Department of Chemical Engineering

Emission of Inorganic Particulate Matter during the Combustion of Biomass, Biochar and Collie Coal

Xiangpeng Gao

This thesis is presented for the Degree of

Doctor of Philosophy

of

Curtin University

October 2011

Declaration

To the best of my knowledge and belief this thesis contains no material previously published by any other person except where due acknowledgment has been made.

This thesis contains no material which has been accepted for the award of any other degree or diploma in any university.

Signature: ……

Date: ……...…….

To my beloved family

ABSTRACT

Coal is an important part of Australia's energy mix and is expected to continue to play an essential role in supplying cheap and secure energy for powering the Australian economy in the foreseeable future. However, coal-based stationary electricity generation is a key contributor to greenhouse gas (e.g. CO_2) emission, which is widely believed to be responsible for global warming and problems related to climate change. Therefore, renewable energy sources such as biomass are becoming increasingly important. In Australia, mallee biomass as a byproduct of managing dryland salinity in agricultural land is a truly sustainable second generation feedstock. Its production is economic, of large scale, high energy efficiency and low carbon footprint. Therefore, mallee biomass and its derived fuels such as biochars can potentially play a key role in the future energy mix of Australia due to significant benefits in Australia's energy security and sustainable development.

Direct combustion of solid fuels (e.g. coal, mallee biomass and its derived biochars etc) is considered to be a matured technology. Coal combustion or coal/biomass co-firing is widely deployed for power generation. However, ash-related issues during solid fuels combustion are notorious and must be considered, particularly the formation/emission of fine inorganic particulate matter (PM). Fine PM is responsible for initiating ash deposition and corrosion on heat exchanger surfaces. PM emission also causes significant adverse impact to human health and environment. Despite the research progress made in this area in the past two decades, there are still significant research gaps in developing credible PM sampling method and understanding on formation/emission of inorganic PM during the combustion of biomass and/or coal.

The present study aims to carry out a systematic study to obtain a thorough understanding on the emission of inorganic PM during the combustion of biomass,

biochar and coal. The specific objectives of this research are to: (1) investigate the effect of sampling temperature on the properties of PM with a size less than 10μm (PM_{10}) produced from pulverized mallee biomass combustion, then develop a proper sampling method for PM produced from the combustion of solid fuels (e.g. biomass and coal); (2) examine the emission behavior and characteristics of PM_{10} produced from pulverized biochar combustion, in order to provide useful data for the design of biochar-based combustion systems; (3) assess the importance and provide direct experimental evidences on the contribution of volatiles combustion to the emission of PM with a size less than 1.0μm (PM_1), and to give insights into fundamental understanding on fine PM formation/emission during biomass combustion; and (4) reveal the significant roles of inherent fine included mineral particles in the emission of PM_{10} during pulverized coal combustion, and propose essential guideline for coal selection on its potential in fine inorganic PM emission during combustion. These objectives have been successfully achieved in this PhD study.

Firstly, sampling temperature is found to influence significantly on the properties of PM_{10} collected from the combustion of pulverized mallee biomass. Although the yield of PM_1 as well as the mass of its dominant elements (e.g. Na, K and Cl) in PM_1 remain constant, the mass-based particle size distribution (PSD) of PM_1 and elemental-mass-based PSDs of Na, K and Cl in PM_1 shift to a larger size at a lower sampling temperature, apparently due to particulate coagulation. However, increasing sampling temperature reduces PM loss due to gravitational settling deposition, leading to an increase in the yields of the PM in a size range of 1.0 – 10 μm ($PM_{1\text{-}10}$) and its dominant elements such as Mg and Ca. Both the yields of $PM_{1\text{-}10}$ and the mass of Mg and Ca in $PM_{1\text{-}10}$ reach constant values at sampling temperatures close to the flue gas temperature (115^{o}C). The sampling temperatures at which drastic shifts in PSD and elemental-mass-based PSDs of PM_{10} take place correlate well with the SO_3 dew points of the flue gas. Therefore, the sampling temperature of PM should be above the flue gas acid dew point to prevent the condensation of acid gas and furthermore be kept close to or same as the flue gas temperature in order to

suppress particulate coagulation and gravitational settling deposition. Based on this important finding, a proper PM sampling method is therefore developed.

Secondly, the PSD of PM_{10} from raw biomass combustion has a bimodal size distribution while the PSDs of PM_{10} from the combustion biochars generally show a unimodal distribution. Most of alkali and alkaline earth metallic species (AAEM species, mainly Na, K, Mg and Ca) are retained in the biochar during pyrolysis. However, the combustion of biochars leads to a significant reduction in the emission of PM_1 (and the mass of Na, K and Cl in PM_1) that dominantly consists of particles smaller than 0.1 μm ($PM_{0.1}$) in comparison to biomass combustion, apparently because of the removal of volatiles and Cl from the raw biomass during pyrolysis for biochars preparation. The results imply that the combustion of volatiles (including the released inorganic species), which is particularly important during biomass combustion, is mainly responsible for PM_1 emission. Meanwhile, a considerable increase in the emission of PM_{1-10} (and the mass of Mg and Ca in PM_{1-10}) is also evident during biochar combustion, most likely as a result of more porous structure and increased ash loading of biochars.

Thirdly, a novel two-stage pyrolysis/combustion system is therefore designed to obtain the direct experimental evidence on the contribution of volatiles combustion to PM emission. The combustion of Na-, K- and Cl-containing volatiles, which are produced *in situ* from the fast pyrolysis of mallee biomass, contributes substantially to PM_1 emission. The PM_1 yield from volatiles combustion is 77.4 – 89.3% of total PM_1 collected from the combustion of both volatiles and char. Oppositely, 97.5 – 99.7% of the yields of total PM_{1-10} are from char combustion. An increase in pyrolysis temperature leads to an increase in the $PM_{0.1}$ yields and the mass of Na, K and Cl in $PM_{0.1}$ from volatiles combustion, as results of enhanced volatilization of Na, K and Cl during pyrolysis. The mass-based PSDs of PM_{10} and elemental-mass-based PSDs of Na, K, and Cl (which are dominantly contained in PM_1) from volatiles combustion generally show a unimodal distribution with a fine

mode range from ~0.022 to ~0.043 μm. The mass-based PSDs of PM_{10} and elemental-mass-based PSDs of Mg and Ca (which are dominantly contained in PM_{1-10}) from char combustion also generally show a unimodal distribution but with a coarse mode of ~6.8 μm. The results clearly demonstrate that the combustion of volatiles (therefore Na, K and Cl included) produced *in situ* from the fast pyrolysis of biomass is a key mechanism responsible for PM_1 emission.

Finally, a density-separated coal sample, with a specific gravity of 1.4 – 1.6, is prepared from Collie coal. As expected, the data of computer-controlled scanning electron microscopy (CCSEM) analysis on the coal show that mineral matter in the coal is of included nature, of which ~90% are fine mineral particles <10 μm. The PM_{10} collected from the combustion of coal and char samples dominantly contains PM_{1-10}, while the yields of PM_1 are limited. PM_{1-10} contains mainly refractory species, including Si, Al, Fe, Mg and Ca. The data also show that PM_1 from char combustion consists of two major fractions with different chemical composition, i.e., $PM_{0.1}$ and PM in a size range of 0.1 – 1 μm ($PM_{0.1-1}$). $PM_{0.1}$ dominantly contains volatile elements (such as Na, K, P and S) and also some refractory elements (e.g. Fe and Si) but $PM_{0.1-1}$ is mainly composed of refractory elements (Al, Fe, and Si). The vast existence of aluminosilicates in $PM_{0.1-1}$ indicates the significant roles of fine included kaolinite and/or Al-silicates particles in the emission of PM_1 from char combustion. Furthermore, the significant roles of inherent fine included mineral particles in PM_{1-10} emission during the combustion of coal and char are clearly evidenced via the identification of the presence of abundant individual but partially-molten quartz ash particles in PM_{1-10}.

ACKNOWLEDGEMENTS

I gratefully acknowledge the Endeavour International Postgraduate Research Scholarship (EIPRS) and Curtin University Postgraduate Scholarship (CUPS), which are provided by Australia's Department of Education, Employment and Workplace Relations and Curtin University, respectively.

I would like to give my sincere acknowledgements to my supervisor, Professor Hongwei Wu, for providing me the precious opportunity for this research and for his invaluable advice, training, guidance, patience, inspiration, persistent support as well as devotion in supervision during the course of this research. Without him, my PhD research would not be possible. I also deeply appreciate him for his thoughtful consideration on not only my research work but also the career development for a young researcher like me.

I am especially indebted to my beloved family-my parents, my wife and my sister, for their support, encouragement and understanding during my PhD study overseas.

I also would like to express my appreciation to Ms. Karen Haynes, Mr. Jason Wright as well as Mr. Zeno Zhang for their laboratory assistance. Thanks also go to the staff from Department of Chemical Engineering for their assistance and the staff from Department of Applied Physics for the help in SEM analysis.

I would like to express my thanks to Dr. Yun Yu, Dr. Hanisom binti Abdullah, Mr. Alan Burton, Mr. Muhammad Usman Rahim, Mr. Syamsuddin Yani, Mr. Sui Boon Liaw, Mr. Dawei Liu, Ms. Yi Li, Ms. Yanwu Yang, Ms.Zhaoying Kong and Ms. Mingming Zhang in our research group for their help in various ways.

LIST OF PUBLICATIONS

Journal Papers

1. **Xiangpeng Gao** and Hongwei Wu. Effect of Sampling Temperature on the Properties of Inorganic Particulate Matter Collected from Biomass Combustion in a Drop-Tube Furnace, *Energy & Fuels* **2010**, 24: 4571–4580.

2. **Xiangpeng Gao** and Hongwei Wu. Biochar as a Fuel: 4. Emission Behavior and Characteristics of PM_1 and PM_{10} from the Combustion of Pulverized Biochar in a Drop-Tube Furnace, *Energy & Fuels* **2011**, 25: 2702–2710.

3. **Xiangpeng Gao** and Hongwei Wu. Combustion of Volatiles Produced *in Situ* from the Fast Pyrolysis of Woody Biomass: Direct Evidence on Its Substantial Contribution to Sub-micrometer Particle (PM_1) Emission, *Energy & Fuels* **2011**, 25: 4172–4181.

4. Hongwei Wu, William Hendrawinata, Yun Yu, **Xiangpeng Gao**, Yi Li, John Bartle, and Peter Grayling. Effect of Hydrodistillation on 1,8-Cineole Extraction from Mallee Leaf and the Fuel Properties of Spent Biomass, *Industrial & Engineering Chemistry Research* **2011**, 50: 11280–11287.

5. Hongwei Wu, Kongvui Yip, Zhaoying Kong, Chun-Zhu Li, Dawei Liu, Yun Yu, and **Xiangpeng Gao**. Removal and Recycling of Inherent Inorganic Nutrient Species in Mallee Biomass and Derived Biochars by Water Leaching, *Industrial & Engineering Chemistry Research* **2011**, 50: 12143–12151.

Conference Papers

1. **Xiangpeng Gao** and Hongwei Wu. Properties of PM_1 collected from biomass combuston in a drop-tube furnace: effect of sampling temperature. *CHEMECA 2010*, 26-29th September, **2010**, Adelaide, Australia.

2. **Xiangpeng Gao** and Hongwei Wu. Emission characteristics of PM_1 generated from pulverised biochar combustion in a drop tube furnace. *Second International Symposium on Gasification and Its Application 2010.* 5-8th December, **2010**, Fukuoka, Japan.

3. **Xiangpeng Gao** and Hongwei Wu. Significant roles of inherent fine included mineral particles in the emission of PM_{1-10} during pulverized coal combustion. *The 7th International Symposium on Coal Combustion* ***2011***, 17-20th July, Harbin, China.

4. Yi Li, **Xiangpeng Gao**, and Hongwei Wu. Roles of Ash Cenosphere Fragmentation in the Formation of Ash and Particulate Matter during Pulverized Pyrite Combustion. *The 7th International Symposium on Coal Combustion* ***2011***, 17-20th July, Harbin, China.

TABLE OF CONTENTS

Declaration ..... **I**

ABSTRACT ..... **III**

ACKNOWLEDGEMENTS ..... **VII**

LIST OF PUBLICATIONS ..... **VIII**

TABLE OF CONTENTS ..... **X**

LIST OF FIGURES ..... **XVI**

LIST OF TABLES ..... **XXIII**

CHAPTER 1 INTRODUCTION **1**

1.1 Background and Motive 1

1.2 Scope and Objectives 3

1.3 Thesis Outline 4

CHAPTER 2 LITERATURE REVIEW **6**

2.1 Introduction 6

2.2 Significance of Collie Coal and Mallee Biomass in Western Australia 7

2.3 The Main Issues Related to Biomass Supply and Motivations of Using Biochar as a Fuel 8

2.4 Ash-Related Problems during Combustion of Pulverized Coal and Biomass 10

2.4.1 Ash Deposition in the Boiler Furnace and Convective Tube Banks 10

2.4.2 Fireside Corrosion 11

2.4.3 Fine PM emission 11

2.5 Sampling Methods of Inorganic PM Produced from the Combustion of Coal and/or Biomass 12

2.5.1 Considerations on Designing PM Sampling Line 13

2.5.2 PM Sample Dilution 13

2.5.3 Importance of Sampling Temperature and its Discrepancies among Various Previous Studies 14

2.6 Ash Formation during Pulverized Biomass Combustion 15

2.6.1 Contents of Inorganic Species in Mallee Biomass 18

2.6.2 Occurrence of Inorganic Species in Biomass 19

2.6.3 Transformation and Release of Inorganic Species during Pulverized Biomass Pyrolysis and Combustion 22

2.6.3.1 Transformation and Release of Cl 23

2.6.3.2 Transformation and Release of S 27

2.6.3.3 Transformation and Release of Alkali Metals ……..28

2.6.3.4 Transformation and Release of Alkaline Earth Metals…35

2.6.4 Important Gas Phase and Gas-Solid Phase Reactions and Their Implications on Mitigating Ash-Related Problems 35

2.6.4.1 Effects of Cl on Fine PM Formation during Biomass Combustion 36

2.6.4.2 Sulfation of Alkali Chlorides to Alkali Sulfates 37

2.6.4.3 Reactions between Alkali Chlorides and Aluminosilicates 38

2.6.5 Ash Formation Mechanisms during Pulverized Biomass Combustion 39

2.7 Ash Formation during Pulverized Coal Combustion 39

2.7.1 Mineral Matter in Coal 39

2.7.2 Transformation of Included Minerals 41

2.7.3 PM Formation Mechanisms during Pulverized Coal Combustion . 45

2.7.3.1 Formation Mechanisms for PM_{1-10} 46

2.7.3.2 Formation Mechanisms for PM_1 49

2.7.4 Effects of Combustion Conditions and Coal Properties on PM Formation during Pulverized Coal Combustion 52

2.8 Conclusions and Research Gaps 54

2.9 Research Objectives of the Present Study 57

CHAPTER 3 RESEARCH METHODOLOGY AND ANALYTICAL TECHNIQUES 59

3.1 Introduction 59

3.2 Methodology 59

3.2.1 Effect of Sampling Temperature on the Properties of Inorganic PM Collected from Biomass Combustion 60

3.2.2 Emission Behavior and Characteristics of PM_1 and PM_{10} from the Combustion of Pulverized Biochar 60

3.2.3 Combustion of Volatiles Produced In Situ from the Fast Pyrolysis of Woody Biomass: Direct Evidence on Its Substantial Contribution to PM_1 Emission 61

3.2.4 Significant Roles of Inherent Fine Included Mineral Particles in the Emission of PM10 during Pulverized Coal Combustion 61

3.3 Experimental 62

3.3.1 Sample Preparations 62

3.3.2 Experimental Rigs 64

3.3.2.1 A Drop-Tube/Fixed-Bed Quartz Reactor System 64

3.3.2.2 A High-Temperature DTF System 66

3.3.2.3 A Novel Two-Stage Pyrolysis/Combustion Reactor 69

3.3.3 Generation of a Stream of Constant PM_{10}-Containing Flue Gas from Biomass Combustion 71

3.3.4 Preparations of Biochar and Coal-Char 72

3.3.4.1 Biochar 72

3.3.4.2 Coal-Char 73

3.3.5 Volatiles Produced In Situ from Fast Pyrolysis of Biomass 74

3.3.6 Combustion of Pulverized Fuel Particles and Volatiles 74

3.3.6.1 Combustion of Pulverized Fuel Particles 74

3.3.6.2 Combustion of Volatiles 75

3.3.7 Sampling of Inorganic PM 76

3.4 Instruments and Analytical Techniques 77

3.4.1 Proximate, Ultimate and Calorific Value Analysis 77

3.4.2 Mass- based Particle Size Distribution of PM_{10} 79

3.4.3 Quantification of AAEM Species and Other Inorganic Species 79

3.4.4 Quantification of S and Cl in PM samples 80

3.4.5 Total Organic Carbon (TOC) Analyzer 81

3.4.6 Micropore Surface Area of Biochars 81

3.4.7 Computer Controlled Scanning Electron Microscopy (CCSEM) 82

3.4.8 Scanning Electron Microscope (SEM) 83

3.4.9 X-Ray Diffraction (XRD) Analysis 83

3.5 Summary 83

CHAPTER 4 EFFECT OF SAMPLING TEMPERATURE ON THE PROPERTIES OF INORGANIC PARTICULATE MATTER COLLECTED FROM BIOMASS COMBUSTION 84

4.1 Introduction 84

4.2 Measured PM Yields and Mass Concentrations in Flue Gas 85

4.3 Mass-Based Particle Size Distribution of PM_{10} 87

4.4 Effect of Sampling Temperature on the Collection and Properties of PM_1 and PM_{1-10} 88

4.5 Possible Mechanisms Responsible for the Effect of Sampling Temperature on the Collection and Properties of PM_{10} 94

4.6 Conclusions 97

CHAPTER 5 EMISSION BEHAVIOR AND CHARACTERISTICS OF PM_1 AND PM_{10} FROM THE COMBUSTION OF PULVERIZED BIOCHAR IN A DROP-TUBE FURNACE 98

5.1 Introduction 98

5.2 Biochar Yields and the Retention of AAEM Species and Cl in Biochars 99

5.3 PM_1 and PM_{10} Yields during the Combustion of Biomass and Biochars 103

5.4 Mass-Based and Elemental Mass-Based Particle Size Distributions (PSDs) of PM_{10} 106

5.5 Further Discussion 109

5.6 Practical Implications 113

5.7 Conclusions 115

CHAPTER 6 COMBUSTION OF VOLATILES PRODUCED IN SITU FROM THE FAST PYROLYSIS OF WOODY BIOMASS: DIRECT EVIDENCE ON ITS SUBSTANTIAL CONTRIBUTION TO PM_1 EMISSION 117

6.1 Introduction 117

6.2 Yields of Volatiles and Release of AAEM Species and Cl with Volatiles Generated in Situ from the Fast Pyrolysis of Pulverized Biomass 118

6.3 PM_1 and PM_{10} Yields during the Combustion of Volatiles and Chars 122

6.4 Properties of PM_1 and PM_{10} Collected from the Combustion of Volatiles and Chars 127

6.5 Further Discussion on the Mechanisms Responsible for the Emission of PM_1 and PM_{1-10} 133

6.6 Conclusions 137

CHAPTER 7 SIGNIFICANT ROLES OF INHERENT FINE INCLUDED MINERAL PARTICLES IN THE EMISSION OF PM_{10} DURING PULVERIZED COAL COMBUSTION 139

7.1 Introduction 139

7.2 Characterisation of Fine Mineral Particles in Coal 140

7.3 Yield and Mass-Based Particle Size Distribution (PSD) of PM_{10} from the Combustion of Coal and Char 144

7.4 Direct Evidences on the Significant Contribution of Fine Included Mineral Particles to PM_{1-10} Emission 147

7.5 Roles of Inherent Fine Included Mineral Particles in PM_1 Emission during Char Combustion 151

7.6 Possible Mechanisms Responsible for the Discrepancies in the Emission Behavior of PM_{10} from the Combustion of Coal and Char 156

7.7 Conclusions 159

CHAPTER 8 CONCLUSIONS AND RECOMMENDATIONS 161

8.1 Introduction 161

8.2 Conclusions 161

8.2.1 Effect of Sampling Temperature on the Properties of Inorganic Particulate Matter Collected from Biomass Combustion 161

8.2.2 Emission Behavior and Characteristics of PM_1 and PM_{10} from the Combustion of Pulverized Biochar in a Drop-Tube Furnace 162

8.2.3 Combustion of Volatiles Produced in Situ from the Fast Pyrolysis of Woody Biomass: Direct Evidence on its Substantial Contribution to PM_1 Emission 163

8.2.4 Significant Roles of Inherent Fine Included Mineral Particles in the Emission of PM_{10} during Pulverized Coal Combustion 164

8.3 Recommendations 166

REFERENCES **167**

LIST OF FIGURES

Figure 1-1: Thesis map..... 5

Figure 2-1: A schematic diagram of particulate matter sampling process..... 13

Figure 2-2: Schematic diagram of the different forms of inorganic species in biomass[114]..... 19

Figure 2-3: Possible reaction pathways and release mechanisms of Cl during biomass pyrolysis and subsequent combustion, summarized based on the findings in refs[117, 125, 130]..... 26

Figure 2-4: Possible reaction pathways and release mechanisms of K and Na during biomass pyrolysis and subsequent combustion, summarized based on the findings in refs[117, 125, 128, 130, 136]..... 34

Figure 2-5: Major ash aerosol formation mechanisms during coal combustion, solid arrows indicate solid-to-particle processes while dotted arrows indicate solid–vapor–particle processes[39]..... 46

Figure 3-1: Research methodology..... 63

Figure 3-2: A Drop-tube/fixed-bed quartz reactor system..... 66

Figure 3-3: Schematic diagram of experimental setup: (1) Feeder, (2) Mass flow controller, (3) Primary air, (4) Cooling water, (5) Secondary air, (6) Water-cooled feeding probe, (7) Dense mullite reaction tube, (8) Two heating-zone furnace, (9) Water-cooled quench probe, (10) Makeup and dilution air, (11) Cyclone, (12) Dekati low pressure impactor, (13) Vacuum pump, (14) Diluter, (15) Quench helium, (16) Exit of quench probe..... 68

Figure 3-4: Gas temperature profile of the DTF..... 70

Figure 3-5: DLPI image (a) and its nominal cut-off size calibrated at 21.5 ^{o}C with a gas flow rate of 10.04 L/min 70

Figure 3-6: A schematic diagram of the two-stage pyrolysis/combustion reactor system used in this study, it consists of a quartz drop-tube/fixed-bed pyrolyser that is cascaded into the DTF as described in Section 3.3.2.2 71

Figure 3-7: Effect of the operation position of cyclone on the (a) particle size distribution of PM_{10} and (b) yield of ash collected by cyclone. The PM sampling temperature was set at 25^{o}C. 76

Figure 3-8: Temperature program of TGA for proximate analysis of coal, coal-char, biomass and biochar 78

Figure 3- 9: A Schematic diagram of quantification of AAEM species and other inorganic species in fuel samples and PM samples collected by DLPI 80

Figure 3-10: Temperature program of ashing fuel samples such as biomass, biochar and coal 81

Figure 4-1: Total PM yield and mass concentration at point A: (a) total PM yield in flue gas, (b) total PM mass concentration in flue gas 85

Figure 4-2: Emission characteristics of PM_{10} at various sampling temperatures: (a) PM_{10} yield in flue gas, (b) PM_{10} mass concentration in flue gas 87

Figure 4-3: Mass-based particle size distribution of particulate matter collected by DLPI at different sampling temperatures: (a) Case-0.1, (b) Case-0.3. Graphs are normalized to the total mass of bark sample (dry basis) fed into the drop-tube reactor in each experiment. 88

Figure 4-4: Elemental Mass Size Distribution at Different Sampling Temperatures in Case-0.1: (a) Na, (b) K, (c) Cl, (d) Mg, (e) Ca, (f) S. Graphs Are Normalized to the Total Mass of Bark Sample (Dry Basis) Fed into the Drop-Tube Reactor in Each Experiment 90

Figure 4- 5: Summary of elements yields at different sampling temperatures in Case-0.1: (a) Na, (b) K, (c) Cl, (d) Mg, (e) Ca, (f) S. Graphs are normalized to the total mass of bark sample (dry basis) fed into the drop-tube reactor in each experiment. 91

Figure 4-6: Elemental mass size distribution at different sampling temperatures in Case-0.3: (a) Na, (b) K, (c) Cl, (d) S. Graphs are normalized to the total mass of bark sample (dry basis) fed into the drop-tube reactor in each experiment. 93

Figure 4-7: Sulfur yields at different sampling temperatures in Case-0.3. Graphs are normalized to the total mass of bark sample (dry basis) fed into the drop-tube reactor in each experiment 94

Figure 4-8: Effect of biomass feeding rate on PSD curves at different sampling temperatures: (a) 25^{o}C, (b) 40^{o}C, (c) 115^{o}C 96

Figure 5-1: Biochar yields from the pyrolysis of raw biomass under various conditions 102

Figure 5- 2: Retentions of AAEM species and Cl in biochars produced from the pyrolysis of raw biomass at different conditions 103

Figure 5-3: PM yields from raw biomass and biochars combustion: (a) PM_1 and (b) PM_{10} yields, normalized to equivalent biomass (db) input into the furnace; (c) PM_1 and (d) PM_{10} yields, normalized to equivalent ash input into the furnace; (e) PM_1 and (f) PM_{10} yield, normalized to equivalent energy input into the furnace. Equivalent biomass input is calculated from the char yields and the mass of biochars fed into the drop tube furnace, equivalent ash input is calculated from the mass of fuel (db) fed into furnace and its ash content (wt%, db), equivalent energy input is calculated from the lower heating value (LHV) of raw biomass and biochars and their mass (db) fed into drop tube furnace. 105

Figure 5-4: Particle size distribution of PM_{10} from the combustion of raw biomass and biochars: (a) graphs normalized to equivalent biomass (db) input into the furnace,

(b) graphs normalized to equivalent ash input into the furnace, and (c) graphs normalized to equivalent energy (LHV) input into the furnace 107

Figure 5-5: Elemental mass size distribution of AAEM species and Cl in PM during the combustion of raw biomass and biochars: (a) Na, (b) K, (c) Cl, (d) Mg and (e) Ca are normalized to the equivalent biomass (db) input into the furnace; (f) Na, (g) K, (h) Cl, (i) Mg and (j) Ca are normalized to the equivalent ash input into furnace; (k) Na, (l) K, (m) Cl, (n) Mg and (o) Ca are normalized to the equivalent energy input (LHV) into the furnace..... 108

Figure 5-6: Elements yields of AAEM species and Cl in PM during the combustion of raw biomass and biochars: (a) Na, (b) K, (c) Cl, (d) Mg and (e) Ca, normalized to equivalent biomass (db) input into the furnace; (f) Na, (g) K, (h) Cl, (i) Mg and (j) Ca, normalized to equivalent ash input into furnace; (k) Na, (l) K, (m) Cl, (n) Mg and (o) Ca, normalized to equivalent energy input (LHV) into the furnace. 110

Figure 5-7: Molar ratio of (Na+K)/Cl in $PM_{0.1}$ collected from raw biomass combustion 111

Figure 5-8: Micropore surface area of biochars produced from the fast pyrolysis of raw biomass, SH–Char–400, SH–Char–500, FH–Char–400 and FH–Char–500 at 1300 ^{o}C in the DTF, analysed by Dubinin-Astakhov equation..... 113

Figure 5-9: The relationship between energy-based ash loading of fuels and energy-based yields of PM1-10 collected from the combustion of raw biomass and biochars 115

Figure 6-1: Products yields from the pyrolysis of raw biomass under various conditions 121

Figure 6-2: Distribution of AAEM species and Cl in chars and volatiles during the pyrolysis of raw biomass under different conditions 124

Figure 6-3: PM yields from the combustion of (a) volatiles, (b) chars and (c) "volatiles + char" (compared with raw biomass combustion). Graphs normalized to the equivalent biomass (db) input into the furnace 127

Figure 6-4: The distribution of PM_{10} yield from the combustion of volatiles and chars, based on the total PM_{10} yield from "volatiles + char" combustion, including the yields of PM with aerodynamic diameters (a) less than 0.1 μm ($PM_{0.1}$), (b) between 0.1 and 1 μm ($PM_{0.1-1}$), (c) less than 1μm (PM_1), (d) between 1 and 10 μm (PM_{1-10}) and (e) less than 10 μm (PM_{10}), respectively 129

Figure 6-5: Particle size distributions (PSDs) of PM_{10} from the combustion of (a) volatiles, (b) chars and (c) "volatiles + char" (compared with biomass combustion). Graphs normalized to the equivalent biomass (db) input into the furnace 130

Figure 6-6: Elemental mass size distribution of AAEM species and Cl in PM_{10} during the combustion of volatiles and chars produced at different temperatures: (a) Na, (b) K, (c) Cl, (d) Mg and (e) Ca are from volatiles combustion; (f) Na, (g) K, (h) Cl, (i) Mg and (j) Ca are from char combustion; (k) Na, (l) K, (m) Cl, (n) Mg and (o) Ca are from "volatiles + char" combustion, also compared with raw biomass combustion. Graphs are normalized to the mass of raw biomass (dry basis) input into the furnace 131

Figure 6-7: Elements yields of AAEM species and Cl in PM_{10} during the combustion of volatiles and chars produced at different temperature: (a) Na, (b) K, (c) Cl, (d) Mg and (e) Ca are from volatiles combustion; (f) Na, (g) K, (h) Cl, (i) Mg and (j) Ca are from char combustion; (k) Na, (l) K, (m) Cl, (n) Mg and (o) Ca are from "volatiles + char" combustion, also compared with raw biomass combustion. Graphs are normalized to the mass of raw biomass (dry basis) input into the furnace 132

Figure 6-8: Possible ash formation/emission mechanisms during pulverized biomass combustion, modified based on the findings in Chapter 6 and previous studies.[39, 277] 133

Figure 6-9: Relationship between PM_1 yield from volatiles combustion between (a) total volatile yield, (b) the content of (Na+K+Cl) in volatiles, (c) the content of (Na+K) in volatiles and (d) the content of Cl in volatiles..... 135

Figure 6- 10: Molar ratio of (Na+K)/Cl in the PM samples with aerodynamic diameters less than 0.1 μm ($PM_{0.1}$) that were collected from the combustion of volatiles and raw biomass. 137

Figure 7-1: Properties of mineral matter in the raw coal: (a) total mineral size distribution; (b) main mineral phases..... 141

Figure 7-2: Inorganic elements distribution afte dilute acid washing..... 144

Figure 7-3: Yield of PM with aerodynamic diameters less than 1μm (PM_1), between 1 and 10μm (PM_{1-10}), and less than 10μm (PM_{10}) from the combustion of coal and char..... 145

Figure 7-4: Mass-based particle size distribution (PSD) of PM_{10} from the combustion of coal and char 146

Figure 7-5: Yield distribution of PM with aerodynamic diameters less than 1μm (PM_1), between 1 and 10μm (PM_{1-10}), and ash collected in cylone from the combustion of coal and char 146

Figure 7-6: Composition of major inorganic elements (reported as oxides) in PM_{1-10} collected from coal/char combustion 147

Figure 7-7: Comparison on the mass percentage of total and water-soluble alkali metals (Na and K) in PM_{1-10} produced from the combustion of coal and char..... 148

Figure 7-8: SEM images and EDS spectrum of PM with an aerodynamic diameter of 4.087 – 6.852 μm in PM_{1-10} collected from coal combustion..... 149

Figure 7-9: XRD patterns of PM with an aerodynamic diameter of (a) 1.624 – 2.438 μm, (b) 2.438 – 4.087 μm, (c) 4.087 – 6.852 μm and (d) 6.852 – 10.174 μm collected from coal combustion..... 150

Figure 7-10: Chemical composition (reported as oxides) of PM with an aerodynamic diameter of (a) less than 0.1µm ($PM_{0.1}$), and (b) 0.1 – 1 µm ($PM_{0.1-1}$) collected from char combustion 152

Figure 7-11: Elemental mass-based particles size distribution of Na, K, Al, and Si in PM_1 collected from char combustion 153

Figure 7-12: SEM images and EDS spectrum of PM with an aerodynamic diameter of (a) 0.043 – 0.077 µm and (b) 0.61 – 0.955 µm in PM_1 collected from char combustion 155

Figure 7-13: Retention of major inorganic elements in char produced from fast pyrolysis of coal at 1000 ^oC 157

Figure 7-14: SEM images and EDS spectrum of ash particles collected by cyclone from the combustion of (a) coal and (b) char 159

LIST OF TABLES

Table 2-1: Summary of PM sampling methods from the combustion of solid fuels (biomass and/or coal) 16

Table 2-2: Inorganic species contents in typical mallee biomass[113] 18

Table 2- 3: Main minerals identified with coals[179] 42

Table 3- 1: Properties of *E.loxophleba lissophloia* mallee bark used in Chapter 4 ... 65

Table 5- 1: Proximate and ultimate analysis of raw biomass and its derived biochars used in this study (SH-Char-xxx: biochar prepared from the slow heating pyrolysis of biomass at xxx °C; FH-Char-xxx: biochar prepared from the fast heating pyrolysis of biomass at xxx °C) 100

Table 5- 2: Contents (wt% db) of inorganic species in raw biomass and its derived biochars used in this study (SH-Char-xxx: biochar prepared from the slow heating pyrolysis of biomass at xxx °C; FH-Char-xxx: biochar prepared from the fast heating pyrolysis of biomass at xxx °C) 101

Table 6- 1: Proximate and ultimate analysis of raw biomass and its derived biochars used in this study (Char-xxx: char prepared from the fast heating pyrolysis of biomass at xxx °C) 119

Table 6- 2: Contents (wt% db) of inorganic species in raw biomass and its derived biochars used in this study (Char-xxx: char prepared from the fast heating pyrolysis of biomass at xxx °C) 120

Table 7- 1: Proximate and ultimate analysis of the coals and coal-chars 143

CHAPTER 1 INTRODUCTION

1.1 Background and Motive

Coal will continue to be the dominant fuel to produce cheap and secure power for the development of the Australian economy in the foreseeable future.[1] However, coal-based stationary electricity generation contributes over 40% of Australia's anthropogenic CO_2 emissions per annum.[2] Greenhouse gas (GHG) such as CO_2 is widely believed to be responsible for global warming and climate change. Therefore, renewable energy, particularly biomass, is becoming increasingly important for future sustainable development. This is particularly the case for Australia, due to the large area, small population and heavy reliance on energy-intensive industries such as mining, energy and mineral processing. For instance, it is predicted by International Energy Agency (IEA) that biomass energy will increase to ~11.7% of the total global energy supply by 2030.[3]

In Australia, mallee biomass is considered to be as a key second-generation bioenergy feedstock[4] because it is a byproduct of managing dryland salinity. Its production is economic on a large scale as well as small carbon and energy footprints.[4-8] Therefore, mallee biomass can potentially play an important role in Australia's energy mix due to its significant benefits in overcoming the challenges of energy crisis and environmental issues.[9-11]

Substantial R&D has been carried out in the past several years on the comprehensive utilization of mallee biomass as a renewable energy feedstock in an efficient and environmentally friendly manner.[12-17] One key research outcome is to use biochar,[14, 15, 17] which can be produced from distributed pyrolysis located near the biomass production areas, as a fuel for further electricity generation via gasification and combustion. Biochar is known to have superb fuel properties, excellent grindability

and high energy density.[14] Using biochar as a fuel addresses the key drawbacks associated with the direct use of biomass as a fuel, including low energy density, high transportation cost, and poor grindability etc.[14]

Therefore, coal and renewable solid fuels (e.g. mallee biomass and its derived biochars) are likely to be key solid fuels for electricity generation in the energy mix of Western Australia, or Australia as a whole. Among various technologies for power generation using solid fuels, direct combustion is a matured technology[18-22] and widely deployed. [23-25]

Combustion of coal and biomass inevitably encounters notorious ash-related issues.[26-28] Among these issues, formation/emission of fine inorganic particulate matter (PM) is an important consideration,[29-35] Fine PM affects the heat transfer in the furnace and has been identified as possibly initiating deposit formation and consequent corrosion on heat exchanger surfaces.[33-35] Once emitted into atmosphere, fine PM will cause significant adverse impact on both human health and environment.[26, 31, 32, 36-38] Therefore, extensive investigations[39-42] have been dedicated to studying the formation/emission of inorganic PM during the combustion of coal and biomass in the past two decades.

Despite the progress made in the formation and emission of inorganic PM during the combustion of biomass and coal, there are still significant research gaps in this area. This is largely due to the complexities of fuels and combustion process. For example, it is still not known how sampling temperature effects the properties of PM collected. Yet such knowledge is essential to developing an adequate sampling method to ensure the PM properties not being distorted by the sampling process. Furthermore, there is also no data on the emission behavior of inorganic PM from the combustion of biochar, such data are believed to be an important criteria for guiding to produce quality biochar fuels. While the previous studies were focused on PM formation/emission during biomass combustion, fundamentally, the contribution of

the combustion of volatiles and char to the formation/emission of fine PM during biomass combustion is still unclear. Last but not least, the roles of fine mineral particles inherent in solid fuels in the formation/emission of PM are largely unknown. Therefore, a fundamental study on the formation/emission of inorganic PM during the combustion of biomass, biochar and coal is of great importance to improve the understanding on the above unknown issues and provide essential knowledge to guide practical applications.

1.2 Scope and Objectives

The present study aims to provide a fundamental understanding on the emission of inorganic PM during the combustion of biomass, biochar and coal. The detailed objectives of this study are to:

(1) Investigate the effects of sampling temperature on the collection and properties of PM_{10} produced from pulverized mallee biomass combustion and aim at developing an adequate sampling method for PM produced from the combustion of solid fuels such as biomass and coal.

(2) Examine the emission behavior of PM_{10} produced from pulverized biochar combustion, aiming to provide useful data for the design of combustion systems using biochar as feed.

(3) Provide direct experimental evidences on the contribution of volatiles combustion to PM_1 emission and mechanistic understanding on fine PM formation/emission during biomass combustion.

(4) Reveal the significant roles of inherent fine included mineral particles in the emission of PM_{10} during pulverized coal combustion and propose essential coal selection guideline in assessing its potential in fine inorganic PM emission during combustion.

1.3 Thesis Outline

There are a total of 8 chapters in this thesis (including this chapter). Each chapter is listed as follows, and the thesis structure is schematically shown in the thesis map (see Figure 1-1).

- Chapter 1 introduces the background and objectives of the present research.
- Chapter 2 reviews the up to date literatures on the inorganic particulate matter emission from the combustion of biomass and coal, finally leading to the identification of existing research gaps in the field and determination of specific objectives of the current research.
- Chapter 3 summarizes the methodology employed to achieve the research objectives, accompanied by the explanations of the experimental equipments, analytical techniques and samples used.
- Chapter 4 investigates the effect of sampling temperature on the properties of PM collected from pulverized biomass combustion and then develops an adequate sampling method for inorganic PM from solid fuels combustion.
- Chapter 5 assesses the emission behavior of inorganic particulate matter from the combustion of a series of biochar produced from the pyrolysis of mallee biomass under conditions related to practical applications.
- Chapter 6 provides direct evidence on the substantial contribution of volatiles combustion to fine PM emission during pulverized biomass combustion.
- Chapter 7 demonstrates the significant roles of fine inherent mineral particles in the emission of fine particulate matter during pulverized coal combustion.
- Chapter 8 concludes the present study and recommends future work.

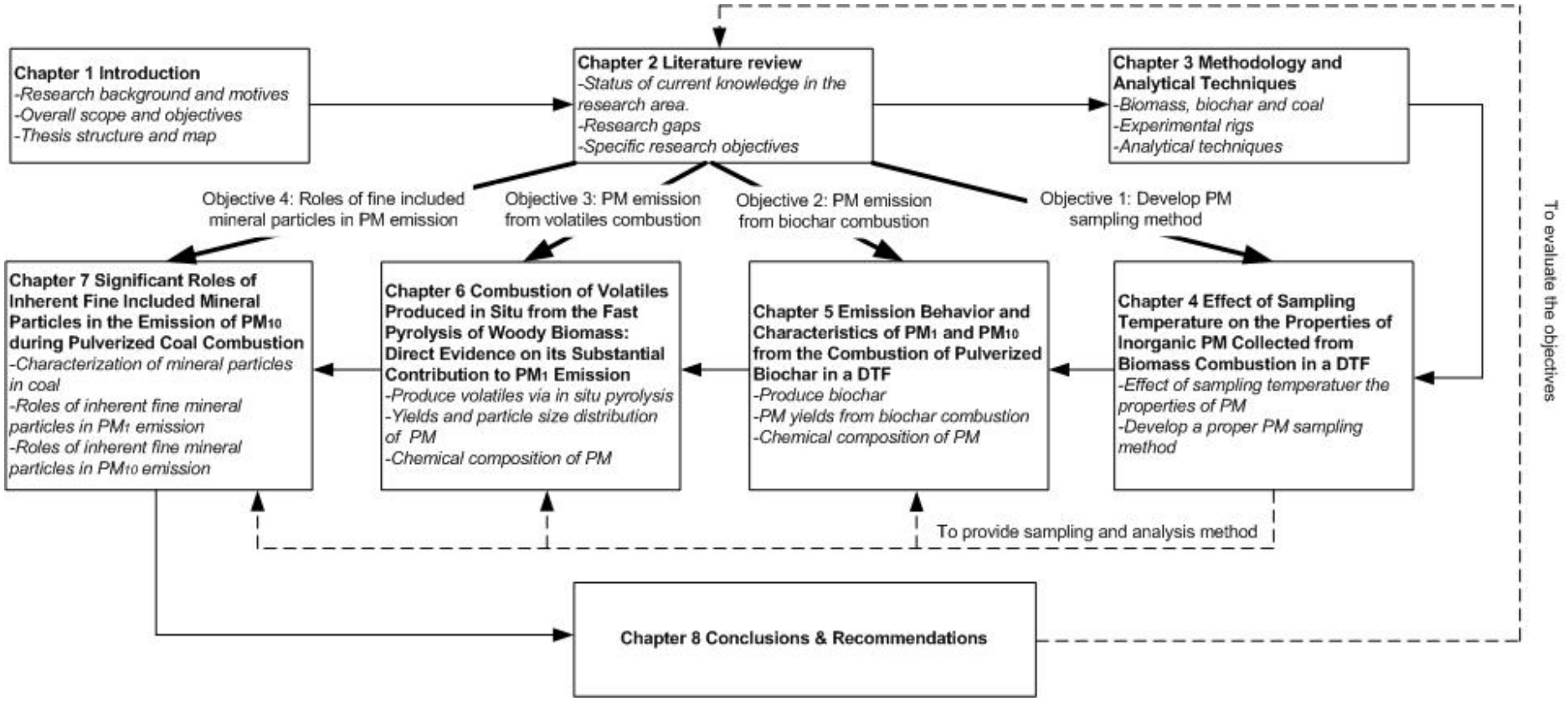

Figure 1-1: Thesis map

CHAPTER 2 LITERATURE REVIEW

2.1 Introduction

Stationary power generation based on the combustion of coal plays an important role in the energy mix of Australia. However, the use of fossil fuel leads to significant emissions, particularly carbon emission which is known to contribute to global warming and climate change. Biomass is projected to be an important renewable source for carbon abatement. Biomass combustion, similar to coal combustion, is a matured technology for electricity generation. However, a key technical challenge associated with the combustion of these solid fuels (biomass or coal) is the emission of fine inorganic particulate matter (PM), which has significant adverse impacts on human health and environment.[31, 32, 43]

Over the past two decades, there have been various research efforts dedicated to the formation/emission of fine PM produced from the combustion of coal and biomass. This chapter aims to review the literature on PM formation/emission during the combustion of coal and biomass, identify the research gaps and outline the research objectives of this thesis. This chapter starts with reviewing the importance of Collie coal and Mallee biomass in Western Australia's energy mix, followed by the key issues related to the use of biomass as direct fuel and the advantages of using biochar as a fuel. A brief review on the ash-related problems associated with the combustion of coal and biomass is also given. The importance of sampling methods for fine PM produced from combustion of pulverized solid fuels (coal and biomass) is then discussed, followed by the detailed mechanisms on the fine PM formation during coal and/or biomass combustion. This chapter concludes with the key research gaps identified and the thesis scope.

2.2 Significance of Collie Coal and Mallee Biomass in Western Australia (WA)

- ***Collie coal***

The Australia relies heavily on coal for electricity generation because of its large coal reserves, coal was used to provide ~75% of the total power generation in Australia in 2009-2010 and is projected to provide ~63.9% in 2029-2030.[1] Hence, coal will continue to be the dominant fuel for electricity production in Australia in the foreseeable future. In WA, Collie coal is the only coal currently being mined[44] and used for electricity generation in coal-fired power stations with a total maximum capacity of more than 2300 MW,[45] playing an important role in supplying cheap energy to the development of state's economy. Collie coal is a sub-bituminous coal of high moisture (20 – 28%), high volatile matter (30-47% dry-ash free basis) and low ash contents (4 – 12% dry basis).[46, 47] Collie coal has been extensively investigated on its pyrolysis behaviours,[48-50] grindability,[51] char reactivity,[46] ash deposition,[52] and mineral matter characterization[53] because of its significance in energy supplements of WA. A unique feature of the coal is that it contains abundant fine included mineral particles[53] (e.g. fine quartz and kaolinite particles, etc.) which are known to be responsible for the initiation and growth of ash deposit.[52]

- ***Mallee Biomass***

As stated above, Collie coal is an important fuel for current power generation in WA. However, as a fossil fuel, coal is finite and its use significantly contributes to various emissions including CO_2, SO_2, NO_X, PM and other pollutants, causing serious environmental problems such as global warming and acid rain. Therefore, renewable energy, particularly biomass is playing increasingly important roles in the global response to the challenges of energy security and sustainable development.

At present, the conversion technologies and markets are well established for the first-generation biofuels which are produced from food crops.[54] However, extensive

utilization of these first-generation biofuels is of low energy efficiency and high carbon footprint, and leads to serious competition with food production.[55, 56] Therefore, sustainable development requires energy/fuels (including biofuels) to be produced from second-generation bioenergy feedstock.

In WA, mallee biomass is considered to be a key second-generation bioenergy feedstock, which has recently attracted extensive R&D due to its economic production on a large scale, small carbon and energy footprints.[4-8] The initial motivation of planting Mallee biomass in WA is to combat the increasing salinity problem in the low-to-medium rainfall (300-600 mm mean annual rainfall) "wheat-belt" agricultural area.[4, 57] Since the early 1990s, more than 14 000 ha (30 million trees) have been planted across the "wheat-belt" region.[58] Mallees are multi-stemmed native eucalypt low tree or shrub species that can be harvested on a short cycle and able to rapidly regenerate as coppice for every 3-4 years. A recent life-cycle energy balance[4] indicates that mallee biomass production in WA achieves an energy ratio (the ratio of total energy outputs and total non-renewable energy inputs) of over 40 and an energy productivity of over 200 GJ ha^{-1} y^{-1}. Such energy performance is considerably better than those achieved by annual energy crops, e.g., canola, which typically have energy ratios less than 7.0 and energy productivities less than 40.0 GJ ha^{-1} y^{-1}. Mallee biomass production is also of large scale, which can be ~10 million dry tones per annum.[5] Overall, the results have indicated that mallee biomass could be the most important secondary generation bioenergy feedstock in WA.

2.3 The Main Issues Related to Biomass Supply and Motivations of Using Biochar as a Fuel

Mallee biomass as a renewable bioenergy resource can contribute significantly to local energy security and regional area development in WA. However, the utilization of mallee biomass has some important technical challenges related to several

undesired characteristics of direct using biomass as a fuel.

- ***Issues related to biomass supply***

The supply chain of biomass mainly consists of transportation, handling, storage, sizing, pre-processing (drying and/or other pre-treatments), and utilization. Biomass is bulky, having high-moisture-content, low-energy-density, and of fibrous nature.[14] In the case of mallee biomass, the green biomass has a moisture content of ~45% and a low energy density of ~10 GJ ton^{-1}.[59] Therefore, it is not economic to transport mallee biomass for a long distance and the capacity of dedicated bioenergy plants using mallee biomass as feedstock is therefore constrained.[6] Furthermore, the bulky and fibrous natures of biomass lead to the biomass's poor grindability, which significantly increases the cost for size reduction of biomass materials as well as other operating and maintenance cost.[14] Moreover, as results of poor grindability of biomass, coarse biomass particles may result in incomplete burn out, blockage/bridging to the feeding system, sedimentation, and poor mixing.[14] Large biomass particles also increase milling costs and require expensive storage.[14] For example, a previous study found that the co-milling of coal and biomass in a pilot scale vertical spindle mill is limited by a maximal 5 wt % biomass blend. Ball mills widely used in coal-fired power stations are not suitable to grind biomass as its gravity impacts and tumbling actions only flatten biomass fibre rather than cutting.

- ***Motivations of using biochar as a fuel***

Various biomass pre-treatment technologies, e.g. drying,[60] pulverizing,[61] baling, briquetting, palletizing,[16] torrefaction, torrefaction combined with pelletizing[62] and pyrolysis,[14, 15] are developed to improve biomass fuel properties. Among these technologies, distributed pyrolysis is a flexible technology[63-67] to convert the bulky raw biomass locally into high-energy-density fuels such as bio-oil[64, 65, 68, 69] and/or biochar.[14, 67, 70] While bio-oil can be transported to centralized plants for further upgrading and refining to produce liquid transport fuels,[64, 65, 71] biochar as a solid fuel

with desired fuel properties, good grindability and high energy density, is therefore suitable for direct combustion and/or co-firing in coal-based power stations.[14, 70, 72]

2.4 Ash-Related Problems during Combustion of Pulverized Coal and Biomass

The potential fuels of interests in this thesis are therefore Collie coal, mallee biomass, and biochar. There are various technological pathways available for power generation from these fuels, including combustion and/or co-firing, gasification and pyrolysis. Direct combustion is a matured technology[18-22] and received extensive investigations.[23-31, 33-35, 73-86] The combustion related issues include fuel conversion rate,[73] flame temperature and stability,[74] gas pollutants emissions and boiler efficiency,[24, 75] and ash-related issues.[26-31, 33-35, 73, 76-86] The ash-related issues are considered to be one of the most important technical challenges of coal and/or biomass combustion as it plays critical roles in the design and operation of coal (and/or biomass) combustion equipments such as pulverized fuel (PF) boilers. The main ash-related issues of the combustion of coal and biomass are ash deposition, fireside corrosion and fine particulate matter emission,[54-72] Biomass combustion also encounters its unique problems such as potential impaction on selective catalytic reduction (SCR) system[76] and fly ash utilization[73] as results of the abundant inherent nutrients species in biomass, including alkali and alkaline earth metallic species (AAEM species, mainly Na, K, Mg and Ca) and chlorine.[77]

2.4.1 Ash Deposition in the Boiler Furnace and Convective Tube Banks

Ash deposition on furnace walls leads to **slagging** when a liquid layer is developed (generally on heat transfer surface and refractory linings in the furnace primarily subjected to radiant heat transfer) and **fouling** when a dry, powdery deposit is formed (mainly in the heat recovery section of the steam generator).[60] Ash sintering is the first step of ash deposition, slagging and fouling. Ash deposition is formed by various processes including inertial impaction (and particle capture), thermophoresis, condensation and heterogeneous reaction.[78] The growth of ash deposition leads to

decline boiler efficiency and sometimes unscheduled shutdown of the facilities.[79]

During coal combustion, the inorganic species of coal are transformed into products such as vapours, aerosols and residual ash particles, which may transfer to furnace walls and form deposits. Iron and sodium are considered to play significant roles in ash slagging and fouling, respectively.[80] The key factors that affect deposition formation are the alkali content of biomass, fluid dynamics, gas and heat transfer surface temperature, and surface interaction and reaction.[79] Therefore, during biomass combustion, ash deposition may be increased because biomass fuels generally contain high contents of AAEM species.

2.4.2 Fireside Corrosion

Fireside corrosion is corrosion of tubes due to chemical attack occurring on the furnace or fireside of heat exchanging surface in coal- and/or biomass-fired furnace.[81] Species such as Na, K, S, Cl and Fe are considered to play significant roles in fireside corrosion.[81] The extent of corrosion is affected by both coal types and combustion conditions.[81] During biomass combustion, high content of Cl in biomass may cause serious corrosion problems.[73, 82] A known strategy to mitigate the chlorine-based corrosion is co-firing biomass with coal, via the reaction between sulfur from coal and alkali compounds from biomass.[83] However, the effectiveness of this mitigation approach may be limited for two reasons. One is that the effect of coal-derived sulfur on corrosion during co-firing only takes place in oxidizing conditions rather than reducing conditions.[83] The other is that the sulfation reaction may be slowed down at lower temperatures in oxidizing conditions as a result of decreasing kinetic rates of conversion to sulfates.[83]

2.4.3 Fine PM emission

Combustion of coal and/or biomass contributes significantly to PM emission,[29-31] especially fine inorganic sub-micrometer particulates (PM_1).[84-86] PM_1 is known to

escape easily from dust cleaning equipment and have significant adverse impact on both human health and environment.[31, 32] Furthermore, fine PM affects heat transfer in furnace and has been identified to be responsible for initiating deposition formation and consequent corrosion on heat exchanger surfaces.[33-35] Therefore, a thorough understanding of PM formation/emission provides essential knowledge for developing solutions for ash-related issues. Therefore, it is **the scope of this study** to carry out a systematic investigation into the emission of inorganic PM during the combustion of biomass and coal. The scope of this thesis also covers the development of a credible PM sampling method so that the properties of PM collected will not be distorted by the sampling process itself.

2.5 Sampling Methods of Inorganic PM Produced from the Combustion of Coal and/or Biomass

Sampling fine inorganic PM from the combustion systems such as a coal and/or biomass firing power stations is difficult due to the high temperatures and moisture contents, and sometimes high acid gas (SO_3, SO_2, HCl, etc.) concentrations of exhaust gases.[87] In order to investigate the inorganic PM formation and/or emission from the combustion of solid fuels such as coal and biomass, a key issue needs to be addressed is the development of a proper method for PM sampling. This is to ensure that the properties of the PM samples collected will not be distorted by the sampling method itself. As shown in Figure 2-1, a PM sampling system generally consists of PM source, sampling line and system followed by PM measurement equipment. An ideal sampling system or method should minimize the sampling loss in the sampling line, properly control the key sampling parameters such as dilution ratio and sampling temperature, in order to obtain representative PM sample from the PM source such as the flue gas channel of a coal-fired power plant and a laboratory-scale experimental rig.

2.5.1 Considerations on Designing PM Sampling Line

One of the most important factors in designing a PM sampling line is to minimize the transport losses of PM through the test rig's ducting and sample lines. If particle losses are high, it will be difficult to achieve a sufficient concentration of large particles for an accurate test, and the differences in the upstream and downstream measurements will be dominated by the particle losses in test duct and sample line, rather than by collection of measurement equipments, therefore fail to obtain representative data from the PM source.

Particle losses associated with the sample lines include inlet losses due to non-isokinetic sampling, losses to the walls of the sample lines due to diffusion, electrostatic charging and gravitational settling, and losses in bends as results of centrifugal force and eddies.[88] Therefore, particle loss at the sample inlet can be minimized by isokinetic sampling. Electrostatic effects are avoided by using conductive and grounded ducting and sample lines such as stainless steel. When possible, tube bends should be avoided, and when needed, a gradual curvature should be considered. Gravitational settling can be reduced by minimizing the effective horizontal length of the sample lines. Additionally, while each sampling system is different, it is often beneficial to have the Reynolds number of the flow be in the high laminar range.[88]

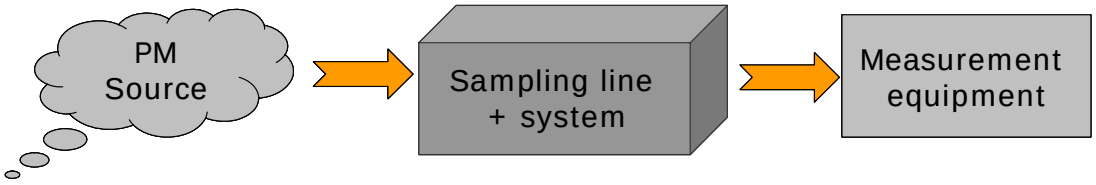

Figure 2-1: A schematic diagram of particulate matter sampling process

2.5.2 PM Sample Dilution

Dilution of PM-containing flue gas is a technique that has been developed to

examine the influence of rapid cooling and dilution on fine particle emission from combustion systems, aiming to simulate the gas-to-particle conversion of semi-volatile or volatile compounds in the flue gas when mixing with ambient air.[89] A specified amount of conditioned air is introduced into the dilution sampler to rapidly mix with the hot flue gas, the dilution allows for processes such as nucleation, condensation, and coagulation to occur.[87] The other important purpose of flue gas dilution is reducing the particle population and the flue gas temperature to prevent overloading and overheating of advanced aerosol measurement instruments such as electrical mobility analyzer (EMA), differential mobility analyzer (DMA) and/or scanning mobility particle sizer (SMPS).[90-93] Various of dilution sampler systems[86, 94, 95] were developed and used to investigate the effects of dilution ratio on the particle size distribution and chemical composition of PM collected from the combustion of coal and/or biomass. Generally, it is concluded that dilution does not influence the particle mass emission rate, but may have significant effect on the size distribution and the total number of particles emitted.[87]

2.5.3 Importance of Sampling Temperature and its Discrepancies among Various Previous Studies

Sampling temperature is speculated to be another key parameter during PM sampling due to the fact that the flue gas from coal and/or biomass combustion generally has a high acid gas (SO_3, SO_2, HCl, etc.) concentration and consequently has a high acid dew point temperature. The condensed acid droplets may significantly change the properties of PM collected. A review on the sampling methods used in some previous studies[26, 86, 96-109] shows that the previous studies used significantly different sampling conditions, particularly various sampling temperatures were also used in those studies, ranging from room temperature to 150 °C. As shown in Table 2-1, such information was not given in some of the studies. Obviously, so far there is no standard method for PM sampling. Although limited attempts were made to study the effects of sampling methods (particularly dilution ratio) on PM properties, there is

significant discrepancy in conclusions drawn in various previous studies.[94, 100] Therefore, the validity is also questionable in comparing the experimental data obtained in different studies.

2.6 Ash Formation during Pulverized Biomass Combustion

Ash is produced from the inherent inorganic species during solid fuels (coal and/or biomass) combustion. The transformation of inorganic species during combustion depends on not only the properties (e.g. concentrations, occurrence, forms, etc) of these inorganic species in the parent fuels,[110, 111] but also combustion conditions.[102] The combustion of a solid fuel particle is generally considered to be in three steps: devolatilization to char and volatiles, volatiles combustion and char combustion.[112] As fuel is injected into the furnace, the first step took place is devolatilization (i.e. pyrolysis). Therefore, the knowledge of the transformations of the inorganic species during devolatilization and subsequent combustion stage are critical to understand ash formation mechanism during biomass combustion. Therefore, the structure of this section is organized as follows. It starts with a brief introduction of inorganic species in mallee biomass, followed by the review on the occurrence of main inorganic elements in biomass. Efforts were then taken to summarize the literature on the transformation and release of key inorganic species during pyrolysis and combustion of biomass, gas phase reactions among the released inorganic species and their important implications. The section concludes with the summarization of ash formation mechanisms.

Table 2-1: Summary of PM sampling methods from the combustion of solid fuels (biomass and/or coal)

Reference	Study type	Fuel	Combustion System	Sampling System	Sampling Temperature	Dilution
Kauppinen et al (1990)[96]	Field study	Bituminous coal	A pulverized coal boiler	BLPI[a]	112-123 °C	NA[h]
Valmari et al (1999)[97]	Field study	Forest residue + Willow	A circulating fluidized-bed boiler	Cyclone + BLPI[a]	110-120 °C	Dilution ratio-80:1
Seames (2003)[26]	Lab-scale	Bituminous + subbituminous coal	A downflow laboratory combustor	Cyclone + BLPI[a]	NA[h]	Dilution applied.
Strand et al (2004)[86]	Field study	Forest residue + peat	A circulating fluidized bed boiler	SMPS[b] + ELPI[c] + DLPI[d]	25 °C	Dilution ratio- 60:1
Johansson et al (2004)[98]	Field study	Wood pellets + Bark pellets + Wood briquettes + Wood logs	Residential boilers	Cyclone + ELPI[c] + DLPI[d]	Room temperature	2 stages dilution
Boman et al (2005)[100]	Field-study	Softwood pellets	A residential pellet stove	Cyclone + DLPI[d]	45 - 75 °C	Dilution ratio-from 3:1~7:1
Jimenez and Ballester (2005)[101]	Lab-scale	Orujillo + Coal + Coke	A down-fired entrained flow reactor	Cyclone + BLPI[a]	~130 °C	NA[h]
Buhre et al (2005)[99]	Lab-scale	Bituminous coal	A drop-tube furnace	Cyclone + CI[f]	Room temperature	NA[h]
Takuwa et al (2006)[103]	Lab-scale	Coal	A drop tube furnace	LPI[e]	NA[h]	Dilution ratio: 10

Liu et al (2006)[102]	Lab-scale	Bituminous coal	A drop-tube furnace	Cyclone + DLPI[d]	NA[h]	NA[h]
Linak et al (2007)[104]	Lab-scale	Pulverized coal	A down-fired lab-scale combustor + A drop tube furnace.	Cyclone + BLPI[a] or MOUDI[g]	80 °C	Dilution applied, without dilution ratio mentioned.
Zhang et al (2008)[105]	Field-study	Sewage sludge	A incineration plant	LPI[e]	Room temperature	dilution ratio- 20:3 (air as dilution gas
Bäfver et al (2009)[106]	Field study	Oat grain	A Combifire boiler	Cyclone + DLPI[d] + ELPI[c]	105 °C	NA[h]
Wiinikka et al (2009)[107]	Lab-scale	Straw pellets	A fixed bed reactor with a pellets burner	Cyclone + DLPI[d]	>150 °C	NA[h]
Ninomiya et al (2009)[108] and (2010)[109]	Lab-scale	Bituminous coals	A drop-tube furnace	Cyclone + LPI[e]	NA[h]	Dilution ratio: ~6, using N_2 as dilution gas

[a] BLPI: Berner-type Low Pressure Impactor; [b] SMPS: Scanning Mobility Particle Sizer; [c] ELPI: Electrical Low Pressure Impactor; [d] DLPI: Dekati Low Pressure Impactor; [e] LPI: Low Pressure Impactor, [f] CI: Cascade Impactor, [g] MOUDI: Micro-Orifice Uniform Deposition Impactor; [h] NA: relevant information Not Available in the publications.

2.6.1 Contents of Inorganic Species in Mallee Biomass

Table 2-2 presents the contents of total ash and inorganic species in the major components (wood, leaf and bark) of a typical mallee biomass. The ash contents of different mallee biomass components are in the order of bark > leaf > wood. The AAEM species are dominant inorganic elements in all components, with Ca being the most abundant, while the contents of Si, Al and Fe are very low. The biomass samples also contain various amounts of P, S, and Cl, which are important nutrient elements in biomass. Therefore, the discussion in Section 2.6.2 will focus on K, Na, Cl, S, Mg, Ca, and P.

Table 2-2: Inorganic species contents in typical mallee biomass[113]

Elements	Components of Mallee biomass		
(wt%)	wood	leaf	bark
Na[a]	0.0212	0.5537	0.2094
K[a]	0.0744	0.3797	0.1105
Mg[a]	0.0364	0.1447	0.0796
Ca[a]	0.1236	0.7652	2.6591
Si[a]	0.0026	0.055	0.0099
Al[a]	0.0025	0.0192	0.0028
Fe[a]	0.0001	0.0142	0.0019
P[a]	0.0182	0.1075	0.0235
S[b]	0.0183	0.1181	0.0509
Cl[b]	0.0323	0.1839	0.2601
Ash content (wt% db)	0.4	3.8	5.5

[a] wt% dry basis; [b] wt% dry-ash-free basis

2.6.2 Occurrence of Inorganic Species in Biomass

Inorganic species in solid fuels (e.g. coal and biomass) can be present in four possible forms (see Figure 2-2): (1) salts present in fuel moisture and pores (these species are easily leachable), (2) inorganic elements associated with the organic structures of biomass, (3) mineral particles included in solid matrix, i.e. included minerals , and (4) free inorganic particles that are free from contact with fuel particles, i.e. excluded minerals (for biomass fuels, these may be inorganic impurities carried into biomass fuels during fuel processing).[114] According to the requirement of most plants growth, the inorganic species present in plants can be grouped into three categories:[115] (1) macronutrients which have a high growth requirement (e.g. Ca, K, S, Mg, and P), (2) micronutrients which have a lower growth requirement (e.g. Cl) and (3) beneficial elements which are stimulate growth but are not essential (e.g. Na). The functions and associations of K, Na, Cl, S, Mg, Ca, and P are discussed below, as these species are the most important elements for ash formation.

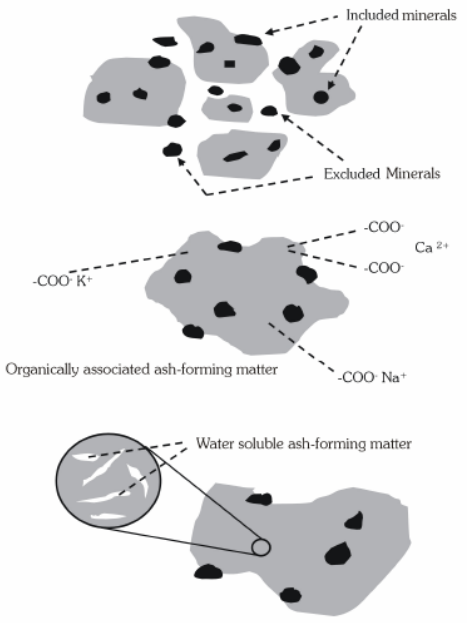

Figure 2-2: Schematic diagram of the different forms of inorganic species in biomass[114]

- ***Potassium (K)***

Potassium is an important inorganic nutrient for plants. The uptake and occurrence of potassium in plants is in the form of a monovalent ion (K^+) that is highly mobile with little structural function.[34] The uptake of potassium is highly selective and correlates with plant metabolic activity.[34] Because of its high mobility and its metabolic function, potassium is often found in regions where plant growth is most vigorous. Tree branches and leaves are generally enriched with potassium compared to stem wood due to its high mobility.[115, 116] During drying of woody biomass, the K originally present as free K^+ ions in the fluids is likely to precipitate in the form of salts, such as KCl, K_2SO_4, KOH, and K_2CO_3.[117] Some of the K in woody biomass may also be organically bound, i.e., ion-exchanged to the oxygen-containing functionalities of the organic structures such as carboxylic groups.[117]

- ***Sodium (Na)***

Sodium is not considered to be an essential element for plants. When its concentration is low (<2%), it may be beneficial to some plants, substituting for potassium in certain functions.[34] At higher concentrations, sodium is generally considered to be toxic.[116] The sodium in woody biomass may exist as salts and/or organically bound structures such as carboxylates.[114]

- ***Chlorine (Cl)***

Chlorine is taken up by plants as the monovalent ion chloride (Cl^-) and served the role of balancing charge.[34] Its concentration is closely related to the nutrient composition of the soils. The levels of chlorine required for optimal plant growth are generally far less than the levels made available by nutrients.[117] Therefore, the differences in chlorine level are usually indicative of soil conditions rather than plant physiology.[34, 115] In plants, chlorine occurs mainly as a free anion or is loosely bound to exchange sites. Chlorine-containing organic compounds such as quaternary

ammonium chloride ($R\text{-}NH_3^+$, Cl^-)[118] may also present in plants, but the function of these compounds is not clear.

- ***Sulfur (S)***

Sulfur is a macronutrient for plants. The most important source of sulfur in plants is sulfate (SO_4^{2-}), which is taken up by the roots.[34] Sulfur may also incorporate into plants via absorption and assimilation of atmospheric SO_2 by aerial parts of the plants.[34] Therefore, the two principle forms of sulfur in plants are sulfates and organic sulfur. The former increases with increasing sulfate in the nutrient supply. The latter is far less sensitive to sulfate supply in most plants.[116] In summary, S can be present in plants as both inorganic S and organically associated S.

- ***Magnesium (Mg) and Calcium (Ca)***

Alkaline earth cations (Mg^{2+} and Ca^{2+}) are macronutrients as common constituents of cell wall and other organic component of cell structure.[34] Particularly for calcium, it occurs almost exclusively in the axoplasm and forms ion-exchangeable bonds with the cell walls and has significant function in cell wall stiffening and the structural integrity of plants.[34] It helps regulate plant growth.[116] Via the advanced analysis, calcium is largely found as ion-exchangeable and acid soluble material. Calcium may also be present as crystallized calcium oxalate ($Ca(COO^-)_2$) in plants.[119]

- ***Phosphorus (P)***

Phosphorus exists in its most oxidized form in biomass fuels and is not reduced during plant metabolism.[34] It is primarily introduced in the form of dihydrogen phosphate ions (H_2PO_4) and either remains in the inorganic form or is incorporated in organic structures by forming esters or pyrophosphates.[120]

2.6.3 Transformation and Release of Inorganic Species during Pulverized Biomass Pyrolysis and Combustion

The typical conditions[121] of a PF fired boiler are of high temperature (1400 – 1650 ^{o}C) and high heating rate (~10^5 K/s). Therefore, laboratory-scale high-temperature drop-tube furnace (DTF) and/or entrained flow reactor (EFR) are commonly used to achieve well-controlled PF combustion conditions. However, there are fundamental challenges in quantification of the release of inorganic species during solid fuels combustion at such high-temperature conditions. As part of the ash-forming species will inevitably react with furnace walls etc, it is hard to obtain mass balance of individual inorganic elements for the whole combustion system. Therefore, it is not surprising that there are scarce studies[121, 122] on the release behavior of inorganic species in biomass during PF combustion at high temperatures, with two essential assumptions. One is that the PM_1 is solely contributed by released elements; the other is that the release of refractory elements (such as Si, Al and Fe) is limited. Such assumptions enable the authors to quantify the release rates of certain elements such as S, Cl, Na, K, Mg and Ca. However, both assumptions may cause considerable errors in quantifying the elements release due to the complexities of both PM_1 formation and the behavior of refractory elements (Si, Al and Fe) during combustion process. Therefore, it is clear that innovative experimental techniques need to be developed in order to provide accurate release data of inorganic species in biomass during biomass combustion for further simulation modeling works.

On the other hand, some investigations[117, 123-125] on the release behaviors of inorganic species (mainly AAEM species, Cl, and S) during biomass combustion were carried out using a fixed-bed reactor or fluidized-bed reactor, to simulate the grate firing systems and fluidized-bed combustion systems, respectively. The combustion conditions such as temperature, particle heating rate, and residence time of grate firing (and fluidized-bed combustion) system are quite different from those of PF combustion. However, from fundamental point of view, the findings from these

combustion systems provide fundamental knowledge that can be useful in assisting to understand the behavior of these species in PF combustion systems.

As devolitalization (i.e, pyrolysis, including drying process) is the first step of pulverized biomass combustion, previous studies[126-129] also investigated the release of Na, K and Cl into gas phase during biomass pyrolysis. Such releases of alkali and Cl are expected to play significant roles in the gas phase reaction and consequent fine PM formation during biomass combustion. Therefore, it is also important to have a thorough understanding on the transformation and release behavior of Cl, S, alkali metals (K and Na), and alkaline earth metals (Mg and Ca) during biomass pyrolysis.

Therefore, the following subsections provide an overview on the main findings from the aforementioned investigations on the release of inorganic species during biomass pyrolysis and combustion under fixed-bed and/or fluidized-bed conditions.

2.6.3.1 Transformation and Release of Cl

Based on the findings in previous studies,[117, 125, 130] the transformation and release mechanisms of Cl during biomass pyrolysis are summarized and schematically illustrated in Figure 2-3, with detailed discussion as follows.

- ***Transformation and release of Cl via primary reactions during pyrolysis***

As discussed in Section 2.6.2, the occurrence of Cl in biomass can be in organically bound forms or inorganic forms such as metal chlorides. A recent study on removal and recycling of inherent inorganic nutrient species in mallee biomass and derived biochars by water leaching[113] indicated that almost all the Cl are in form of chlorides. Similar observations were also noted in annual biomass such as straw.[127] Therefore, for mallee biomass that is of interest in this study, the transformation and release of inorganic Cl seems to be more relevant than that of organic Cl.

It was proposed that upon thermal processing, organic Cl generally releases as HCl

via the decomposition of organic Cl-containing structure.[125] With respect to the inorganic Cl, considerable amount (10 – 60%) of Cl is reported to be released at temperatures as low as 200 – 400 ^{o}C during the pyrolysis of either biomass[131] or brown coal.[130] Zintl et al.[132] proposed a release mechanism where carboxylic groups or other proton-donating sites interact with alkali chlorides at low temperature (< 500^{o}C) in the solid phase to produce HCl that was subsequently released to gas phase, e.g., by the following reaction:

$$Char\text{-}COOH + ACl(s) \rightarrow Char\text{-}COOA + HCl(g) \quad (1)$$

where *Char* represents the char matrix and *A* represents alkali metals (potassium or sodium). Furthermore, van Lith et al.[117] found that such Cl release mechanism at low temperatures (< 500^{o}C) is more important for the biomass with a lower Cl content in the set of woody biomass samples such as spruce, beech, fiber board and bark investigated (Cl content ≤ 0.05% db). Such a difference was hypothesized to be due to the possible differences in the availability of proton-donating sites for reactions with metal chlorides among different biomass samples.

- ***Secondary reactions involved in the release of Cl during pyrolysis***

After the primary release of Cl (mainly as HCl, as discussed above) at low temperature during biomass pyrolysis, two possible secondary reactions between volatiles (including the released Cl) and char (including AAEM species in char) were proposed. **One** is that the Cl-containing volatiles may interact with nascent char at higher temperature (600 – 800 ^{o}C for the pyrolysis of Victorian brown coal) with a fast heating rate (10^3 – 10^4 K s^{-1}), leading to a significant retention of Cl in char.[130] An important feature of a fluidized-bed/fixed-bed reactor system used in the study[130] is the realization of continuous contact between volatiles and char. During pyrolysis at a higher temperature and fast heating rate, Cl-containing species in volatiles (e.g. HCl) might have combined with the reactive sites generated inside the char. The exact nature of the bonds between Cl and the char matrix remains unclear, such

bonds seem to be not very strong, because the volatilization of Cl increases to more than 50% with further increasing temperature to 900°C.[130] Furthermore, an almost complete volatilization of Na at 900 °C[130] confirms the existence of char-bound Cl, rather than NaCl.[130] The retention of Cl in char increased from ~1% to ~80% with the increase of temperature from 500 to 900°C during biomass pyrolysis,[128] indicating the interactions between Cl-containing volatiles and char being strongly temperature dependent.

The other possible secondary reaction[117] is between the HCl (g) produced at low temperature pyrolysis and the metal species (e.g., potassium carbonates and char-bond potassium) in the char. The released HCl (g) from the lower part of the fuel bed can diffuse through the char layer on top in a fixed-bed reactor (heating rate: ~30 – 170 K min^{-1}), leading to interactions between HCl (g) and alkali metals in char.[125] Such interactions are hypothesized to be responsible for the observed reduction in Cl release below 700°C, above which the evaporation of metal chlorides formed by this secondary reaction is considered to dominate Cl release.[125]

- ***Transformation and release of Cl during char combustion***

During char combustion, both char-bond Cl and metal chlorides (s) are likely to be released as metal chlorides (g) via a series of reaction and/or evaporation at high temperature (~1150 °C).[125]

Overall, the transformation and release of Cl during biomass pyrolysis may depend on many factors such as biomass properties, heating rate and reaction temperatures. However, almost all the Cl in biomass are likely to end up as HCl (g) and/or metal chlorides (g) in gas phase during subsequent char combustion phase.

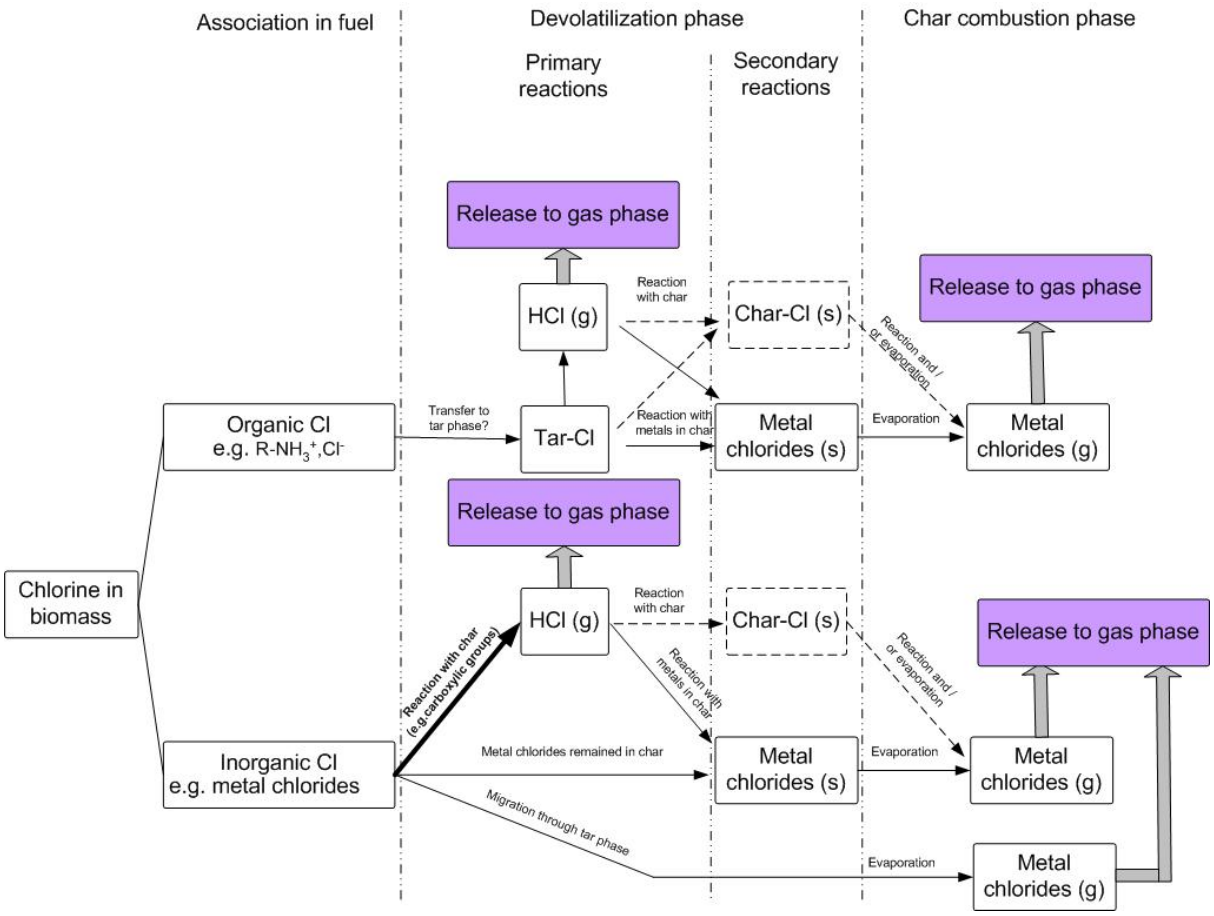

Figure 2-3: Possible reaction pathways and release mechanisms of Cl during biomass pyrolysis and subsequent combustion, summarized based on the findings in refs[117, 125, 130]

2.6.3.2 Transformation and Release of S

Understanding the transformation and release of S is important to control the emission of both SO_2 and fine PM during biomass combustion.[124] A number of investigations were carried out to reveal the mechanisms of S transformation during biomass combustion in fixed-bed reactors and fluidized-bed reactor systems.[117, 118, 123-125, 127, 133, 134] Possible reaction pathways and release mechanisms of S during pyrolysis and combustion of biomass are summarized as follows.

- ***Transformation and release of S during pyrolysis***

As discussed in section 2.6.2, S can be present in biomass as both inorganic S and organically-bound S. The release behavior of S during biomass pyrolysis highly depends on the mode of S occurrence in the fuel. Under fixed-bed conditions, a significant amount of S can be released as SO_2[117, 135] at low temperature (500 °C) due to the decomposition of organic S compounds that are thermally unstable, rather than the decomposition of inorganic sulfates during the pyrolysis stage. This is coincidence with the good correlation between the quantity of S released at 500 °C and the amount of organic S in the fuel,[117] further supporting this proposed S release mechanism at low temperatures.[117, 123, 127, 135] Additionally, there are also possible secondary reactions between released SO_2 (g) and char or inorganic species in the char (resulting in inorganic sulfates). This was the mechanism proposed to explain the effects of bed size on S release during biomass pyrolysis at low temperatures (500 – 850 °C) in a fixed-bed reactor.[125] It was also confirmed that the SO_2 (g) released from the lower parts of the bed was mainly captured in the upper char layer via reactions with organic char matrix rather than inorganic species in the char.[133]

- ***Transformation and release of S during char combustion***

During char combustion at a slow heating rate (~30 – 170 K min^{-1}) under fixed-bed

conditions, the char-bound S is most likely transformed into sulfates which are stable at a temperature below 900 °C,[125] leading to a very little additional S was released in the temperature range of 500 − 850 °C. However, a steep increase in the release of S with temperature above 850 °C and a complete release at 1150 °C was observed by van Lith.[125] At a temperature higher than 850 °C, the sulfur release is thought to be mainly due to the decomposition and/or evaporation of alkali metal sulfates.[117, 123]

However, the release of a portion of S preferential to K above 1000°C [123] suggests that there are other mechanisms responsible for the release of S during biomass combustion at high temperature (above 1000°C). van Lith et al.[125] proposed that the reactions between sulfates of AAEM species and silicates (and/or aluminosilicates) may also be an important mechanism for S release as SO_2 (g).

The inorganic S (e.g. metal sulfates) originally presented in biomass may remain stable in pyrolysis stage.[125] However, during char combustion, it can be released as SO_2 and/or metal sulfates vapor as results of decomposition of metal sulfates, reactions between AAEM sulfates and silicates (and/or alumino-silicates), and/or the evaporation of alkali sulfates.[125]

Overall, many factors can influence the transformation and release of S during biomass pyrolysis and combustion, including mode of S occurrence in biomass, temperature, ash composition (particularly Na, K, Mg, Ca, Si and Al etc.). S is likely to be either released as SO_2 and/or alkali sulfates vapors, or retained in the ash as sulfates of refractory metals (e.g. Mg and Ca) after the char burnout.

2.6.3.3 Transformation and Release of Alkali Metals (K and Na)

Figure 2-4 summarizes the transformation and release mechanisms of K and Na during biomass pyrolysis and subsequent combustion, based on the findings in previous studies.[117, 125, 128, 130, 136] The detailed discussion is given below.

- ***Transformation and release of K and Na via primary reactions during pyrolysis***

As discussed in Section 2.6.2, alkali metals in biomass are mainly present as salts (chlorides and sulfates), organically bound structures (e.g. carboxylates[128]), free ions and/or aluminosilicates (such as microcrystalline quartz-like backbone in straw). It is known that the mode of occurrence of alkalis is important for their transformation and release during pyrolysis.[118]

A number of previous studies[123, 126, 128] reported that considerable amounts of alkali metals can be released at temperatures as low as 500 °C or below during biomass pyrolysis. It is suggested that the thermal decomposition of carboxylates in the biomass from large molecular mass structures and the subsequent release of light alkali-containing carboxylates (–COOK or –COONa) is an important mechanism for the release of alkali metals during biomass pyrolysis at low temperature.[128, 129] Even of relatively low vapor pressure, carboxylates of K and Na may also be released from biomass particles due to the entrainment with the volatiles.[128] The larger molecular carboxylates that are not able to be released may retain in char matrix and form char-bond alkalis.[128] Further increasing pyrolysis temperature to 900^{o}C at slow heating rate (fixed-bed condition) leads to little additional release of Na and K, indicating the bonds between char matrix and alkalis are relatively temperature-stable.[128]

Another proposed mechanism for K release during biomass pyrolysis at low temperatures (400 – 600 ^{o}C) is that the organically bond K (e.g. carboxylates) may start to decompose at below 400 °C and release atomic K, followed by the released K being bound to phenol groups in the char at <600 °C.[117] The phenol groups may at the same time also start to degrade above 400 °C, leading to the release of K to the gas phase, probably as K(g). However, this mechanism can not explain the release of K at 180^{o}C as observed by Olsson et al.[126] Furthermore, it was found that the

carboxylates such as acetate and formate were still found in the product gas from the pyrolysis at 900°C.[128] This suggests that some of the structures such as –COOK and –COONa can survive and be carried away by volatiles during pyrolysis, instead of their complete decomposition to produce CO_2.[128] This further supports that the release of alkali-containing light carboxylates seems to be more likely the mechanism for the release of K and Na below 500°C during pyrolysis.

For alkali chlorides (KCl or NaCl), during pyrolysis, some of alkalis must be bound with char matrix to form char-bond alkalis, accompanied by the release of Cl (see Section 2.6.3.1) at low temperature (< 500°C). This suggests that reactions between chlorides and char (e.g. carboxylic groups) must have taken place. The char-bond alkalis may further experience secondary reactions and then be either released or retained in char, depending on the char temperature time history. The remained alkali chlorides in char may evaporate as alkali chlorides (g) at high temperatures, or released as chlorides (g) during char combustion, which will be discussed later.

- ***Secondary reactions involved in the release of K and Na during pyrolysis***

Secondary reactions involved in the release of alkali metals (K and Na) may include the reactions between volatiles (including the released alkali metals in volatiles) and char during biomass pyrolysis at high temperatures (>500 °C).[117, 128]

Firstly, during biomass pyrolysis at a slow heating rate (fixed-bed conditions), the released K or Na species could experience repeated desorption and adsorption from/onto char particles within the fixed-bed, as hypothesized by Knudsen et al.[123] and experimentally demonstrated by Hayashi et al.[137, 138] The repeated desorption and adsorption of K and Na allowed these species be chemically transformed into thermally stable char-bond forms and/or non-volatile species such as silicates.[137, 138] van Lith et al.[125] also attributed this phenomenon to the intercalation of K into the char matrix.

Secondly, it was observed that at temperatures > 500°C, substantial release of alkali metals was observed during pyrolysis in a fluidized-bed reactor at a fast heating rate, while such an observation is absent during pyrolysis at slow a heating rate.[128, 129] Such a phenomenon is explained well by "volatiles-char interactions", which was firstly developed by Wu et al.[139] Briefly, under fast heating rate condition, it is expected that the volatiles contain significant amounts of reactive species (hypothesized as free radicals, especially H radicals) produced from thermal cracking. Such reactive species can interact with char and take part in substitution reactions allowing the release of alkali species, represented symbolically as below:

$$R + CM\text{-}X \rightarrow CM\text{-}R + X \qquad (2)$$

where *CM* denotes the char matrix, *X* represents the alkali species and *R* represents reactive species (hypothesized as free radicals, including H radicals) in the volatiles. This observation is of great importance to fluidized-bed pyrolyser or gasifier, which has an important feature of continuous contact between volatiles and char.

- ***Transformation and release of K and Na during char combustion***

During char combustion, both char-bound K (or Na) and intercalated K (or Na) are suggested be oxidized to carbonates, followed by the decomposition and/or reaction via K_2O (or Na_2O) and finally released to gas phase as K(g) or Na(g).[117] After vaporization, K(g) or Na(g) may react with other species present in the gas phase. For example, when water is present in the gas phase, K(g) or Na(g) will convert to KOH(g) or NaOH(g), in the presence of HCl, the conversion of alkalis (g) to alkali chlorides (g) is more favored.[117] For the alkali sulfates, which can be originally present in biomass and/or products of alkali metals sulfation reaction, may release to gas phase in forms of alkali sulfates (g).[125, 136] It is also possible that K or Na may interact with silicates in the ash, resulting in a possible reduction in the release of K or Na via the formation of refractory K-silicates or Na-silicates. Beside the availability of Si, Mg and Ca may also influence K release as Mg and Ca would

compete for positions in the silicate matrix with K or Na.[136]

- ***Roles of Cl in the release of K and Na during pyrolysis and combustion***

There are debates on whether Cl can enhance the release of K and Na during biomass pyrolysis and/or subsequent combustion. Some researchers[126, 140, 141 136] suggested Cl is the main facilitator for the release of K or Na during pyrolysis and subsequent combustion. However, others[128, 130] argued that so far there is insufficient evidence to prove the facilitating roles of Cl in enhancing the release of K and Na during pyrolysis of both biomass and brown coal. Based on the analysis in Sections 2.3.6.1 and 2.3.6.3, the roles of Cl in the release of K and/or Na during pyrolysis and subsequent are discussed separately as follows.

Some researchers[126, 140, 141] suggested that Cl may be able to facilitate the release of alkali metals due to the relatively low melting point temperatures of KCl (770 ^{o}C) and NaCl (801 ^{o}C). However, this seems not to be credible because of the release of K and Na at lower temperature (<500 ^{o}C), which are due to thermal decomposition of K- and Na-containing organic structures such as carboxylates.[114] Furthermore, at a slow heating rate under fixed-bed conditions, the majority of Cl (even exist as chlorides) is found to be released presumably as HCl, which is most likely formed from ion-exchange reactions of functional groups in the organic matrix of biomass at lower temperature (<500 ^{o}C).[132] This suggests that the alkali metals (K and Na), which are initially presented as chlorides in biomass, must bound to char matrix to form char-bound alkalis. Additionally, during pyrolysis at a fast heating rate particularly under fluidized bed conditions, substantial Cl can be recombined with char matrix to form char-bound Cl rather than chlorides.[130] All of these evidence suggest that alkali metals and Cl are released separately during pyrolysis and are likely to be bound into char matrix separately after pyrolysis.

Therefore, the roles of Cl in the release of K and Na (if nay) during pyrolysis are likely to be at least influenced by three factors: (1) the occurrence of alkali metals in

biomass; if majority of alkali metals are in forms of organically bound structure, their release behavior particularly at low temperature (<500^{o}C) may not be affected by Cl; (2) the molar ratio of Cl/(K+Na), a higher molar ratio of chlorine to alkali metals means a higher possibility of Cl to facilitate the release of alkali metals (if any), and (3) the thermal stability of the chemical bonds between char and alkali metals. The role of Cl in the release of alkalis during pyrolysis will depend on the net effect of these factors. For example, if the char-bound alkali metals are stable at a temperature higher than the melting points of alkali chlorides (e.g. 770 or 801^{o}C), the presence of alkali chlorides in the fuels are likely to lead to significant release of alkali metals during pyrolysis at a temperature > the melting point temperature of alkali chlorides. In summary, thus far there are no direct experimental evidences to clarify the roles of Cl in the release of alkali metals during biomass pyrolysis.

During char combustion, the presence of Cl in char or the HCl released to gas phase may facilitate the reactions with alkali compounds (e.g. K, KOH, Na and NaOH) in the gas phase.[142] This may potentially lead to the preferential formation of alkali chlorides which are relatively stable in combustion conditions, and consequently enhance the release of alkali metals.

Overall, the transformation and release of alkali metals (K and Na) during biomass pyrolysis may depend on many factors such as biomass properties, heating rate and temperature, and ash composition. However, majority of alkali metals in biomass is likely to be released to gas phase as atomic alkalies, chlorides, sulfates and/or hydroxides during subsequent char combustion stage.

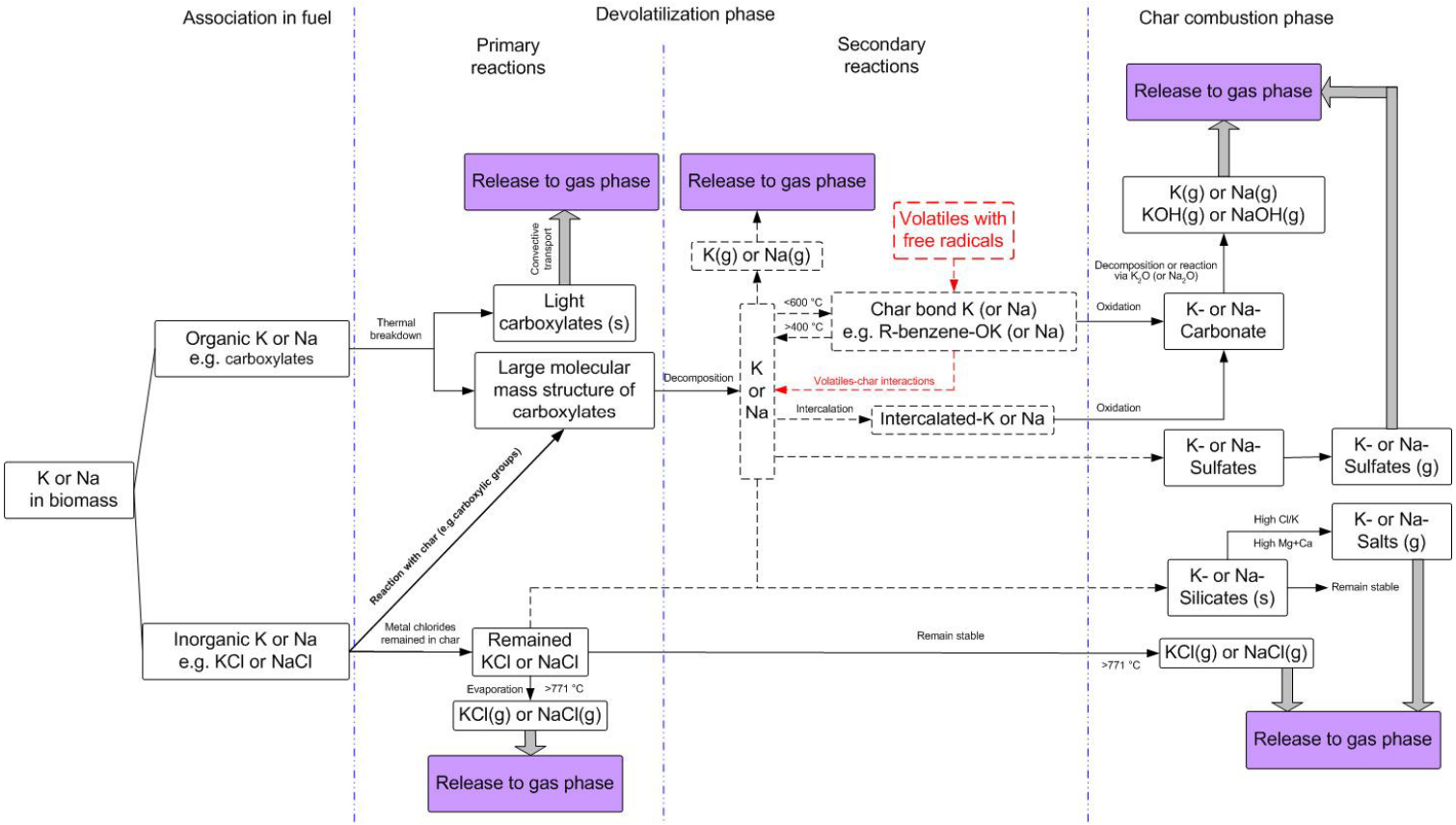

Figure 2-4: Possible reaction pathways and release mechanisms of K and Na during biomass pyrolysis and subsequent combustion, summarized based on the findings in refs[117, 125, 128, 130, 136]

2.6.3.4 Transformation and Release of Alkaline Earth Metals (Mg and Ca)

As discussed in Section 2.6.1, significant amounts of Mg and Ca in biomass may be molecularly dispersed in the fuel and bound to carboxylic groups.[128, 129] During pyrolysis at low temperature (around 500 ^{o}C), similar to alkalis (Na and K), the organically bound Mg and Ca are likely to be released as light carboxylates due to the decomposition of Mg-and Ca-containing organic structure. While at high temperatures above 600 ^{o}C,[128] the breakage of bonds between Mg (and/or Ca) and char matrix seems to be the dominant mechanism for the release of Mg and Ca [143], following the similar mechanisms for the release of Na and K (see Section 2.6.3.3). However, the amounts of released Mg and Ca are generally lower than those of K and Na as observed in the pyrolysis of both sugar cane biomass[128] and Victorian brown coal,[139, 143] probably due to the difference in the nature of valence, i.e., monovalent of K (and Na) and divalent of Mg (and Ca).

During combustion, Mg and Ca are likely to be transformed to oxides and/or carbonates.[144] It is also possible that Mg and Ca can preferentially react with aluminosilicates (if any) in comparison to Na and K.[145, 146] Therefore, higher levels of Mg and Ca in the fuel may cause more alkali metals to remain in gas phase as alkali chlorides, sulfates, oxides and/or hydroxides even at 800– 1150 ^{o}C.[117]

2.6.4 Important Gas Phase and Gas-Solid Phase Reactions and Their Implications on Mitigating Ash-Related Problems

Most biomass fuels generally have higher contents of alkali metals and chlorine than other solid fuels such as coal.[120, 147] As discussed in Section 2.6.3, substantial amounts of these elements can be released to gas phase mainly as alkali chlorides and/or hydroxides during combustion.

Once in the gas phase, these species may react with HCl, SO_3, and CO_2 to form

chlorides, sulfates, and carbonates via a series of **gas phase reactions**. These species are also mainly responsible for the formation of fine particles which either deposit in the furnace or transport into the flue gas.

In addition, gas phase alkali species may also react with silicates and/or aluminosilicates existed in coarse fly ash particles via **gas-solid reactions**, leading to the retention of alkali metals in bottom ash and/or in coarse fly ash fraction. Among these alkali species, alkali chlorides (particularly KCl) are notorious for leading to numerous ash-related problems[148-151] such as slagging, fouling, corrosion, deactivation of de-NO_X catalysts, and serious harm to human health and environment.

Therefore, the roles of Cl in alkali-containing fine particulate matter formation, sulfation reaction of alkali chlorides and the reactions between alkali metals and aluminosilicates were extensively investigated in the past years. The main objectives were to elucidate the formation mechanisms of alkali chlorides and mitigate their adverse impacts on combustion system, human health and environment. Such important gas phase and gas-solid phase reactions and their implications on mitigating the ash-related problems are discussed below.

2.6.4.1 Effects of Cl on Fine PM Formation during Biomass Combustion

A number of investigations were performed on fine particles formation during biomass combustion using both fluidized-bed reactor and entrained flow reactor. The fine particles are mainly composed of alkali chlorides and sulfates, indicating that both Cl and S play important roles in fine particle formation.[152-154] By introducing additional HCl gas into combustion, previous studies demonstrated that the addition of HCl clearly increases number concentration and mass concentration of fine particles with a size less than 1μm (PM_1). This may be due to the increased release of ash-forming elements (mainly Na and K) into fine particles and consequently the deceased amounts of these elements reacted with silicates and/or aluminosilicates (if

any). These experimental data suggest that Cl increases the amounts of alkali metals transformed into PM_1 via possibly forming alkali chlorides, which are known to be relatively stable under combustion conditions.[142]

2.6.4.2 Sulfation of Alkali Chlorides to Alkali Sulfates

The sulfation of alkali chlorides to less troublesome alkali sulfates is an attractive way to minimize the chlorine-associated corrosion problems.[155] According to Lind et al.[156] and Sippular et al.[157], when a sufficient amount of SO_2 is supplied in a chlorine rich combustion system (S/Cl molar ratio ranges from 4.7 to 7.5), most of the HCl remain in the gaseous phase. The release of ash-forming elements also decreased, so do the fine particle concentrations, as results of possible enhanced retention of alkali metals in the coarse particle fraction during sulfation process.[156]

The sulfation of alkali chlorides to alkali sulfates is assumed to take place via the following global reaction:[157]

$$MCl+SO_2+1/2O_2+H_2O \rightarrow M_2SO_4+2HCl \qquad (3)$$

where M=K or Na. It was also found that the alkali metal sulfation reactions in large-scale combustion conditions take place dominantly in the gas phase. [158, 159]

This finding is of particularly importance in biomass combustion. Because the sulfation reaction raises nucleation/condensation temperatures of alkali metal vapors, the particle formation is most likely initiated by the gas phase sulfation reactions.[160] Additionally, the reactions between alkali chlorides and sulfur are important to the corrosion in biomass-fired boilers, as the corrosive and sticky deposits on heat exchangers are generally created by alkali chloride particles. Via sulfation reactions, chlorine in alkali chlorides is released as HCl, leading to significant reduction in deposit formation and corrosion in power plants operating with chlorine rich fuels.[161] The source of sulfur oxides can be a coal (co-firing)[162], or a sulfur containing

additive such as ammonium sulfate.[163]

2.6.4.3 Reactions between Alkali Chlorides and Aluminosilicates

Apart from the sulfation reactions of corrosive alkali chlorides as discussed in Section 2.6.4.2, gas-solid reactions between alkali chlorides and aluminosilicates, particularly kaolinite ($Al_2Si_2O_5(OH)_4$), were also extensively investigated[164-168] under both fluidized-bed and pulverized fuel combustion conditions. These reactions are known to provide another feasible way to capture inorganic vapors, particularly corrosive alkali chlorides vapors in combustion conditions.[164-168] The overall reactions between kaolinite and alkali chlorides at high temperature have been presented as:[169]

$$Al_2Si_2O_5(OH)_4 + 2MCl \rightarrow 2MAlSiO_4 + H_2O + 2HCl \quad (4)$$

$$Al_2Si_2O_5(OH)_4 + 2MCl + 2\,SiO_2 \rightarrow 2MAlSiO_6 + H_2O + 2HCl \quad (5)$$

where M=K or Na.

The kaolinite may capture alkali chlorides vapors by chemical reaction and/or physical sorption, which seem to be independent of gas oxygen concentration or slightly promoted in a reducing atmosphere.[164] Chemical reaction is the dominant sorption mechanism for alkali chlorides captured by kaolinite when water vapor is present in the system[164] and only physical adsorption takes place in the absence of water vapor.[170] The adsorption efficiency of vaporized salts is dependent on the temperature. It was found that the adsorption efficiency decreases with increasing temperature from 900 to 1300 °C, then increases with further increasing temperature from 1300 to 1500 °C.[164] Kaolinite after reaction with KCl in typical CFB combustion temperatures (800–900 °C) has a similar porosity as the unreacted kaolinite.[164] As the temperature increases above 1300 °C, both reacted and unreacted kaolin become sintered, resulting in decrease in porosity and surface area. At a

temperature higher than 1300 °C, it was also proposed that the capture of potassium is due to the formation of a molten phase.[164]

2.6.5 Ash Formation Mechanisms during Pulverized Biomass Combustion

Ash formation mechanisms during biomass combustion under fluidized-bed[28, 163, 171-176] and fixed-bed[111] conditions were well documented in the past decade, however, little studies have been done on the ash formation mechanisms during biomass combustion under PF combustion conditions.[177, 178] It is reasonable to speculate that the inorganic species in biomass may experience more severe combustion conditions during PF combustion, leading to enhanced release of inorganic species into gas phase in comparison to that of fluidized-bed and/or fixed-bed conditions. Considering the discussion in Sections 2.6.1 to 2.6.4, and the ash formation mechanisms during pulverized coal combustion (will be discussed in Section 2.7) together, the ash formation mechanisms, particularly for PM with a size less than 10μm (PM_{10}), are summarized as follows.

The PM_{10} produced from biomass combustion can be described to consist of two fractions, i.e., PM_1 and PM in a size range of 1-10 μm (PM_{1-10}). It is believed that PM_1 are mainly formed from the constituents (e.g., Na, K, S, Cl and heavy metals) that are easily vaporized, followed by homogeneous nucleation and/or heterogeneous condensation/reaction of these inorganic vapors.[84-86] On the other hand, PM_{1-10} are generally considered to be formed by the refractory elements such as Mg and Ca during char combustion.[28, 84-86]

2.7 Ash Formation during Pulverized Coal Combustion

2.7.1 Mineral Matter in Coal

During coal combustion, ash is produced from mineral matter.[179] The major inorganic elements found in coal are Si, Al, Ca and Fe, while the minor inorganic

elements include K, Mg, Na, Ti and P. Trace inorganic elements with a concentration less than 100 ppm may also present, including Hg, As and Sr etc. The inorganic elements are found in three principle forms:[179]

- Dissolved in the pore water, the most common elements found dissolved in the pore water are sodium and chlorine.

- Combined chemically with the organic materials (either ion exchanged or as metal-organics), alkali and alkaline earth elements such as sodium and calcium, are found replacing protons on oxygenated functional groups of the organic matter. Trace elements may be present as metal-organic substances.

- Discrete mineral particles, inorganic elements occur in coal predominantly in this form.

The mineral matter in coal can be classified into different groups such as silicates, oxyhydroxides, sulphates, carbonates, sulphides, phosphates, chlorides and other mineral species. The main minerals identified with coals are shown in Table 2-3.[179]

The coals from a particular region may contain similar minerals. However, these coals may have different mineral proportions, modes of occurrence and origin. The quantities of these minerals in coal will affect its performance during combustion, depending upon the roles of the abundant minerals. Generally, the approximate quantitative distribution of the mineral classes in coal, in decreasing order of significances is:[180] silicates > carbonates > oxyhydroxides > sulphides > sulphates > phosphates > others. It is also observed that the distribution of minerals in coal are affected by coal ranks,[181] coal particle size[182], and density fractions.[183, 184]

Mineral matter in coal can be categorized into two classes[185] according to carbon-mineral association:

- Included (inherent) mineral matters, which are derived from inorganic species originally exist in peat forming plants. This fraction of minerals is in an intimate association with carbonaceous matrix, so it cannot be removed easily from coal.

- Excluded (extraneous) mineral matters, where the minerals originate from inorganic constituents that have been conveyed to coal forming deposit from surrounding. Since this type of minerals is not included closely in the carbonaceous matrix, it can be removed from coal via beneficiation processes. Excluded mineral particles are characterised by high percentage of minerals.

Generally, the main excluded mineral matters include quartz, kaolinite, illite, pyrite and calcite. The transformation of these minerals during coal combustion is well known.[34, 182, 186-191] The contribution of excluded minerals on particulate matter formation during coal combustion has also been well documented.[182, 192, 193] Therefore, those information can be found in those publications and are not included in this review.

The transformation of included minerals during pulverized coal combustion includes vaporization, condensation and nucleation, coalescence, and char fragmentation. Such processes are complicated due to the included minerals may experience a higher temperature,[34] locally reducing environment within a burning coal particle and coalescence with other included mineral particles within the same coal particle.[34] Therefore, the transformation of included minerals are reviewed and discussed in Section 2.7.2.

2.7.2 Transformation of Included Minerals

The transformation of included minerals involve several mechanisms including coalescence, char fragmentation, shedding of ash particles from burning char surface, and vaporization followed by condensation, nucleation and aggregation. Such mechanisms are mainly responsible for the formation of ash and PM_{10} during coal

combustion, as will be detailed in Section 2.7.3.

This section will mainly discuss the transformation of typical included minerals including quartz, pyrite, clay minerals (kaolinite and illite), and organically bound sodium and calcium.

Table 2- 3: Main minerals identified with coals[179]

Mineral	Formula
Silicates	
Quartz	SiO_2
Kaolinite	$Al_4Si_4O_{10}(OH)_8$
Illite	$KAl_2(AlSi_3O_{10})(OH)_2$
Biotite	$K(Mg, Fe)_3(AlSi_3O_{10})(OH)_2$
Oxyhydroxides	
Hemitite	Fe_2O_3
Magnetite	Fe_3O_4
Rutile	TiO_2
Sulphates	
Gypsum	$CaSO_4 \cdot 2H_2O$
Jarosite	$(Na,K)Fe_3(SO_4)_2(OH)_6$
Melanterite	$FeSO_4 \cdot 7H_2O$
Barite	$BaSO_4$
Carbonates	
Siderite	$FeCO_3$
Calcite	$CaCO_3$
Ankerite	$(Ca, Fe, Mg)CO_3$
Dolomite	$(Ca, Mg)CO_3$
Sulphides	
Pyrite	FeS_2
Marcasite	FeS_2
Chlorides	
Halite	NaCl
Sylvite	KCl
Bischofite	$MgCl_2 \cdot 6H_2O$
Phosphates	
Apatite	$Ca_2(PO_4)_3(F, Cl, OH)$

- ***Quartz transformation***

Although quartz has high melting point of 1723 ^{o}C,[34] release of Si into gaseous phase may take place for included quartz particle because the formation of silicon monoxide (SiO) can be formed in the presence of carbon and other mineral species.[34] Therefore, the extent of Si release and the subsequent fume formation are dependent upon the formation of silicon monoxide when silica or silicates react with carbon and hydrogen.[182] In the presence of carbonates and clays, the volatilization of silicon monoxide has been reported to start at ~1649 °C while in the presence of pyrites or metallic iron, volatilization begins at ~1560 °C and continues rapidly until all the Si is volatilized.[34] The volatilized SiO may be subsequently oxidised and condensed as small SiO_2 fume particles in low-temperature or oxidising zones.[190] It is also important to note that the degree of Si volatilization in pulverized coal boilers is minimal under normal conditions due to the low concentration of CO and H_2 in the flue gas.[182]

Another mechanism involved in quartz transformation is coalescence with other minerals withtin the same burning coal particle. However, there are still arguments on whether finely dispersed included quartz will interact with the molten silicates during coal combustion.[193] As reported by ten Brink et al.[194], the included silica is in contact with each other as the coal is shrinking in the burn-off phase, resulting in the clustering of silica particles due to the adhesion forces among small particles hence the formation of silica cluster after combustion. Nevertheless, according to Baxter,[195] the average diameter of the silica grains decreases by a factor of 5 and there is a proportional increase in the number density as well. Baxter[195] concluded the differences with results observed by ten Brink[196] are mainly the occurrence forms of silica, in addition, it is mentioned that no significant interaction between silica and inorganic species or gas phase is noticed during the combustion process.

- ***Pyrite transformation***

Included pyrite will decompose to form molten pyrrhotite and gaseous sulphur as a result of higher temperature of burning char.[197, 198] As included pyrite within the char experiences a locally reducing environment during char combustion, the oxidation of pyrrhotite will not proceed rapidly until the completion of char combustion.[197] Once exposed to the gas atmosphere, pyrrhotite will either undergo oxidation as in the case for excluded pyrite, or mix with the silicates or alumino-silicates present. When pyrite-derived ash particles contact with silicate/alumino-silicates, there are two possible glass formation ways: one is the contact of pyrrhotite with silicate/aluminosilicates and the other involves the oxidation of pyrrhotite to molten FeO before contacting the silicates/alumino-silicates. Additionally, the original pyrite particles also seem to fragment to form two or three fragments during the thermal decomposition, and the resultant ash particles are likely to be pyrrhotite or iron oxides.[195]

- ***Clay minerals (kaolinite and illite) transformation***

The included clay minerals such as kaolinite and illite will form soft spherical ash particles during combustion.[190] Included clay minerals are expected to melt and coalesce to form bigger particles, while sodium will interact with alumino-silicates to form sodium aluminosilicates when the coal has high acid-extractable sodium levels.[193] As kaolinite and other clay minerals within the coal serve as an absorbent for alkali and alkaline earth metals, they play an important role in ash deposition.[34] Under typical combustion conditions, included illite will melt and release gases (mainly water) to form molten silicate particles without significant change in particle size due to fragmentation or swelling.[199] Include illite might also interact with other minerals to form ash particles of different chemical composition.

- ***Organically bound sodium and calcium transformation***

Under reducing conditions, organically-bound sodium is released as metallic sodium and the rate of release is dependent upon total surface, pore size, pore diffusivity and bulk diffusivity.[34] As for sodium chloride, volatilization begins at about 750 ^{o}C, once released, the dominant sodium-bearing gas is Na(OH), and is free to react with excluded silicates present as well as the char and included silicates to form Na_2SiO_3 and Na_2SiO_5. The sodium, as sodium chloride, reacts far more extensively with kaolinite than with silicates.[182] The role of sodium in ash deposition manifests in several ways, such as a low-melting silicate responsible primarily for very high-temperature slagging and fouling, and an initiator of fouling by forming low melting sodium sulphate just above convection bank superheater or reheater tube temperature.

Organically bound calcium has been reported to form fumes of reactive submicron CaO and calcium silicate cenosphere.[34] Calcium in the form of chloride will volatilize in the boiler flame and convert to sulfate in a manner similar to sulfation of volatilized NaCl.[182] Released calcium fume initiates furnace wall deposits and calcium-sulphate-bounded deposits at low temperature convection bank heat transfer surface.[34] Organically bound calcium reacts quickly with aluminosilicate and quartz within the coal matrix to form lower melting point phases such as $CaSiO_3$.[190] The presence of calcium may perpetuate the growth of partially developed slag as semi-molten anorthite or gehlenite.[34]

2.7.3 PM Formation Mechanisms during Pulverized Coal Combustion

The particle size distribution of PM_{10} produced from coal combustion generally shows a bimodal distribution,[102, 200] i.e., a coarse mode located between 1 and 10μm (PM_{1-10}) and fine mode with a mode diameter less than 1μm (PM_1), indicating their formation and/or emission are governed by different mechanisms. The PM emission mechanisms during pulverized coal combustion have been extensively studied[201-204]

for decades, a recently state of the art review[39] has summarized the PM formation mechanisms and also the properties of PM produced from coal combustion. As shown in Figure 2-5, the major processes governing the PM formation can be generally divided into two categories, i.e., the solid-to-particle process which mainly produces PM_{1-10} and the solid-vapor-solid process that is mainly responsible for PM_1 formation. The detailed formation mechanisms for PM_{1-10} and PM_1 during pulverized coal combustion are briefly discussed as follows.

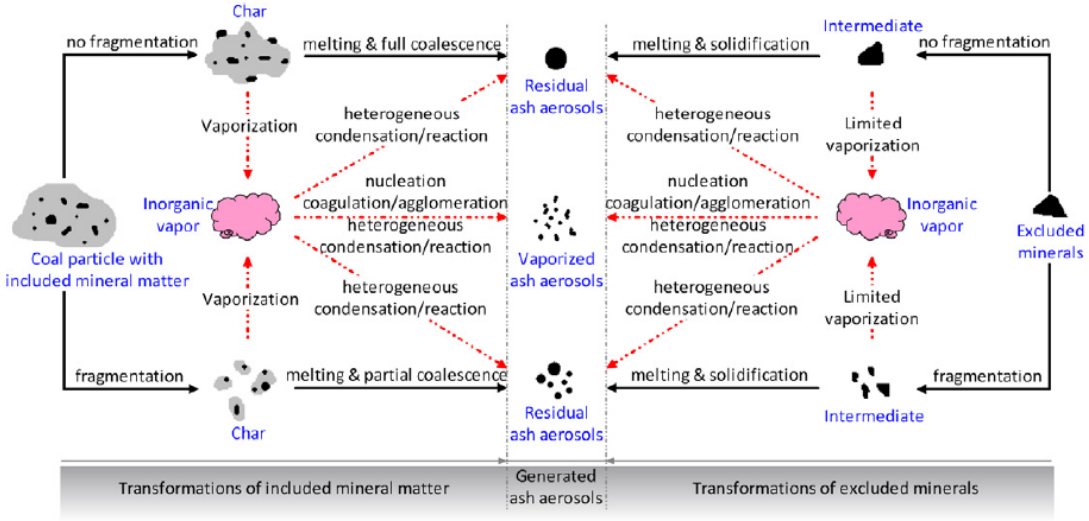

Figure 2-5: Major ash aerosol formation mechanisms during coal combustion, solid arrows indicate solid-to-particle processes while dotted arrows indicate solid–vapor–particle processes[39]

2.7.3.1 Formation Mechanisms for PM_{1-10}

As shown in Figure 2-5, at least three mechanisms, i.e., coalescence of included minerals, char fragmentation and excluded mineral fragmentation, are responsible for the formation and emission of PM_{1-10}.

- ***Coalescence of included minerals***

Coalescence of included minerals takes place when the individual ash particles agglomerate and/or sinter to form larger particles.[205, 206] Basically, only the minerals

in the same coal particle are likely to coalesce because the excluded minerals or the minerals in different coal particles have very few opportunities to contact with each other. Several conditions which are necessary for mineral coalescence were suggested[205], including more than one mineral grain in the same coal particle, temperature is above the melting points of minerals presented in coal, and the possibilities for the molten particles to get in contact with each other.

It is suggested that the coalescence of included minerals occurs on the external surfaces burning char particles mainly during the middle and later stages of burnout.[207] Therefore, both particle temperature and mineral properties such as chemical composition and particle size distribution will affect the extent of mineral coalescence. Under typical pulverised fuel combustion temperature (1600–2000 K)[208], the minerals such as kaolinite and iron oxides in the same fuel particle would melt and coalesce completely to form one large ash particle in case of no fragmentation.[209, 210] Additionally, mineral properties such as chemical composition and particle size distribution are found to be another main controlling factor to the extent of coalescence.[193]

However, char fragmentation will also take place as a competition process to coalescence and diminish mineral coalescence.[211, 212] In this case, the included minerals only underwent partial coalescence, resulting in a number of smaller particles from each fuel particle.[212] Three models have been proposed to account for different scenarios of mineral coalescence, namely, full-coalescence, no-coalescence, and partial-coalescence.[206, 213-215]

Due to mineral coalescence, the final ash particles have a coarser average particle size than that of the original coal minerals. In addition, they have a relatively more homogeneous composition compared with the original minerals.

- ***Char fragmentation***

Char fragmentation significantly influences the particle size distribution of fly ash produced from coal combustion.[209, 212, 216] At high temperatures, char fragmentation dominates the fly ash formation, followed by coalescence with in the resulting fragments. Char fragmentation can take place through the percolation mechanism[217] or from the burn-off of bridges connecting regions of a char particle of irregular shape.[218] With char fragmentation, one coal particle will break into a number of smaller particles, which might each contributes to one ash particle and results in the formation of more than one ash particle form one char particle. This process will also in turn reduce the possibility of included mineral coalescence and hence, results in the formation of more fine ash particles, the number of which may vary from 3–5 to 200–500.[219]

Char fragmentation is strongly affected by coal rank, particle size, and system pressure, which contribute to the difference in char structure particularly macroporosity of the char.[211, 220] Char macroporosity was considered to be an important controlling parameter for char fragmentation.[212] Since the macropores provide oxygen with easy access to the inner part of the particle, oxidation reactions can take place on both the internal and external surfaces. As the macropores broaden with the conversion, the char structure becomes more and more lacy and eventually breaks apart into a number of fragments of all sizes.[217] Aside from the char structure, mineral properties and combustion conditions are also important factors influencing the char fragmentation.

- ***Fragmentation of excluded minerals***

Most excluded minerals evolve directly into residual ash particles due to the limited particle interactions during combustion, but some may undergo fragmentation. The fragmentation of different excluded minerals on rapid heating was studied and summarized by Raask.[182] Three key findings were drawn in his study: (1) no

fragmentation was observed for the silicate minerals, quartz, illite, and muscovite, (2) pyrite particles could fragment due to the vigorous evolution of sulfur gas, and (3) carbonates, i.e., siderite, ankerite, and calcite fragmented extensively on rapid heating because of the release of carbon dioxide. It was then concluded that mineral fragmentation was the result of thermal shock and gas evolution. Additionally, the fragmentation of excluded minerals is believed mainly contributed to PM_{1-10} rather than PM_1, as investigated by Wang et al..[221]

2.7.3.2 Formation Mechanisms for PM_1

The formation of PM_1 is of particular importance due to their significant adverse impact on combustion systems as well as environments. It was generally believed that PM_1 were formed via vaporization and condensation mechanism, as proved by the dominant existence of vaporized elements in PM_1. Indeed, the vaporization and condensation mechanism contributes significantly to the formation of PM_1. However, some other possible mechanisms which may be responsible for the formation of PM_1 were also proposed, including surface ash shedding, cenosphere bubble bursting, direct carryover of fine mineral particles, and convective transport of mineral matter.

- ***Vaporization and condensation***

Vaporization and condensation processes during pulverized coal combustion have been extensively investigated by Sarofim's group in Massachusetts Institute of Technology (MIT) since 1980s.[40, 219, 222, 223] During pulverized coal combustion, small amounts of mineral matters may vaporize and release into gas phases at high temperatures.[224] The degree of vaporization of mineral matters depends on a number of factors such as inherent volatility, mode of occurrence in coal, particle temperature, and combustion atmosphere.[225, 226] The inherent volatility for pure elements decreases in the order of Na, K, Fe, Mg, Ca, Si and Al.[27] However, these elements exist as different chemical forms in coal and therefore the observed volatility was different from that of the pure element.[201] For a specific element, the organically

bound portion could easily vaporize at the early stage of coal combustion, but the portion associated with silicates and/or aluminosilicates was much more difficult to release.[223] Vaporization is intensified by higher particle temperatures and more reducing environments.[223] Fuel properties such as coal particle size can also have influence. The vaporization mechanism for refractory elements (Si, Al, Fe, Ca, and Mg) is generally believed to be the reduction of these species to more volatile sub-oxides (SiO and AlO) and metals (Fe, Ca, and Mg).[223] Therefore, the reducing conditions which are commonly in fuel-rich regions and within burning char particles enhance the vaporization of refractory elements. However, the extent of vaporization can be affected by other factors.[227] As high temperatures may lead to more severe interactions between volatile species and solid materials such as silicates and/or aluminosilicates, and consequently suppress the vaporization.

After diffusing away from the char particle, the vaporized species will undergo a series of gas phase reactions.[222] The gas phase may become supersaturated due to a lowered vapor pressure of the new compound formed and/or simply due to the cooling of the flue gas, and consequently homogeneous nucleation takes place to form a very large number of extremely small particles (probably<0.01 μm[224]). Once new particles formed, they will collide with each other due to their relative motion and adhere to form larger particles as results of Brownian motion and/or external forces,[88] such process is known as coagulation, leading to the growth of particle size. The heterogeneous condensation/reaction will also occur between inorganic vapours and pre-existing fine particles formed through homogeneous nucleation, and consequently increases the particle size. Additionally, such heterogeneous condensation favors smaller particles due to their higher surface area-to-volume ratios. As results of homogeneous nucleation, heterogeneous condensation and coagulation, the morphology of particles formed via vaporization-condensation mechanism appears to be spherical and/or aggregate-like.

- ***Other possible mechanisms responsible for the formation of PM_1***

As discussed above, the main formation mechanism for PM_1 during coal combustion is believed to be vaporization and condensation. However, some other researchers have proposed other mechanisms which are speculated to be responsible for PM_1 formation. These possible mechanisms are summarized as follows.

Surface ash shedding is likely caused by fast rotating of burning char particles as a result of rapid evolution of gas jets of volatiles.[216] It was found that 200–500 ash particles on the order of 1 μm are generated per coal particle due to both ash shedding and char fragmentation.[219] Some researchers[40, 223] suggested that ash shedding is an important process contributing to the formation of fine particles. However, other researchers argued that shedding would not occur for molten ash from the burning char particle via mathematical calculation on the centrifugal forces generated by char particle rotation.[212]

Cenosphere bubble bursting is caused by the rapid evolution of gases such as H_2O, CO, CO_2 and SO_2, which result the formation of gas bubbles inside the liquid particles[228] during coal combustion. When the viscosity of the liquid particles are not high enough to hold on to the evolving gases due to the increase of temperature, the particles may burst and form a shower of much smaller particles.[229] As claimed by Ramsden,[230] the bursting of gas bubbles inside the liquid particles might lead to the formation of submicron ash particles. However, so far, there is no direct experimental evidence to prove this mechanism.

Carryover of fine fuel particles during coal combustion was first proposed by Holve.[231] However, the hypothesis was based on the finding that the pulverized coal sample and the resulting fly ash had similar particle size distributions and chemical composition in the submicron size range. Sadakata et al.[232] claimed that ~50% of the submicron fly ash was simply carried over from the submicron coal particles. However, thus far no direct experimental evidences are available to prove this

mechanism.

Convective transport of mineral matter is caused by rapid release of volatiles during coal devolatilization. Baxter et al.[233] proposed that convective transport during devolatilization could contribute to the mass loss of atomically dispersed or very fine-grained inorganic materials. Recently, Zhang et al.[234] also found the presence of major ash-forming inorganic elements in the condensed volatile matter smaller than 1 μm during coal pyrolysis. However, so far, there is no direct experimental evidence to prove that those fine ash particles are due to the direct convective transport of mineral matter in the parent fuels.

2.7.4 Effects of Combustion Conditions and Coal Properties on PM Formation during Pulverized Coal Combustion

Due to the complexity of the mineralogy of coal and the combustion process, the actual particle size distributions (PSDs) and characteristics of PM_{10} may therefore be governed by a combination of the mechanisms discussed in Section 2.7.3, so that are largely dependent on combustion conditions and coal properties, particularly the characteristics of mineral matter in coal.

- ***Effects of combustion conditions***

The effects of combustion conditions on the PM formation during coal combustion is of great importance as they may provide direct guidelines for the operation conditions of the pulverized coal boiler in terms of reducing the PM formation and/or emission. Several attempts were made to investigate the effects of combustion conditions such as temperature[102, 235] and oxygen content[236, 237] in combustion gas. According to Liu et al.[102] and Zhang et al.,[235] increasing combustion temperature generally increases the yields of both PM_1 and PM_{1-10}, they attributed this phenomenon as results of intensified inorganic elements vaporization (for PM_1) and increased char fragmentation coupled with increased liberation of fine included

mineral particles from the burning char surface. With respect to combustion atmosphere[236], an enhanced oxygen concentration seems to increase the formation of PM_1, probably due to the increased char-burning temperature and enhanced reducing properties of the gas environment.

- ***Effects of coal properties***

The formation and/or emission of PM_{10} may also largely depend on the coal properties such as particle size, density fraction, mode of occurrence of inorganic species, and most importantly, characteristics of mineral matter. Coal with a smaller particle size may produce more PM_{10}.[102] According to Liu et al.,[200] The combustion of a coal with heavy density fraction (>2 g cm^{-3}), which dominantly contains excluded minerals, may produce less PM_{10} compared with that of coals with medium (1.4-2.0 g cm^{-3}) and light density fractions (<1.4 g cm^{-3}) which are of included nature. Such results suggest that the PM_{10}-producing ability of excluded minerals may be much lower than that of included minerals. The mode of occurrence of inorganic species in coal may significantly influence the formation of PM_1, by collecting and identifying the inorganic species released during coal pyrolysis, Zhang et al.[234] speculated that the organically bound elements which are released during pyrolysis may contribute significantly to the formation of ultrafine particles during subsequent combustion.

The characteristics such as composition and particle size distribution of minerals in coal are believed to play important roles in the formation of PM_{10} during pulverized coal combustion. As one aspect of characteristics of minerals in coal, mineral composition and the interactions among inherent minerals have been studied by Zhang et al.[238] and Wang et al.,[239] they concluded that the interactions between included minerals and excluded minerals, and those interactions among inherent minerals significantly affect the formation of both PM_1 and PM_{1-10} during coal combustion. The association of inherent minerals with carbonaceous matrix is

important for determining their transformation into PM1, the possible interactions between inherent Si- and Al-containing minerals and excluded ($CaO+Fe_2O_3$) may affect the formation of both PM_1 and PM_{10}.[238, 239] Such interactions among mineral matters in coal are of practical importance, several methods based on the minerals interactions have been proposed to control the formation and/or emission PM_{10} (particularly PM_1) including blending of coals with different mineralogy[240] and the development of Mg-based additives.[241] On the other hand, the particle size distribution of minerals in coal is another basic but important characteristic and may play an important role in the formation of PM_{10} during coal combustion. Unfortunately, little studies have been done on this important aspect. Teramae et al.[242] mentioned the amount of SiO_2 in the particles smaller than 0.22 μm was related to the amount of fine included quartz and clay minerals in the parent coals.

2.8 Conclusions and Research Gaps

Upon the review of the literatures, the main conclusions are drawn as follows:

(1) Collie coal and mallee biomass are two important solid fuels in WA.

(2) Direct combustion of coal (or biomass) fuels is a matured technology for electricity generation.

(3) One important challenge during solid fuels (coal or biomass) combustion is the emission of inorganic particulate matter (PM), which is known to have adverse impacts on combustion system, human health and environment.

(4) Using biomass as a fuel directly suffers from several key drawbacks including high moisture content, low-energy density, poor grindability so that long-distant transport of biomass is not economic and a process using biomass as feedstock must of small scales;

(5) Distributed pyrolysis is a flexible technology to produce bio-oil and biochar from

biomass. While bio-oil can be updated and refined to produce liquid transport fuel, biochar as a solid fuel has superb fuel properties, good grindability and high energy density therefore is suitable for direct combustion and/or co-firing in coal-based power stations.

(6) A proper sampling method is of critical importance to studying PM produced from the combustion of solid fuels such as coal and biomass. Dilution ratio and sampling temperature are known to be two key parameters need to be considered when designing sampling systems. The effects of dilution on the properties of PM collected from the combustion system have been extensively studied, and consequently various dilution technologies are developed.

(7) Transformation and release of key inorganic species (K, Na, Mg, Ca, Cl and S etc.), and PM formation mechanisms during biomass combustion under fluidized-bed and fixed-bed conditions were extensively investigated.

(8) The properties and formation mechanisms of PM produced from pulverized coal combustion have been well studied. Several factors influencing the PM formation and/or emission during coal combustion are also investigated, including combustion temperature, oxygen concentration in the combustion gas, coal particle size and chemical composition minerals in coal.

Based on the above summary of previous studies performed on the formation and/or emission of inorganic PM produced from the combustion of biomass and coal, **firstly**, it is clear that the sampling temperature is another key parameter that must be considered in designing a credible PM sampling system but little consideration has been given on this aspect so far. **Secondly**, biochar has shown excellent fuel properties in applications such as direct combustion and co-firing with coal. However, as a key assessment criteria fuels for combustion application, inorganic PM emission behavior during biochar combustion is not yet studied. **Thirdly**, the transformation and release behaviors of key inorganic species during biomass combustion under PF

combustion conditions remain unclear. **Fourthly**, current understanding on PM formation and/or emission is based on the experimental data of the whole biomass combustion (including volatile and char). The contributions of the combustion of volatiles and char to PM emission are still unknown. **Fifthly**, up to now, the roles of fine inherent minerals in the parent fuels in the emission of PM_{10} during coal combustion is still largely unclear.

Overall, further R&D is therefore needed to improve the fundamental understandings on the emission of inorganic PM during the combustion of biomass, biochar and Collie coal, including:

(1) Developing a proper method for inorganic PM sampling from the combustion of biomass and coal. This requires a systematic experimental study to provide thorough understanding on the effects of sampling temperature on the collection and properties of PM.

(2) Emission behavior of inorganic PM from biochar combustion. It is of great importance to assess PM emission during biochar combustion. Such information is in urgent need to improve the fuel evaluation criteria of biochar, in order to promote the utilization of biochar for combustion application.

(3) Contribution of volatiles combustion to PM emission. As a high-volatile fuel, substantial amounts of volatiles (including inorganic species released in the volatiles) are produced during biomass prolysis. Subsequent combustion of the volatiles may contribute substantially to the PM emission. However, little work has been done on this aspect so far.

(4) Roles of fine inherent mineral particles on the emission of PM produced from pulverized coal combustion. As one of the basic but important properties of mineral matter in coal, the size distributions of mineral particles and its roles in PM emission are still not well understood yet.

(5) Transformation and release behaviors of key inorganic species (such as Na, K, Mg, Ca, S, and Cl etc.) in biomass during biomass combustion under PF combustion conditions. Such work is required to provide accurate data on the release of the above elements to further simulation and modeling works.

(6) Effects of Cl on the release of alkali metals. The roles of Cl in the release of alkali metals during pyrolysis and combustion of biomass remain unclear. Further investigation is needed to provide a fundamental understanding on the formation and control of Cl-associated aerosols during biomass combustion.

(7) Co-firing mallee biomass with Collie coal. It is of strong demand to carry out systematic investigation on the emission of inorganic PM during co-firing of mallee biomass and Collie coal. Although co-firing is not specifically reviewed in this chapter, it is generally believed to be an attractive near-term option for reducing the net CO_2 emissions from existing coal-fired power stations, because of its low cost, ability to provide a rapid solution and flexibility to the vast existing infrastructures.[75, 243]

2.9 Research Objectives of the Present Study

As identified by the above literature review, there are various research gaps in the research field. However, it is impossible to carry out research to fill all of these research gaps within a period of 3.5 year for PhD study. Therefore, this study will focus on the emission of inorganic particulate matter during the combustion of biomass, biochar and Collie coal. The main research objectives of this study are:

(1) To investigate the effects of sampling temperature on the collection and properties of PM_{10} produced from pulverized mallee biomass combustion. A proper PM sampling method will then be developed.

(2) To examine the emission behaviors of PM_{10} produced from pulverized biochar

combustion, in order to provide the data which are useful in designing combustion systems such as PF boiler for biochar.

(3) To provide direct experimental evidences on the substantial contribution of volatiles combustion to PM_1 emission.

(4) To study the significant roles of fine inherent mineral particles in the emission of PM_{10} from pulverized coal combustion.

CHAPTER 3 RESEARCH METHODOLOGY AND ANALYTICAL TECHNIQUES

3.1 Introduction

This chapter describes the general research methodologies employed to achieve the thesis objectives which were outlined in Chapter 2. Experimental and analytical techniques are then given in details.

3.2 Methodology

Two important solid fuels are considered in this thesis, i.e. Collie coal that is a sub-bituminous coal and the only coal currently being mined in Western Australia (WA), and mallee biomass that is a key renewable energy source in the state. A series of systematical experiments were then carried out, including:

- pyrolysis of raw pulverized fuels in a drop-tube/fixed-bed reactor system to produce their derived fuels such as coal-char and biochar for further characterization and combustion experiments.
- combustion of the prepared fuels under well-controlled conditions via a high temperature drop-tube furnace (DTF) to produce a constant stream of flue gas which contains particulate matter (PM) with a size less than 10μm (PM_{10}) for further PM sampling and analysis.
- collection of PM samples using a cyclone followed by a Dekati low pressure impactor (DLPI) under well controlled conditions.
- analyses of the collected PM samples via a series of techniques such as gravimetrical, chemical composition and morphology analysis, etc.

In this research, experiments and analyses were repeated to ensure the reproducibility of the results. The overall research methodology to achieve the research objectives is shown in Figure 3-1, with further explanations as follows.

3.2.1 Effect of Sampling Temperature on the Properties of Inorganic PM Collected from Biomass Combustion

As discussed in Section 2.9 of Chapter 2, a key issue needs to be addressed is the development of a proper method for the sampling of PM produced from the combustion of solid fuels (biomass or coal). This is to ensure that the properties of the PM samples collected will not be distorted by the sampling process itself. It is suspected that sampling temperature is a key parameter. Therefore, in this thesis, a series of experiments were carried out to produce PM samples from the combustion of a typical pulverized woody biomass (mallee bark, see Section 3.3.1) in a laboratory-scale DTF system (see Section 3.3.2.2) at 1300 ^{o}C, followed by sampling PM samples by Dekati cyclone and Dekati low pressure impactor (DLPI) at various sampling temperature (25 – 115 ^{o}C). The collected PM samples were then subject to mass analysis and chemical composition analysis to investigate the effect of sampling temperature on collection and properties of PM generated from pulverized biomass combustion. A new sampling method, which is also suitable for sampling PM produced from coal and biomass combustion, was then developed in Chapter 4 and employed in the studies reported in this thesis.

3.2.2 Emission Behavior and Characteristics of PM_1 and PM_{10} from the Combustion of Pulverized Biochar

To achieve the research objective 2 outlined in Section 2.9 of Chapter 2, a series of systematical experiments were then designed and carried out. Firstly, six biochar samples were produced from both slow and fast pyrolysis of mallee bark via a quartz drop-tube/fixed-bed reactor system (see Section 3.3.2.1) at 400 – 550 ^{o}C, respectively – such temperatures are typically used for biochar and/or bio-oil production in practice. Secondly, to investigate the emission behavior and characteristics of PM with a size less than 1.0μm (PM_1) and PM_{10}, the raw biomass and its derived biochar samples were combusted in a DTF (see Section 3.3.2.2) at

1300 ^{o}C, followed by PM sampling and analysis using the suitable method developed in Chapter 4. The detailed results and discussion for this work are presented in Chapter 5.

3.2.3 Combustion of Volatiles Produced In Situ from the Fast Pyrolysis of Woody Biomass: Direct Evidence on Its Substantial Contribution to PM_1 Emission

The results in Chapter 5 show that combustion of biochars leads to a substantial reduction in the emission of PM_1 in comparison to that of biomass combustion, such results imply that the combustion of volatiles (including the released inorganic species) is mainly responsible for PM_1 emission. In Chapter 6, a novel two-stage pyrolysis/combustion system (see Section 3.3.2.3) was then designed to obtain direct evidence on the substantial contribution of volatiles combustion to PM_1 emission. Volatiles, which were produced in situ from the fast pyrolysis of a mallee biomass at 800 – 1000 ^{o}C, were immediately combusted in a DTF (see Section 3.3.2.2) at 1300 ^{o}C to investigate the contribution of volatiles combustion to PM_1 emission. The results of this work are presented in Chapter 6.

3.2.4 Significant Roles of Inherent Fine Included Mineral Particles in the Emission of PM10 during Pulverized Coal Combustion

To investigate the roles of inherent fine included mineral particles in coal in the formation of inorganic PM during pulverized coal combustion, a WA sub-bituminous coal (Collie Coal, see Section 3.3.1) was density-separated, size-narrowed, and washed with dilute acid to produce a coal sample that is free of organically-bound inorganic species and contains dominantly discretely included mineral particles. The computer-controlled scanning electron microscopy (CCSEM) analysis was carried out to quantify the particle size and chemical compositions of fine included mineral particles in the coal. The PM produced from coal combustion was carefully sampled and analyzed using various analytical techniques including inductively coupled

plasma-atomic emission spectroscopy (ICP-AES), scanning electron microscope equipped with an energy dispersive X-ray spectrometer (SEM-EDS), and X-Ray diffraction (XRD) analysis. The significant roles of fine included mineral particles in coal in the emission of PM_{10} during combustion were then clearly evidenced. The detailed results of this part of work are reported in Chapter 7.

3.3 Experimental

3.3.1 Sample Preparations

Mallee Biomass. A batch of woody biomass sample (mallee bark) was prepared by separating the bark component from the green mallee trees (*E.loxophleba lissophloia*), which were harvested from Narrogin, WA. After dried at 40 °C in a large lab oven, the bark sample was then cut, milled and sieved into the size fraction of 75–150 μm. The prepared sample was stored in sealed double bags in a freezer under -4 °C for further experiments. The fuel properties of the prepared mallee bark sample are summarized in Table 3-1. It should be noted that this mallee bark sample is different with the batch listed in Table 2-2. It is clear that the mallee bark sample has high contents of alkali and alkaline earth metallic (AAEM, mainly Na, K, Mg and Ca) species (~96% of the total inorganic species in bark) and Cl, while the contents of Si and Al are very low (<2% of the total inorganic species in bark). Such unique features of the bark sample provide a simple system for this study. Therefore, the chemical composition analysis of the PM generated from biomass combustion in this study focused on AAEM species, S and Cl.

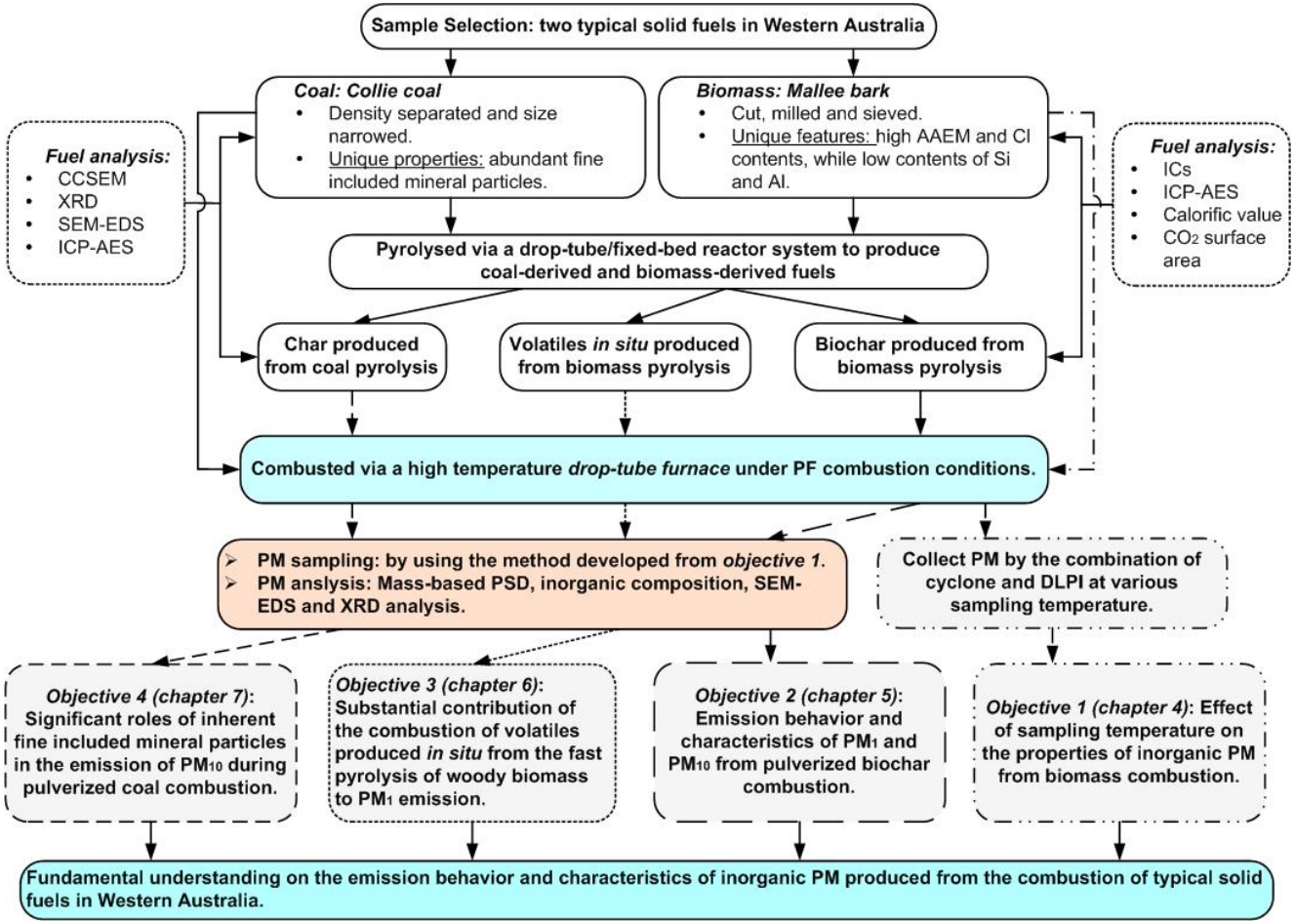

Figure 3-1: Research methodology

Collie Coal. Collie coal was sampled from the mine site in Collie, WA, crushed and sieved to prepare a coal sample of narrow size fraction (63 – 90 μm). The sample was then density separated via sink-float method to yield a coal sample with a density fraction of 1.4–1.6 g/cm^3. The coal sample was then washed with acetone to remove the heavy liquid remained after density separation, followed by drying in argon at 105 °C for 2 hours to completely evaporate the acetone. Then the acetone washed coal was termed as "raw coal". The raw coal was then washed by dilute acid (0.1 M HCl acid) for 24 hours to prepare an acid-washed coal for the experiments in Chapter 7.

3.3.2 Experimental Rigs

3.3.2.1 A Drop-Tube/Fixed-Bed Quartz Reactor System

The pyrolysis experiments were carried out to prepare biochar and coal-char samples using a quartz drop-tube/fixed-bed reactor. A schematic diagram of the reactor system is shown in Figure 3-2, it mainly consists of a quartz reactor with a inner diameter of 40 mm and a two-heating zone electrical furnace. A key feature of the reactor system is that it can be used for pyrolysis experiments at both slow- and fast-heating rates. For pyrolysis experiments at a slow-heating rate, the sample was firstly loaded into the reactor that was then heated from ambient to the desired pyrolysis temperature at a heating rate of 10 Kmin^{-1} with a further holding of 30 min. For pyrolysis experiments at a fast-heating rate, the reactor has the features of both a drop-tube reactor and a fixed-bed reactor. The reactor was firstly pre-heated to the desired pyrolysis temperature. The fuel particles were then fed into the reactor at a feeding rate of ~0.05–0.1 g min^{-1} via a feeder (see Section 3.3.2.2). Once the pulverized fuel particles were injected into the hot reactor zone, rapid pyrolysis took place (similar to a normal drop-tube reactor). However, different to a normal drop-tube reactor, the char particles formed in this reactor system after pyrolysis remained on the frit of the reactor while volatiles were swept away. Once a pyrolysis

experiment was completed, the reactor was lifted out of the furnace immediately and cooled naturally with argon continuously flowing through the reactor.

Table 3- 1: Properties of *E.loxophleba* ***lissophloia*** mallee bark used in Chapter 4

Proximate analysis	
Moisture, % after air-dried	4.9
Ash, %db	4.9
Volatile Matter, %db	68.1
Fixed Carbon, %db	27.0
Ultimate analysis, % daf	
Carbon	52.0
Hydrogen	5.78
Nitrogen	0.41
Sulfur	0.04
Chlorine	0.18
Oxygen (calculated by difference)	41.59
Contents of Inorganic Species, %db	
Na[a]	0.2729
K[a]	0.1353
Mg[a]	0.0992
Ca[a]	2.4717
Si[b]	0.0478
Al[b]	0.0093
Ba[b]	0.0062
Fe[b]	0.0065
Pb[b]	0.0289
Sr[b]	0.0317
Ti[b]	0.0004
[a]analysed by IC; [b]analysed by ICP-AES	

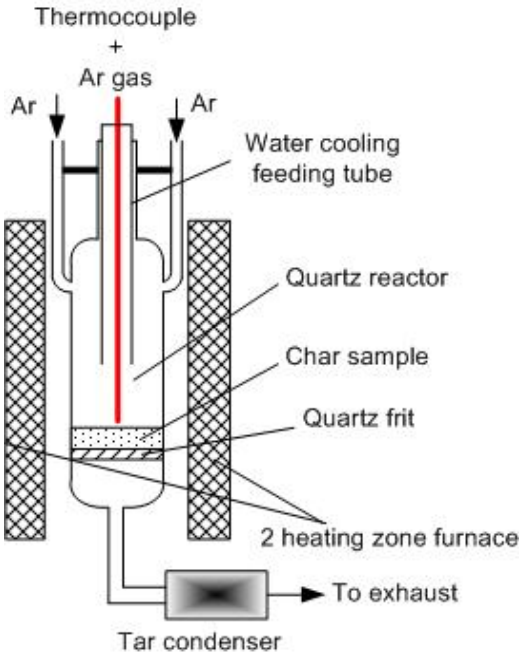

Figure 3-2: A Drop-tube/fixed-bed quartz reactor system

3.3.2.2 A High-Temperature DTF System

All the combustion experiments in this study were conducted using a laboratory-scale high-temperature DTF system, as shown in Figure 3-3. The DTF can be operated at 1 atm and a maximum temperature of 1600 °C under various atmospheres. The whole system consists of a feeding system, a main drop-tube reactor and a PM sampling system, which are detailed as follows.

Feeding system. The feeding system is similar to the one used in a previous study[130] but modified for feeding both pulverized coal and biomass. It includes an entrained flow feeder, primary air, mass flow controller and a water-cooled feeding probe. As illustrated in Figure 3-3, the entrained flow feeder consists of 1/4" stainless steel tubing which is inserted into a 3/8" stainless steel tubing being placed inside a glass tube with pre-loaded pulverized fuel samples. The primary air, controlled by mass flow controller, passes through the annular space between 1/4" and 3/8" stainless steel tubing at a sufficiently high velocity. This enables the feeding gas entrain the pulverized fuel particles through the 1/4" stainless steel tubing and then feed the fuel

particles into the main drop-tube reactor via a water-cooled feeding probe inserted into the top section of the furnace. The secondary air is introduced through the water-cooled feeding probe to provide a laminar flow profile in the heated zone of the reactor.

The main drop-tube reactor. The main drop-tube reactor is a vertical dense mullite tube (inner diameter of 54mm, length of 1200mm) which is heated electrically. The furnace is divided into 2 heating zones and has an isothermal zone of ~600mm. The gas temperature profile of the DTF is shown in Figure 3-4.

The PM sampling system. The PM sampling system consists of a water-cooled quench probe, a diluter, a Dekati cyclone (Model SAC-65) with a nominal cut-off size of ~10μm, a Dekati low pressure impactor (DLPI) with backup filter and a vacuum pump (Leybold Sogevac SV25). The water-cooled quench probe, using helium as quench medium (1 L/min in this study), is designed not only for quick quenching and diluting the particle stream with high purity helium to minimize the interaction among particles, but also for forcing the nucleation of vaporized materials during quenching.

The DLPI used in this study is composed of 13 collection stages and a backup filter stage, calibrated by the manufacturer, as shown in Figure 3-5. The inlet and outlet pressure of the DLPI is controlled at 1013.3mbar and 100mbar respectively. The bottom stage of DLPI acts as a sonic orifice to control the flow rate at nominal value (~10L/min). Because the total gas stream flow rate (including primary air, secondary air and quench helium) is lower than 10L/min under the experimental conditions, a small stream (~3.4 L/min) of instrument grade air was introduced through the diluter as makeup and dilution air (with a dilution ratio of 1.5). Because the feeding rate of fuel particles is very low, the PM_{10} concentration in the flue gas at furnace exit is low (<30 mg/Nm^3) so that no further dilution was carried out during sampling.

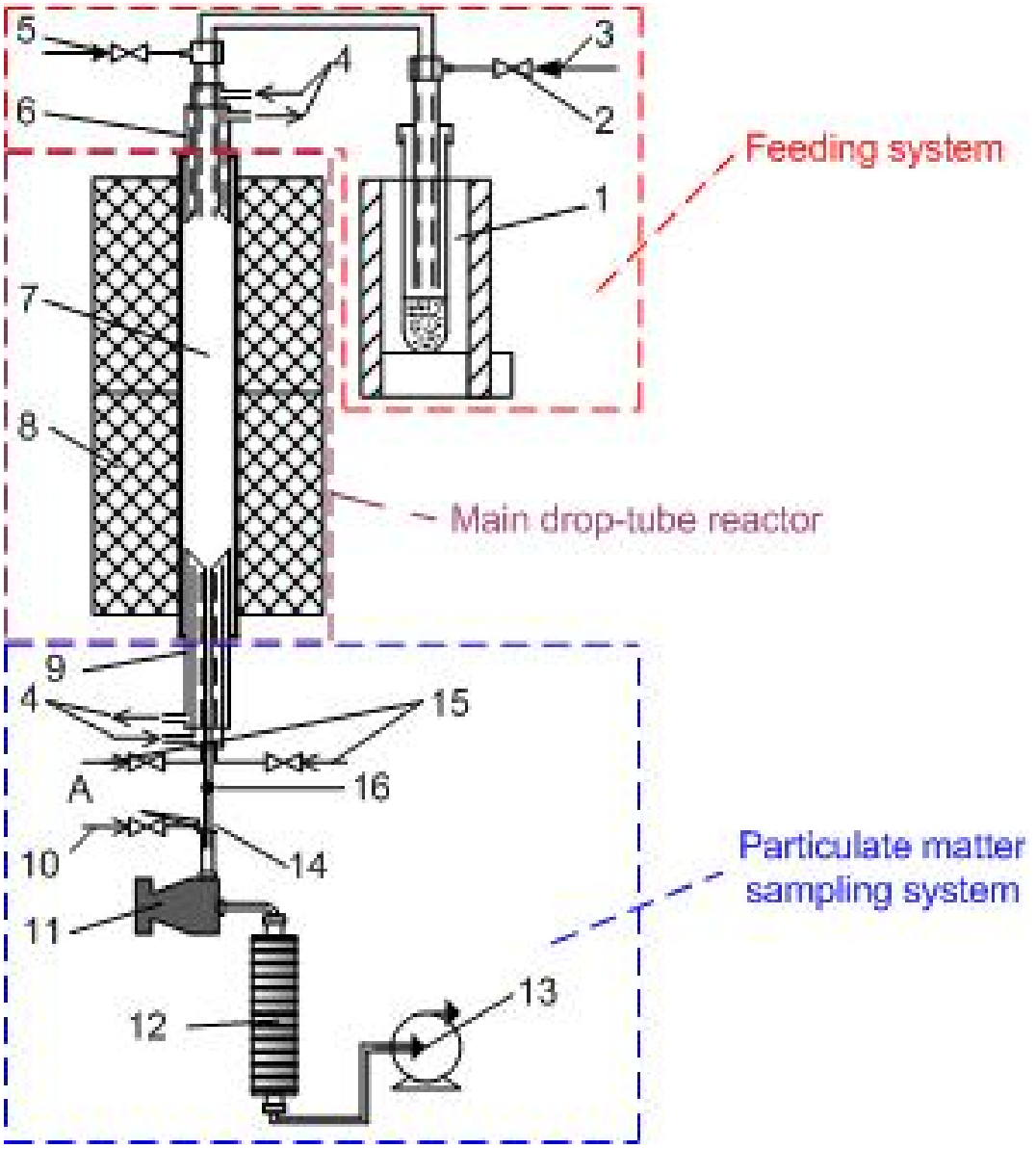

Figure 3-3: Schematic diagram of experimental setup: (1) Feeder, (2) Mass flow controller, (3) Primary air, (4) Cooling water, (5) Secondary air, (6) Water-cooled feeding probe, (7) Dense mullite reaction tube, (8) Two heating-zone furnace, (9) Water-cooled quench probe, (10) Makeup and dilution air, (11) Cyclone, (12) Dekati low pressure impactor, (13) Vacuum pump, (14) Diluter, (15) Quench helium, (16) Exit of quench probe.

3.3.2.3 A Novel Two-Stage Pyrolysis/Combustion Reactor System

In this study, a novel two-stage pyrolysis/combustion reactor system was developed to investigate the combustion of volatiles and its contribution to PM_1 emission, as illustrated in Figure 3-6. The two-stage reactor system is fundamentally a combination of two reactors connected fluidly. One is a novel quartz drop-tube/fixed-bed pyrolyser as the first-stage, which is similar to the one described in Section 3.3.2.1. The other is a DTF as the second-stage, which is the same as the one described in Section 3.3.2.2. The pyrolyser is cascaded into the DTF.

The drop-tube/fixed-bed pyrolyser is a drop tube with the installation of a quartz frit at the exit of the reactor, having the features of both a conventional drop-tube reactor and a fixed-bed reactor. During experiments, solid fuel particles are injected into the reactor (similar to that into a conventional drop-tube reactor), with UHP argon as carrier gas. The presence of the quartz frit achieves the separation of char that remains on the frit during pyrolysis (with the features of a conventional fixed-bed reactor) from volatiles which are swept out of reactor via the frit then immediately combusted in the DTF. Therefore, the key innovation of the two-stage pyrolysis/combustion reactor system in Figure 3-6 is that the pyrolyser can be considered as an *in situ* generator/feeder of volatiles. It truly achieves the separation of volatiles combustion from char combustion, enabling the investigation on the PM emission from subsequent volatiles *in situ* combustion in the DTF.

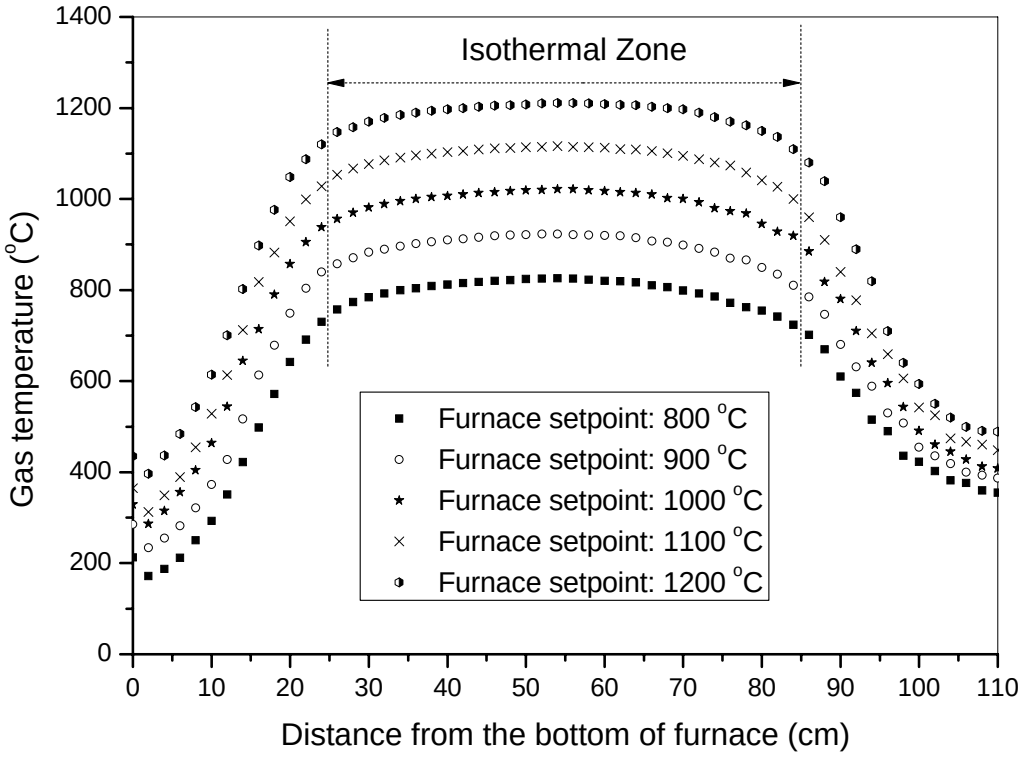

Figure 3-4: Gas temperature profile of the DTF

(a)

Stage	D50% (μm)
Filter	~0
1	0.0275
2	0.0542
3	0.0927
4	0.155
5	0.26
6	0.38
7	0.609
8	0.942
9	1.59
10	2.37
11	3.97
12	6.64
13	9.85

(b)

Figure 3-5: DLPI image (a) and its nominal cut-off size calibrated at 21.5 °C with a gas flow rate of 10.04 L/min

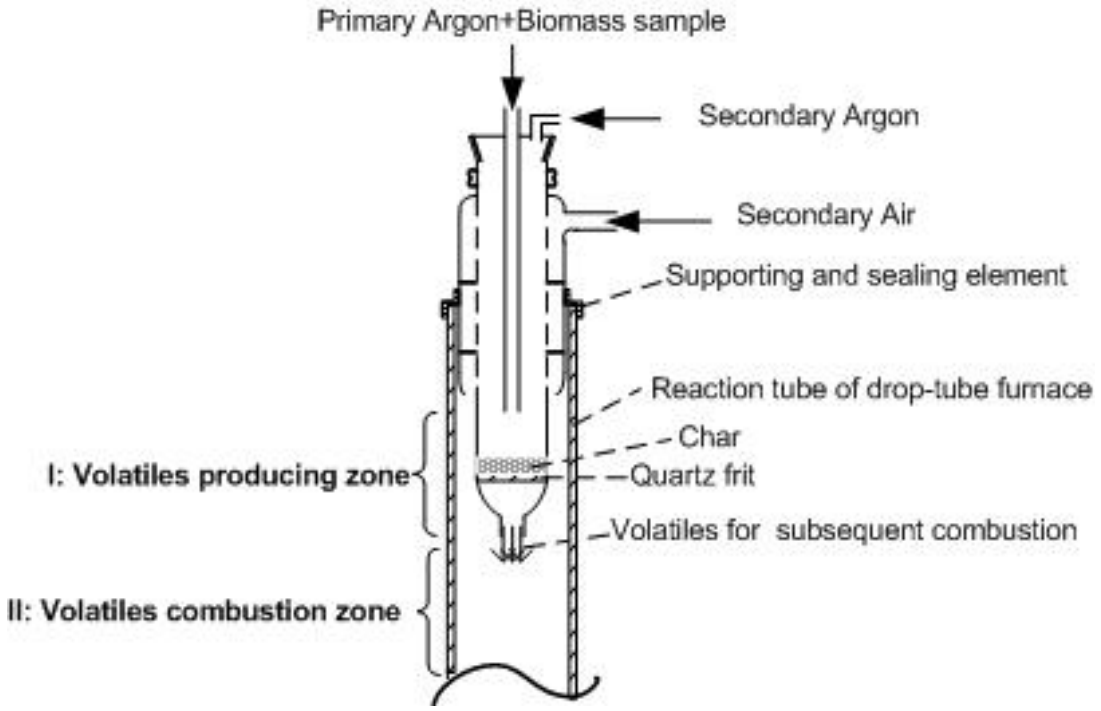

Figure 3-6: A schematic diagram of the two-stage pyrolysis/combustion reactor system used in this study, it consists of a quartz drop-tube/fixed-bed pyrolyser that is cascaded into the DTF as described in Section 3.3.2.2

3.3.3 Generation of a Stream of Constant PM_{10}-Containing Flue Gas from Biomass Combustion

In Chapter 4, the effect of sampling temperature on the properties of PM produced from the combustion of pulverized biomass (75 – 150 μm, see Section 3.3.1) in a DTF system (see Section 3.3.2.2) at 1300 ^{o}C was investigated. Two different streams of constant PM_{10}-containing flue gas with different particle mass concentrations and acid gas (mainly SO_3 and HCl) concentrations at the outlet of water-cooled quench probe (termed as point A, see Figure 3-3) were produced by using two fuel feeding rates (~0.1 and ~0.3g/min, denoted as "Case-0.1" and "Case-0.3" hereafter) with all other experimental conditions kept unchanged. The total combustion air flow rate was 5.6L/min (primary air of 1 L/min and secondary air of 4.6 L/min). The residence time of pulverized biomass particles in the isothermal zone was estimated as ~1.7s.

In all experiments of this study, the flue gas temperature at the exit of the quench probe (point A, see Figure 3-3) was adjusted at 115 °C.

It is important to note that all combustion experiments were carefully designed and carried out under conditions with substantial excessive air. The values of Lambda (λ, expressed as the ratio of actual air-fuel ratio to stoichiometric air-fuel ratio) in Case-0.1 and Case-0.3 are ~13 and ~4.3 respectively. The high furnace temperature (1300 °C), fine biomass particle size (75–150 μm) and substantial excessive air facilitate operation conditions which achieve complete combustion. Indeed, the total organic carbon (TOC, see Section 3.4.6) analysis of the extracts of PM samples shows that little organic carbon is present in the PM samples collected from all experiments.

3.3.4 Preparations of Biochar and Coal-Char

3.3.4.1 Biochar

In Chapter 5, six biochar samples were prepared from the pyrolysis of the raw biomass sample using a quartz drop-tube/fixed-bed reactor as described in Section 3.3.2.1. It should be noted that the batch of raw biomass sample is different from the one used in Section 3.3.3. Pyrolysis experiments at both slow-heating rate and fast-heating rate were carried out at 400 – 550 ^{o}C using argon (UPH 99.999%, 2.0 L min-1) as a carrier gas, such temperatures are typically used for biochar and/or bio-oil production in practice. Hereafter in this study, the biochar samples produced from slow pyrolysis at 400, 450, 500 and 550 ^{o}C are referred as “SH–Char–400”, “SH–Char–450”, “SH–Char–500” and “SH–Char–550” while those produced from fast pyrolysis at 400 and 500 ^{o}C as “FH–Char–400” and “FH–Char–500”.

In Chapter 6, in order to compare the contribution of the combustion of volatiles and biochars to PM emission, the drop-tube/fixed-bed pyrolyser (Section 3.3.2.3) was also used to prepare biochar samples from the fast pyrolysis of raw biomass which is

same as the one used in Chapter 5 at 800, 900 and 1000 ^{o}C, following the identical conditions used for *in situ* volatiles generation (see Section 3.3.5) in the two-stage pyrolysis/combustion reactor system. Hereafter, biochar samples produced from fast pyrolysis of raw biomass at 800, 900 and 1000 ^{o}C are denoted as "Char–800", "Char–900" and "Char–1000", respectively.

In Chapter 5, fast pyrolysis experiments at 1300 ^{o}C were carried out for the raw biomass, "SH–Char–400", "SH–Char–500", "FH–Char–400" and "FH–Char–500" in a DTF system detailed in Section 3.3.2.2 using argon as a carrier gas, to investigate the structure change of chars produced from the fast pyrolysis of these fuels at 1300 ^{o}C. A total gas flow rate of 5.6 L min^{-1} argon passed through the reactor in two streams, a primary stream of argon (1 L min-1,) via the feeder and a secondary stream of argon (4.6 L min-1) via the reactor inlet. A fuel feeding rate of ~0.05 g min-1 was used. Hereafter in Chapter 5, the biochar samples produced from the fast pyrolysis of raw biomass, "SH–Char–400", "SH–Char–500", "FH–Char–400" and "FH–Char–500" at 1300 ^{o}C are denoted as "Char–1300–raw biomass", "Char–1300–SH–Char–400", "Char–1300–SH–Char–500", "Char–1300–FH–Char–400" and "Char–1300–FH–Char–500", respectively.

3.3.4.2 Coal-Char

In Chapter 7, the coal-char was also prepared from the fast pyrolysis of the acid washed coal at 1000 ^{o}C using a quartz drop-tube/fixed-bed reactor detailed in Section 3.3.2.1, using argon as carrier gas (UHP, 1.5 L min-1). About 1 g of coal particles were fed into the pyrolysis reactor in 20 min at a feeding rate of ~0.05 g min^{-1}. The reactor was then held in the furnace for 10 min before it was lifted out of the furnace and cooled rapidly with argon continuously following through the reactor. The residence time of coal particles in the isothermal zone of the reactor was ~1s.

3.3.5 Volatiles Produced In Situ from Fast Pyrolysis of Biomass

To investigate the role of volatiles combustion in PM_1 emission, the key challenge is to carry out experiments that separate the combustion of volatiles from char produced *in situ* from biomass pyrolysis under various conditions. In Chapter 6, volatiles were produced *in situ* from the fast pyrolysis of woody mallee biomass which is the same one used in Chapter 5 using the novel two-stage pyrolysis/combustion reactor system as described in Section 3.3.2.3. The temperature of DTF was kept as 1300 ^{o}C. However, as the pyrolyser is made of quartz, limited by its working temperature in such applications, *in situ* volatiles were generated at 800 – 1000 ^{o}C by adjusting its position in the reaction tube of the DTF. A total gas flow rate of 2.0 L min^{-1} argon (UHP, 99.999%) was used as a carrier gas and passed through the pyrolyser in two streams: a primary stream of argon (1 L min^{-1}) via a feeder to feed ~1g of raw biomass samples into the pyrolyser in 10 min at a feeding rate of ~0.1 g min^{-1}, and a secondary stream of argon (1 L min^{-1}) via the pyrolyser inlet to assist in sweeping the produced volatiles through the quartz frit. Once the biomass particles were injected into the hot zone of the pyrolyser, rapid pyrolysis took place and the volatiles generated *in situ* were swept out of the pyrolyser then immediately combusted in the DTF, while the char particles were retained on the quartz frit of the pyrolyser. Hereafter, the volatiles generated from fast pyrolysis at 800, 900 and 1000 ^{o}C are referred to as "Votatiles-800 ^{o}C", "Volatiles-900 ^{o}C" and "Volatiles-1000 ^{o}C", respectively.

3.3.6 Combustion of Pulverized Fuel Particles and Volatiles

3.3.6.1 Combustion of Pulverized Fuel Particles

The combustion experiments of raw biomass, biochars, coal and coal-char were carried out using the DTF system detailed in Section 3.3.2.2. The furnace temperature was kept at 1300 ^{o}C and 1400 ^{o}C for the combustion of raw biomass /biochar and coal/coal-char samples, respectively. During combustion, the primary

and secondary air flow rates were 1.0 L min^{-1} and 4.6 L min^{-1}, respectively. The fuel feeding rate was ~0.05 g min^{-1}. The value of lambda (λ, expressed as the ratio of actual air–fuel ratio to stoichiometric air–fuel ratio) was ~26 and ~19 for the combustion of biomass and coal, respectively. The residence times of biomass and coal particles in the isothermal zone of the DTF were estimated as ~1.7 and ~1.5s, respectively. Under the experimental conditions in this study, complete combustion was achieved.

3.3.6.2 Combustion of Volatiles

In Chapter 6, the combustion experiments for volatiles generated *in situ* from fast pyrolysis of biomass were carried out in the same DTF system detailed in Section 3.3.2.2. The furnace temperature was kept at 1300 ^{o}C. During experiment, the volatiles generated *in situ* were swept out of the quartz drop-tube/fixed-bed pyrolyser that is cascaded in the DTF (see Figure 3-6). The volatiles were then immediately combusted in the DTF, via the introduction of an additional stream of secondary air (3.6 L min^{-1}) into DTF via the annular tube of the pyrolyser (see Figure 3-6). Volatiles combustion experiments were finished as soon as biomass feeding was complete without extra holding at the pyrolysis temperatures.

Additionally, as the pyrolyser is made of quartz, it is possible that the quartz pyrolyser (SiO_2) may interact with volatiles under the conditions and such interactions can potentially influence PM emission. Therefore, blank tests were also carried out by feeding a suitable amount of ash-free microcrystalline cellulose (Avicel PH-101, particle size: 30~50 μm) into the pyrolyser for 10 min to generate a stream of ash-free volatiles at 1000 ^{o}C (the highest pyrolysis temperature) for subsequent combustion and PM collection. The amount and feeding rate of cellulose were calculated by considering the yields of volatiles from the pyrolysis of both raw biomass and cellulose under the prevailing conditions in order to generate a similar amount of volatiles.

3.3.7 Sampling of Inorganic PM

The PM_{10}-containing flue gas (after dilution, PM_{10} concentration < 30mg/Nm^3) was firstly separated by the cyclone to remove the coarse ash particles (aerodynamic diameter >10 μm), then directed to the DLPI for size-segregated collection (0.0275–10 μm) and the ultrafine particles (<0.0275 μm) were collected by the backup filter. As suggested by the manufacturer (Dekati), the cyclone was placed horizontally for all the experiments to minimize the effect of the tube bend in the sampling line (see Figure 3-3). A close investigation demonstrates that the operation position of cyclone has little effect on mass-based particle size distribution of PM_{10}, (see Figure 3-7a) but the yield of ash collected by cyclone during horizontally sampling increases substantially in comparison to that of vertically sampling (see Figure 3-7b), apparently due to the reduction in the mass of ash lost in the tube bend, this further confirms the advantages of placing cyclone horizontally. Aluminum foils and polycarbonate filters were used as collection substrates for the mass concentration and chemical analysis, respectively. The collection substrates were covered by Apiezon-H vacuum grease to prevent particle bounce, and was pretreated at 115 °C for 12 hours to avoid mass losses (if any) during sampling.

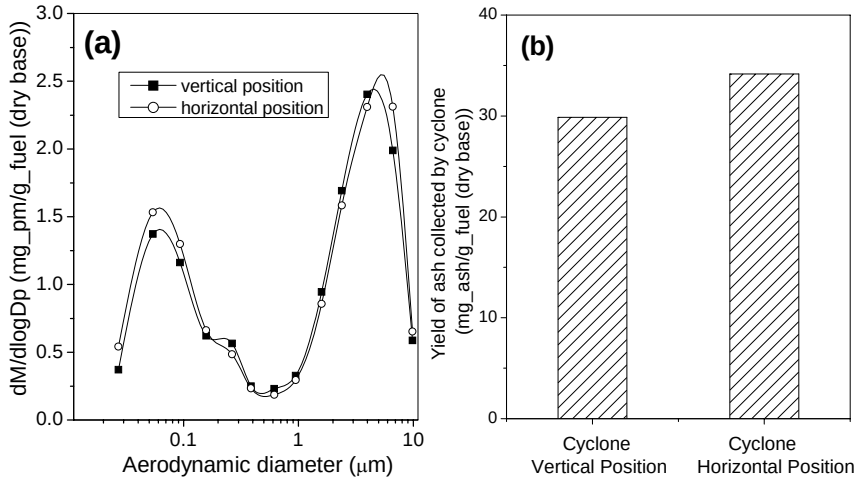

Figure 3-7: Effect of the operation position of cyclone on the (a) particle size distribution of PM_{10} and (b) yield of ash collected by cyclone. The PM sampling temperature was set at 25°C.

In Chapter 4, to study the effect of sampling temperature on PM collection, the sampling system (including diluter, cyclone, DLPI and the stainless steel sampling lines) was adjusted at various temperatures (25 – 115 °C) via external electrical heating. At different sampling temperatures, the actual cutoff aerodynamic diameters of cyclone and DLPI were different with the calibration values and were properly corrected by the calculation program provided by the manufacturer (Dekati). In Chapters 5–7, the sampling system was kept at a temperature (~115 °C) same as that of the flue gas at the sampling probe exit, in order to avoid possible acid gas condensation and suppress particle coagulation during the sampling process, as concluded in Chapter 4.

After experiment, the collection substrates were carefully disassembled and put in a desiccator. The collection substrates were analyzed gravimetrically with a 0.001mg micro-balance (see Section 3.4.2). The relative standard errors of PM mass size distribution are ±4%. The ash particles collected by the cyclone and deposited in the sampling tubing were washed by acetone and weighed after the evaporation of acetone.

3.4 Instruments and Analytical Techniques

3.4.1 Proximate, Ultimate and Calorific Value Analysis

Proximate analysis of biomass, biochar and coal samples was determined by a METTLER thermogravimetric analyzer (TGA) based on American Society for Testing and Materials (ASTM) international standard ASTME870-82[244] and ASTMD7582-10,[245] the temperature program of TGA is shown in Figure 3-8. Briefly, ~10 mg of fuel sample was loaded into the TGA sample crucible, purged with Ar for 15 min and then heated to 110 °C followed by holding at this temperature for 20 minutes until no further weight loss was observed. The total weight loss was recorded as moisture content of the sample. The sample was then further heated to 950 °C at a heating rate of 50 K min^{-1} in Ar and held at the temperature for 20 min,

followed by decreasing the temperature to 600 and 750 °C for biomass and coal, respectively. The weight loss was recorded as volatile matter and the remaining material as char. The char residue was then exposed to air to be oxidized for 30 min until no weight loss was observed. The weight of the residual ash in the sample crucible is used to calculate the ash content of the fuel, while the difference between the weights of the char and residue ash is calculated as the fixed carbon content of the fuels.

Ultimate analysis of these fuels was determined via a series of analytical techniques, total carbon, hydrogen and nitrogen contents were determined using a LECO Truspec Analyser according to Australian standard AS1038.6.4,[246] while the total sulfur and chlorine contents were determined by inductively coupled plasma-optical emission spectrometer (ICP-OES), following combustion of the samples under "Eschka" mixture and acid digestion, based on Australian standard AS1038.6.3.1[247] and AS1038.8.1.[248] The oxygen content was determined by the difference from the C, H, N, S and Cl contents of the samples, on a dry-ash-free (daf) basis. The calorific values of selected fuel samples were measured using a Leco AC-350 analyser.

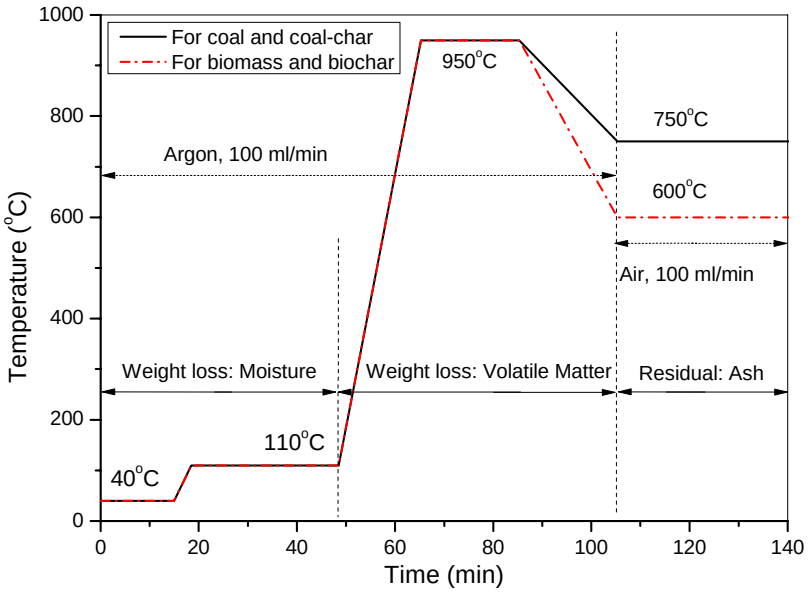

Figure 3-8: Temperature program of TGA for proximate analysis of coal, coal-char, biomass and biochar

3.4.2 Mass- based Particle Size Distribution of PM_{10}

The mass-based particle size distribution (PSD) was obtained by measuring the mass of PM collected in each stage of DLPI using a Mettler MX5 microbalance (accuracy: 0.001 mg).

3.4.3 Quantification of AAEM Species and Other Inorganic Species

The AAEM species (mainly Na, K, Mg and Ca) and other inorganic species (e.g. Al, Ba, Fe, Mn, Ni, P, Si, Sr, Ti and V) in the fuel samples and PM collected by DLPI were determined via a procedure described in a previous study.[72] The quantification procedure is schematically illustrated in Figure 3-9. Briefly, about 20~30mg of fuel sample was put in a Pt crucible, then it was ashed in air following a specially designed heating program (see Figure 3-10) to ensure no loss of these species during ashing.

For the AAEM species, the ash sample together with the Pt crucible was then put in a Teflon vial for acid digestion with a mixture of HNO_3:HF (1:1) solution at 120 °C for 12h. After the evaporation of excessive acids on a hot plate, the digested ash was dissolved in 20mM methanesulfonic acid (MSA) solution. The AAEM species in the solution was quantified using a Dionex ICS-3000 ion chromatography with a CS12A column and 20mM MSA solution as eluent. The contents of AAEM species in PM sample from each stage of DLPI were also quantified via the same procedure described above but the ashing step was omitted. The relative standard errors of the elemental-mass-based particle size distribution of Na and K are ±5%, while those of Mg and Ca are ±6% and ±8%, respectively.

Other inorganic species (e.g. Al, Ba, Fe, Mn, Ni, P, Si, Sr, Ti and V) in the fuel samples were analyzed by inductively coupled plasma-atomic emission spectroscopy (ICP-AES), following borate fusion and acid digestion. Briefly, 1–3 mg of ash was decomposed by fusion with the X-Ray flux (35.3% lithium tetraborate and 64.7%

lithium metaborate for biomass ash, or 50% lithium tetraborate and 50% lithium metaborate for coal ash with high iron content) in a Pt crucible at 950 ^{o}C for 2 h. The ratio of ash to X-ray flux was about 1:30. The fusion bead was dissolved in dilute redistilled nitric acid (10% v/v) and subject to the analysis for the above inorganic species using a Varian Vista Axial CCD Simultaneous ICP-AES instrument. For the analysis of above elements in PM samples collected on polycarbonate filters in each stage of DLPI, the PM-loaded polycarbonate filters were placed in a Pt crucible and heated to 600 ^{o}C at a slow heating rate of 2 K min^{-1} in air followed by holding at 600 ^{o}C for 2 h to completely burn the polycarbonate filter, followed by ICP-AES analysis using the same procedure as described above.

3.4.4 Quantification of S and Cl in PM samples

The PM-loaded polycarbonate filters were dissolved into Milli-Q water for sufficient long (24 hours) till all S and Cl were dissolved. The S and Cl in the solution were quantified using a Dionex ICS-1000 ion chromatography with an AS14 column and 3.5mM NaCO3/1.0mM NaHCO3 solution as eluent. The relative standard errors of the elemental-mass-based particle size distribution Cl and S are ±5%.

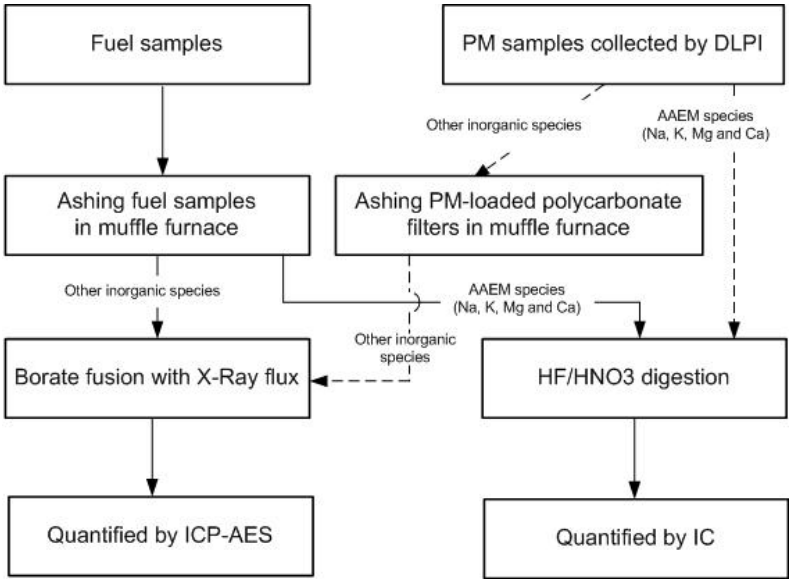

Figure 3- 9: A Schematic diagram of quantification of AAEM species and other inorganic species in fuel samples and PM samples collected by DLPI

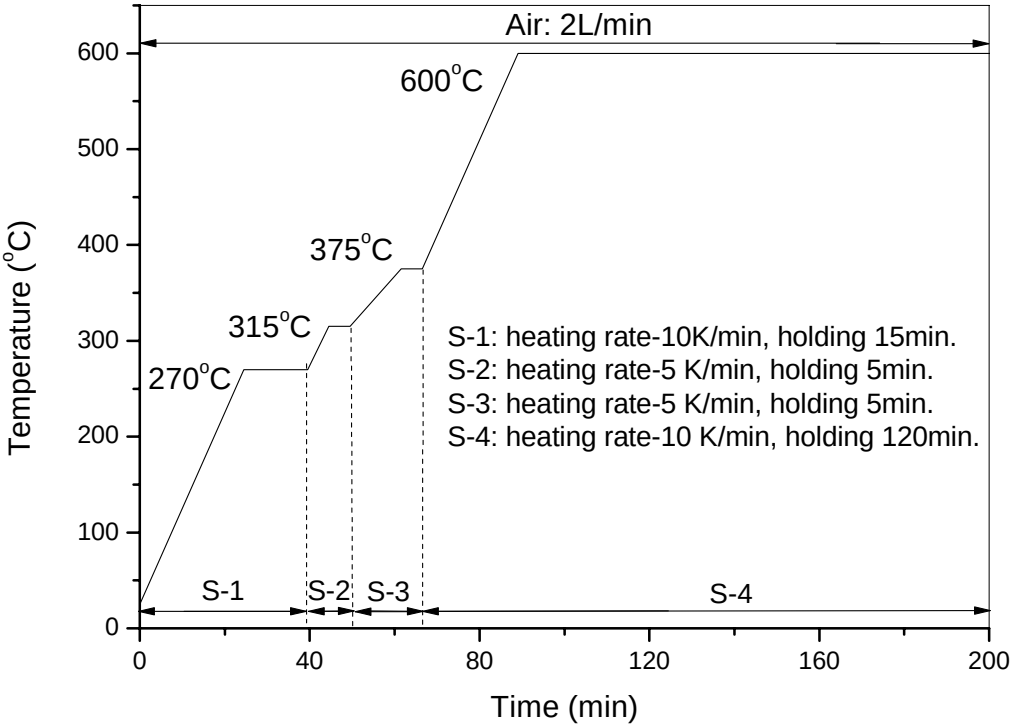

Figure 3-10: Temperature program of ashing fuel samples such as biomass, biochar and coal

3.4.5 Total Organic Carbon (TOC) Analyzer

In selected experiments of this study, the PM samples were extracted in MilliQ water for 24 hr followed by the total organic carbon (TOC) analysis using a TOC analyzer (Shimadzu TOC-V_{CPH}). Generally, the sample is injected via the sample pre-treatment/injection system into the combustion chamber filled with catalyst, the carbon in the sample is oxidized to CO_2 after combustion at 680 ^oC under zero grade air, the gas containing CO_2 was then introduced to the non-dispersive infrared detector (NDIR) for carbon detection.

3.4.6 Micropore Surface Area of Biochars

The micropore surface area analysis of the biochars produced from fast pyrolysis at 1300 ^oC was conducted at HRL Technology Pty Ltd (Melbourne, Australia), via CO_2

adsorption analyzed by the Dubinin – Astakhov (DA) equation. The DA equation is written as:[249, 250]

$$W = W_0 \exp\left[-\left(\frac{A}{\beta E_0}\right)^n\right] \quad (1)$$

where W is the amount of CO_2 adsorbed at a given relative pressure P/P_0; W_0 is the micropore volume; A is the differential molar work defined by $A = RT\ln(P/P_0)$, T is the absolute temperature; β is the affinity coefficient taken as 0.46 for CO_2 at 273 K; and E_0 is the characteristic adsorption energy. The exponent n reflects the width of the energy distribution and can be determined by fitting the experimental data to the linear form of Eq.(1).[249]

3.4.7 Computer Controlled Scanning Electron Microscopy (CCSEM)

Computer controlled scanning electron microscopy (CCSEM) analysis for density separated (1.4-1.6 g/cm^3) and size narrowed (63-90 μm) collie coal was carried out at Chubu University in Japan to quantify the particle size distributions and compositions of mineral particles present in the coal. To perform CCSEM analysis, coal sample was first mixed with molten carnauba wax. After the sample was cooled to a solid, the pellet was carefully cross-sectioned, polished, and carbon-coated. During CCSEM analysis, the back-scattered electron (BSE) images were continuously collected. Compared with the wax and coal carbonaceous matrix, the coal minerals are usually the brightest because of their heavy molecular weights.[251] The properties of each mineral particle were automatically determined by an energy dispersive x-ray spectrometer (EDS). Mineral particles in coal were then determined according to the elemental composition of individual particle analyzed, the mineral categories based on the composition criteria developed by Zygarlicke and Steadman[252] were employed to determine the compositions of mineral particles in coal.

3.4.8 Scanning Electron Microscope (SEM)

Selected coal and coal char samples, PM samples and ash samples collected in cyclone were characterized using a Zeiss EVO 40XVP scanning electron microscopy equipped with an energy dispersive X-ray spectrometer (SEM-EDS) for morphology and chemistry analysis. Morphology of selected PM samples was also examined using a Zeiss Neon EsB focused ion beam scanning electron microscopy (FIBSEM).

3.4.9 X-Ray Diffraction (XRD) Analysis

The mineralogy investigation of selected PM samples from coal combustion was conducted using a Bruker-AXS D8 advance type X-ray Diffractometer (XRD) via Cu radiation and a LynxEye position sensitive detector. The data were collected in a 2θ range from 5 to 60^{o} with a nominal step size of 0.009^{o} and a time per step of 1.2s. Crystalline phases were identified by using Search/Match algorithm, EVA 16.0 (Bruker-AXS, Germany) to search the Powder Diffraction File (PDF4+ 2009 edition).

3.5 Summary

A mallee bark (75 – 150 μm) biomass sample and a Collie coal (with a density of 1.4–1.6 g/cm^3 and a size fraction of 63–90 μm) were carefully selected as typical solid fuels in WA. The raw fuel samples were then pyrolysed using quartz drop-tube/fixed-bed reactor system to prepare their derived fuels, such as biochars, volatiles, and coal-char, for further combustion experiments, which were carried out using a high-temperature DTF system to produce constant streams of PM_{10} containing flue gas for PM sampling. The raw fuels, their derived fuels, and ash particles collected in cyclone and DLPI were characterized via various analytical techniques as detailed in Section 3.4. The fundamental understandings on the emission of inorganic PM produced from the combustion of biomass, biochars and coal were then achieved.

CHAPTER 4 EFFECT OF SAMPLING TEMPERATURE ON THE PROPERTIES OF INORGANIC PARTICULATE MATTER COLLECTED FROM BIOMASS COMBUSTION

4.1 Introduction

Mallee biomass is a key second-generation bioenergy feedstock for the future sustainable development of rural and regional Australia.[4, 6, 8] Direct biomass combustion or co-firing of biomass and coal is matured technology for power generation from mallee biomass but may contribute significantly to particulate matter (PM) emission. Particularly, PM with an aerodynamic diameter less than 1.0 μm (PM_1) and 2.5 μm ($PM_{2.5}$), and those less than 10.0 μm (PM_{10}) are known to have significant adverse impact on both human health and environment.[31, 32, 253] Therefore, a thorough understanding on PM properties and formation during biomass combustion is required for minimizing PM emissions from the combustion of biomass such as mallee.

Sampling of PM from solid fuel (coal or biomass) combustion systems typically employs a combination of cyclone and low pressure impactor (LPI). As summarized in Table 2-1 of Chapter 2, a review on the sampling methods used in some previous studies[26, 86, 96-109] shows that the previous studies used significantly different sampling conditions. Dilution is for both quenching flue gas and preventing particle overloading in sampling instruments. It is clear that the previous studies employed very different dilution conditions. Various sampling temperatures were also used in those studies, ranging from room temperature to 150 °C. As shown in Table 2-1, such information was not given in some of the studies. Obviously, there is no standard method for PM sampling. Although limited attempts were made to study the effects of sampling methods (particularly dilution ratio) on PM properties, there is

significant discrepancy in conclusions drawn in different studies.[94, 100] Therefore, the validity is also questionable in comparing the experimental data in different studies.

Therefore, sampling conditions are clearly important considerations to ensure that the properties of PM collected are not distorted by the sampling process. The key objective of Chapter 4 is to carry out a systematic investigation on the effect of sampling temperature on the properties of particulate matter generated from biomass combustion, while other conditions are kept unchanged. A mallee bark sample is combusted in a drop-tube furnace system under constant conditions to generate 2 constant streams of PM_{10}-containing flue gas (exit temperature: 115 °C, see Section 3.3.3 in Chapter 3). A proper method is then developed and employed in the following chapters for sampling and characterizing the PM collected, corresponding to the first research objective outlined in Chapter 2.

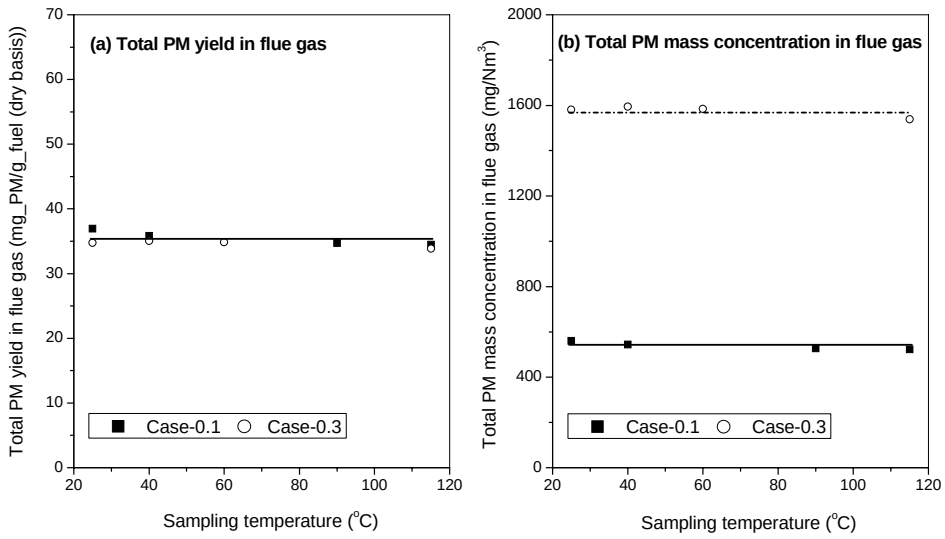

Figure 4-1: Total PM yield and mass concentration at point A: (a) total PM yield in flue gas, (b) total PM mass concentration in flue gas

4.2 Measured PM Yields and Mass Concentrations in Flue Gas

At a given biomass feeding rate (0.1 or 0.3 g/min), the total PM yield (normalized to the amount of biomass combusted) and mass concentration are constant in all

experiments at various sampling temperatures (see Figure 4-1). The PM mass concentration at 0.3 g/min biomass feeding rate is about 3 times as that at 0.1 g/min biomass feeding rate, while the total PM yield normalized to the amount of biomass combusted remains unchanged. This is expected as the configuration of the PM collection system is designed to achieve a complete collection of the PM in the flue gas. The total PM is dominantly collected in the cyclone (~90%) while the PM_{10} collected in the DLPI contributes to only ~10% of the total PM.

Figure 4-2 presents the similar data on the yields and mass concentrations of PM_1, the particulate matter with an aerodynamic diameter between 1.0 and 10.0 μm (PM_{1-10}) and PM_{10}. Three key observations can be made from the data in Figure 4-2. First, regardless the biomass feeding rate (0.1 or 0.3 g/min), the yield and mass concentration of PM_{10} actually increases with increasing sampling temperature from 25 to 105 °C and then levels off with a further increase to 115 °C. It seems that unless the sampling temperature is close to the flue gas temperature (115 °C), some of PM_{10} was collected by the sampling system before entering into the DLPI. Second, it is interesting to see that the sampling temperature has little effect on the yield and mass concentration of PM_1. Therefore, although the sampling temperature does influence the yield and mass concentration of PM_{10}, such influence is mainly on PM_{1-10} as clearly illustrated in Figure 4-2. Third, at the same sampling temperatures < 105 °C (such as 25 or 40 °C), increasing biomass feeding rate from 0.1 to 0.3 g/min has little effect on the yield of PM_{10}. However, increasing biomass feeding rate does lead to an appreciable reduction in the yield of PM_1 and interestingly, such a reduction is accompanied with an increase in the yield of PM_{1-10}. Therefore, the data in Figure 4-2 clearly suggest that the sampling temperature significantly influence the measured yield and mass concentration of PM_{10} in the flue gas and such influence is also dependent on the source PM_{10}-containing flue gas.

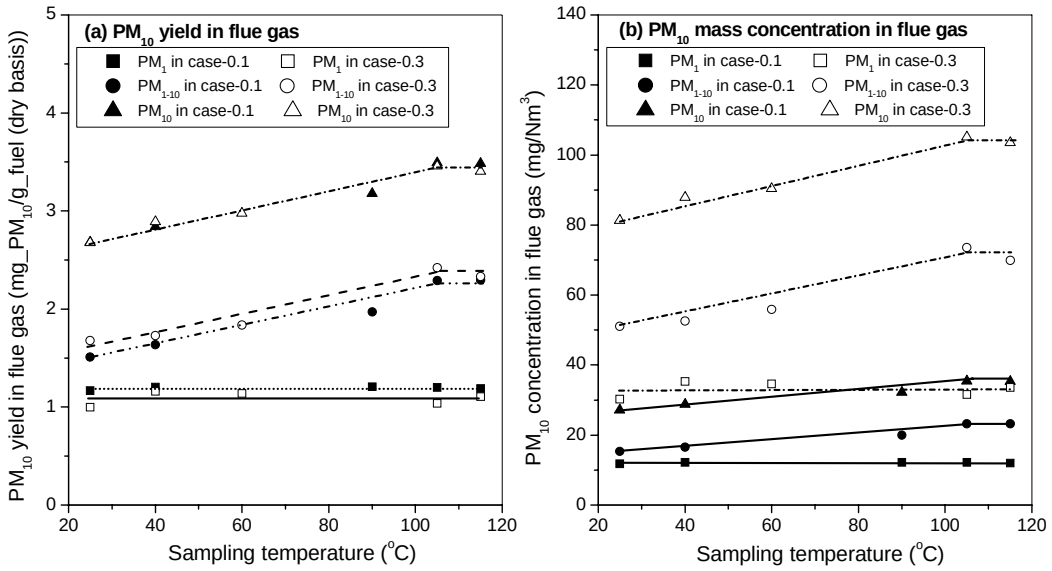

Figure 4-2: Emission characteristics of PM_{10} at various sampling temperatures: (a) PM_{10} yield in flue gas, (b) PM_{10} mass concentration in flue gas

4.3 Mass-Based Particle Size Distribution of PM_{10}

Further efforts were then made to investigate the mass-based particle size distribution (PSD) of PM_{10} collected at various sampling temperatures (see Figure 4-3). It can be seen clearly that the PSD of PM_{10} has a bimodal size distribution, i.e. a fine and a coarse mode. For example, at a biomass feeding rate of 0.1 g/min, the fine mode is located between 0.03 and 0.1 μm with a mode diameter of ~0.05 μm while the coarse mode is located between 2.37 and 6.64 μm with a mode diameter of ~3.97 μm. Such an observation is in agreement with the results on a bimodal PSD of PM_{10} reported in previous studies.[28, 41]

However, the most important results in Figure 4-3 are the fact that the PSD of PM_{10} is significantly influenced by the sampling temperature. Although sampling temperature has little effect on the yield of PM_1 (see Figure 4-2), increasing sampling temperature shifts the PSD of PM_1 to smaller particle size. For $PM_{1\text{-}10}$, sampling temperature does not seem to influence the shape of the PSD curves. Rather, the mount of $PM_{1\text{-}10}$ collected increases as the sampling temperature increases from 25 to

105 °C and levels off from 105 to 115 °C, in consistent with the data on PM_{10} yield in Figure 4-3. Clearly, the data in Figures 4-2 and 4-3 show that the influence of sampling temperature is distinctly different for PM_1 and PM_{1-10}, suggesting that there are likely different fundamental mechanisms governing the influence of sampling temperature on the collection and properties of PM_1 and PM_{1-10}. These aspects are discussed in the following sections.

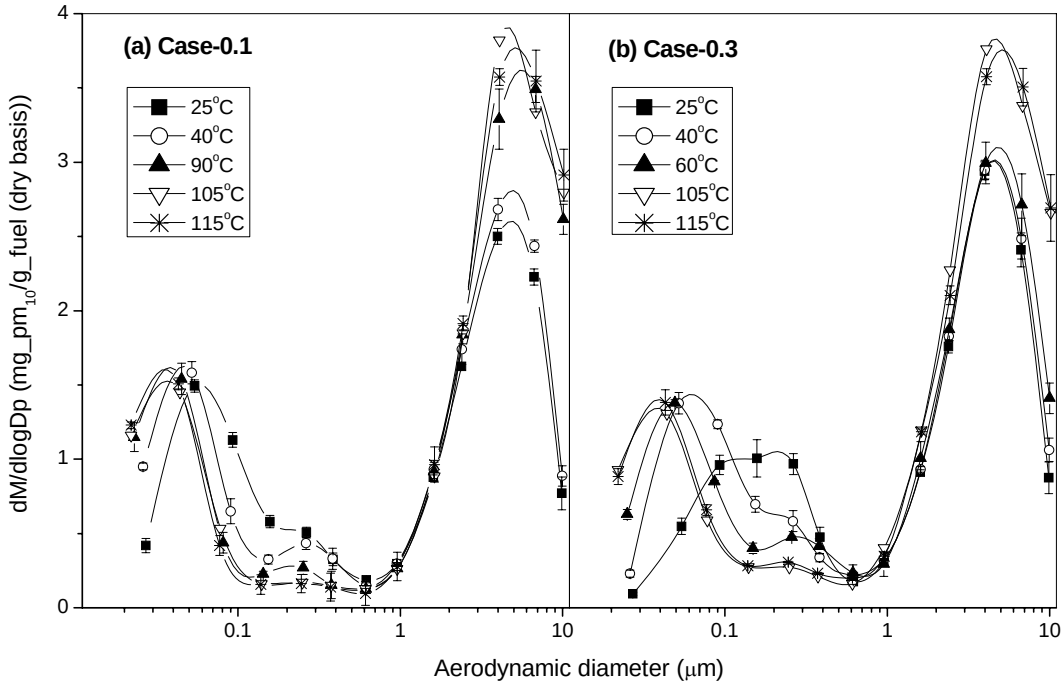

Figure 4-3: Mass-based particle size distribution of particulate matter collected by DLPI at different sampling temperatures: (a) Case-0.1, (b) Case-0.3. Graphs are normalized to the total mass of bark sample (dry basis) fed into the drop-tube reactor in each experiment.

4.4 Effect of Sampling Temperature on the Collection and Properties of PM_1 and PM_{1-10}

Figures 4-2 and 4-3 indicate that the yield and PSD of PM_1 remain unchanged as the sampling temperature decreases from 115 to 105 °C. A further decrease in the sampling temperature leads to a decrease in the mass of PM with a size range from

0.03 to 0.05 μm, coupled with an increase in the mass of PM with a size range from 0.1 to 0.61 μm. While such a decrease is progressive, it becomes drastic as the sampling temperature decreased from a "turning point" temperature to 25 °C. The "turning point" temperature here refers to the sampling temperature where the PSDs of PM_1 start to change drastically. The PSD of PM_1 is drastically influenced by the sampling temperature when it is below the "turning point" temperature. Such a "turning point" temperature is also dependent on the sampling source of the flue gas. For example, the "turning point" temperature increases from ~40 to ~60 °C as the biomass feeding rate increases from 0.1 to 0.3 g/min. With respect to PM_{1-10}, the amount of PM with a size range from 2.37 to 10 μm increases substantially as the sampling temperature increases from 25 to 105 ^{o}C, and remains unchanged as the sampling temperature further increases to 115 ^{o}C (see Figures 4-2 and 4-3).

Figure 4-4 (for Case-0.1) shows the elemental mass size distribution of Na, K, Mg, Ca, Cl and S. It is shown that Na, K, Mg, Ca and Cl all have a unimodal distribution. Na, K and Cl is dominantly contained in PM_1 in a single mode with a mode diameter around 0.05μm, while Mg and Ca are concentrated in PM_{1-10} in a single mode with a mode diameter around 3.97 μm. The unimodal distribution of Na, K and Cl in PM_1 is known to be result of either homogeneous nucleation or heterogeneous condensation on small particles. [28, 84, 85, 88, 254] The unimodal distribution of Mg and Ca suggests that the PM_{1-10} are likely produced from refractory elements (Mg and Ca) in the burning char particles.[28, 84, 85, 254] However, S shows a clear biomodal distribution as shown in Figure 4-4f, with a fine mode around 0.05μm and a coarse mode around 3.97μm. The S in PM_1 mainly exists as the sulfates of alkali metals,[255] formed via either homogeneous[256-258] and/or heterogeneous[259-261] mechanisms. The S in PM_{1-10} may be formed via the reactions between S and Ca,[142] condensation of alkali sulfates on the surface of coarse particles,[97] coagulation of S-rich small particles on the coarse particles, and/or condensation of SO_3 during sampling process.

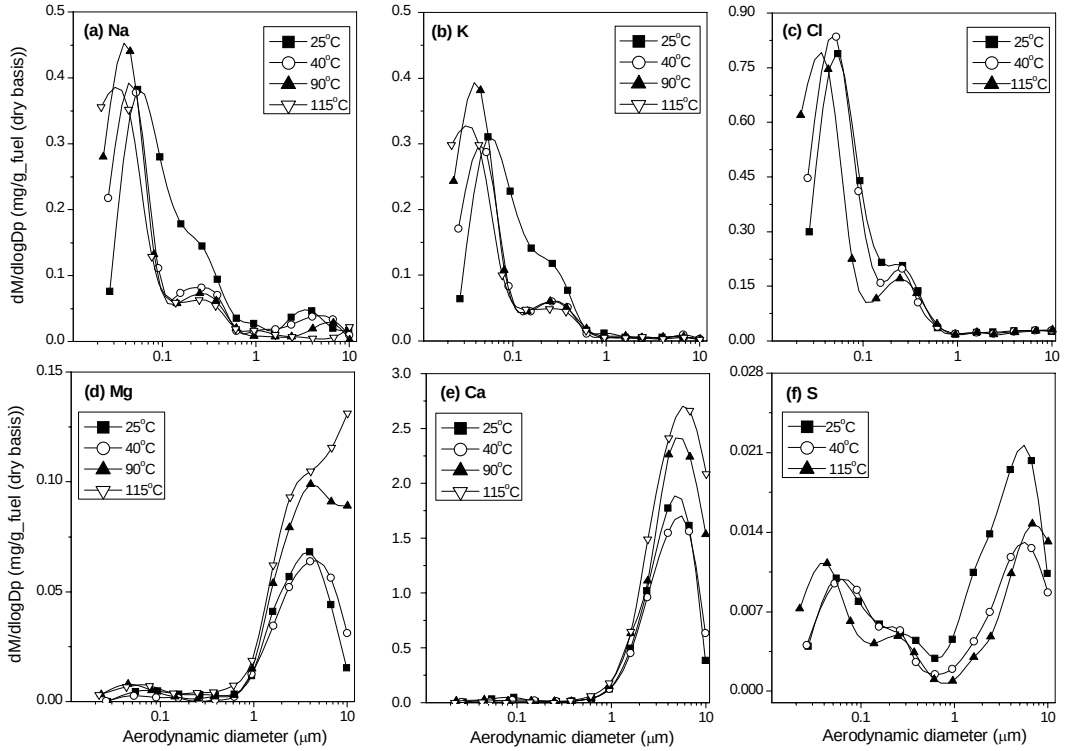

Figure 4-4: Elemental Mass Size Distribution at Different Sampling Temperatures in Case-0.1: (a) Na, (b) K, (c) Cl, (d) Mg, (e) Ca, (f) S. Graphs Are Normalized to the Total Mass of Bark Sample (Dry Basis) Fed into the Drop-Tube Reactor in Each Experiment

Figure 4-4 also clearly shows that for PM_1, decreasing sampling temperature results in a progressive decrease in the mass of Na, K and Cl in the size range of 0.03 to 0.05 μm, and an increase in the mass of these elements in the size range of 0.1 to 0.61 μm. The changes in the Na, K and Cl distribution curves as a function of sampling temperature also exhibit a "turning point" temperature of 40 °C, in consistence with that of the PSD curves (see Figure 4-3a). However, the mass of Mg and Ca in $PM_{1\text{-}10}$ increases as the sampling temperature increases from 25 to 105 °C, and remains unchanged from 105 to 115 °C (see Figures 4-5d and 4-5e). With respect to S (see Figure 4-4f), as the sampling temperature decreases, the S mass also shifts to larger size in PM_1. The S distribution curve at the "turning point" temperature (40 °C) has a similar trend with that of 25 °C in the size range of 0.03 to 0.38 μm but there is a considerable increase in the mass of S in the size range of 0.38 to 6.64 μm

when the sampling temperature decreases to 25 °C. Furthermore, the S distribution curve in PM_{1-10} at the turning point temperature (40 °C) is similar with that of 115 °C, while S in the size range of 0.942 to 6.64 μm increases significantly as the sampling temperature decreases to 25 °C. The results suggest that S have condensed from the stage with a D_{50} of ~0.38 μm at sampling temperatures blow the "turning point" temperature (40 °C).

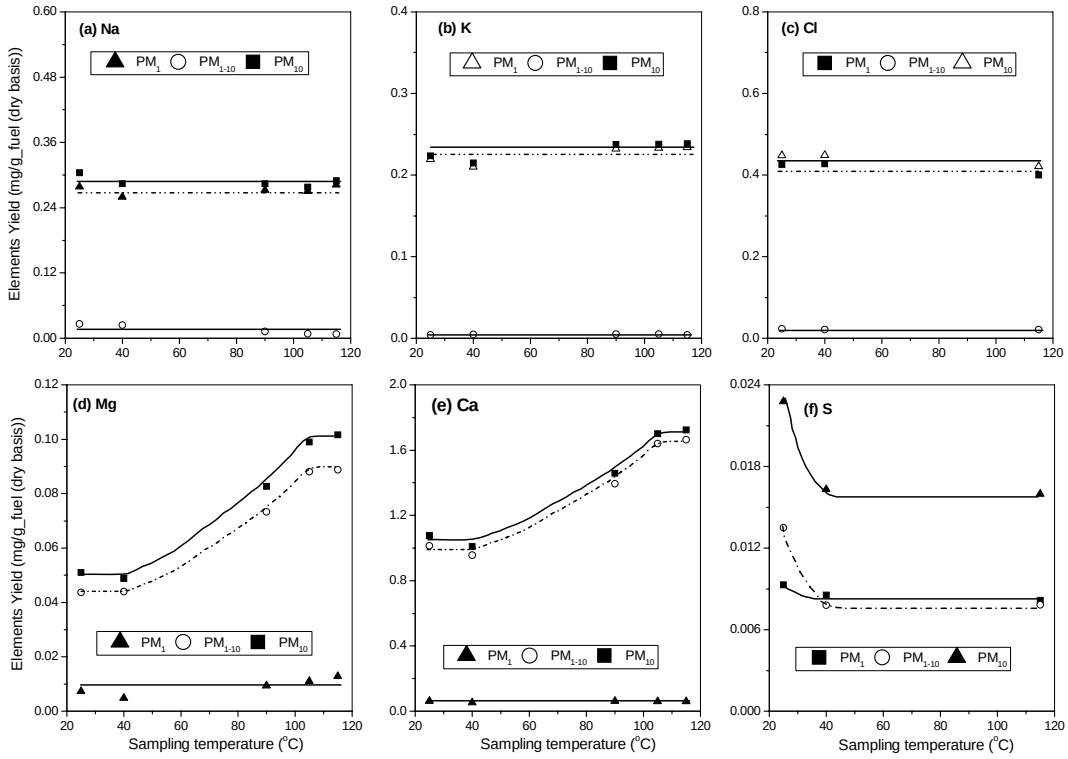

Figure 4- 5: Summary of elements yields at different sampling temperatures in Case-0.1: (a) Na, (b) K, (c) Cl, (d) Mg, (e) Ca, (f) S. Graphs are normalized to the total mass of bark sample (dry basis) fed into the drop-tube reactor in each experiment.

Therefore, the data in Figures 4-3 to 4-4 suggest that the presence of the "turning point" temperature in the mass and elemental mass PSD curves is related to the condensation of sulfur. Based on the flue gas compositions, the dew point temperature of SO_3 and HCl in the flue gas can be estimated using the following well-known equations:[262, 263]

$$T_{d,SO_3} = 1000 / \left\{ 2.276 - 0.0294 \ln\left(P_{H_2O}\right) - 0.0858 \ln\left(P_{SO_3}\right) + 0.0062 \ln\left(P_{H_2O}\right) \times \ln\left(P_{SO_3}\right) \right\} \quad (1)$$

$$T_{d,HCl} = 1000 / \left\{ 3.7368 - 0.1591 \ln\left(P_{H_2O}\right) - 0.0326 \ln\left(P_{HCl}\right) + 0.00269 \ln\left(P_{H_2O}\right) \times \ln\left(P_{HCl}\right) \right\} \quad (2)$$

where T_{d,SO_3} and $T_{d,HCl}$ are the dew point temperature of SO_3 and HCl (K) and P_{H_2O}, P_{SO_3} and P_{HCl} are the partial pressure of H_2O, SO_3 and HCl in the flue gas (mmHg). It should be noted that the acid dew point temperature decreases from top stage to bottom stage of the DLPI because the flue gas pressure decreases progressively from 1013.3mbar in top stage to 100 mbar in bottom stage of DLPI and the partial pressure of acid gas decreases in the downstream of the DLPI as results of progressive condensation. The SO_3 and HCl dew point temperatures at top stage of DLPI are estimated to be 45 and 4 °C, respectively. Indeed, the "turning point" temperature of PSD curves correlates well with the calculated SO_3 dew point temperature as HCl is not likely to condense in the collection system even at the lowest sample temperature (25 °C). Additionally, the temperature of flue gas (115 °C) in this study is low enough for the complete nucleation and condensation of alkali vapors,[264] complete combustion of biomass in the DTF system was also achieved so that little organic species vapors would be present in the flue gas. Therefore, SO_3 condensation is a key mechanism governing the effect of sampling temperature on the properties of collected PM_1.

Furthermore, as shown in Figure 4-4f, the amount of S condensed in PM_1 and PM_{1-10} is very small in comparison to the PM_1 and PM_{1-10} yield (see Figure 4-2) hence contributes little to the total mass of PM_1 and PM_{1-10}. However, the data in Figure 4-5f show that the amount of S has a considerable increase in PM_1 and a significant increase in PM_{1-10} at the sampling temperature below the "turning point" temperature (40 °C), and S condenses mainly on coarse particles due to the SO_3 dew point temperature being lower in the downstream stages of the DLPI.

To further identify the relationship between the "turning point" temperature of PSD

curves and the calculated SO_3 dew point temperature, the biomass feeding rate was increased to 0.3 g/min. In this case, the dew point temperatures of SO_3 and HCl in flue gas at top stage of the DLPI are estimated to be 65 °C and 15 °C respectively due to the higher acid gases concentration compared with that at 0.1 g/min, note that HCl is still not likely to condense even at the lowest sampling temperature (25 °C). As shown in Figures 4-6 and 4-7, it is clearly that SO_3 starts to condense at the sampling temperature below 60 °C, which is in good agreement with the calculated SO_3 dew point temperature. Furthermore, the "turning point" temperature of 60 °C observed from PSD curves (see Figure 4-3b) and elemental mass size distribution curves (see Figure 4-6) indeed correlates well with the calculated SO_3 dew point temperature.

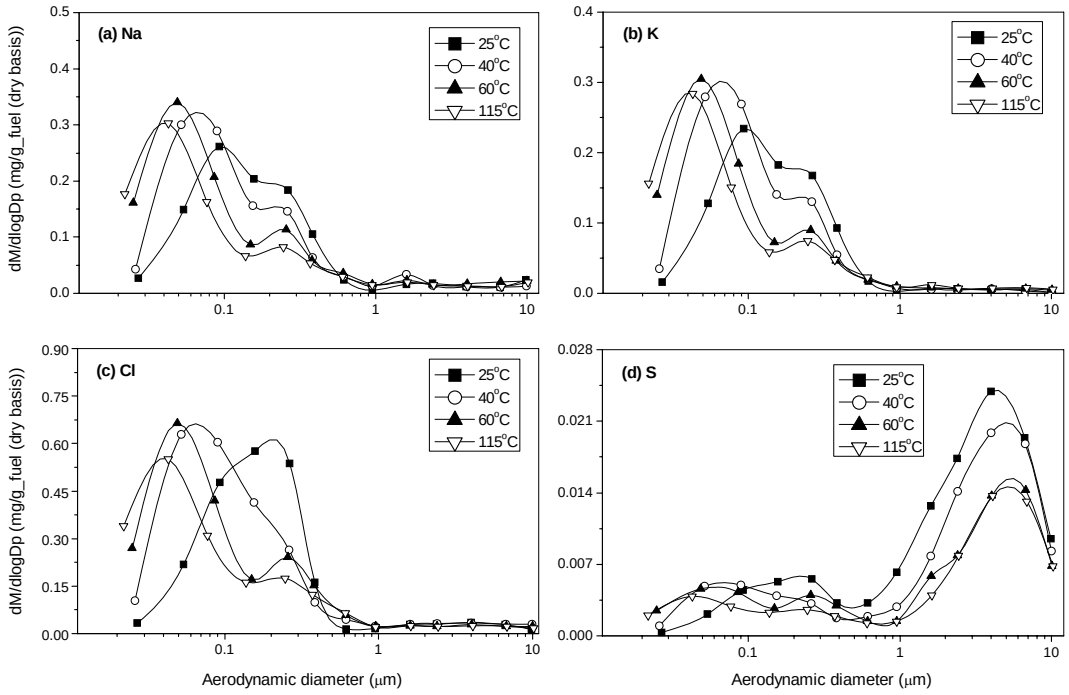

Figure 4-6: Elemental mass size distribution at different sampling temperatures in Case-0.3: (a) Na, (b) K, (c) Cl, (d) S. Graphs are normalized to the total mass of bark sample (dry basis) fed into the drop-tube reactor in each experiment.

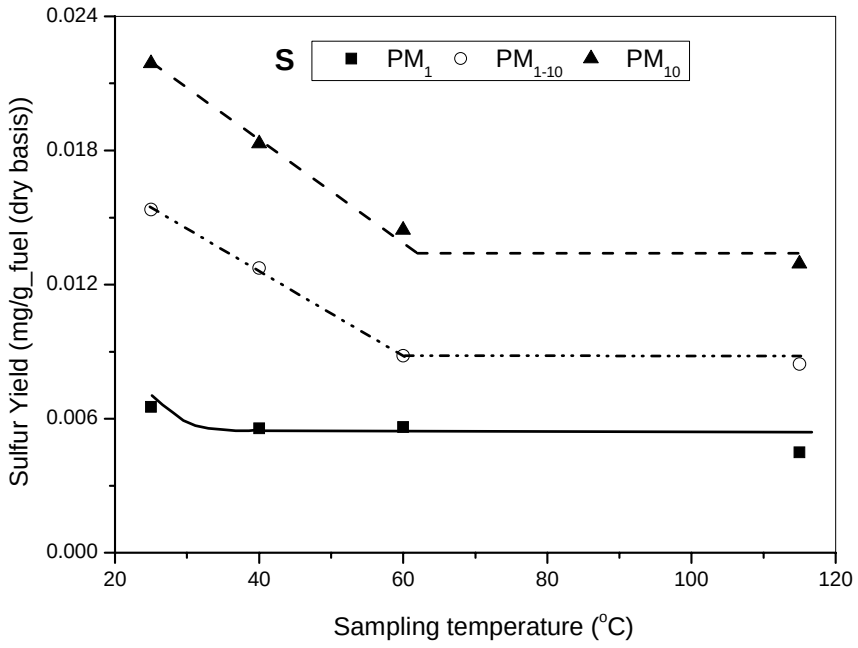

Figure 4-7: Sulfur yields at different sampling temperatures in Case-0.3. Graphs are normalized to the total mass of bark sample (dry basis) fed into the drop-tube reactor in each experiment

4.5 Possible Mechanisms Responsible for the Effect of Sampling Temperature on the Collection and Properties of PM_{10}

Three mechanisms may be responsible for the effect of sampling temperature on the collection and properties of PM_{10}, i.e. thermophoresis deposition, coagulation of fine particulate matter and gravitational settling deposition. Thermophoresis, mainly influencing the transport loss of sub-micron particles,[265] is a result of a temperature gradient in the surrounding gas, resulting in a particle being drawn into the direction of decreasing temperature.[88] Particle coagulation is a process where fine particles collide with one another due to their relative motion and adhere to form larger particles, as results of Brownian motion and/or external forces.[88] Gravitational settling deposition takes place due to the gravity and affects more on coarse particles than fine particles.[88]

Relevant to this study, thermophoresis deposition is not expected to be important due

to the small temperature differences. In fact, the nearly constant amount of PM_1 under different sampling temperature (see Figure 4-2) already indicates that the effect of thermophoresis deposition is negligible under the experimental conditions.

Coagulation of fine particles appears to be the key mechanism as it does not change the total PM_1 mass but only shift the PSD of PM_1. Coagulation process is also influenced by temperature.[266] As flue gas temperature decreases, the flue gas velocity decreases, resulting in enhanced relative motions among the particulate particles, and consequently, the coagulation process is enhanced. This is indeed the case as seen in Figure 4-3 which shows a progressive growth of particle size in PM_1 as sampling temperature decreases. Coagulation of fine particles is also accelerated by the sulfuric acid droplets at the sampling temperature below "turning point" temperature (also SO_3 dew point temperature as discussed), although SO_3 condensation contributes little to the PM_{10} yield. The accelerated coagulation causes a significant shift of particle mass to larger size in PM_1 (see Figure 4-3). As discussed, the "turning point" temperature in PSD curves correlates well to the calculated SO_3 dew point. Therefore, SO_3 condensation plays an important role in the coagulation process and therefore the effect of sampling temperature on the properties of collected PM_1.

Further elemental analysis shows that the total amounts of Na, K, and Cl in PM_1 are nearly constant at all the sampling temperatures (see Figure 4-5). The shifts of size distribution curves of these elements at different sampling temperatures (see Figure 5) is therefore most likely due to the coagulation of Na-, K-, and Cl-containing particles. So is the mass shift of S in a size range of 0.03 to 0.38 μm (see Figure 4-4f). Therefore, all the data suggest that coagulation of fine particulate matter is the key mechanism responsible for the shifts of PSD and elemental mass size distribution curves of PM_1.

The coagulation process seems to be also influenced by the concentration of

particulate matter in flue gas. Figure 4-8 is based on the data in Figure 4-3 and clearly shows as the biomass feeding rate increases from 0.1 to 0.3 g/min (i.e. Case-0.1 and Case-0.3, corresponding to an increase in the PM concentration in the flue gas by 3 times), the particle mass shifts to larger size in PM_1 when the particle number concentration increases at the sampling temperature of 25 and 40 °C. However, such an effect diminishes at a sampling temperature close to the flue gas temperature (115 °C), suggesting that a sampling temperature close to the flue gas temperature is required in order to suppress particle coagulation. Although the PM_{10} yield is nearly constant for both Case-0.1 and Case-0.3, the PM_1 yield in Case-0.3 is slightly lower and the PM_{1-10} yield is slightly higher compared to those in Case-0.1 (see Figure 4-2), suggesting that some fine particles in PM_1 have coagulated with coarse particles in PM_{1-10} due to the higher PM concentration in Case-0.3.

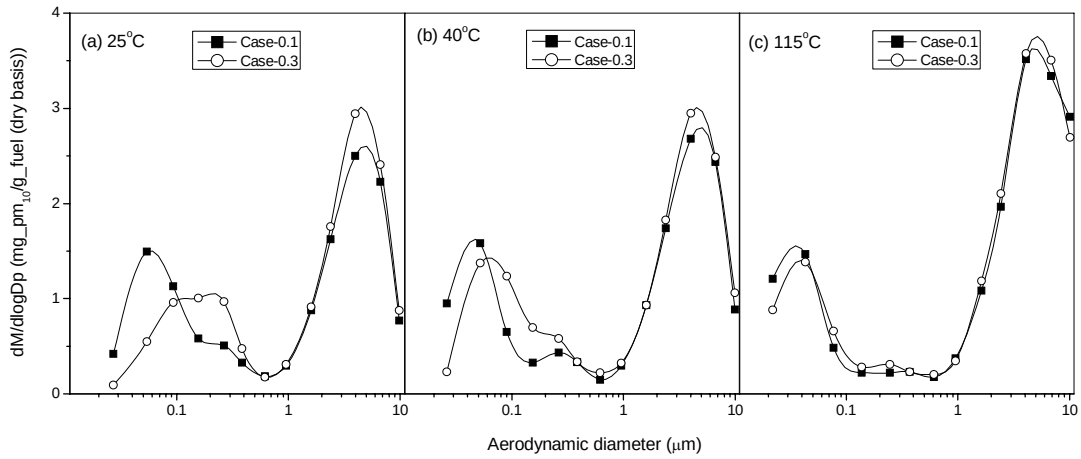

Figure 4-8: Effect of biomass feeding rate on PSD curves at different sampling temperatures: (a) 25°C, (b) 40°C, (c) 115°C

Gravitational settling deposition affects more on coarse particles.[88] In fact, as the sampling temperature decreases, the particle loss caused by gravitational settling deposition increases as a result of decreasing flue gas velocity, resulting part of in an increasing loss of PM before the PM_{10}-containing flue gas enters into the DLPI. This is indeed the case as both the yield of PM_{1-10} and the mass of Mg and Ca in PM_{1-10} decreases with decreasing sampling temperature (see Figures 4-2 to 4-5). The similar

trend of PSD curves at the sampling temperature of 105°C and 115°C (see Figure 4-3) further suggests that in order to eliminate the influence of gravitational settling deposition on the collection of PM_{1-10}, the sampling temperature must be close to or same as the flue gas temperature (115°C).

4.6 Conclusions

The experimental data in this Chapter clearly demonstrate the significant effects of sampling temperature on the collection of PM_{10} and its properties. Coagulation of fine particles appears to be the key mechanism responsible for the shift of PM_1 mass to larger size as the sampling temperature decreases, although the total yield of PM_1 remains unchanged. The chemical composition of PM_1 is dominantly Na, K and Cl and the mass distribution of these elements also shifts to larger size in PM_1 as the sampling temperature decreases, as results of the coagulation of Na-, K, and Cl-containing fine particles. However, the PM_{1-10} contains dominantly of Mg and Ca, the mass PM_{1-10} and the mass of Mg and Ca in PM_{1-10} increases with increasing sampling temperature and levels off at a sampling temperature close to the flue gas temperature (115°C). The reduction in the collection of Mg- and Ca-containing coarse particles in PM_{1-10} as the sampling temperature decreases appears to be mainly due to gravitational settling deposition. The "turning point" temperature of PSD and elemental mass size distribution curves seems to correlate well with the SO_3 dew point of the flue gas. Therefore, to ensure the proper collection of PM_{10}, the sampling temperature should be above the flue gas acid dew point temperature to prevent acid gas condensation and furthermore be kept at a temperature close to or same as the flue gas temperature.

CHAPTER 5 EMISSION BEHAVIOR AND CHARACTERISTICS OF PM_1 AND PM_{10} FROM THE COMBUSTION OF PULVERIZED BIOCHAR IN A DROP-TUBE FURNACE

5.1 Introduction

As discussed in Section 2.2 of Chapter 2, mallee biomass is an important second-generation renewable feedstock for the future energy security and sustainable development in rural and regional Australia, because of the fact that it is a byproduct of dryland salinity management of premium agriculture land and enhances (rather than compete with) food production.[5, 8] The production of mallee biomass is of large-scale, economic and has small carbon and energy footprints.[4-7] However, the major hurdles that limit the use of biomass as fuel are the biomass's bulky nature, high moisture content, high transport cost and poor grindability.[18-22]

As biomass is typically produced/available in rural and regional areas, an attractive utilisation strategy to address aforementioned issues is to deploy distributed pyrolysis as a flexible technology[63-67] to convert the bulky raw biomass locally into high-energy-density fuels such as bio-oil[64, 65, 68, 69] and/or biochar.[14, 67, 70] While bio-oil can be transported to centralized plants and has the potential for further upgrading and refining to produce liquid transport fuels,[64, 65, 71] biochar as a solid fuel has superb fuel properties, good grindability and high energy density therefore is suitable for applications such as gasification and combustion, as well as co-firing in coal-based power stations.[14, 70, 72]

Direct biomass combustion or co-firing biomass with coal are matured technologies[18-22] for power generation and promising short-term solutions for

reducing CO_2 emission from power generation. However, biomass combustion/co-firing contributes significantly to the fine particulate matter (PM) emission[26, 41, 84-86, 98, 101, 264, 267], especially submicron particles (PM_1) which are easy to escape from dust cleaning equipment. Biochar also contains abundant inherent inorganic species[72, 268, 269] that may potentially lead to significant PM emission. However, while the emission behaviour of PM_1 and PM_{10} (PM with an aerodynamic diameter less than 10.0 μm) from raw biomass combustion were investigated previously,[28, 97, 98] little work has been done so far on PM_{10} emission from biochar combustion.

Therefore, a good understanding on the emission behaviour and characteristics of PM_1 and PM_{10} from biochar combustion is important to practically utilising biochar is used as a fuel in direct combustion or co-firing applications. The key objective of Chapter 5 is therefore to carry out a systematic investigation on the properties of PM_1 and PM_{10} emitted from the combustion of biochars (produced from biomass pyrolysis under controlled conditions relevant to practical biochar production) in a laboratory-scale drop-tube furnace system, to address the second research objective listed in Chapter 2.

5.2 Biochar Yields and the Retention of AAEM Species and Cl in Biochars

The fuel properties of raw biomass and its derived biochars are shown in Table 5-1 and Table 5-2. It can be seen that the inorganic species in these fuels are dominantly AAEM species and Cl, with very low contents of Al and Si. It should be noted that the S contents in both raw biomass and biochars are also very low, with an extremely low S/Cl ratio of ~0.1 in raw biomass, the sulphation effect of S plays insignificant role because a much higher S/Cl ratio (from 4.7 to 7.5) is required to cause significant sulphation reactions during biomass combustion.[157] Therefore, such unique features of the fuel samples simplify the study as the chemical composition analysis can be focused on AAEM species and Cl.

Table 5- 1: Proximate and ultimate analysis of raw biomass and its derived biochars used in this study (SH-Char-xxx: biochar prepared from the slow heating pyrolysis of biomass at xxx °C; FH-Char-xxx: biochar prepared from the fast heating pyrolysis of biomass at xxx °C)

Samples	Raw Biomass	SH–Char–400	SH–Char–450	SH–Char–500	SH–Char–550	FH–Char–400	FH–Char–500
				Proximate Analysis			
M[a], % ad	5.6	5.8	4.0	4.4	3.1	5.1	4.6
Ash, % db	4.0	9.0	10.8	11.3	12.0	10.3	13.7
VM[b], % db	74.2	34.1	26.6	24.3	19.3	39.6	31.9
FC[c], % db	21.8	56.9	62.6	64.4	68.7	50.1	54.4
				Ultimate Analysis (% daf)			
C	51.02	74.95	82.85	85.12	88.98	72.07	80.18
H	5.61	3.61	3.25	2.92	2.39	3.77	3.22
N	0.26	0.51	0.56	0.66	0.64	0.63	0.66
S	0.02	0.04	0.02	0.03	0.02	0.04	0.06
Cl	0.17	0.02	0.01	0.02	0.01	0.07	0.24
O[d]	42.92	20.87	13.31	11.25	7.96	23.42	15.64
				Lower Heating Value (LHV) (MJ/kg, ad)			
	17.2	24.1	25.7	26.1	27.4	23.6	23.4

[a] moisture; [b] volatile matter; [c] fixed carbon; [d] by difference; [e] not detected.

Table 5- 2: Contents (wt% db) of inorganic species in raw biomass and its derived biochars used in this study (SH-Char-xxx: biochar prepared from the slow heating pyrolysis of biomass at xxx °C; FH-Char-xxx: biochar prepared from the fast heating pyrolysis of biomass at xxx °C)

Samples	Inorganic species content (wt% db)							
	Na[a]	K[a]	Mg[a]	Ca[a]	Al[b]	Si[b]	Fe[b]	P[b]
Raw Biomass	0.2550	0.1407	0.0869	1.3937	0.0017	0.0021	0.0016	0.0257
SH–Char–400	0.6360	0.3108	0.2118	3.6168	0.0077	0.0102	0.0182	0.0626
SH–Char–450	0.7465	0.3238	0.2450	3.8316	0.0062	0.0149	0.012	0.0672
SH–Char–500	0.7424	0.3668	0.2333	4.2265	0.0047	0.0196	0.0057	0.0717
SH–Char–550	0.8477	0.3704	0.2721	4.175	0.0053	0.0134	0.0049	0.0722
FH–Char–400	0.7082	0.3472	0.2179	3.9313	0.0059	0.0071	0.0041	0.0726
FH–Char–500	0.9677	0.4236	0.3187	5.5712	0.0132	0.0108	0.0103	0.1086
FH–Char–800	0.7519	0.4866	0.5191	7.994	0.0151	0.022	0.0493	0.1017
FH–Char–900	0.6097	0.5763	0.622	9.5566	0.0154	0.0309	0.0599	0.1248
FH–Char–1000	0.3768	0.5083	0.6635	9.2845	0.0198	0.042	0.0928	0.1368

[a] analyzed by IC; [b] analyzed by ICP-AES.

Figure 5-1 shows the biochar yields from pyrolysis of raw biomass at various conditions on a dry basis. As expected, at a given pyrolysis temperature, a higher biochar yield is obtained in slow pyrolysis in comparison to that of fast pyrolysis. A higher pyrolysis temperature also leads to a lower biochar yield, in either slow or fast pyrolysis of biomass. Therefore, "SH–Char–400" (i.e. the biochar produced from slow pyrolysis at 400 °C, see Section 3.3.4.1 in Chapter 3) has the highest biochar yield of ~37.0% while the "FH–Char–500" (i.e. the biochar produced from fast pyrolysis at 500 °C) has the lowest yield of ~26.7%.

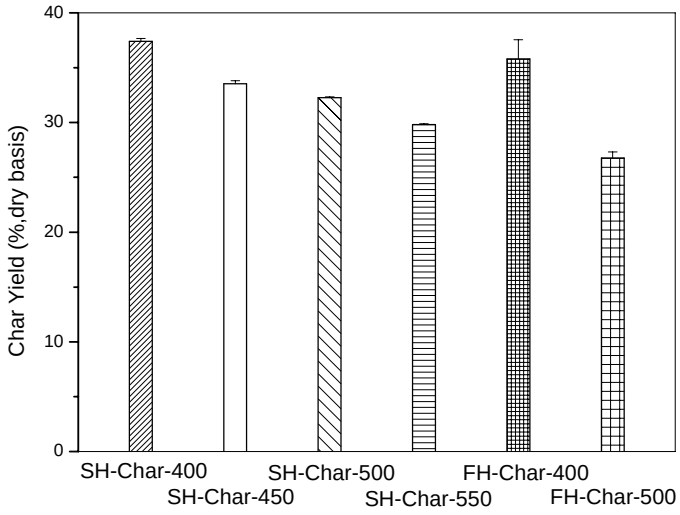

Figure 5-1: Biochar yields from the pyrolysis of raw biomass under various conditions

Figure 5-2 further shows the retention of AAEM species and Cl in the biochars after biomass pyrolysis under various conditions. It is clear that after pyrolysis, the majority of the AAEM species in biomass have been retained in the biochars, with retentions of AAEM species around 78.5 – 100.0%. This is also expected given the low pyrolysis temperatures (400 – 550 °C). Even at such low temperatures, a small proportion of AAEM species were volatilised. Such a phenomenon is known to be possible due to the volatilisation of AAEM species along with the release of carboxylate structures during pyrolysis, as observed in previous studies.[126, 270] Ca has the highest retention of around 92.2 – 100.0% while K appears to have the lowest

retention of around 78.5 – 88.3%. Contrary to AAEM species, the majority of Cl was volatilised at such low temperature as 400 – 550 ^{o}C during the pyrolysis of raw biomass, with retentions of around 2.0 – 33.4%. It is also interesting to note that the retentions of Cl in fast pyrolysis are higher than those of slow pyrolysis. Particularly, for fast pyrolysis at 500 ^{o}C, Cl retention is ~33.4%, possibly due to the strong interactions between Cl and char matrix during pyrolysis.[130]

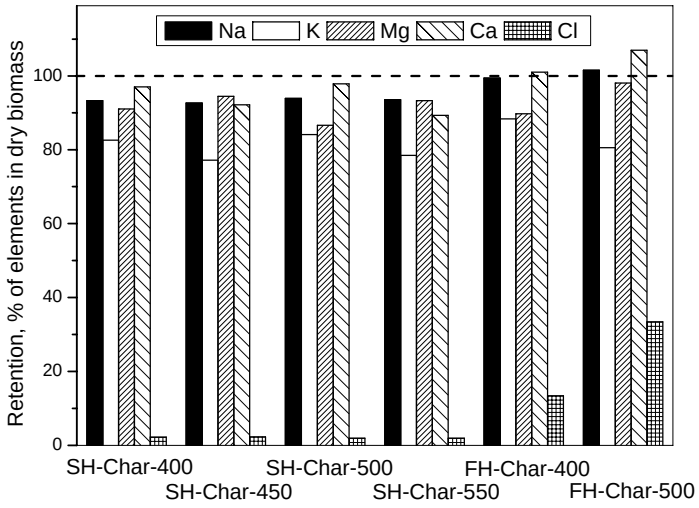

Figure 5- 2: Retentions of AAEM species and Cl in biochars produced from the pyrolysis of raw biomass at different conditions

5.3 PM_1 and PM_{10} Yields during the Combustion of Biomass and Biochars

Figure 5-3 presents the data on PM_{10} yields from the combustion of the raw biomass and its derived biochars. For meaningful comparisons, it is important to note that the PM_{10} yields are normalized to three different bases (i.e. equivalent biomass, ash and energy input) and presented in Figure 5-3a–b, Figure 5-3c–d and Figure 5-3e–f, respectively.

Figure 5-3a–b presents the PM_1 and PM_{10} emission data normalized to the equivalent amount of starting raw biomass (db), enabling to provide insights into the effect of pyrolysis as a technology for biomass pretreatment (i.e. for biochar production) on PM emission during biomass/biochars combustion. It is interesting to note that at an

equivalent amount of raw biomass, the PM_1 yields from the combustion of biochars are substantially lower than that from direct raw biomass combustion (see Figure 5-3a). Clearly, the use of biochars from the biomass pyrolysis in fuel applications may lead to substantial reduction in PM_1 emission, likely related to the removal of volatiles (including the released inorganic species). One exception is in the case of fast-heating char at 500 °C, the PM_1 yield is higher than other chars, implying fuel properties may also play an important role. On the contrary, the PM_{10} yields from the combustion of biochars are higher than that from direct biomass combustion (see Figure 5-3b). As the PM_1 yields during biochars combustion are reduced, such significant increases in PM_{10} yields are clearly due to the increase in the yields of coarser particulates with an aerodynamic diameter between 1 and 10 μm (PM_{1-10}) during biochars combustion. As supermicron PM is generally produced from char fragmentation during combustion, the results seem also to suggest that the pretreatment of the fuel via pyrolysis also leads to a significant enhancement of char fragmentation during combustion.

After low-temperature pyrolysis, the ash content of the fuel is increased substantially from 4.0% db for biomass to 9.0 – 13.7% db for biochars depending on pyrolysis conditions (see Table 3-2 of Chapter 3). Therefore, the PM_{10} yields during a fuel combustion normalized to fuel ash content will further provide some plausible indication on the ability of the unit mass of ash-forming species in the fuel for PM emission. Such data are presented in Figure 5-3c–d. It is not surprising that in this case, the shapes of Figure 5-3c–d are similar to those of Figure 5-3a–b, because the majority of ash-forming elements such as AAEM species were retained in biochars after low-temperature biomass pyrolysis (see Figure 5-2). Clearly, compared to those in the biomass, the ash-forming species in the char has a much poorer ability in PM_1 emission but a significantly enhanced ability in PM_{1-10} emission.

The substantial reductions in PM_1 yields during biochars combustion, based on an equivalent biomass mass and unit ash input, respectively, are important findings.

Such data demonstrate another good feature of using biochar as a fuel, in addition to its high-energy-density, good grindability and good fuel properties for better matching with coal in co-firing application.[14, 70] The data normalised to equivalent energy input into the furnace will be discussed in Section 5.6.

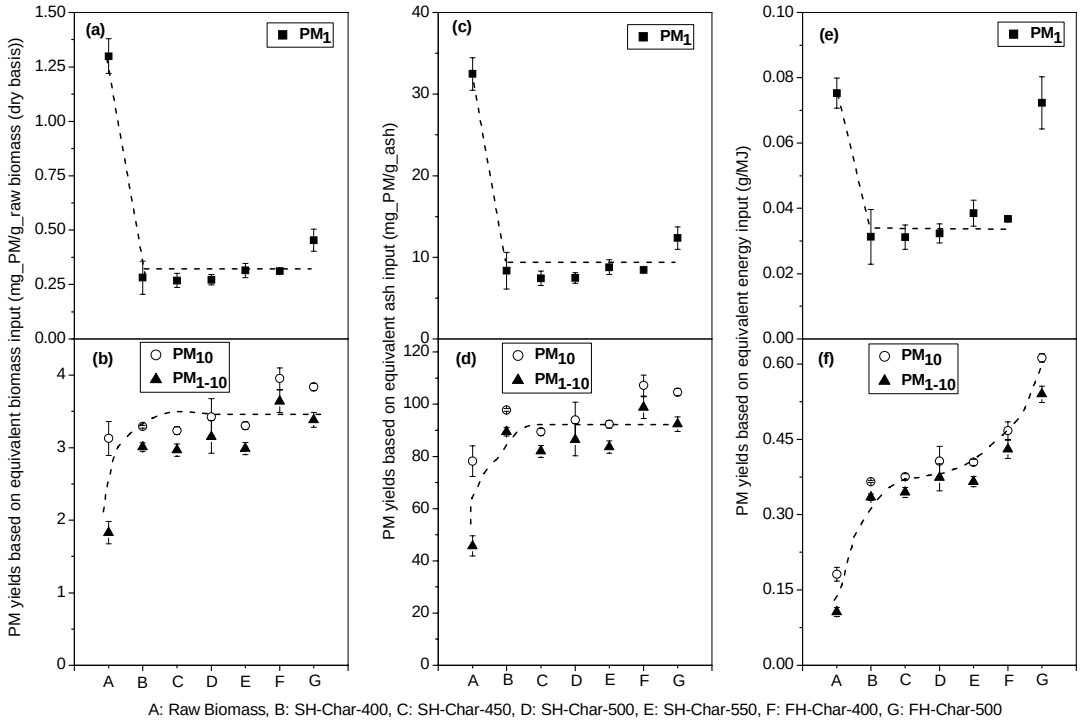

Figure 5-3: PM yields from raw biomass and biochars combustion: (a) PM_1 and (b) PM_{10} yields, normalized to equivalent biomass (db) input into the furnace; (c) PM_1 and (d) PM_{10} yields, normalized to equivalent ash input into the furnace; (e) PM_1 and (f) PM_{10} yield, normalized to equivalent energy input into the furnace. Equivalent biomass input is calculated from the char yields and the mass of biochars fed into the drop tube furnace, equivalent ash input is calculated from the mass of fuel (db) fed into furnace and its ash content (wt%, db), equivalent energy input is calculated from the lower heating value (LHV) of raw biomass and biochars and their mass (db) fed into drop tube furnace.

5.4 Mass-Based and Elemental Mass-Based Particle Size Distributions (PSDs) of PM_{10}

To further understand the characteristics of PM_{10} emission during the combustion of biomass and biochars, analyses were done to obtain the data on mass-based and elemental mass-based PSDs of PM_{10}. The data on mass-based and the elemental mass-based PSDs of PM_{10} are plotted in Figures 5-4 and 5-5, respectively.

As shown in Figure 5-4, the mass-based PSD of PM_{10} collected from raw biomass combustion normalized to equivalent raw biomass has a bimodal size distribution, i.e., a fine mode with a mode diameter of ~0.022 μm and a coarse mode with a mode diameter of ~6.8 μm. However, the PSDs of PM_{10} from biochars combustion generally show a unimodal distribution with only a coarse mode of ~6.8 μm. The fine mode generally disappears in the PM_{10} produced from biochars combustion, leading to the significantly low PM_1 yields as shown in Figure 5-3. The only exception is the PSD of PM_{10} from "FH–Char–500" combustion, which also shows a fine mode with a mode diameter less than ~0.022 μm, possibly due to the char's high Cl content as discussed in next section. Furthermore, the data on the mass-based PSDs of PM_{10} in Figure 5-4 clearly show that the significant PM_1 generated from biomass combustion dominantly contains particulate matter with a size less than 0.1 μm ($PM_{0.1}$). It is clear that the significant reductions in PM_1 emission during biochars combustion are due to the very low $PM_{0.1}$ yields for all biochar samples (see Figures 5-3a, 5-3c and Figures 5-4a, 5-4b).

Furthermore, the data on elemental mass size distributions of PM_{10} normalized to the unit mass of equivalent raw biomass (db), further show that Na, K and Cl also generally have a unimodal distribution from the combustion of both raw biomass and biochars (see Figure 5-5). Na, K and Cl are dominantly contained in PM_1 (more precisely $PM_{0.1}$) in a single mode with a mode diameter of ~0.022 μm, which is same as the mode diameter of the fine mode in the mass-based PSDs of PM_{10} (see Figure

5-4). The data on the elemental yields of AAEM species and Cl (see Figure 5-6) further demonstrates the dominant presence of Na, K and Cl in PM_1 is most likely due to the known mechanisms such as homogeneous nucleation and/or heterogeneous condensation of the Na, K and Cl-containing vapours on fine particulates.[28, 84, 85, 88, 254]

Additionally, the data in Figure 5-5 also show that Mg and Ca also have a unimodal distribution in PM_{10} from the combustion of both raw biomass and biochars. However, Mg and Ca are concentrated in $PM_{1\text{-}10}$ in a single mode with a mode diameter of ~6.8 μm which is also same as the coarse mode in the mass-based PSDs of PM_{10} (see Figure 5-4). The data in Figure 5-6 clearly show that the $PM_{1\text{-}10}$ are mainly produced from the refractory elements (Mg and Ca) in the burning char particles, in agreement with previous studies.[28, 84, 85, 254]

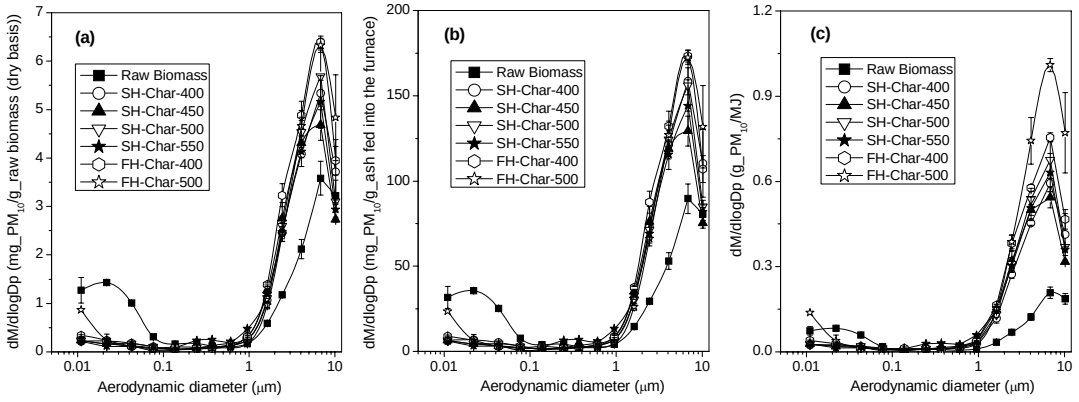

Figure 5-4: Particle size distribution of PM_{10} from the combustion of raw biomass and biochars: (a) graphs normalized to equivalent biomass (db) input into the furnace, (b) graphs normalized to equivalent ash input into the furnace, and (c) graphs normalized to equivalent energy (LHV) input into the furnace

Not only the PM_1 yield (see Figures 5-3 and 5-4), but also the mass of Na, K and Cl which are dominantly contained in PM_1 are substantially reduced during biochars combustion in comparison to those from raw biomass combustion (see Figures 5-5a–c, f–h). As Na, K and Cl are dominantly contained in $PM_{0.1}$, such particle mass

and elements (Na, K and Cl) mass reductions in PM_1 mainly take place in the ultra fine particles ($PM_{0.1}$). Oppositely, the data in Figure 5-4 demonstrate a substantial increase in the mass of PM in the size range of 1.6 – 10.2 μm (with a mode diameter of 6.8 μm) from biochars combustion in comparison to that from raw biomass combustion. As shown in Figures 5-5d–e, i–j, such increases in the coarse PM yields are due to the substantial increases in the mass of Mg and Ca in $PM_{1\text{-}10}$ within the size range of 1.6 – 10.2 μm.

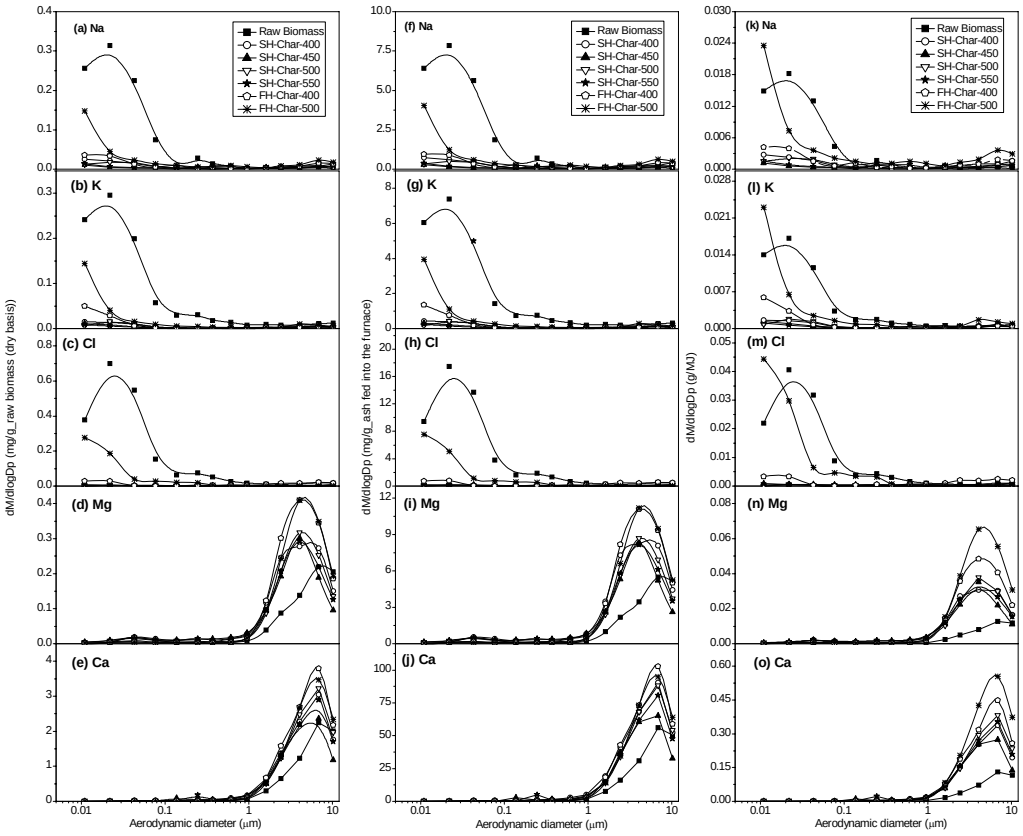

Figure 5-5: Elemental mass size distribution of AAEM species and Cl in PM during the combustion of raw biomass and biochars: (a) Na, (b) K, (c) Cl, (d) Mg and (e) Ca are normalized to the equivalent biomass (db) input into the furnace; (f) Na, (g) K, (h) Cl, (i) Mg and (j) Ca are normalized to the equivalent ash input into furnace; (k) Na, (l) K, (m) Cl, (n) Mg and (o) Ca are normalized to the equivalent energy input (LHV) into the furnace.

5.5 Further Discussion

Considering the data in sections 5.2–5.4 together, the possible mechanisms responsible for the significant discrepancies in the emission characteristics of PM_1 and PM_{10} from the combustion of raw biomass and biochars may be deduced. A key difference between biomass and biochars as fuels is the removal of volatiles (including released inorganic species) during biomass low-temperature (400 – 550 °C) pyrolysis for biochar production. Furthermore, it should be noted that during biomass pyrolysis for biochar preparation, the majority of the AAEM species (78.5 – 100.0%) are retained in biochars (see Figure 5-2). However, the AAEM species retained in the biochars, although in substantial amounts, are not responsible for the significantly higher $PM_{0.1}$ yield during the combustion of raw biomass, as the contribution of biochars combustion to $PM_{0.1}$ yield is limited (see Figures 5-4a–b). In other words, the combustion of volatiles (including the released inorganic species) seems to be the dominant mechanism for $PM_{0.1}$ formation, although there are only small proportions (7 – 20%) of Na and K released with volatiles during pyrolysis (see Figure 5-2). Therefore, the significant reductions in PM_1 (or $PM_{0.1}$) yields and the mass yields of Na, K and Cl (dominantly contained in $PM_{0.1}$) from biochars combustion in comparison to those from raw biomass combustion (see Figures 5-3–5-6) are most likely due to the lack of the contribution of volatiles (including the released inorganic species) combustion to PM_1 formation, although majority of AAEM species are retained in the biochars.

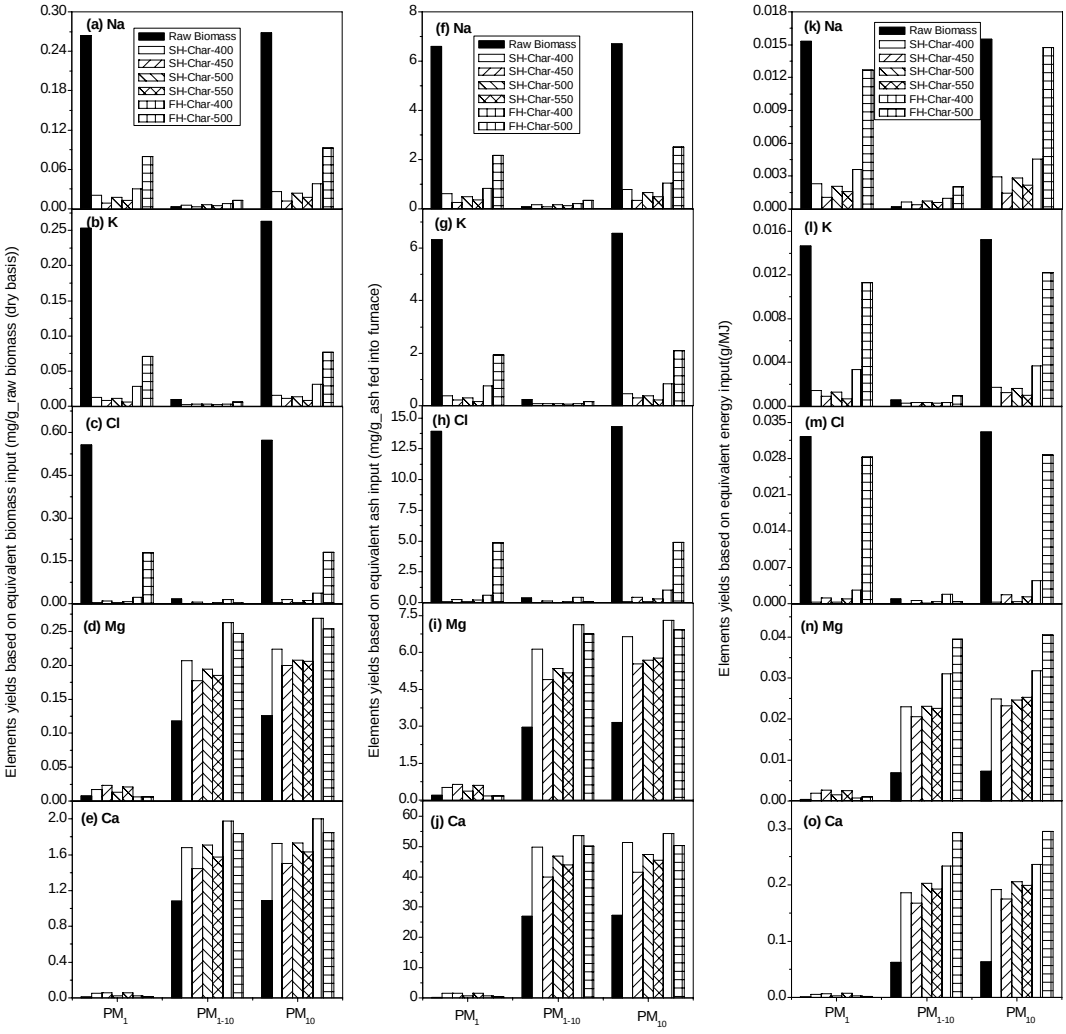

Figure 5-6: Elements yields of AAEM species and Cl in PM during the combustion of raw biomass and biochars: (a) Na, (b) K, (c) Cl, (d) Mg and (e) Ca, normalized to equivalent biomass (db) input into the furnace; (f) Na, (g) K, (h) Cl, (i) Mg and (j) Ca, normalized to equivalent ash input into furnace; (k) Na, (l) K, (m) Cl, (n) Mg and (o) Ca, normalized to equivalent energy input (LHV) into the furnace.

As $PM_{0.1}$ contains dominantly Na, K and Cl (see Figure 5-5), further analyses clearly show that the molar ratios of (Na+K)/Cl in samples collected in related different DLPI stages (that make up $PM_{0.1}$) from raw biomass combustion are all close to 1 (see Figure 5-7), suggesting that the $PM_{0.1}$ generated from raw biomass combustion is mainly composed of alkali (Na and K) chlorides. This also demonstrates the important role of Cl in the formation of ultra fine PM. It is known that Cl is a key

element that can substantially enhance the volatilization of alkali metals during biomass pyrolysis.[126] Furthermore, the formation of alkali chloride is also stable under combustion conditions,[142] leading the subsequent formation of ultra fine PM via either homogeneous nucleation and/or heterogeneous condensation of the alkali chloride vapors on small particles.[28, 84, 85, 88, 254] Figure 5-2 clearly shows that the majority (66.6 – 98.0%) of Cl were volatilised as part of volatiles during preparation of biochars even at 400 ^{o}C. Therefore, the removal of volatiles during low-temperature pyrolysis of biomass for biochars production leads to not only the lack of the contribution of volatiles combustion during biochars combustion but also the lack of Cl in the fuels. This reduces the volatilization of Na and K during biochars combustion, in despite of the abundant Na and K were retained in biochars (see Figure 5-2), consequently, the PM_1 yields from biochars combustion are substantially reduced. Such reasoning also seems to be consistent with the higher PM_1 yield during the combustion of fast pyrolysis biochar produced at 500 °C as this char has a substantially higher Cl content.

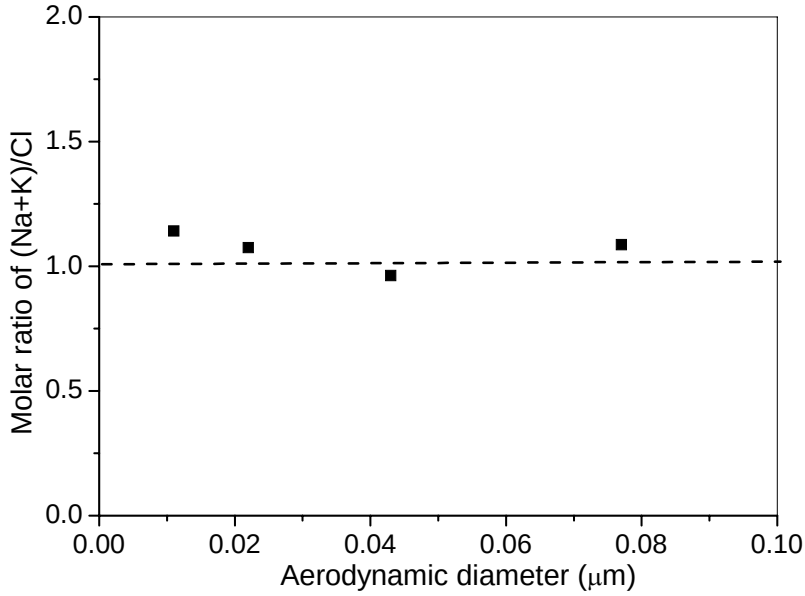

Figure 5-7: Molar ratio of (Na+K)/Cl in $PM_{0.1}$ collected from raw biomass combustion

For PM_{1-10}, it is clearly seen in Figures 5-3 to 5-6 that there are substantial increases in the yields of PM_{1-10} which dominantly contains Mg and Ca. Particularly, when normalised to equivalent ash input into the furnace (see Figures 5-4b and Figures 5-5i–j), the data clearly demonstrate that the contribution of Mg and Ca for PM_{1-10} emission is significantly enhanced during biochars combustion. As already normalised to ash content, the data suggest that such a significant increase must be related to an enhanced char fragmentation during combustion, as results of changes in char structure. During char combustion, char fragmentation followed by the release of refractory elements in the burning char is known as a principle mechanism responsible for the formation of PM_{1-10} from both coal and biomass combustion.[28, 84, 85, 212, 254, 271] Previous investigations showed that the fragmentation of char is strongly dependent on the char structure.[212] An increase in char macroporosity[212] and surface area[271] can lead to intensified fragmentation of porous chars. Therefore, further experiments and analysis were then carried out to prepare and characterise the structure of the chars. It should be noted that because the combustion of biomass and biochars were undertaken at 1300 °C, only the chars prepared from the pyrolysis of the fuels (biomass and biochars) at 1300 °C are relevant, using the same drop-tube furnace under similar conditions (with argon as carrier gas instead of air). Indeed, as shown in Figure 5-8, the micropore surface area of chars produced from biochars are much higher than that from biomass under pyrolysis conditions pertinent to the combustion conditions. Therefore, the substantial increases in the yields of PM_{1-10} during biochars combustion are likely due to the enhanced char fragmentation resulting from more porous chars from the pyrolysis of biochars under the combustion conditions, in comparison to that from biomass.

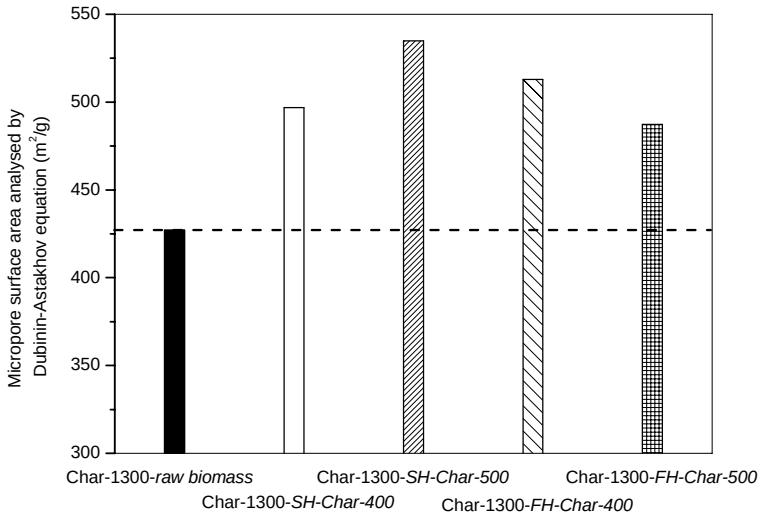

Figure 5-8: Micropore surface area of biochars produced from the fast pyrolysis of raw biomass, SH–Char–400, SH–Char–500, FH–Char–400 and FH–Char–500 at 1300 ^{o}C in the DTF, analysed by Dubinin-Astakhov equation

5.6 Practical Implications

From a practical point of view, it becomes more important to assess the ability of a particular fuel in PM_1 and PM_{10} emissions, normalized to the unit useful energy (lower heating value) input into the furnace. Such results are presented in Figures 5-3e–f (for PM_1 and PM_{10} yield), Figures 5-6k–o (for elemental yields in PM_1 and PM_{10}), Figure 5-4c (for mass-based PSDs) and Figures 5-5k–o (for elemental mass-based PSDs). There are three important observations of practical significance can be made based on the data presented in these figures.

First, per unit energy input, as shown in Figures 5-3e, the PM_1 yields from biochars combustion may have considerable reductions compared to that from raw biomass combustion. On an elemental basis, as shown in Figures 5-6k–m, substantial reductions in the yields of Na, K and Cl in PM1 are observed. Again, one exception is the fast pyrolysis char prepared at 500 °C that has a high PM_1 yield, possibly related to the high Cl content in the char. As almost all of the PM_1 are actually $PM_{0.1}$ (see Figure 5-4c and Figures 5-5k–m), the data clearly demonstrate the potential

advantage of using biochar as a fuel (via pyrolysis as a fuel pretreatment technology) in effective reduction of submicron (and ultrafine) PM emission during combustion. This has important practical implications because it is known that the PM_1 can easily escape from dust cleaning equipment. Therefore, while bio-oil is a product from biomass pyrolysis for further upgrading and refining to produce liquid transport fuels, the use of the other product – biochar as a fuel offers a simple alternative solution for reducing the release of alkali metal vapors and subsequent PM_1 emission during combustion, in comparison to other strategies such as removing alkali in the fuel by washing[127] or adding kaolin.[106]

Second, during biochars combustion, the substantial reductions in PM_1 yields are however accompanied with substantial increases in PM_{1-10} emission. For example, per energy input basis, the combustion of "SH–Char–400" and "FH–Char–500" results in increases of PM_{10} yields by 100% and 240% (see Figure 5-3f), respectively, in comparison to that from biomass combustion. The substantial increases in PM_{10} yields are also reflected in the significant increases in the yields of Mg and Ca in PM_{10} (see Figures 5-6n–o). Therefore, such increases in PM_{1-10} emission during biochars combustion are likely to increase the load of dust cleaning equipment.

Third, it is also noteworthy that on an equivalent energy input basis, the mass yields of PM_{1-10} (see Figure 5-3f) and the yields of dominant elements in PM_{1-10} (Mg and Ca, see Figures 5-6n–o) during the combustion of different biochars are significantly different. As shown in Figure 5-8, after pyrolysis at 1300 °C, the selected four biochars, "Char–1300–SH–Char–400", "Char–1300–SH–Char–500", "Char–1300–FH–Char–400" and "Char–1300–FH–Char–500" have similar values of surface area, therefore the differences in char structure do not seem to be the reason. A close investigation reveals that different biochars are significantly different in energy-based ash loading, i.e. the amount of ash input into the furnace during combustion normalised to equivalent energy input. The energy-based PM_{1-10} yields during biochars combustion are then plotted again the energy-based ash loading, as

presented in Figure 5-9. A strong correlation between the two is clearly evidenced. Such reasoning is plausible as more ash inputs would have led to higher PM_{1-10} emissions.

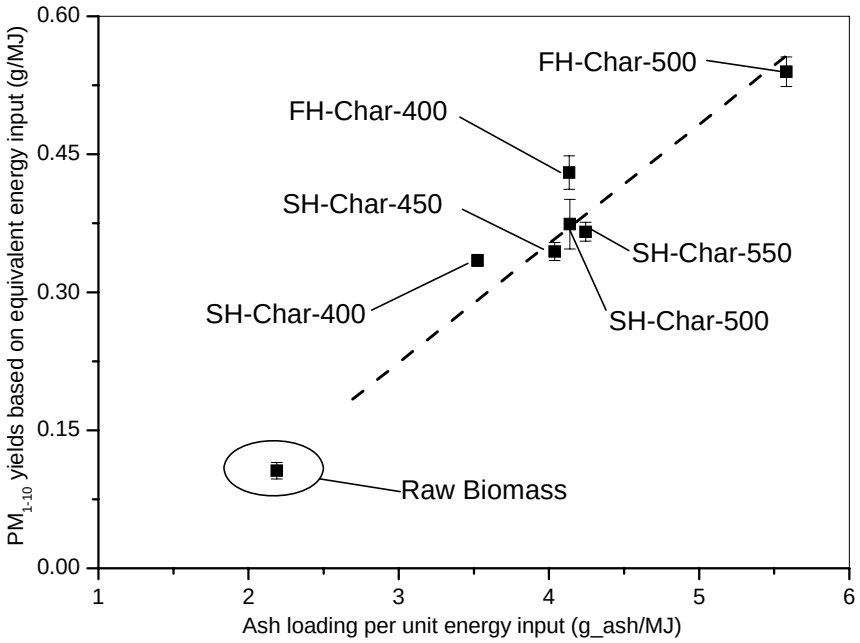

Figure 5-9: The relationship between energy-based ash loading of fuels and energy-based yields of PM1-10 collected from the combustion of raw biomass and biochars

5.7 Conclusions

This Chapter investigates the emission behavior and characteristics of PM_1 and PM_{10} during the combustion of biomass and its derived biochars (produced from low-temperature pyrolysis at both slow- heating (at 400, 450, 500 and 550^oC) and fast-heating rates (at 400 and 500 ^oC)) using a laboratory-scale drop-tube furnace system. The major conclusions are drawn as follows:

(1) The biochar yields during biomass pyrolysis range from 26.7 to ~37.0% depending on pyrolysis conditions. At such low temperatures, the majority (78.5 – 100.0%) of AAEM species are retained in biochars after pyrolysis, while the

retention of Cl in biochars is only 2.0 – 33.4%.

(2) The PSD of PM_{10} from raw biomass combustion has a bimodal size distribution, i.e., a fine mode (mode diameter: ~0.022 μm) and a coarse mode (mode diameter: ~6.8 μm). However, the PSDs of PM_{10} from biochars combustion generally show a unimodal distribution with only a coarse mode (mode diameter: ~6.8 μm).

(3) The combustion of biochars leads to substantial reductions in both PM_1 yields and the mass of Na, K and Cl in PM1 in comparison to direct biomass combustion, such reduction is most likely due to the lack of the contribution of volatiles (including released inorganic species) combustion to PM_1 formation and the volatilisation of Cl during low-temperature pyrolysis of biomass for biochars preparation.

(4) Biochars combustion also results in significant increases in the yields of PM_{1-10} and the mass of Mg and Ca in PM_{1-10} compared with those from raw biomass combustion, most likely due to the significant changes in char structures.

(5) Based on an equivalent energy input into furnace, there is a strong correlation between the energy-based PM_{1-10} yields and the energy-based ash loading during biochars combustion. An increase in biochar ash loading leads to a significantly increased PM_{1-10} emission.

CHAPTER 6 COMBUSTION OF VOLATILES PRODUCED IN SITU FROM THE FAST PYROLYSIS OF WOODY BIOMASS: DIRECT EVIDENCE ON ITS SUBSTANTIAL CONTRIBUTION TO PM_1 EMISSION

6.1 Introduction

Previous studies[28, 84-86, 88, 97, 254] suggested that during the combustion of solid fuels including biomass, PM_1 are mainly formed from the constituents (e.g., Na, K, S, Cl and heavy metals) that are easily vaporized, followed by homogeneous nucleation and/or heterogeneous condensation of these inorganic vapors. However, as fuel particles are injected into the reactor, pyrolysis of biomass particles takes place as the first step to produce volatiles and chars for combustion. The present understanding on PM_1 emission from biomass combustion is largely on that from the whole biomass combustion, including the contributions from the combustion of both volatiles and char. Little is known on which of the two (volatiles combustion and char combustion) plays a more important role in PM_1 emission.

Chapter 5 investigated PM_1 and PM_{10} emission from the combustion of pulverized biochars at 1300 °C in a drop-tube furnace. The biochars were produced from low-temperature biomass pyrolysis at 400 – 550 °C which is considered to be a preprocessing technology for upgrading biomass fuels. The results in Chapter 5 show that biochar combustion leads to substantial reductions in the yield of PM_1 in comparison to raw biomass combustion. Inorganic elements were also previously identified in carbon-rich submicron particles produced from the pyrolysis of five bituminous coals, collected by a low-pressure impactor.[234] In a quasi one-dimensional pulverized coal combustor[272], PM in the ultrafine mode and intermediate mode were collected from coal flame zone. Previous studies were also

carried out to understand aerosol formation from various stages in an updraft fired fixed-bed combustor, ranging from hot flame zone to flue gas channel during the combustion of wood pellets via spatially resolved measurements.[273, 274] These experimental data all imply that the combustion of volatiles may play an important role in PM_1 emission during solid fuels combustion. Unfortunately, thus far there has been no work done to provide direct experimental evidence on the contribution of volatiles combustion to PM_1 emission during solid fuels combustion.

Therefore, it is the objective of Chapter 6 to carry out a series of experiments for obtaining direct experimental evidence on the significant contribution of volatiles combustion to PM_1 emission during pulverized woody biomass combustion. A novel two-stage pyrolysis/combustion reactor system was designed to achieve the combustion of the volatiles (at 1300 °C), which were produced in situ from fast pyrolysis of a mallee bark biomass at 800 – 1000 ^{o}C. PM generated from volatiles combustion only were collected by a cyclone and low pressure impactor to investigate the fundamental mechanisms responsible for PM_1 and PM_{10} emission from the combustion of pulverized woody biomass, corresponding to the third research objective outlined in Chapter 2.

6.2 Yields of Volatiles and Release of AAEM Species and Cl with Volatiles Generated in Situ from the Fast Pyrolysis of Pulverized Biomass

The fuel properties of raw biomass and its derived char samples are shown in Tables 6-1 and 6-2. It can be seen that the inorganic species in these fuels are dominantly AAEM species and Cl, with very low contents of Al and Si. Therefore, such unique features of the fuel samples simplify the study as the chemical composition analysis can be focused on AAEM species and Cl.

Table 6- 1: Proximate and ultimate analysis of raw biomass and its derived biochars used in this study (Char-xxx: char prepared from the fast heating pyrolysis of biomass at xxx °C)

Samples	Raw Biomass	Char–800	Char–900	Char–1000
M[a], % ad	5.6	4.1	3.4	3.1
Ash, % db	4.0	23.7	26.8	31.7
VM[b], % db	74.2	14.7	13.0	11.6
FC[c], % db	21.8	61.6	60.2	56.7
C	51.02	94.89	96.72	97.39
H	5.61	1.57	1.23	1.17
N	0.26	0.47	1.15	1.16
S	0.02	0.04	0.07	0.09
Cl	0.17	0.20	0.12	0.05
O[d]	42.92	2.83	0.71	0.14

[a] moisture; [b] volatile matter; [c] fixed carbon; [d] by difference.

Figure 6-1 presents the data on yields (db) of volatiles generated in situ from fast pyrolysis of raw biomass in the drop-tube/fixed-bed pyrolyser at 800 – 1000 °C. It is evident that an increase in pyrolysis temperature from 800 to 1000 °C leads to an increasing yield of volatiles from 83.7 to 87.4 wt% (db), corresponding to a decrease in char yield from 16.3 to 12.6% wt% (db). For low-rank fuels such as biomass or lignite, at pyrolysis temperatures > 700 °C, the yields of volatiles and char are insensitive to the pyrolysis temperature as pyrolysis would be largely completed at 700 °C.[48] Therefore, the reduction in char yields in Figure 6-1 as the pyrolysis temperature increases from 800 to 1000 °C is mainly due to the unique configuration of the drop-tube/fixed-bed pyrolyser. As the nascent chars produced from biomass pyrolysis are remained on the quartz frit, steam is continuously generated from the inherent moisture in biomass subsequently fed into the reactor and the pyrolytic

water produced from the pyrolysis of these fuel particles. Therefore, the steam produced would continuously interact with the nascent chars on the quartz frit, leading to significant in situ steam gasification of the nascent chars during pyrolysis. This phenomenon is also called "self-gasification" of char during pyrolysis as it was also observed in the pyrolysis of Collie coal in a similar reactor system.[48]

Table 6- 2: Contents (wt% db) of inorganic species in raw biomass and its derived biochars used in this study (Char-xxx: char prepared from the fast heating pyrolysis of biomass at xxx °C)

Samples	Inorganic species content (wt% db)			
	Raw Biomass	Char-800 °C	Char-900 °C	Char-1000 °C
Na[a]	0.2550	0.7519	0.6097	0.3768
K[a]	0.1407	0.4866	0.5763	0.5083
Mg[a]	0.0869	0.5191	0.6220	0.6635
Ca[a]	1.3937	7.9940	9.5566	9.2845
Al[b]	0.0017	0.0151	0.0154	0.0198
Si[b]	0.0021	0.0220	0.0309	0.0420
Fe[b]	0.0016	0.0493	0.0599	0.0928
P[b]	0.0257	0.1017	0.1248	0.1368

[a] analyzed by IC; [b] analyzed by ICP-AES.

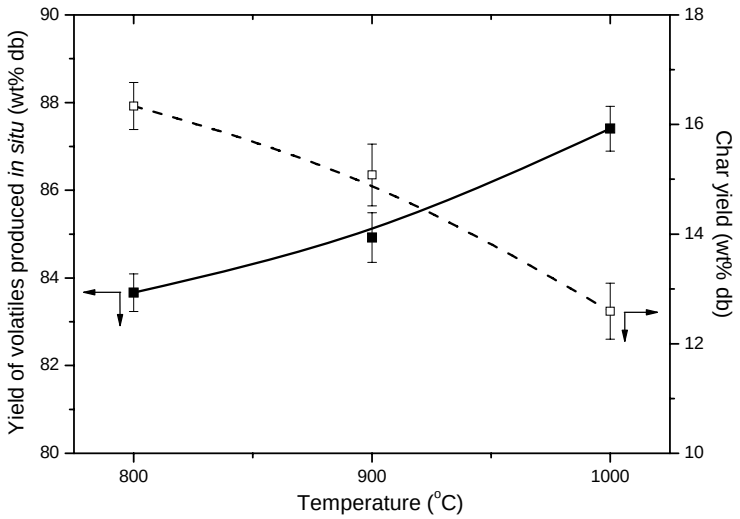

Figure 6-1: Products yields from the pyrolysis of raw biomass under various conditions

The data in Figure 6-1 clearly demonstrate that biomass processing contains dominantly reactions that are in gaseous phase. It is possible that at least a proportion of AAEM species and Cl may also likely be released and/or volatilised with the volatiles. Figure 6-2 therefore presents the release and/or volatilisation of AAEM species and Cl in the volatiles produced in situ from biomass pyrolysis under various conditions. Indeed, the release and/or volatilisation of both AAEM species and Cl can be significant under the experimental conditions and strongly dependent on temperature. A higher pyrolysis temperature leads to a substantial increase in the release and/or volatilisation of these elements with volatiles. As shown in Figure 6-2, as the pyrolysis temperature increases from 800 to 1000 ^{o}C, the release and/or volatilisation of Na, K, Mg and Ca increases from 51.8 to 81.4%, 43.5 to 54.5%, 2.5 to 9.3% and 6.3 to 16.1%, respectively. There are at least two possible mechanisms responsible. One is that as temperature increases, the chemical bonds between these species and char matrix becomes thermally unstable.[143] The other is due to the unique configuration of the drop-tube/fixed-bed pyrolyser. During continuous feeding, as nascent char produced is remained on the quartz frit, the volatiles produced from the rapid pyrolysis of the biomass particles subsequently fed into the reactor system

would continuously interact with the char on the frit, leading to the so-called "volatiles-char interactions". It is known that volatiles-char interactions are key mechanisms for the release and/or volatilisation of inorganic species during solid fuel pyrolysis and become more intensified at high temperatures.[139] Furthermore, the release and/or volatilisation of AAEM species is also strongly dependent on the valency of the inorganic species. While there are 43.5 – 81.4 % of Na and K were released into volatile phase, only small amounts (2.5 – 16.1%) of Mg and Ca were released while the majority of them were retained in char. It is known that the divalent species (Mg and Ca) are more stable than monovalent species (Na and K) during low-rank fuels pyrolysis.[143] It should be also noted that 85.2– 97.2% of Cl were volatilised during pyrolysis, suggesting the bonds between Cl and char matrix are unstable under the pyrolysis conditions. The (Na+K)/Cl molar ratios for Na, K and Cl volatilised with the volatiles are found to be 1.8 – 2.4 at 800 – 1000 ^{o}C, clearly suggesting that at least part of alkali metals (Na and K) were volatilised separately with Cl, rather than as alkali chlorides, in consistent with previous results on brown coal pyrolysis.[275]

6.3 PM_1 and PM_{10} Yields during the Combustion of Volatiles and Chars

The data in figure 6-2 demonstrate that significant amount of Na, K and Cl in biomass can be volatilised and become part of volatiles produced in situ from the pyrolysis of raw biomass even at 800 – 1000 °C. As the chemical compositions of PM_1 from biomass combustion dominantly consist of these elements, it is very likely that the subsequent combustion of these volatiles may lead to substantial PM_1 emission. However, the drop-tube/fixed-bed pyrolyser (see Figure 3-6 of Chapter 3) for generating volatiles in situ from raw biomass pyrolysis is made of quartz. It is important to note that under reducing atmosphere, SiO_2 may be reduced to form volatile SiO vapours, which can be subsequently reoxidised during combustion to form fumes as part of PM_1.[223, 276] Therefore, the contribution from such possible reactions between the quartz reactor and volatiles generated in situ to PM_1 emission

needs to be understood. In this chapter, an ash-free microcrystalline cellulose sample (Avicel PH-101, particle size: 30~50 μm) was fed into the drop-tube/fixed-bed pyrolyser of the two-stage pyrolysis/combustion reactor system to generate ash-free volatiles at 1000 ^{o}C for subsequent combustion and PM collection. It was found that the formation of PM_{10} from the combustion of the volatiles generated in situ from cellulose fast pyrolysis is negligible, as shown in Panel (a) of Figure 6-3 and Figure 6-5, which will be discussed later. Further ICP-AES analysis of the PM collected from the combustion of volatiles produced in situ from fast pyrolysis of cellulose shows that there is little Si present in those PM samples. Therefore, these data demonstrate that the effect of the potential reactions between quartz pyrolyser and volatiles on PM emission can be neglected under the experimental conditions in this chapter. The PM collected from the two-stage pyrolysis/combustion reactor system is truly contributed by the combustion of volatiles produced in situ from the pyrolysis of raw biomass under those conditions.

Figure 6-3 presents the data on the yields of PM with aerodynamic diameters in the size ranges of less than 0.1 μm ($PM_{0.1}$), 0.1 – 1 μm ($PM_{0.1-1}$), less than 1μm (PM_1), 1 – 10 μm (PM_{1-10}) and less than 10 μm (PM_{10}), respectively, from the combustion of volatiles and chars produced from raw biomass fast pyrolysis at 800 – 1000 °C. It is important to note that the total PM_{10} yields are calculated as the sum of those from volatiles and chars combustion, benchmarking against that from the direct combustion of raw biomass in the DTF under the same combustion conditions. The PM yields are normalized to the equivalent amount of starting raw biomass (db), as shown in panel a, b, and c of Figure 6-3, respectively. Several important points can be observed from the data in Figure 6-3.

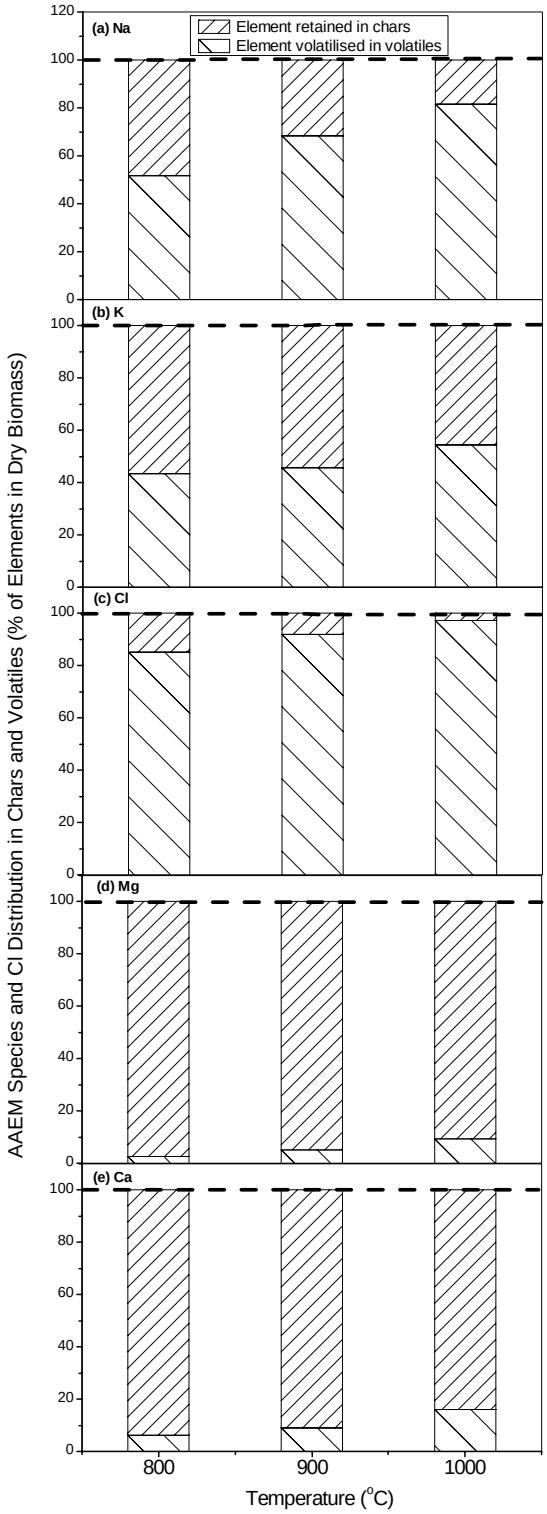

Figure 6-2: Distribution of AAEM species and Cl in chars and volatiles during the pyrolysis of raw biomass under different conditions

Firstly, the combustion of volatiles indeed produces substantial amounts of PM_{10}, which are dominantly PM1, accounting for 95.6 – 98.4% of total PM_{10} collected from volatiles combustion. This is as expected because the majority of alkali metals (Na and K) and chlorine that are mainly responsible to PM_1 emission[28, 85, 254] were volatilised, while the majority of refractory elements (Mg and Ca) that are the main compositions of PM_{1-10} were retained in chars during biomass pyrolysis (see Figure 6-2). In fact, the data presented in panel (a) of Figure 6-3 clearly demonstrate that significant PM_1 generated from volatiles combustion are dominantly contained the ultra-fine particles with a size less than 0.1μm ($PM_{0.1}$).

Secondly, the combustion of volatiles produced in situ from biomass fast pyrolysis at higher temperatures results in a clear increase in the $PM_{0.1}$ yields (therefore PM_1 and PM_{10} yields). This appears to correlate well with the increased volatilisation of Na, K and Cl as the temperature of the drop-tube/fixed-bed pyrolyser increases from 800 to 1000 °C (see Figure 6-2).

Thirdly, it is important to note in Figure 6-3b that opposite to the combustion of volatiles, the combustion of chars contributes mainly the emission of PM_{1-10}, which accounts for 84.4– 98.4% of the total yield of PM_{10} collected from char combustion. An increase in pyrolysis temperatures from 800 to 1000 °C appears to have little effect on the yields of PM_{1-10} produced from the combustion of chars. The yields of PM_1 from the combustion of chars produced from raw biomass fast pyrolysis at 800 – 1000 °C are small. However, a decrease in the PM_1 (including mainly $PM_{0.1}$) yield from char combustion is also evident as pyrolysis temperature increases from 800 to 1000 ^{o}C, which appear to correlate well with the decreasing Cl content in the char as pyrolysis temperature increases (see Table 3-2 of Chapter 3).

Lastly, the sum of PM yields from the combustion of both volatiles and chars (denoted as “volatiles + char” hereafter) are presented in Figure 6-3c, benchmarking against the PM yield from direct combustion of the raw biomass in the DTF at 1300

°C under the same conditions. It is important to note that it is not possible to obtain the data on PM emissions from the combustion of volatiles generated in situ from biomass fast pyrolysis at 1300 °C due to the limitation of the quartz pyrolysis reactor. It is interesting to see that the yields of $PM_{0.1}$, PM_1 and PM_{10} from the "volatiles + char" combustion (pyrolysis takes place at 800 – 1000 °C) are slightly higher than those from direct biomass combustion. While the exact reasons are unknown at present, several responsible mechanisms may be speculated. For example, the volatiles-char interactions (10 mins) would be prolonged for the cases of "volatiles + char" combustion, in comparison to that during direct biomass combustion. Additionally, there would be significant differences in the properties of both volatiles (including any AAEM species and Cl in the volatiles) and chars produced at 800 – 1000 ^{o}C with those at 1300 ^{o}C. Furthermore, during direct biomass combustion, there would also possibly be potential synergies in PM emissions between volatiles and char combustion, such synergies are absent in the case of "Volatiles + Char" combustion. In summary, it is obvious that future work is required to clarify this important point via innovative reactor design, achieving the operation of the first-stage pyrolysis at the same temperature of the second-stage combustion.

To further illustrate the important role of volatiles combustion in PM emission, the contribution of volatiles and char combustion to the total yields of PM_1 and PM_{10} (i.e. the sum of "volatiles + char" combustion in Figure 6-3c) are presented in Figure 6-4. It is clear that PM_1 (both $PM_{0.1}$ and $PM_{0.1\text{-}1}$) emission was dominantly contributed by volatiles combustion, accounting for 77.4 – 89.3% of the yield of PM_1 from "volatiles + char" combustion. As discussed, the contribution of volatiles combustion to total $PM_{0.1}$ yields appears to increase with pyrolysis temperature, which is likely as results of enhanced volatilisation of Na, K and Cl. The contribution of char combustion to PM_1 emission is limited. However, char combustion is dominantly responsible for $PM_{1\text{-}10}$ emission, accounting for almost all (97.5 – 99.7%) of $PM_{1\text{-}10}$ from the "volatiles + char" combustion. The pyrolysis temperature seems to have little effect on the contribution of char combustion to total $PM_{1\text{-}10}$ emission.

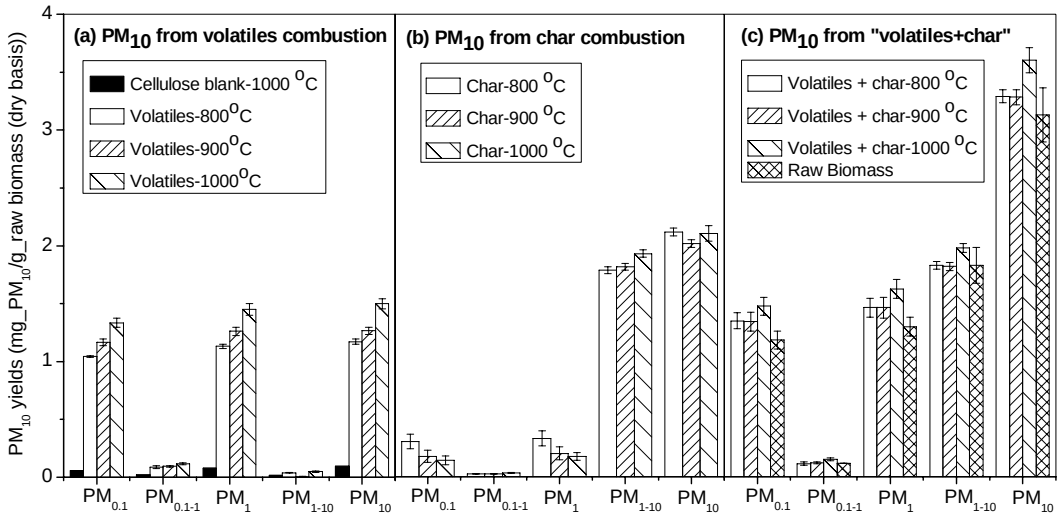

Figure 6-3: PM yields from the combustion of (a) volatiles, (b) chars and (c) "volatiles + char" (compared with raw biomass combustion). Graphs normalized to the equivalent biomass (db) input into the furnace

6.4 Properties of PM_1 and PM_{10} Collected from the Combustion of Volatiles and Chars

To further understand the properties of PM_1 and PM_{10} produced from the combustion of volatiles and chars, analyses were carried out to obtain the data on mass-based PSDs of PM_{10} and elemental mass-based PSDs of Na, K, Mg, Ca and Cl in PM_{10}. As shown in Figure 6-5a, the mass-based PSDs of PM_{10} from volatiles combustion, normalized to equivalent raw biomass, generally show a unimodal size distribution, i.e., with a fine mode ranges from ~0.022 to ~0.043μm. It is also clear that increasing pyrolysis temperature leads to an increase on the mass of particulate matter < 0.077μm, possibly due to the increased volatilisation of inorganic species with volatiles at higher pyrolysis temperature. Figure 6-5b presents the data on PSDs of PM_{10} from char combustion, normalized to equivalent raw biomass, generally shows a unimodal distribution, i.e., a coarse mode with a mode diameter of ~6.8μm. An exception is the PSD of PM_{10} from "Char-800 ^{o}C" combustion, which also shows a fine mode with a mode diameter < 0.022 μm, probably because of the high Cl content in "char-800 ^{o}C". The mass of particles in the size range of 0.955 – 10.174

μm remains almost unchanged from the combustion of chars prepared at different temperatures, although increasing pyrolysis temperature causes a considerable reduction in the mass of particles less than 0.1 μm, in agreement with the decrease of $PM_{0.1}$ yield from char combustion (see Figure 6-3b), possibly due to the low Cl content in the chars (see Table 3-2 of Chapter 3). Considering the data in Figure 6-5a and 6-5b together, the PSDs of PM_{10} from "volatiles + char" combustion show a biomodal distribution with a fine mode in the range of 0.022 – 0.043 μm and a coarse mode with a mode diameter of ~6.8μm, which is similar to that of raw biomass combustion (see Figure 6-5c).

The data on elemental-mass-based size distributions of AAEM species and Cl in PM_{10}, normalized to the unit mass of equivalent raw biomass (db) are presented in Figure 6-6. It is clear that Na, K and Cl all have a unimodal distribution from the combustion of volatiles (see Figures 6-6a-c) with a single mode ranges from ~0.022 to ~0.043μm, in consistence with the mass-based PSDs of PM_{10} from volatiles combustion (see Figure 6-5a). The mass of Na, K and Cl in particulates < 0.077μm shows a substantial increase at a higher pyrolysis temperature (see Figures 6-6a–c), which is in consistence with the trend observed in mass-based PSDs of PM_{10} from volatiles combustion (see Figure 6-5a). The data on the elemental yields (see Figure 6-7a-c) further demonstrate the dominant presence of Na, K and Cl in PM_1 (particularly $PM_{0.1}$) produced from volatiles combustion and the significance influence of pyrolysis temperature. It should also be noted that there are still low (but not zero) concentrations of Mg and Ca present in PM_{1-10} samples emitted from volatiles combustion.

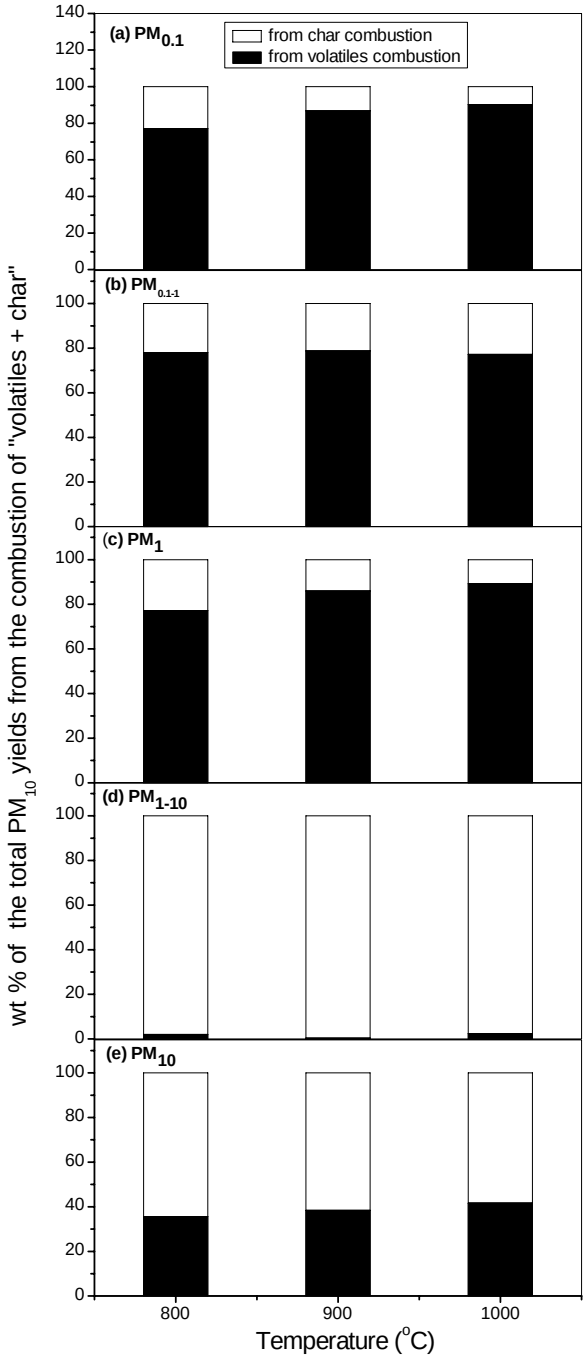

Figure 6- 4: The distribution of PM_{10} yield from the combustion of volatiles and chars, based on the total PM_{10} yield from "volatiles + char" combustion, including the yields of PM with aerodynamic diameters (a) less than 0.1 µm ($PM_{0.1}$), (b) between 0.1 and 1 µm ($PM_{0.1-1}$), (c) less than 1µm (PM_1), (d) between 1 and 10 µm (PM_{1-10}) and (e) less than 10 µm (PM_{10}), respectively

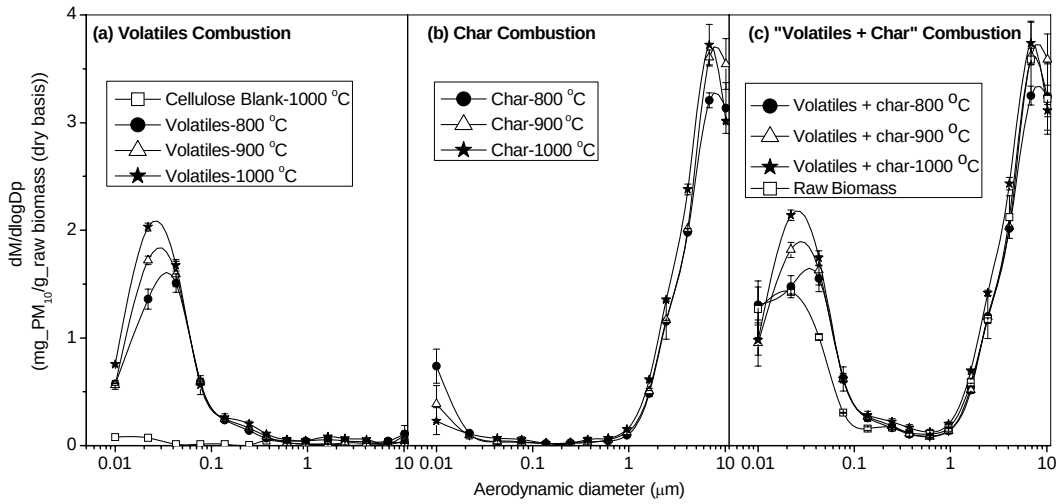

Figure 6- 5: Particle size distributions (PSDs) of PM_{10} from the combustion of (a) volatiles, (b) chars and (c) "volatiles + char" (compared with biomass combustion). Graphs normalized to the equivalent biomass (db) input into the furnace

The elemental-mass-based PSDs of Mg and Ca from char combustion show a unimodal distribution in PM_{10} with a coarse mode of ~6.8 μm (see Figures 6-6i-j), which is also same as the coarse mode in the mass-based PSDs of PM_{10} (see Figure 6-5b). The dominant presence of Mg and Ca in PM_{1-10} is in agreement with the results reported in Chapter 5 and also previous studies.[28, 84, 85, 254] The responsible mechanisms are generally considered to be ash formation from these refractory elements during the combustion of char particles.[84, 85] Oppositely, there is little Na, K and Cl present in PM_{10} from char combustion. An exception is the PSDs of Na, K and Cl from the combustion of "Char-800 °C", that show a fine mode with a mode diameter less than ~0.022μm, most likely due to the high Cl content in the char. In despite of the low concentrations of Na, K and Cl in PM_{10} from char combustion, these elements are still dominantly presented in $PM_{0.1}$, which generally has decreased yields of these elements in $PM_{0.1}$ with increasing pyrolysis temperature (see Figures 6-7f–h). The dominant presence of Na, K and Cl in PM_1 from the combustion of both volatiles and chars are known to be results of homogeneous nucleation and/or heterogeneous condensation of the Na, K and Cl-containing vapors on fine

particulates.[28, 84, 85, 88, 254]

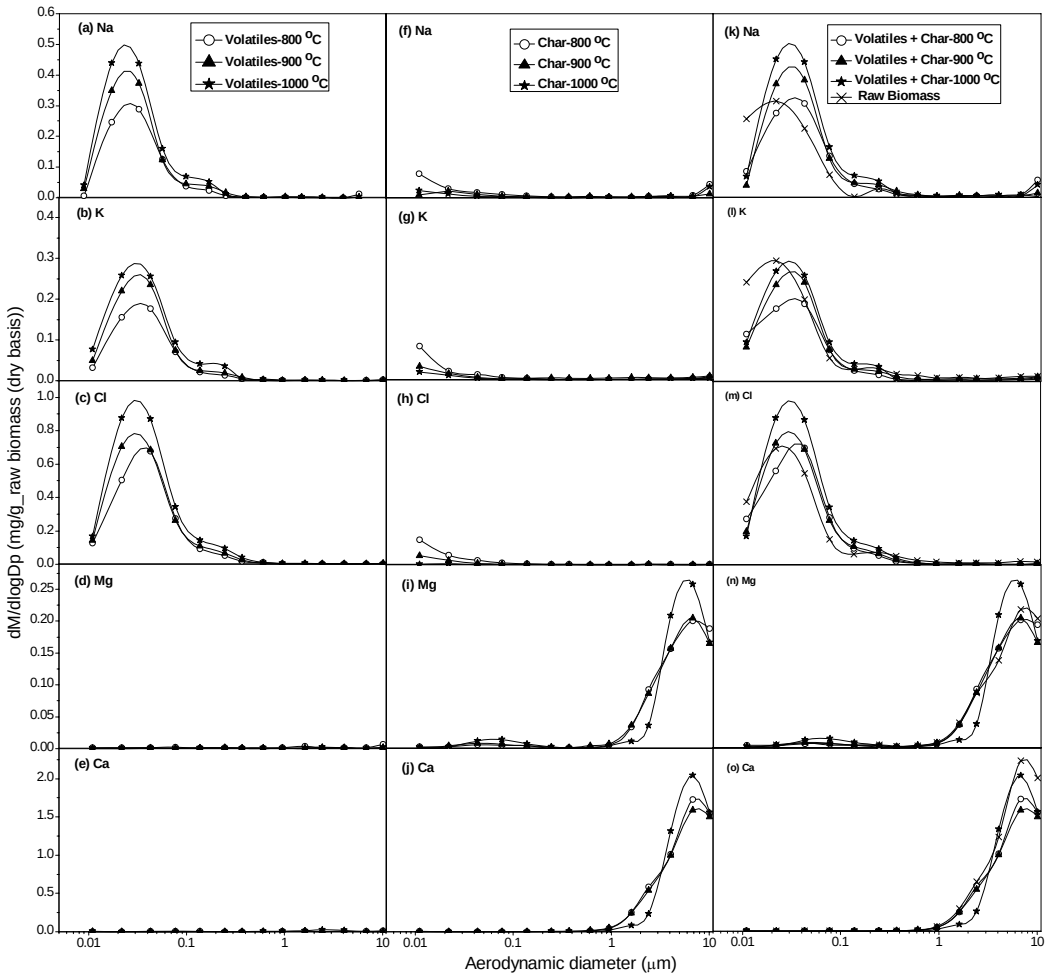

Figure 6-6: Elemental mass size distribution of AAEM species and Cl in PM_{10} during the combustion of volatiles and chars produced at different temperatures: (a) Na, (b) K, (c) Cl, (d) Mg and (e) Ca are from volatiles combustion; (f) Na, (g) K, (h) Cl, (i) Mg and (j) Ca are from char combustion; (k) Na, (l) K, (m) Cl, (n) Mg and (o) Ca are from "volatiles + char" combustion, also compared with raw biomass combustion. Graphs are normalized to the mass of raw biomass (dry basis) input into the furnace

Considering the AAEM species and Cl in the PM_{10} from the combustion of both volatiles and chars together, the PSDs of and yields of these elements in PM_{10} from "volatiles + char" combustion are presented in panels k-o of Figures 6-6 and 6-7, respectively. Similar with the case of raw biomass combustion, the Na, K and Cl are

dominantly contained in PM_1 (account for 95 – 99% based on the mass of these elements in PM_{10}) with a fine mode in the range of ~0.022 to ~0.043μm. However, Mg and Ca are concentrated in PM_{1-10} with a mass percentage of 91 – 99% based on the total elements in PM_{10} with a coarse mode of ~6.8 μm (see panels n – o of Figures 6-6 and 6-7).

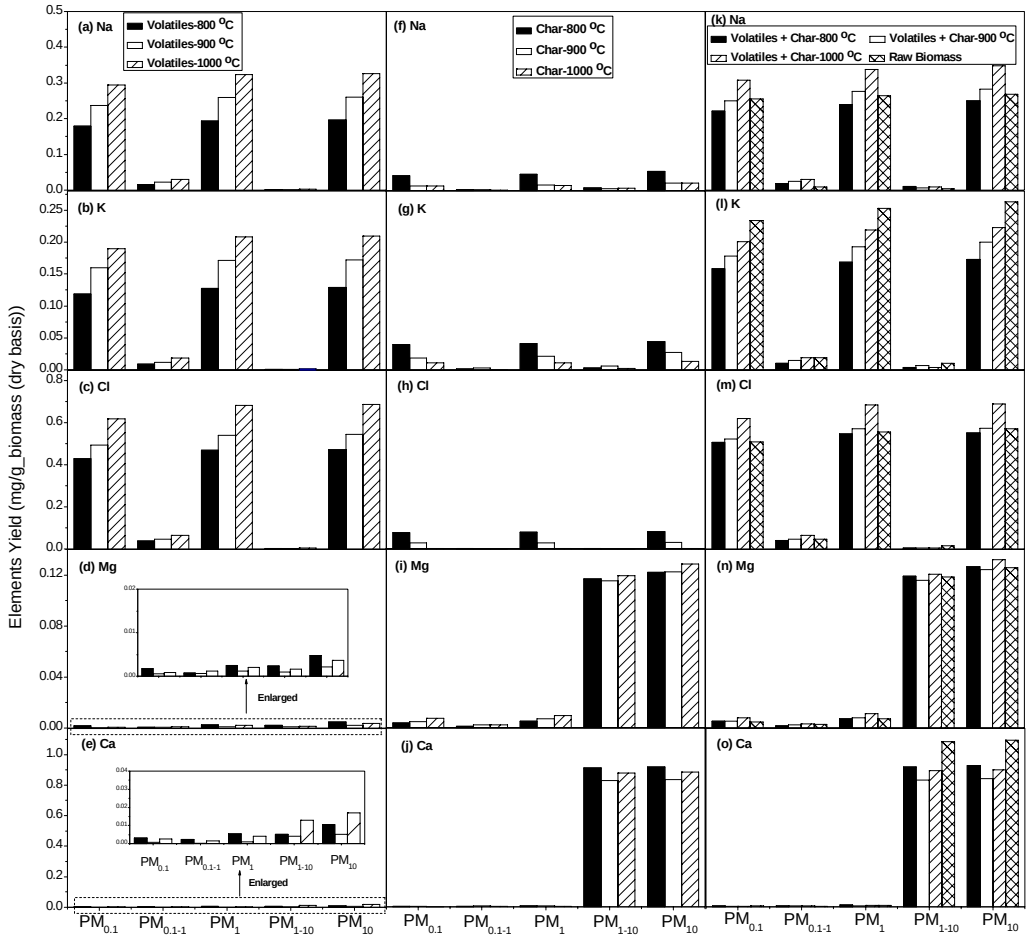

Figure 6-7: Elements yields of AAEM species and Cl in PM_{10} during the combustion of volatiles and chars produced at different temperature: (a) Na, (b) K, (c) Cl, (d) Mg and (e) Ca are from volatiles combustion; (f) Na, (g) K, (h) Cl, (i) Mg and (j) Ca are from char combustion; (k) Na, (l) K, (m) Cl, (n) Mg and (o) Ca are from "volatiles + char" combustion, also compared with raw biomass combustion. Graphs are normalized to the mass of raw biomass (dry basis) input into the furnace

6.5 Further Discussion on the Mechanisms Responsible for the Emission of PM_1 and PM_{1-10}

The data in sections 6.2–6.4 suggest as the first time in the field on the significant contribution of volatiles combustion to PM_1 emission. Based on this finding, new possible mechanisms responsible for PM formation/emission during biomass combustion are proposed and schematically illustrated in Figure 6-8.

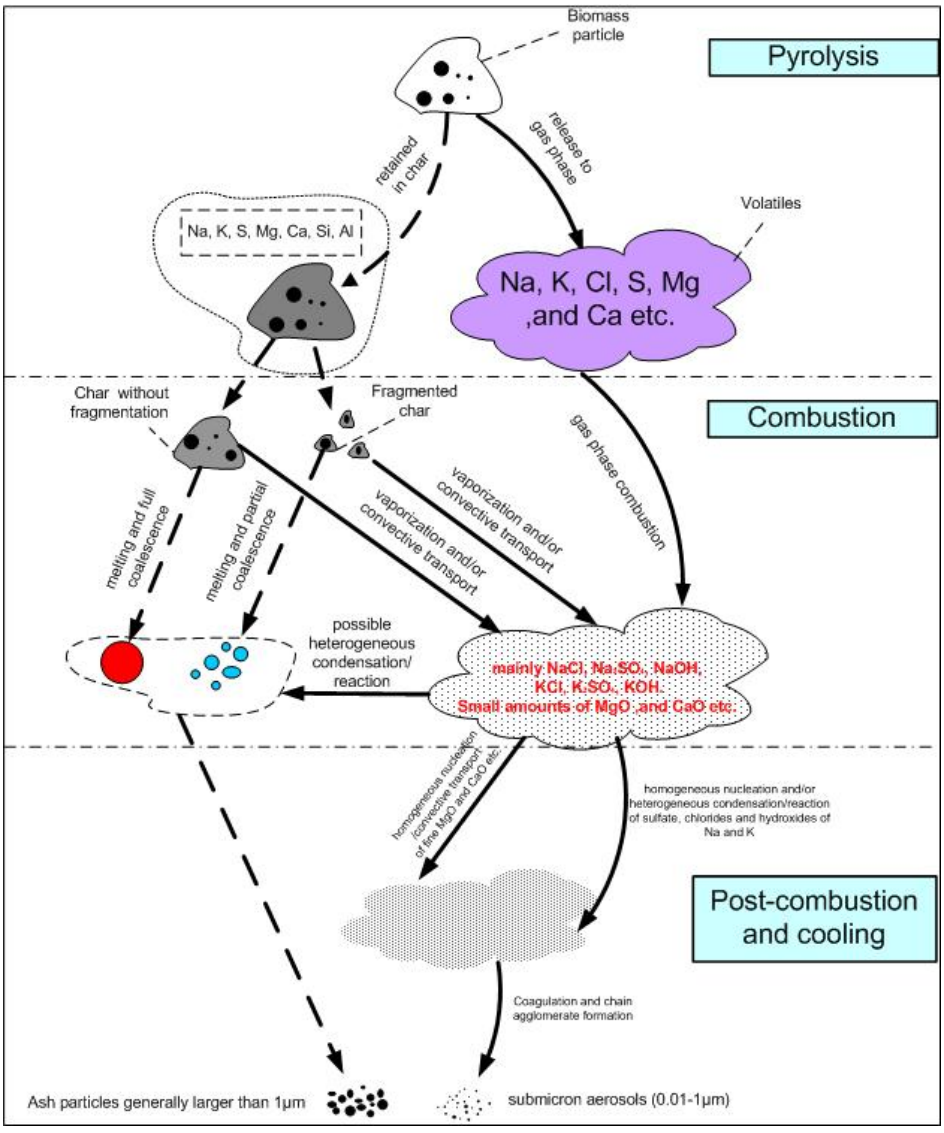

Figure 6-8: Possible ash formation/emission mechanisms during pulverized biomass combustion, modified based on the findings in Chapter 6 and previous studies.[39, 277]

6.5.1 PM_1 Rormation/Emission Mechanisms

- ***Volatiles combustion***

As shown in Figure 6-8, considerable amounts of organically bound AAEM species (particularly Na and K) may be released into gas phase during pyrolysis, so do almost all the Cl and organic S.[117] The released volatiles (including inorganic species released) may combust immediately and undergo a series of gas phase reactions to form different components of AAEM species, S and Cl (e.g. alkali chlorides, alkali sulfates and oxides of alkaline earth metals, etc.).

Furthermore, these compounds in gaseous phase may become supersaturated due to the lowered vapour pressure of the new compounds formed and/or due to the cooling of the flue gas. The supersaturation of the respective compounds may result in homogeneous nucleation to form new particles and/or heterogeneous condensation (and/or reaction) on existing particle surface (either aerosols or coarse ash particles). It is suggested that formation of particles by nucleation and condensation of vapors on existing particle surfaces are always competing processes. The higher the surface area of existing particles is the more the formation of particles by nucleation is suppressed and the growth of existing particles by condensation is preferred. Therefore, it is generally observed that the inorganic vapors may prefer to condense more on smaller particles rather than on the bigger ones, because of the high surface to volume ratio of small particles. Once the particles are formed, they collide with each other and may adhere or coalesce, which leads to a decrease of particle numbers in the flue gas but an increase of particle diameters, and consequently the PM_1 is formed via the above processes.

Indeed, the data in sections 6.2–6.4 have clearly demonstrated that the volatilisation and subsequent combustion of Na, K and Cl with volatiles produced in situ from biomass fast pyrolysis is a key mechanism responsible for PM_1 emission. Furthermore, the PM_1 yields from volatiles combustion increase with an increase in the pyrolysis temperature for in situ volatiles generation (see Figure 6-3). The results

suggest the enhanced release of volatiles (see Figure 6-9a) and the enhanced release and/or volatilisation of AAEM species and Cl (see Figures 6-9b-d) at higher pyrolysis temperatures. A close investigation shows that the compositions of the volatiles influence PM_1 emission significantly during volatiles combustion. Figures 6-9b-d demonstrate a strong correlation between the PM_1 yields and the content of (Na+K+Cl), (Na+K) and Cl in the volatiles.

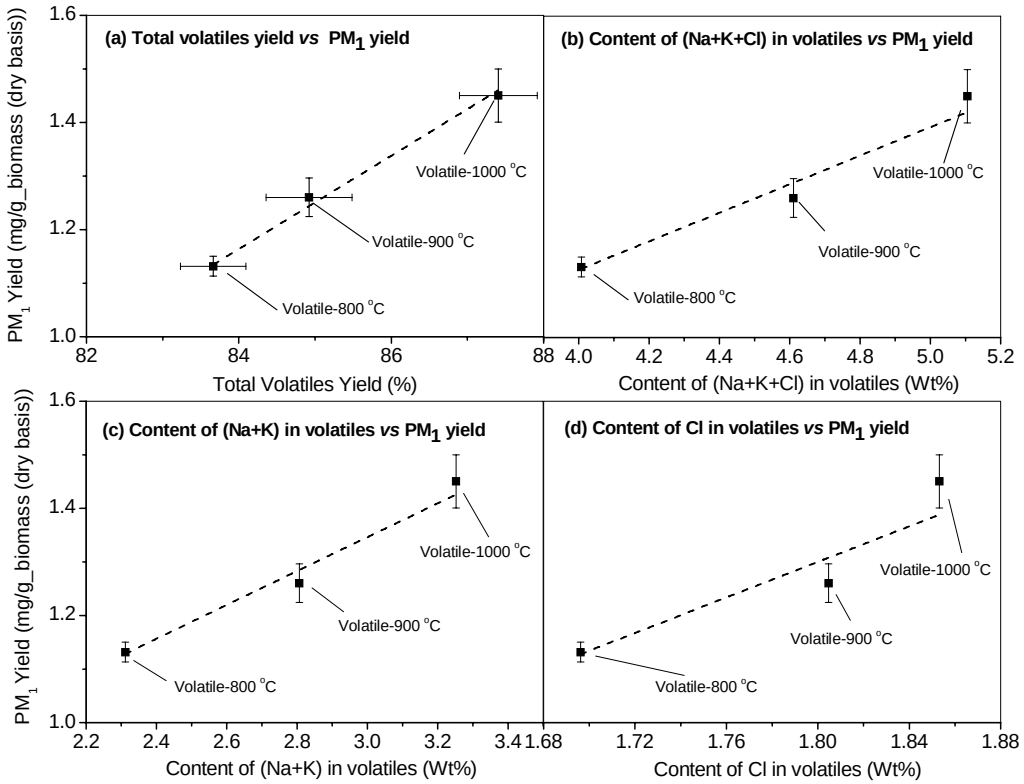

Figure 6-9: Relationship between PM_1 yield from volatiles combustion between (a) total volatile yield, (b) the content of (Na+K+Cl) in volatiles, (c) the content of (Na+K) in volatiles and (d) the content of Cl in volatiles

It is also interesting to note that the combustion of volatiles also results in the presence of refractory elements (Mg and Ca) in either PM_1 or PM_{1-10} (particularly for "volatiles–1000^{o}C" combustion), although the amount is very low. This phenomenon directly demonstrates that a small amount of Mg and Ca species will be carried out with volatiles during pyrolysis and consequently contribute to PM_1 (and also PM_{1-10}) emission during volatiles combustion. Similar phenomenon of the presence of Mg

can Ca in PM_1 was also found by Lind et al.[156] and Sippula et al.[157]

- ***Char combustion***

As shown in Figure 6-8, the alkali metals and tiny amount of Cl retained in the char possibly release to gas phase during char combustion, the released components may follow similar gas phase reactions to that of the components formed via volatiles combustion. Once the gas phase components formed, they may contribute to the formation/emission of PM_1 as results homogeneous nucleation and/or heterogeneous condensation (and/or reaction), and subsequent coagulation and agglomeration, which are similar to those processes of volatiles combustion. There are also small amount of Mg and Ca in PM_1 from char combustion (see Figures 6-6 and 6-7), which is likely due to the liberation of fine Mg- and Ca-containing particles (less than 1 um) which are originally present in the biomass.

However, the results in Sections 6.2 to 6.4 suggest that the contribution of char combustion to PM_1 emission is limited, possibly due to the absence of Cl in the char. Such similar result is also found in Chapter 5, indicating the significant roles of Cl in the emission of PM_1. Additionally, the molar ratios of (Na+K)/Cl in $PM_{0.1}$ (which are dominantly contained in PM_1) from the combustion of volatiles and raw biomass are all close to 1 (see Figure 6-10), further supporting that volatiles combustion rather than char combustion, is the main mechanism responsible for PM_1 emission.

6.5.2 PM_{1-10} Formation/Emission Mechanisms

The data in Sections 6.2 to 6.4 suggest that the liberation of refractory elements (such as Mg and Ca) during char combustion is a key mechanism for PM_{1-10} formation/emission. The refractory elements may be liberated to flue gas followed the possible processes of char fragmentation and ash melting and/or coalescence, and consequently, Ash particles formed by the above mechanisms generally have a wide range of compositions, shapes and sizes (normally larger than 1μm), related to the

characteristics of the parent biomass. Heterogeneous condensation and/or reaction between inorganic vapors and these larger particles may also take place in a limited extent. Therefore, particles formed via these processes consist mainly of refractory species such Mg and Ca

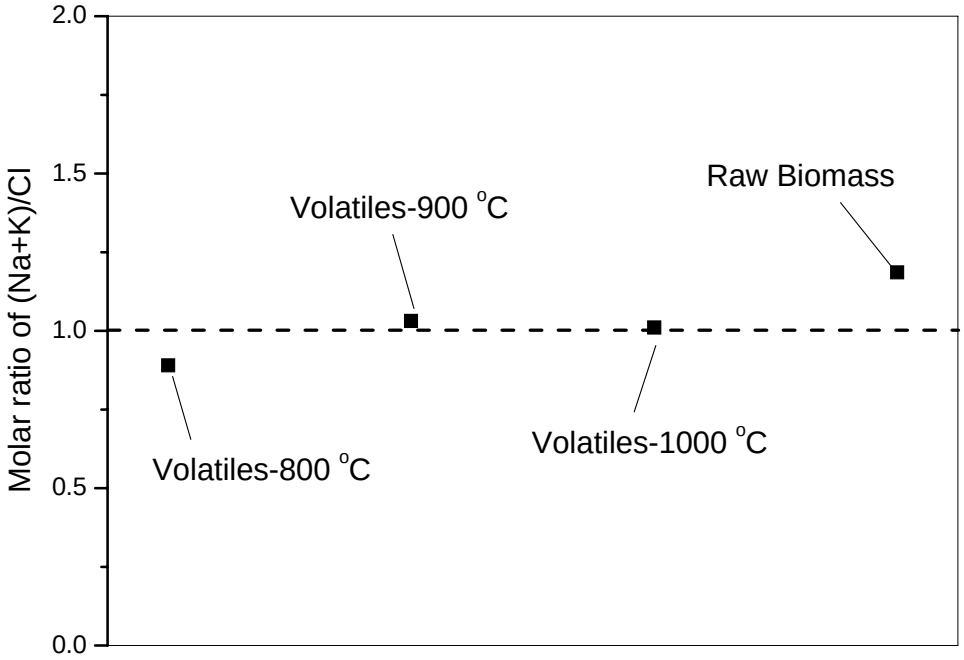

Figure 6- 10: Molar ratio of (Na+K)/Cl in the PM samples with aerodynamic diameters less than 0.1 μm ($PM_{0.1}$) that were collected from the combustion of volatiles and raw biomass.

6.6 Conclusions

This chapter reports the direct experimental evidence on the substantial contribution of volatiles combustion to PM_1 emission during biomass combustion, via a series of experiments by using a novel two-stage pyrolysis/combustion reactor system. The major conclusions are drawn as follows:

(1) An increase in pyrolysis temperature from 800 to 1000 °C leads to an increase in the yield of volatiles from 83.7% to 87.4% (db), and the release and/or volatilisation of Na, K, Mg ,Ca and Cl from 51.8 to 81.4%, 43.5 to 54.5%, 2.5 to 9.3%, 6.3 to

16.1% and 85.2 to 97.2%, respectively.

(2) Based on the data from the combustion of volatiles produced in situ from raw biomass pyrolysis at 800 – 1000 °C, volatiles combustion contributes to 77.4 – 89.3% of the yield of total PM_1 while char combustion contributes to 97.5 – 99.7% of the yield of total PM_{1-10}.

(3) PM_1 from volatiles combustion is dominantly $PM_{0.1}$ and consists of mainly Na, K and Cl, with little Mg and Ca. The mass-based PSDs of PM_{10} and elemental-mass-based PSDs of Na, K, and Cl (which are dominantly contained in PM_1) from volatiles combustion generally show a unimodal distribution with a fine mode range from ~0.022 to ~0.043 μm. A higher pyrolysis temperature leads to a significant mass increase of the particles (and the mass of Na, K and Cl dominantly contained in these particles) with a size less than ~0.077 μm.

(4) The mass-based PSDs of PM_{10} and elemental-mass-based PSDs of Mg and Ca (dominantly contained in PM_{1-10}) from char combustion generally show a unimodal distribution with a coarse mode of ~6.8 μm. Increasing char preparation (i.e., pyrolysis) temperature leads a considerable mass decrease of particles with a size less than 0.022 μm (and also Na, K and Cl in these particles) during char combustion, possibly due to the reduction of Cl content in chars.

(5) The volatilisation and subsequent combustion of Na, K and Cl with volatiles produced in situ from biomass fast pyrolysis are the key mechanism responsible for PM_1 emission. There are strong correlations between the PM_1 yields and the contents of (Na+K+Cl), (Na+K) and Cl in the volatiles from volatiles combustion. The dominant presence of alkali (Na and K) chlorides in $PM_{0.1}$ collected from the combustion of volatiles and raw biomass is also evident.

CHAPTER 7 SIGNIFICANT ROLES OF INHERENT FINE INCLUDED MINERAL PARTICLES IN THE EMISSION OF PM_{10} DURING PULVERIZED COAL COMBUSTION

7.1 Introduction

Inorganic particulate matter (PM) with an aerodynamic diameter of less than 10 μm (i.e. PM_{10}) is a major aerosol pollutant emitted from stationary coal-fired powerstations, drawing worldwide attention due to its adverse health and environmental impact. The need for controlling PM emission leads to extensive investigations on the formation and/or emission mechanisms of PM_{10} over the past decade. A number of mechanisms have been proposed to be responsible for PM with an aerodynamic size less than 1 μm (PM_1), such as inorganic species vaporization, condensation, and aggregation,[223, 276] surface ash shedding during char combustion,[40, 278] bursting of cenosphere,[229, 279] and convective transport of organically bound and possibly small-grained inorganic species away from coal particle during coal devolatilization,[233] etc. The proposed mechanisms for the formation and/or emission of PM with an aerodynamic size between 1 and 10μm (PM_{1-10}) from coal combustion are included minerals coalescence[206, 280], char fragmentation[212, 281] and excluded minerals fragmentation.[189, 278, 282] The particle size distributions (PSDs) and characteristics of PM_{10} may therefore be governed by a combination of these mechanisms so that are largely dependent on combustion conditions and coal properties,[281, 283] particularly the characteristics of mineral matter in coal.[27, 284]

In Western Australia, Collie coal is the only coal currently being mined and plays an important role in supplying cheap energy to power the state's economy. It is a sub-bituminous coal of high-moisture and high-volatile.contents. A unique feature of the coal is that it contains abundant fine included mineral matter (e.g. fine quartz and

kaolinite particles etc.) which are known to be responsible for ash deposit initiation and growth.[285] As results of the presence of these fine mineral matter particles, it is reasonable to speculate that these fine included mineral particles in the coal matrix may substantially contribute to PM_{10} formation during coal combustion. Unfortunately, little works thus far has been done on this important aspect, which is the main objective of this chapter. Therefore, a unique coal sample which is known to contain fine included mineral matter only was prepared. After that, a series of experiments were then conducted to investigate the roles of fine included mineral particles inheriented in coal in the emission of PM_{10} during coal combustion via using a drop-tube furnace (DTF, see Section 3.3.2.2 of Chapter 3).

7.2 Characterisation of Fine Mineral Particles in Coal

A Collie coal samples was firstly crushed and sieved to a narrow size fraction of 63–90 μm, followed by density separation to a density fraction of 1.4–1.6 g/cm^3 via sink-float method. The size-narrowed and density-seperated coal sample was then washed with acetone to remove the heavy liquid remained after density separation, followed by drying in argon at 105 °C for 2 hr to completely evaporate the acetone. Then the acetone washed coal was termed as "raw coal" (see Section 3.3.1 of Chapter 3), which was subsequently analyzed by CCSEM to obtain the data on the characteritics of fine mineral particles, as shown in Figure 7-1. Approximately 56.0% of the total mineral matters are in the form of fine mineral particles with a size < 5μm, furthermore, the mineral particles of a size < 10 μm account for ~90% of the total mineral matters in coal (see Figure 7-1a). It should be noted that the the coal is expected to dominantly contain included mineral matter, as either included mineral particles or organically-bound inorganic elements, due to the low coal density, because excluded minerals generally have a much higher densities (> 2.4 g/cm^3).[34] Indeed, CCSEM analysis shows no excluded mineral matter in the coal so that the abundant fine mineral particles are all fine included mineral particles inherently present in the coal matrix. Quartz, kaolinite and iron-bearing minerals are found to be

key minerals and the presence of K Al-silicate is also evident (see Figure 7-1b). It should be noted in Figure 7-1 that ~35% of mineral particles are categorized as "unclassified". A close examination suggests that an "unclassified" mineral particle typically consists of multiple mineral phases, mainly as mixtures of Fe and Ca Al -silicates, plus some with less extent of Ti- and P-containing minerals.

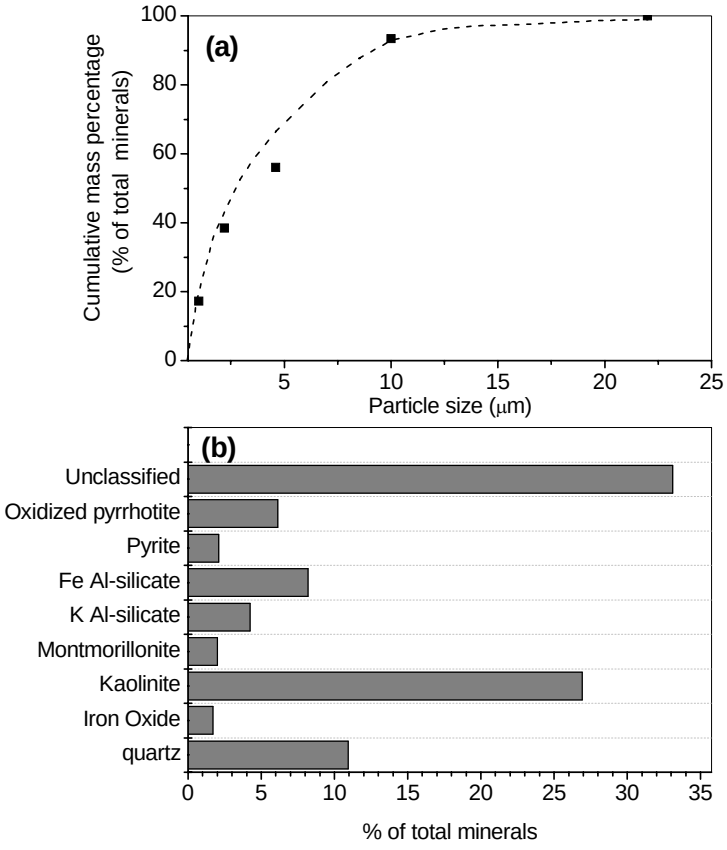

Figure 7- 1: Properties of mineral matter in the raw coal: (a) total mineral size distribution; (b) main mineral phases

To isolate the contributions of fine included mineral particles and organically-bound elements to PM formation during coal combustion, the raw coal sample was then washed using dilute acid (0.1 M HCl acid) for 24 hours and subsequently rainsed with Milli-Q water repeatedly to prepare the acid washed coal for further experiments. Acid washing using dilute acid removes acid soluble inorganic speices (mainly organically-bound elements, plus acid-solube minerals e.g. carbonates etc.), yielding a coal sample consisting of only discrete included mineral particles.

Hereafter in this chapter, the acid washed coal and its derived char prepared from fast pyrolysis at 1000°C (see Section 3.3.4.2 of Chapter 3) are simply denoted as "**coal**" and "**char**", respectively. The typical fuel properties of "raw coal", "coal" and its derived char are summarized in Table 7-1.

Figure 7-2 further presents the elemental distribution of mineral matter after the raw coal was washed with 0.1M HCl acid. As expected, the majority of Ai and Si are retained in the acid-washed coal, suggesting that Al and Si are not organically-bound in the coal matrix but mainly in acid-insoluble forms as included discrete mineral particles. Meanwhile, only small amounts (0.5–1.7%) of K, Mg, S and Ti are washed away by dilute acid, indicating that K, Mg and Ti mainly present in acid-insoluble forms such as alumino-silicates, S may mainly occurs in the coal substance and/or in the mineral fraction such as sulfides which are acid-insoluble.[286] However, Figure 7-2 shows that ~7.1–33.0% of Ca, Sr, Ba, Na, P and Fe were removed by acid washing, suggesting that small proportions of these elements are present in the raw coal in either organically-bound forms and/or acid-soluble minerals e.g. carbonates and phosphates. It is known that Na, Ca, Sr, Ba, Fe and P may be organically bound in coal (particularly low-rank coals) and/or exist as carbonates[287, 288] and phosphates.[289]

Based on the data in Figures 7-1 and 7-2, it is clear that the "raw coal" contains abundant fine included mineral particles of an included nature, plus possibly small proportions of organically-bound ash-forming species. Therefore, acid-washing indeed removes the acid-soluble mineral matter and delivers an excellent coal sample that contains only included mineral particles. Such unique property of the coal and char sample simplify the experimental program and enables us to purposedly investigate the effect of included mineral matter particularly the fine discrete included mineral particles on PM_{10} emission.

Table 7- 1: Proximate and ultimate analysis of the coals and their derived coal-chars

Samples	Raw coal	Acid-washed coal (termed as "coal")	Char-acid-washed coal (termed as "char")
Proximate analysis:			
M[a] (% ad)	6.0	6.5	6.8
Ash (% db)	5.6	5.1	7.8
VM[b] (% db)	37.8	37.3	3.8
FC[c] (% db)	56.6	57.6	88.4
Ultimate analysis (% daf):			
C	70.63	71.44	94.96
H	4.00	3.92	0.41
N	1.74	1.96	1.96
S	0.68	0.69	0.12
O[d]	22.95	21.99	2.55
Contents of inorganic species (wt% db)			
Si	1.3774	1.2168	1.8605
Al	0.8140	0.7357	1.1762
Fe	0.3368	0.2488	0.4514
Ca	0.0580	0.0480	0.0869
Mg	0.0208	0.0163	0.0280
K	0.0453	0.0171	0.0189
Na	0.0078	0.0063	0.0066
P	0.0680	0.0590	0.0964
Ba	0.0281	0.0184	0.0289
Sr	0.0213	0.0177	0.0279
Ti	0.0498	0.0435	0.0761

[a] moisture; [b] volatile matter; [c] fixed carbon; [d] by difference.

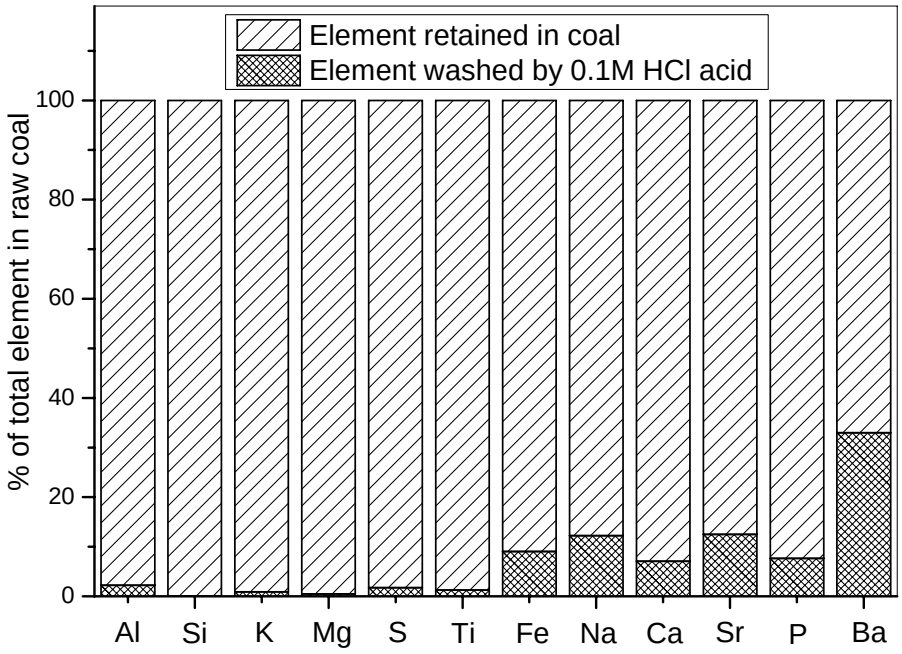

Figure 7-2: Inorganic elements distribution afte dilute acid washing

7.3 Yield and Mass-Based Particle Size Distribution (PSD) of PM_{10} from the Combustion of Coal and Char

Figures 7-3 and 7-4 present the yields and PSDs of PM_{10} produced from the combustion of coal and char in the DTF. It should be noted that the ash contents in the coal and char are 5.1 and 7.8% db, respectively (see Table 3-4 of Chapter 3). Therefore, the PM data are then normalized to the unit mass of ash input in order to directly compare the ability of mineral matter in different fuels on PM_{10} emission.

As shown in Figure 7-3, the yields of PM_{10} from the combustion of coal and char are 150.1 and 142.6 mg/g_ash input, respectively. It is clear that the PM_{10} dominantly contains PM_{1-10} with a yield of 136.2 and 125.9 mg/g_ash from the combustion of coal and char, respectively, while the yields of PM_1 are limited (13.9 and 16.7 mg/g_ash from the combustion of coal and char, respectively). This is not surprising due to the majority of organically bound elements, which are expected to have significant contribution to PM_1 emission,[235] were removed by acid washing of the "raw coal".

The PSDs of PM_{10} (see Figure 7-4) from the combustion of coal and char exhibit a bimodal distribution with a coarse mode diameter of ~4.087 μm, which is in agreement with the repored values in previous studies[102, 200] on PM_{10} from coal combustion, and a fine mode diameter in the range of ~0.022–0.043 μm (see zoom in figure of Figure 7-4). Further mass balance analysis indicates that given a collect efficiency of ~68% achieved in sample collection of the DTF system, the amounts of PM_1 and PM_{1-10} account for ~2.3% and ~19.4% based on the total ash collected in DLPI and cyclone (see Figure 7-5). Particular attentions are then given to PM_{1-10} due to its high proportion in ash, which appears to correlate well with the unique feature of mineral matter in the coal samples, i.e. the occurrence of abundant fine included mineral particles.

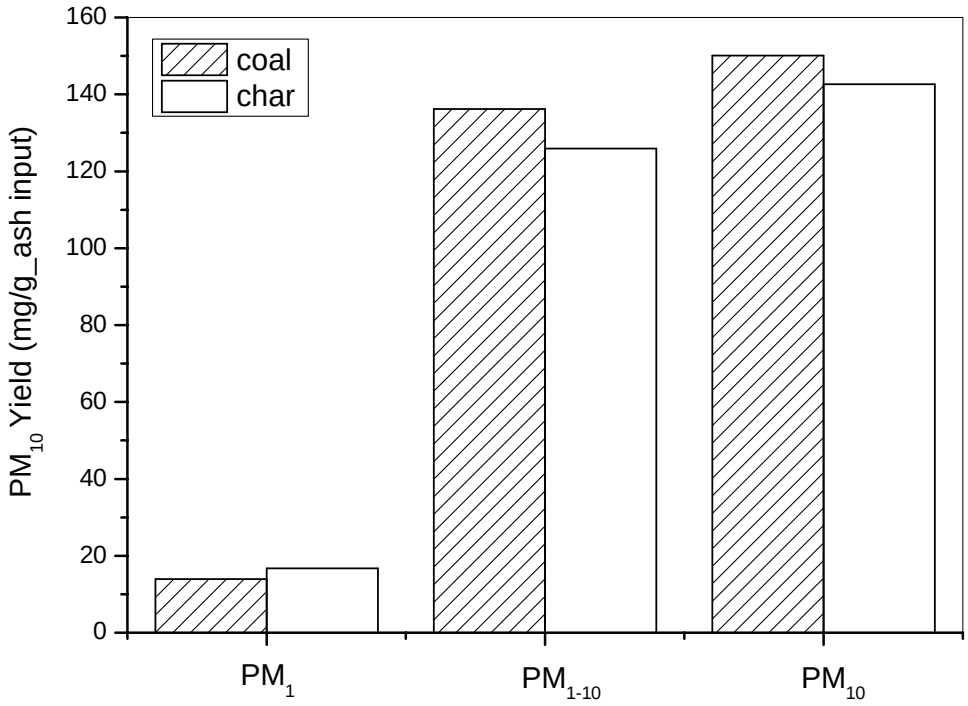

Figure 7- 3: Yield of PM with aerodynamic diameters less than 1μm (PM_1), between 1 and 10μm (PM_{1-10}), and less than 10μm (PM_{10}) from the combustion of coal and char

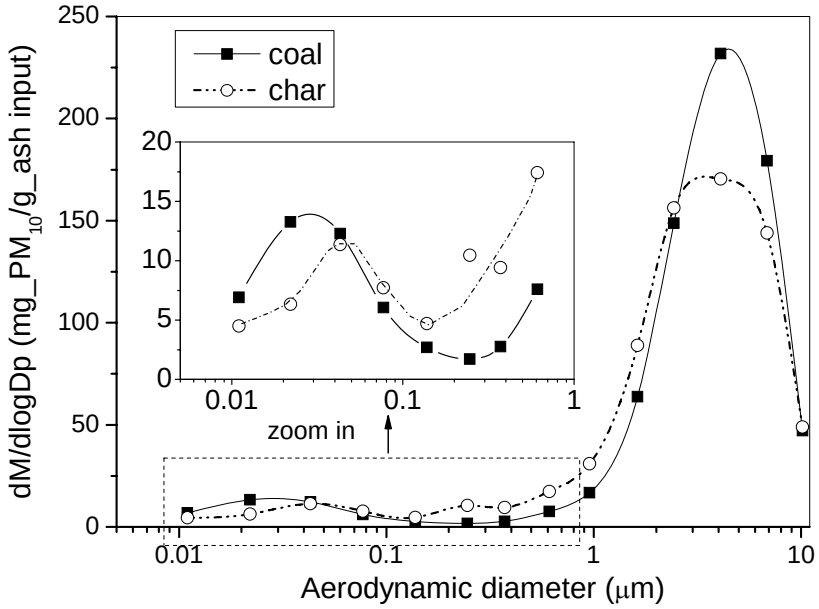

Figure 7- 4: Mass-based particle size distribution (PSD) of PM_{10} from the combustion of coal and char

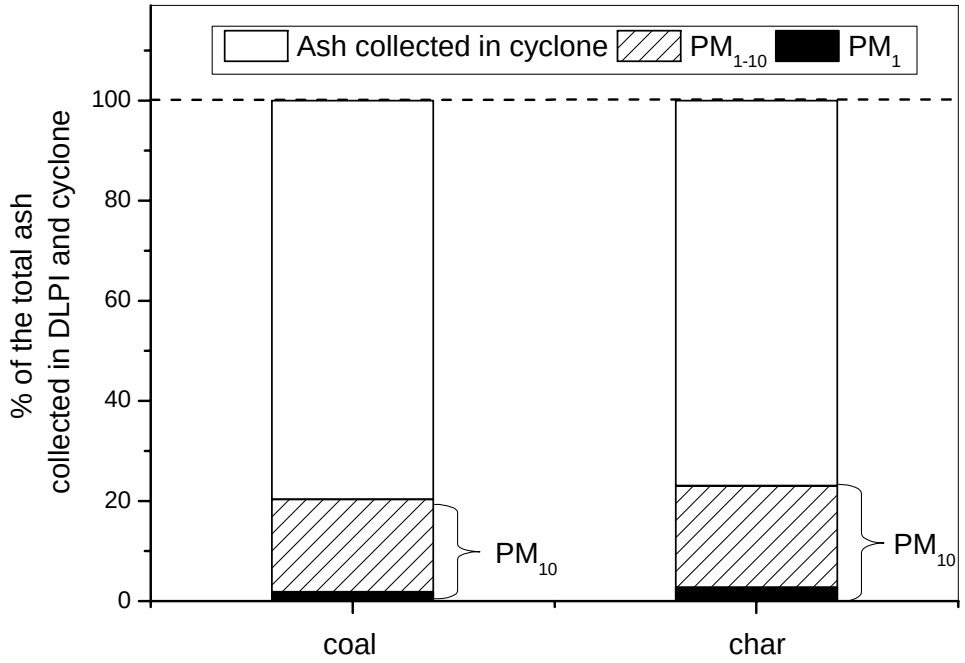

Figure 7- 5: Yield distribution of PM with aerodynamic diameters less than 1μm (PM_1), between 1 and 10μm (PM_{1-10}), and ash collected in cylone from the combustion of coal and char

7.4 Direct Evidences on the Significant Contribution of Fine Included Mineral Particles to PM_{1-10} Emission

As discussed in Section 7.3, the high mass proportion of PM_{1-10} based on the total ash collected indicates a good correlation with the occurrence of abundant fine included mineral particles in coal and char. Furthermore, the PM_{1-10} samples contain dominantly refractory elements (including Si, Al, Fe, Mg and Ca) and alkai metals (Na and K). Reported as oxides, the sum of SiO_2, Al_2O_3, Fe_2O_3, MgO, CaO, Na_2O and K_2O contribute to close to 95.0% of the total mass of PM_{1-10} (see Figure 7-6). A close investigation shows that the amounts of water soluble Na and K in PM_{1-10} from the combustion of both coal and char are limited (see Figure 7-7), indicating the forms of Na and K in PM_{1-10} are probably in water-insoluble minerals such as Na- and K- aluminosilicates and/or silicates. Indeed, the chemistry of PM_{1-10} correlated well with that of the mineral matter in the parent fuels (i.e., coal and char, see Table 3-4 of Chapter 3 and Figure 7-1b). The data further suggest that the fine included mineral particles are the main source of PM_{1-10} emission.

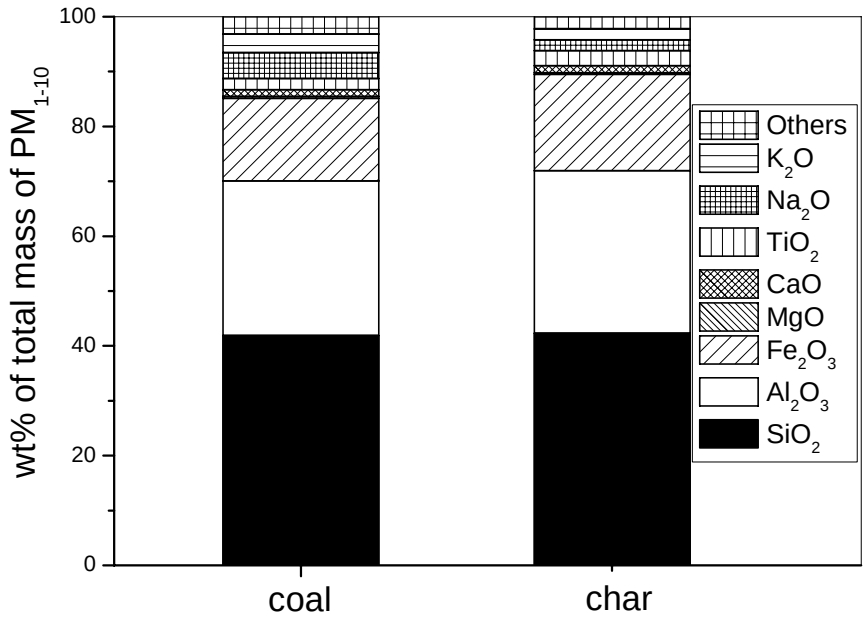

Figure 7- 6: Composition of major inorganic elements (reported as oxides) in PM_{1-10} collected from coal/char combustion

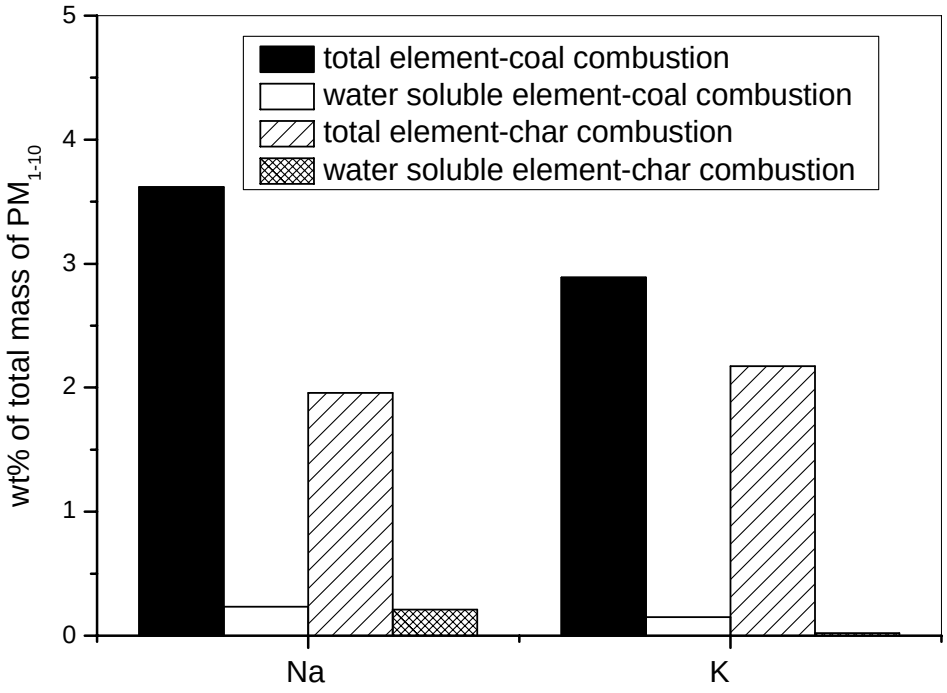

Figure 7- 7: Comparison on the mass percentage of total and water-soluble alkali metals (Na and K) in PM_{1-10} produced from the combustion of coal and char

Efforts were then taken to investigate PM_{1-10} morphology. Figure 7-8 presents a typical SEM image acquired from the ash particles present in the size fraction 4.087 –6.852 μm of the PM_{1-10} sample from coal combustion. The fine ash particles are dominantly spherical- or oval- shaped. The energy dispersive X-ray Spectrums (EDS, see Figure 7-8) of selected fine ash particles suggest that the spherical particles (also with smooth surfaces) contain mainly Si, Al, Fe, K and O possibly as mullite and/or aluminosilicates, indicating these particles experienced complete melting during combustion. This is not surprising given the abundant kaolinite and Al-silicates particles in coal mineral matter and the burning coal particles are known to reach a peak temperature several hundred degrees higher than the surrounding gas temperature.[290, 291] The oval-shaped particles contain Si and O only, suggesting these fine ash particles are originated from the abundant fine included quartz (SiO_2) particles in coal but have only experienced partial melting during combustion. Furthermore, XRD diffractograms of the PM_{1-10} samples clearly show (see Figure 7-9)

that the mineral phases in PM_{1-10} are mainly quartz, mullite, plus aluminum phosphate and iron silicates. Although the quantitive analysis of mineral phases in PM_{1-10} is difficult to achieve due to limited samples available, the XRD diffractograms clearly suggest the presence of abundant quartz particles in PM_{1-10}.

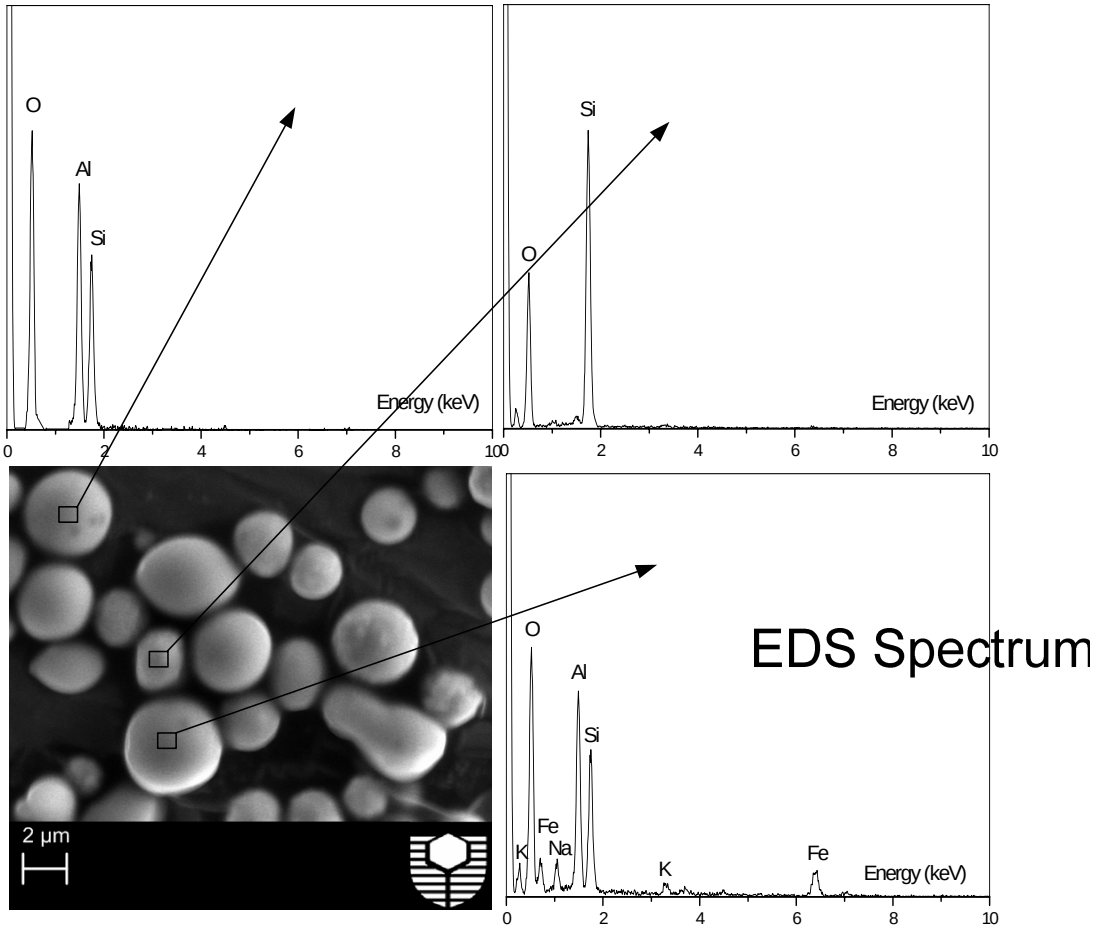

Figure 7- 8: SEM images and EDS spectrum of PM with an aerodynamic diameter of 4.087 – 6.852 µm in PM_{1-10} collected from coal combustion

The results presented in Figures 7-6 to 7-9 have significant implications in revealing the fundamental PM_{1-10} formation mechanisms. As quartz particles in PM_{1-10} are not likely to be the product of other reactions of coal mineral matter during combustion, all the fine quartz ash particles in PM_{1-10} must be formed from the direct transformation of the fine included quartz particles originally present as included

mineral matter in the parent fuels (coal or char samples). It was reported that fragmentation of quartz (particularly included quartz in coal particles) are unlikely during pulverized coal combustion.[34] The morphology of quartz particles in Figure 7-8 also suggests that although experienced partial melting during combustion, the quartz particles are largely individual ash particles with little evidence of coalescence with other quartz particles included in the same burning coal particles. Therefore, the results in Figures 7-6 to 7-9 provide direct experimental evidence for direct transformation of fine included quartz mineral particles into fine quartz ash particles in PM_{1-10} as an important mechanism for PM_{1-10} formation.

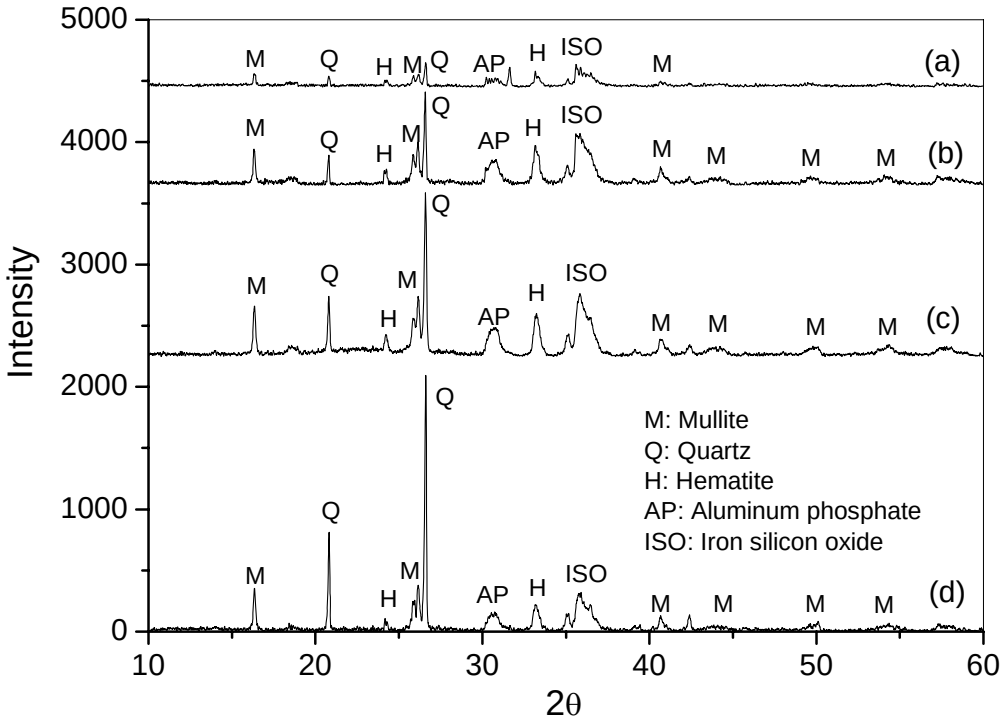

Figure 7- 9: XRD patterns of PM with an aerodynamic diameter of (a) 1.624 – 2.438 µm, (b) 2.438 – 4.087 µm, (c) 4.087 – 6.852 µm and (d) 6.852 – 10.174 µm collected from coal combustion

Similarly, it is therefore also possible that the contribution of other fine mineral particles (such as fine kaolinite, Fe Al–silicates, pyrite etc.) in coal to PM_{1-10} formation can also be substantial, although different mineral reactions and various

extents of coalescence of these fine included mineral particles may take place within the burning coal particles. This is clearly supported by the major mineral phases identified in PM_{1-10}, as shown in Figure 7-9. For example, mullite is known to be the major product of kaolinite thermal decomposition.[34] The presence of hematite in PM_{1-10} is a clear indication on the direct transformation of pyrite combustion with minimal coalescence with other ash particles.

7.5 Roles of Inherent Fine Included Mineral Particles in PM_1 Emission during Char Combustion

Recent studies[234, 235, 272] suggest that PM_1 consits two major fractions including PM with an aerodynamic diameter of less than 0.1 μm ($PM_{0.1}$) and 0.1–1 μm ($PM_{0.1-1}$), both organically bound metals and the inherent fine mineral particles in coal play significant roles in its formation and/or emission. As aforementioned, the organically bound metals in the coal were removed by dilute acid washing (see Section 7.2). To further exclude the contribution of volatiles (including the inorganic species carried out by volatiles) combustion to PM_1 emission (see Chapter 6), the char produced via fast pyrolysis at 1000 ^{o}C was combusted to investigate the contribution of vaporization-condensation of included minerals and direct transformation of inherent fine mineral particles to PM_1 emission during char combustion.

Figure 7-10 presents the chemical composition of $PM_{0.1}$ and $PM_{0.1-1}$, which accounts for ~34.4% and ~65.6% based on total mass of PM_1 collected, respectively. As expected, $PM_{0.1}$ dominantly contains volatile elements (such as Na, K, P and S) and refractory elements (Fe and Si), with little amount of Al and other alkaline earth metals (such as Ca, Mg, Ba and Sr), reported as oxides, the sum of Na, K, P, S, Cl, Fe, and Si contributes to close to 92.7% of the total mass of $PM_{0.1}$. Oppositely, $PM_{0.1-1}$ are mianly composed of refractory elements (Al, Si and Fe), which account for ~84.3% of the total $PM_{0.1-1}$ based on the mass of their oxides, while of the amounts of volatile elements such as Na, K, P, S and Cl are relatively low. Such an obvious

difference on the composition of $PM_{0.1}$ and $PM_{0.1-1}$ indicates that their formation and/or emission are governed by different mechanisms.

The elemental mass-based particle size distributions of the key elements including Na, K, Al and Si in PM_1 are then plotted in Figure 7-11. There are three important observations from the data presented. Firstly, increasing particle size leads a gradual increase in the mass of Si and Al in $PM_{0.1}$, but a drastic increase of those in $PM_{0.1-1}$, which are in agreement with the higher contents of both Al and Si in $PM_{0.1-1}$ in comparison to those in $PM_{0.1}$. Secondly, the mass of Al in $PM_{0.1}$ is much lower than that of Si, however, the PSDs of Al and Si follow a similar trent in $PM_{0.1-1}$. Thirdly, PSDs of Na and K show a similar trend, which slightly decrease with the increase in PM size.

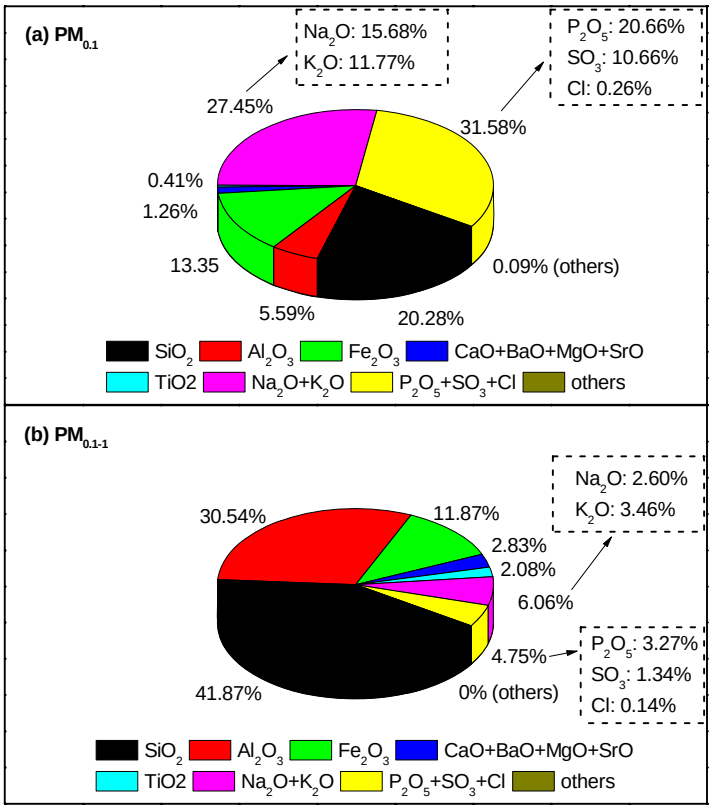

Figure 7- 10: Chemical composition (reported as oxides) of PM with an aerodynamic diameter of (a) less than 0.1µm ($PM_{0.1}$), and (b) 0.1 – 1 µm ($PM_{0.1-1}$) collected from char combustion

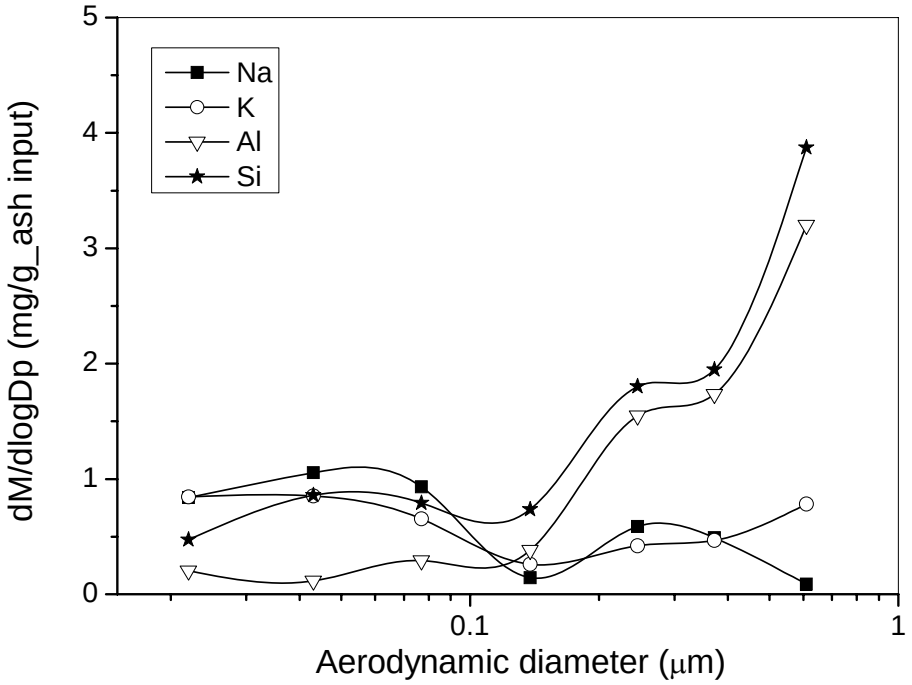

Figure 7- 11: Elemental mass-based particles size distribution of Na, K, Al, and Si in PM_1 collected from char combustion

The data in Figures 7-10 and 7-11 provide important insight into the mechanisms responsible for the formation and/or emission of $PM_{0.1}$ and $PM_{0.1\text{-}1}$. The volatile elements such as Na, K, P, S and Cl in PM_1, particularly in $PM_{0.1}$, are genrally known[40, 222, 292] to be formed via vaporization at high temperature during solid fuels combustion, followed by a serious of gas phase reaction, homogeneous nucleation and/or heterogenous condensation and/or reaction on the surface of existing particles. Particle coagulation and agglomeration may also be involved.[39] On the contrast, for refractory species (e.g. Si and Al) in $PM_{0.1}$, a generally accepted mechanism for the vaporization of these oxides is the reduction to more volatile sub-oxides (SiO and AlO) under the locally reducing atmosphere in fuel-rich regions and within the burning-char particles.[223] Furthermore, Al is suggested to be harder to vaporize compared with Si,[235] explaining well with the dominant existence of SiO_2, rather than Al_2O_3 in $PM_{0.1}$ (see Figures 7-10a and 7-11). The abundant fine inherent quartz particles in the coal/char may contribute to the formation of $PM_{0.1}$ in two

mechanisms. One is that these fine quartz particles provide substantial surface area for reduction reaction within the burning coal/char particle, enhancing the release of SiO that would be further reoxidised in the flame zone to form SiO_2 fume. The other is that there are possibly ultrafine inherent quartz particles (e.g. those < 0.1μm) in the coal. The direct liberation of such ultrafine quartz (if any) can lead to the formation of $PM_{0.1}$. Direct libration of ultrafine inherent mineral particles appears to be possible. The morphology of PM samples with a size fraction of 0.043 – 0.077 μm is shown in Figure 7-12a. apart from the spherical or aggregate-like particles as results of vaporization-condensation mechanism, the existence of oval-shaped and individual particle is also evident.

Opposite to $PM_{0.1}$, both Si and Al are dominantly contained in $PM_{0.1\text{-}1}$, besides, the PSD of Al corresponds closely to that of Si in the size range of 0.1 – 1 μm (see Figure 7-10b and Figure 7-11). Such data clearly suggest the direct transformation of fine (about 1μm) Al-and Si-containing minerals (such as Al-silicates, montmorillonite and kaolinite, see Figure 7-1b) into $PM_{0.1\text{-}1}$. Furthermore, the molar ratio of Si/Al in $PM_{0.1\text{-}1}$ is ~1.16, which is much lower compared to the ratio of ~3.11 in $PM_{0.1}$. Such a substantial decrease in Si/Al molar ration in $PM_{0.1\text{-}1}$ compared to that in $PM_{0.1}$ further confirms the different transformation mechanisms of Al-containing minerals into $PM_{0.1}$ and $PM_{0.1\text{-}1}$, i.e., Al in $PM_{0.1}$ is likely to be a result of limited vaporization and condensation,[223] while the direct transformation of fine Al- and Si-containing minerals seems to be responsible for the abundance of both Al and Si in $PM_{0.1\text{-}1}$. Additionally, such a molar ratio (~1.16) of Si/Al in $PM_{0.1\text{-}1}$ suggests the dominant existence of aluminosilicates in $PM_{0.1\text{-}1}$, as the molar ratio of Si/Al in majority of aluminosilicates such as Na- and K- aluminosilicates is known to be ~1. The existence of aluminosilicates in $PM_{0.1\text{-}1}$ is also indicated by the EDS analysis of selected spherical particle with size range of 0.61 – 0.955 μm, as shown in Figure 7-13b. Considering the data presented in Figures 7-10 to 7-12 together, it is clear that Al in $PM_{0.1\text{-}1}$ is originated from the fine (about 1μm) Al- and Si-containing mineral particles presented in char, and most likely to exist as aluminosilicates in $PM_{0.1\text{-}1}$ as

results of a series of mineral reactions during char combustion.

It should be noted that the fine mineral particles in char may come from two parts. One is the fine mineral particles originally existed in coal. In deed, CCSEM data have shown that about 17% of the total mineral particles are in form of particles with a size around 1μm (see Figure 7-1a). The other may be the fine mineral particles produced during char preparation. In fact, the char was prepared at 1000°C, the primary decompositions of included mineral matters such as kaolinite[34] and/or pyrite[278] (see Figure 7-1b) are likely to take place to fragment into smaller mineral particles, probably accompanied by char fragmentation. Overall, the transformation of inherent fine particles (particularly kaolinite and/or Al-silicates) originally existed in the coal, and/or the fine mineral particles produced during char preparation plays a significant role in $PM_{0.1\text{-}1}$ emission.

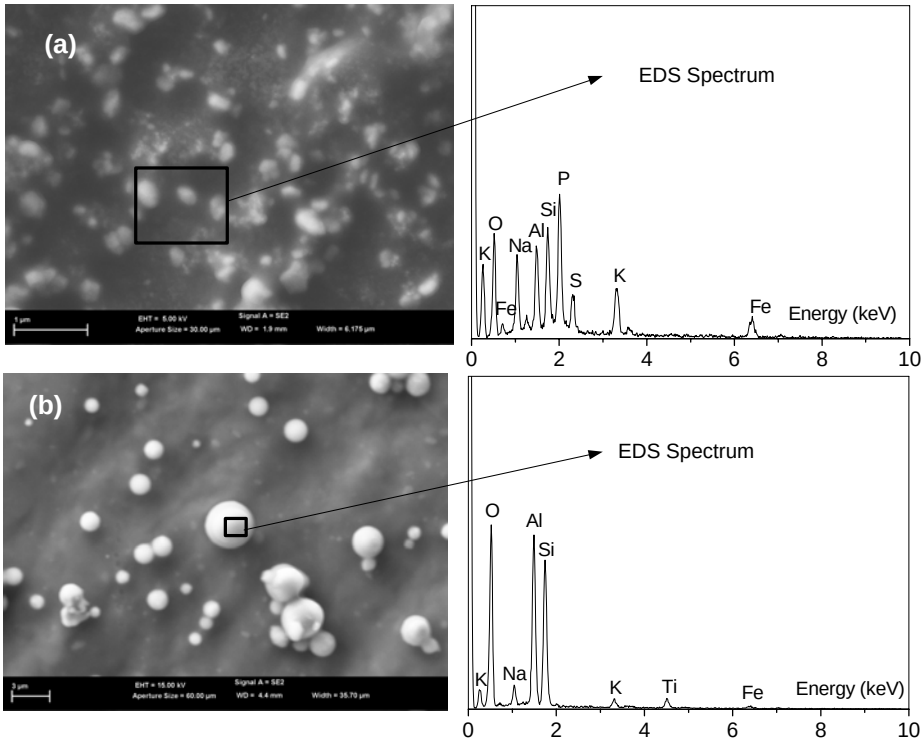

Figure 7- 12: SEM images and EDS spectrum of PM with an aerodynamic diameter of (a) 0.043 – 0.077 μm and (b) 0.61 – 0.955 μm in PM_1 collected from char combustion

In summary, the results in Sections 7.4 and 7.5 clearly indicate that the inherent fine included mineral particles originally presented in parent fuels (coal and char) can substantially contribute to the formation of fine ash particles in PM_{10} (includeing both PM_1 and PM_{1-10}). This finding is of practically importance as it shows that the properties (e.g. PSDs and mineral compositions) of inherient fine mineral matter in coal may also need to be considerd as a key criterion in coal selection guideline for assessing the potential of a particular coal in forming PM_{10} during combustion.

7.6 Possible Mechanisms Responsible for the Discrepancies in the Emission Behavior of PM_{10} from the Combustion of Coal and Char

It is also noteworthy that considerable discrepancies were also observed on the emission behavior and characteristics of PM_{10} from the combustion of coal and char (see Figures 7-3 and 7-4). The PSD of PM_{10} (particular at sizes between 0.1 and 2.438μm) from char combustion appears to slightly shift to smaller sizes in comparison to that from coal combustion, accompanied by a considerable reduction in the mass yield of PM with a size range of 4.087–10.174μm. Consequently, the yields of PM_{1-10} from char combustion are ~5.3% lower than that from the combustion of its parent coal. However, there is no obviouse difference in the yields of PM_1 from the combustion of coal and char. While the exact mechanisms responsible for such differences in the emission of PM_{1-10} between char and coal combustion are unknown at present, there are at least two possible mechanisms which may be responsible.

One is the absence of volatile matter in a char compared to its parent coal. During coal pyrolysis, the release of volatiles may be accompanied by the volatilization of inorganic species so that it is important to investigate the retentions of major inorganic elements (Si, Al, Fe, Na, K, Mg and Ca) in the char produced from the fast pyrolysis of coal. Considering the char yield (51.8% db) and the contents of these elements in char or coal samples (see Table 3-4 of Chapter 3), the data on the

retentions of Si, Al, Fe, Na, K, Mg and Ca are determined. As presented in Figure 7-13, although the majorities (80–98%) of Si, Al, Fe, Mg and Ca were retained in chars, there are still 2–20% of these elements and ~44.3% of Na and K were released during pyrolysis. Apart from the volatilization of Na and K, which is probably because of ash vaporization, the releases of the refractory elements (Si, Al, Fe, Mg and Ca) are more likely as results of physical carryover mechanisms, particularly fine mineral particles inherented in the coal being released as part of volatiles jets from the pyrolysing coal particles, or fine mineral fragments being released from the decomposition of carbonates and/or pyrite etc. The releases of these species during pyrolysis may be responsible for the slight reduction on the yields of $PM_{1\text{-}10}$ during char combustion.

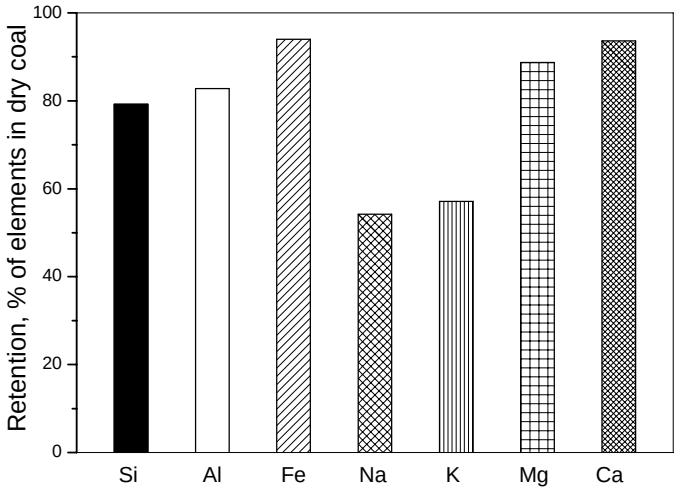

Figure 7- 13: Retention of major inorganic elements in char produced from fast pyrolysis of coal at 1000 ^{o}C

The other is the differences in the combustion conditions between char combustion and its parent coal combustion. During coal combustion, the intensified release of volatiles during coal combustion would lead to rapid rotations of burning coal particles.[293] Therefore, such rotations would be much faster for burning coal particles during coal combustion in comparison to the burning char particles during char combustion, leading to significantly enhanced shedding of ash particles from the fast

receding surface of char hence increased PM_{1-10} yield during coal combustion. Additionally, the absence of volatiles combustion during the combustion of char may lead to a lower particle temperature during char combustion than that during coal combustion.[294-297] It is known that at a lower combustion temperature, the weaken shedding of ash particles from burning coal/char particles may consequently lead to decreased liberation of fine included mineral particles within a burning coal/char particles.[284] As a result, the fine included mineral particles would have increased time to coalescence, leading to decreased PM_{1-10} yield during char combustion. Indeed, as shown in Figure 7-14, coalescence of included mineral particles in burning char/coal particles obvisously took place during coal/char combustion because there are substantial amount of large ash agglomerates (> 10μm) present in the ash samples collected in the cyclone from the combustion of either coal or char. Most importantly, the intensified coalescence and agglomeration of fine included mineral particles during char combustion are also clearly evidenced because the ash agglomerates collected in cyclone from char combustion are considerably bigger than those from coal combustion. It is also interesting to note that the ash agglomerates formed during char combustion consist of mainly small ash particles of irregular shapes but experienced partially melting, in comparison to sphereical particles (experienced complete melting) during coal combustion, as shown in Figure 7-14.

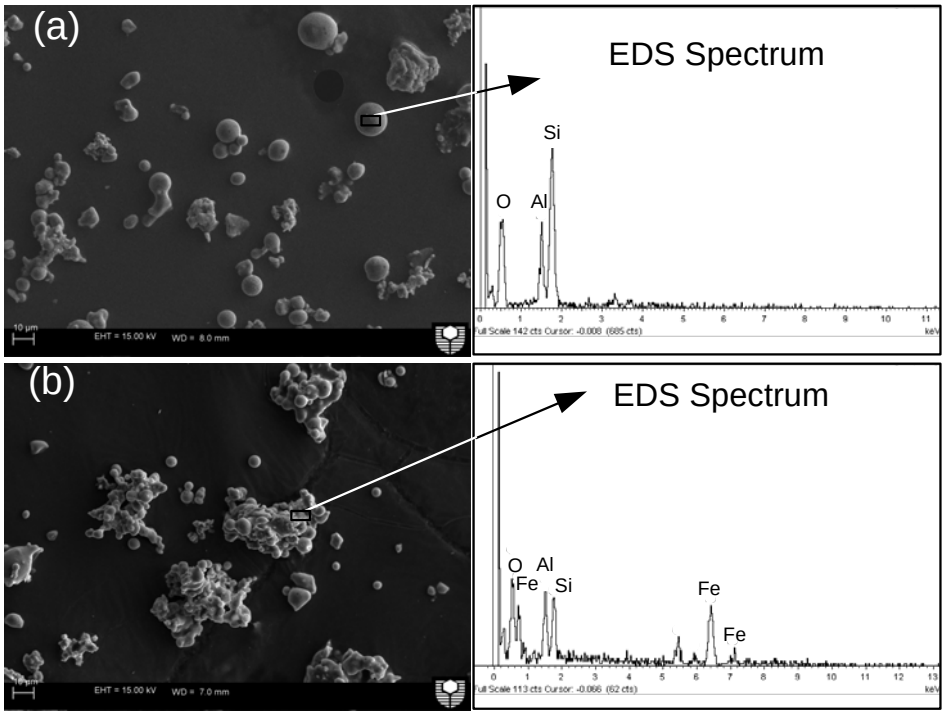

Figure 7- 14: SEM images and EDS spectrum of ash particles collected by cyclone from the combustion of (a) coal and (b) char

7.7 Conclusions

This chapter reports the significant roles of fine included mineral particles in the formation and/or emission of PM_{10} during pulverized coal and char combustion. The main conclusions are drawn as follows:

- CCSEM results show that ~90% of the total mineral particles in the Collie coal sample are fine included mineral particles with a size <10 μm. The major included minerals are quartz, kaolinite and iron-bearing minerals.

- The PM_{10} collected from the combustion of coal and char samples dominantly contains PM_{1-10}, of which the yields are 136.2 and 125.9 mg/g_ash input for coal and char combustion, respectively. However, the yields of PM_1 are limited, of which are 13.9 and 16.7 mg/g_ash input for coal and char combustion, respectively. As a result, the amounts of PM_1 and PM_{1-10} account for ~2.3% and

~19.4% of the total ash colleted from the combustion of both coal and char, respectively.

- PM_{1-10} contains dominantly refractory species, including Si, Al, Fe, Mg and Ca, Na and K which are mainly in the forms of water-insoluble are also evident.

- PM_1 from char combustion consits two major fractions ($PM_{0.1}$ and $PM_{0.1-1}$) with different chemical compostion. $PM_{0.1}$ dominantly contains volatile elements (such as Na, K, P and S) and refractory elements (Fe and Si), with little amounts of Al and other alkaline earth metals (such as Ca, Mg, Ba and Sr). Oppositely, $PM_{0.1-1}$ are mianly composed of refractory elements (Al, Fe, and Si), which account for ~84.3% of the total $PM_{0.1-1}$ based on the mass of their oxides, while the amounts of volatile elements such as Na, K, P, S and Cl are relatively low.

- The significant roles of fine included mineral particles in PM_{1-10} emission during coal and char combustion are clearly evidenced via the identification of the presence of abundant individual but partially-molten quartz ash particles in PM_{1-10}. Furthermore, the significant roles of fine included kaolinite and/or Al-silicates particles in the emission of PM_1 from char combustion are also evident based on the vast existence of aluminosilicates in $PM_{0.1-1}$.

- The differences in PSDs and yields of PM_{10} between the combustion of coal and char maybe due to the release of inorganic species (mainly Si, Al, Fe, Na, K, Mg and Ca) during coal pyrolysis for char preparation and the differences in the prevailing combustion conditions.

CHAPTER 8 CONCLUSIONS AND RECOMMENDATIONS

8.1 Introduction

This chapter summarizes the key research outcomes from this PhD study. Overall, the thesis has delivered new insights into fundamental understanding on the emission of inorganic PM during the combustion of solid fuel such as biomass, biochar and coal. Firstly, this research has developed a new PM sampling method that minimizes the distortion of ash properties by sampling process. Secondly, this research has also reported as the first time in the field on the emission behavior and characteristics of inorganic PM produced from the combustion of various biochars. Thirdly, a novel two-stage pyrolysis/combustion reactor system was deployed to successfully separate volatiles combustion from char, providing direct experimental evidence on the substantial contribution of volatiles combustion to PM_1 emission. Finally, direct evidence is also obtained on the significant roles of fine inherent mineral particles in the emission of PM_{10} during pulverized coal combustion. Additionally, based on the data and findings so far, some recommendations are also given on the future work required on several important aspects in this research area.

8.2 Conclusions

8.2.1 Effect of Sampling Temperature on the Properties of Inorganic Particulate Matter Collected from Biomass Combustion

- Sampling temperature is found to influence significantly on the properties of PM_{10} collected from the combustion of pulverized biomass.

- Coagulation of fine particles appears to be the key mechanism responsible for the shift of PM_1 mass to larger size as the sampling temperature decreases, although the total yield of PM_1 remains unchanged.

- The chemical composition of PM_1 is dominantly Na, K and Cl and the mass distribution of these elements also shifts to larger size in PM_1 as the sampling temperature decreases, as results of the coagulation of Na-, K, and Cl-containing fine particles.

- The PM_{1-10} contains dominantly of Mg and Ca, the mass PM_{1-10} and the mass of Mg and Ca in PM_{1-10} increases with increasing sampling temperature and levels off at a sampling temperature close to the flue gas temperature (115^{o}C).

- The reduction in the collection of Mg- and Ca-containing coarse particles in PM_{1-10} as the sampling temperature decreases appears to be mainly due to gravitational settling deposition.

- The "turning point" temperature of PSD and elemental mass size distribution curves seems to correlate well with the SO_3 dew point of the flue gas.

- To ensure the proper collection of PM_{10}, the sampling temperature should be above the flue gas acid dew point temperature to prevent acid gas condensation and furthermore be kept at a temperature same as (or close to) the flue gas temperature.

8.2.2 Emission Behavior and Characteristics of PM_1 and PM_{10} from the Combustion of Pulverized Biochar in a Drop-Tube Furnace

- The biochar yields during biomass pyrolysis range from ~26.7 to ~37.0% depending on pyrolysis conditions. At such low temperatures, the majority (78.5 – 100.0%) of AAEM species are retained in biochars after pyrolysis, while the retention of Cl in biochars is only 2.0 – 33.4%.

- The PSD of PM_{10} from raw biomass combustion has a bimodal size distribution, i.e., a fine mode (mode diameter: ~0.022 μm) and a coarse mode (mode diameter: ~6.8 μm). However, the PSDs of PM_{10} from biochars combustion generally

show a unimodal distribution with only a coarse mode (mode diameter: ~6.8 μm).

- The combustion of biochars leads to substantial reductions in both PM_1 yields and the mass of Na, K and Cl in PM_1 in comparison to direct biomass combustion, such reduction is most likely due to the lack of the contribution of volatiles (including released inorganic species) combustion to PM_1 formation and the volatilization of Cl during low-temperature pyrolysis of biomass for biochars preparation.
- Biochars combustion also results in significant increases in the yields of PM_{1-10} and the mass of Mg and Ca in PM_{1-10} compared with those from raw biomass combustion, most likely due to the significant changes in char structures.
- Based on an equivalent energy input into furnace, there is a strong correlation between the energy-based PM_{1-10} yields and the energy-based ash loading during biochars combustion. An increase in biochar ash loading leads to a significantly increased PM_{1-10} emission.

8.2.3 Combustion of Volatiles Produced in Situ from the Fast Pyrolysis of Woody Biomass: Direct Evidence on its Substantial Contribution to PM_1 Emission

- An increase in pyrolysis temperature from 800 to 1000 ^oC leads to an increase in the yield of volatiles from 83.7% to 87.4% (db), and the release and/or volatilization of Na, K, Mg ,Ca and Cl from 51.8 to 81.4%, 43.5 to 54.5%, 2.5 to 9.3%, 6.3 to 16.1% and 85.2 to 97.2%, respectively.
- Based on the data from the combustion of volatiles produced in situ from raw biomass pyrolysis at 800 – 1000 °C, volatiles combustion contributes to 77.4 – 89.3% of the yield of total PM_1 while char combustion contributes to 97.5 – 99.7% of the yield of total PM_{1-10}.
- PM_1 from volatiles combustion is dominantly $PM_{0.1}$ and consists of mainly Na,

K and Cl, with little Mg and Ca. The mass-based PSDs of PM_{10} and elemental-mass-based PSDs of Na, K, and Cl (which are dominantly contained in PM_1) from volatiles combustion generally show a unimodal distribution with a fine mode range from ~0.022 to ~0.043 μm. A higher pyrolysis temperature leads to a significant mass increase of the particles (and the mass of Na, K and Cl dominantly contained in these particles) with a size less than ~0.077 μm.

- The mass-based PSDs of PM_{10} and elemental-mass-based PSDs of Mg and Ca (dominantly contained in PM_{1-10}) from char combustion generally show a unimodal distribution with a coarse mode of ~6.8 μm. Increasing char preparation (i.e., pyrolysis) temperature leads a considerable mass decrease of particles with a size less than 0.022 μm (and also Na, K and Cl in these particles) during char combustion, possibly due to the reduction of Cl content in chars.
- The volatilisation and subsequent combustion of Na, K and Cl with volatiles produced in situ from biomass fast pyrolysis are the key mechanism responsible for PM_1 emission. There are strong correlations between the PM_1 yields and the contents of (Na+K+Cl), (Na+K) and Cl in the volatiles from volatiles combustion. The dominant presence of alkali (Na and K) chlorides in $PM_{0.1}$ collected from the combustion of volatiles and raw biomass is also evident.

8.2.4 Significant Roles of Inherent Fine Included Mineral Particles in the Emission of PM_{10} during Pulverized Coal Combustion

- CCSEM results show that ~90% of the total mineral particles in the Collie coal sample are fine included mineral particles with a size <10 μm. The major included minerals are quartz, kaolinite and iron-bearing minerals.
- The PM_{10} collected from the combustion of coal and char samples dominantly contains PM_{1-10}, of which the yields are 136.2 and 125.9 mg/g_ash input for coal and char, respectively. However, the yields of PM_1 are limited, of which are 13.9 and 16.7 mg/g_ash input for coal and char, respectively. As a result, the amounts

of PM_1 and PM_{1-10} account for ~2.3% and ~19.4% of the total ash colleted from the combustion of both coal and char, respectively.

- Chemical analysis of PM_{1-10} shows that PM_{1-10} contains dominantly refractory species, including Si, Al, Fe, Mg and Ca, Na and K which are mainly in the forms of water-insoluble are also evident.
- PM_1 from char combustion consits two major fractions ($PM_{0.1}$ and $PM_{0.1-1}$) with different chemical compostion. $PM_{0.1}$ dominantly contains volatile elements (such as Na, K, P and S) and refractory elements (Fe and Si), with little amounts of Al and other alkaline earth metals (such as Ca, Mg, Ba and Sr). Oppositely, $PM_{0.1-1}$ are mianly composed of refractory elements (Al, Fe, and Si), which account for ~84.3% of the total $PM_{0.1-1}$ based on the mass of their oxides, while the amounts of volatile elements such as Na, K, P, S and Cl are relatively low.
- The significant roles of fine included mineral particles in PM_{1-10} emission during coal and char combustion are clearly evidenced via the identification of the presence of abundant individual but partially-molten quartz ash particles in PM_{1-10}. Furthermore, the significant roles of fine included kaolinite and/or Al-silicates particles in the emission of PM_1 from char combustion are also evident based on the vast existence of aluminosilicates in $PM_{0.1-1}$.
- The differences in PSDs and yields of PM_{10} between the combustion of coal and char maybe due to the release of inorganic species (mainly Si, Al, Fe, Na, K, Mg and Ca) during coal pyrolysis for char preparation and the differences in the prevailing combustion conditions.
-

8.3 Recommendations

Based on the conclusions in this study, the future research is suggested below:

1. The roles of Cl in the release of alkali metals (Na and K) during biomass pyrolysis and combustion remain unclear. It is therefore important to carry out additional research to systematically investigate the role of Cl in alkali metals release and subsequent fine PM formation and/or emission.

2. In this thesis, the volatiles were generated via fast pyrolysis of biomass at a max temperature of 1000 ^{o}C due to the limitation of working temperature of quartz feeder (see Chapter 6). Advanced experimental techniques are desired to achieve the same temperature between volatiles generation and subsequent combustion.

3. Future research is also needed on the combustion of other high–energy-density fuels such as bioslurry, particularly on the emission behavior and characteristics of inorganic PM.

4. Co-firing biomass with coal in existing coal-based power stations is an attractive short-term option for reducing the CO_2 emission and using biomass in a large scale for electricity generation. Therefore, it is important to investigate the inorganic PM formation and/or emission from various co-firing options, including coal-biomass, coal-biochar and coal-combustible-gases produced form biomass gasification.

REFERENCES

1. Australian Bureau of Agriculture and Resource Economics (ABARE), Energy updates 2011. http://www.abare.gov.au.
2. Dave, N.; Do, T.; Palfreyman, D.; Feron, P. H. M., Impact of liquid absorption process development on the costs of post-combustion capture in Australian coal-fired power stations. *Chemical Engineering Research and Design* **2011,** 89, (9), 1625-1638.
3. IEA, "World Energy Outlook 2009", OECD/IEA, 2009.
4. Wu, H.; Fu, Q.; Giles, R.; Bartle, J., Production of Mallee Biomass in Western Australia: Energy Balance Analysis. *Energy Fuels* **2008,** 22, (1), 190-198.
5. Bartle, J.; Olsen, G.; Don, C.; Trevor, H., Scale of Biomass Productionfrom New Woody Crops for Salinity Control in Dryland Agriculture in Australia. *Int.J.Global Energy Issues* **2007,** 27, (2), 115-137.
6. Yu, Y.; Bartle, J.; Li, C. Z.; Wu, H., Mallee Biomass as a Key Bioenergy Source in Western Australia: Importance of Biomass Supply Chain. *Energy Fuels* **2009,** 23, (6), 3290-3299.
7. Yu, Y.; Wu, H., Bioslurry as a Fuel. 2. Life-Cycle Energy and Carbon Footprints of Bioslurry Fuels from Mallee Biomass in Western Australia. *Energy & Fuels* **2010,** 24, 5660-5668.
8. Bartle, J. R.; Abadi, A., Toward Sustainable Production of Second Generation Bioenergy Feedstocks. *Energy Fuels* **2010,** 24, (1), 2-9.
9. Peter, M., Energy production from biomass (part 1): overview of biomass. *Bioresource Technology* **2002,** 83, (1), 37-46.
10. Senelwa, K.; Sims, R. E. H., Fuel characteristics of short rotation forest biomass. *Biomass and Bioenergy* **1999,** 17, (2), 127-140.
11. Mohan, D.; Pittman, C. U.; Steele, P. H., Pyrolysis of Wood/Biomass for Bio-oil: A Critical Review. *Energy & Fuels* **2006,** 20, (3), 848-889.
12. Garcia-Perez, M.; Wang, X. S.; Shen, J.; Rhodes, M. J.; Tian, F.; Lee, W.-J.; Wu, H.; Li, C.-Z., Fast Pyrolysis of Oil Mallee Woody Biomass: Effect of Temperature on the Yield and Quality of Pyrolysis Products. *Industrial & Engineering Chemistry Research* **2008,** 47, (6), 1846-1854.
13. Wu, H.; Yip, K.; Tian, F.; Xie, Z.; Li, C.-Z., Evolution of Char Structure during the Steam Gasification of Biochars Produced from the Pyrolysis of Various Mallee Biomass Components. *Industrial & Engineering Chemistry Research* **2009,** 48, (23), 10431-10438.
14. Abdullah, H.; Wu, H., Biochar as a Fuel: 1. Properties and Grindability of Biochars Produced from the Pyrolysis of Mallee Wood under Slow-Heating Conditions. *Energy & Fuels* **2009,** 23, (8), 4174-4181.
15. Abdullah, H.; Mediaswanti, K. A.; Wu, H., Biochar as a Fuel: 2. Significant Differences in Fuel Quality and Ash Properties of Biochars from Various Biomass

Components of Mallee Trees. *Energy & Fuels* **2010,** 24, (3), 1972-1979.
16. Khan, A. A.; de Jong, W.; Jansens, P. J.; Spliethoff, H., Biomass combustion in fluidized bed boilers: Potential problems and remedies. *Fuel Processing Technology* **2009,** 90, (1), 21-50.
17. Yip, K.; Xu, M.; Li, C.-Z.; Jiang, S. P.; Wu, H., Biochar as a Fuel: 3. Mechanistic Understanding on Biochar Thermal Annealing at Mild Temperatures and Its Effect on Biochar Reactivity. *Energy & Fuels* **2010,** 25, (1), 406-414.
18. Boylan, D. M., Southern Company tests of wood/coal cofiring in pulverised coal units. *Biomass and Bioenergy* **1996,** 10, (2-3), 139-147.
19. Hughes, E. E.; Tillman, D. A., Biomass cofiring: status and prospects 1996. *Fuel Processing Technology* **1998,** 54, 127-142.
20. Prinzing, D. E.; Hunt, E. F., Impacts of wood cofiring on coal pulverization at the Shawville Generating Station. *Fuel Processing Technology* **1998,** 54, 143-157.
21. Zulfiqar, M. H.; Moghtaderi, B.; Wall, T. F. *Co-milling of coal and biomass in pilot-scale vertical spindle mill*; Cooperative Research Centre for Coal in Sustainable Development (CCSD), QCAT, Technology Transfer Centre, Pullenvale, Quensland.: 2006.
22. Zulfiqar, M.; Moghtaderi, B.; Wall, T. F., Flow properties of biomass and coal blends *Fuel Processing Technology* **2006,** 87, 281-288
23. Wendt, J. O. L., Fundamental coal combustion mechanisms and pollutant formation in furnaces. *Progress in Energy and Combustion Science* **1980,** 6, (2), 201-222.
24. Sami, M.; Annamalai, K.; Wooldridge, M., Co-firing of coal and biomass fuel blends. *Progress in Energy and Combustion Science* **2001,** 27, (2), 171-214.
25. William T, R., The relation of mineral composition to slagging, fouling and erosion during and after combustion. *Progress in Energy and Combustion Science* **1984,** 10, (2), 159-169.
26. Seames, W. S., An initial study of the fine fragmentation fly ash particle mode generated during pulverized coal combustion. *Fuel Processing Technology* **2003,** 81, (2), 109-125.
27. Zhang, L.; Ninomiya, Y., Emission of suspended PM10 from laboratory-scale coal combustion and its correlation with coal mineral properties. *Fuel* **2006,** 85, (2), 194-203.
28. Lind, T. T.; Valmari, E.; Kauppinen, K.; Nilsson, K.; Sfiris, G.; Maenhaut, W., ASH formation mechanisms during combustion of wood in circulating fluidized beds. *Proc. Combust. Inst.* **2000,** 28, (2), 2287–2295.
29. Chen, Y.; Shah, N.; Huggins, F. E.; Huffman, G. P.; Linak, W. P.; Miller, C. A., Investigation of primary fine particulate matter from coal combustion by computer-controlled scanning electron microscopy. *Fuel Processing Technology* **2004,** 85, (6-7), 743-761.
30. Ninomiya, Y.; Zhang, L.; Sato, A.; Dong, Z., Influence of coal particle size on particulate matter emission and its chemical species produced during coal combustion. *Fuel Processing Technology* **2004,** 85, (8-10), 1065-1088.
31. Lind, T.; Valmari, T.; Kauppinen, E. I.; Sfiris, G.; Nilsson, K.; Maenhaut, W.,

Volatilization of the Heavy Metals during Circulating Fluidized Bed Combustion of Forest Residue. *Environ.Sci.Technol.* **1999,** 33, (3), 496–502.
32. Maynard, A. D.; Maynard, R. L., A derived association between ambient aerosol surface area and excess mortality using historic time series data. *Atmos. Environ.* **2002,** 36, (36-37), 5561-5567.
33. Mikkanen, P., Fly ash particle formation in kraft recovery boilers. Academic Dissertation; VTT Publications 421: Espoo, Finland, 2000.
34. Bryers, R. W., Fireside slagging, fouling, and high-temperature corrosion of heat-transfer surface due to impurities in steam-raising fuels. *Progress in Energy and Combustion Science* **1996,** 22, (1), 29-120.
35. Grabke, H. J.; Reese, E.; Spiegel, M., The effects of chlorides, hydrogen chloride, and sulfur dioxide in the oxidation of steels below deposits. *Corrosion Science* **1995,** 37, (7), 1023-1043.
36. Seames, W. S.; Wendt, J. O. L., Partitioning of arsenic, selenium, and cadmium during the combustion of Pittsburgh and Illinois #6 coals in a self-sustained combustor. *Fuel Processing Technology* **2000,** 63, (2-3), 179-196.
37. Seames, W. S.; Wendt, J. O. L., Regimes of association of arsenic and selenium during pulverized coal combustion. *Proceedings of the Combustion Institute* **2007,** 31, (2), 2839-2846.
38. Herek L, C., Bimodal fly ash size distributions and their influence on gas-particle mass transfer during electrostatic precipitation. *Fuel Processing Technology* **2006,** 87, (11), 987-996.
39. Xu, M.; Yu, D.; Yao, H.; Liu, X.; Qiao, Y., Coal combustion-generated aerosols: Formation and properties. *Proceedings of the Combustion Institute* **2011,** 33, (1), 1681-1697.
40. Quann, R. J.; Neville, M.; Janghorbani, M.; Mims, C. A.; Sarofim, A. F., Mineral matter and trace-element vaporization in a laboratory-pulverized coal combustion system. *Environmental Science & Technology* **1982,** 16, (11), 776-781.
41. Lind, T.; Kauppinen, E. I.; Hokkinen, J.; Jokiniemi, J. K.; Orjala, M.; Aurela, M.; Hillamo, R., Effect of Chlorine and Sulfur on Fine Particle Formation in Pilot-Scale CFBC of Biomass. *Energy Fuels* **2005,** 20, (1), 61-68.
42. Spliethoff, H.; Hein, K. R. G., Effect of co-combustion of biomass on emissions in pulverized fuel furnaces. *Fuel Processing Technology* **1998,** 54, (1-3), 189-205.
43. WHO, Air quality guidelines: Global update 2005, World Health Organization, ISBN: 9289021926, 2007 Edition.
44. DIOR, 2005 - 06 Western Australian Mineral and Petroleum STATISTICS DIGEST. Department of Industry and Resources, Government of Western Australia: Perth, Australia, 2006.
45. http://en.wikipedia.org/wiki/List_of_power_stations_in_Western_Australia.
46. Esther, N., Investigation of Char Reactivity of Collie Coals. Ph.D. Thesis, Department of Chemical Engineering, Curtin University of Technology, Australia, 2006. .
47. Clark, K.; Meakins, R.; Attalla, M.; Craig, K., Report on Project C3100: Agglomeration and Stabilisation of Collie Coals by Binderless Briquetting;

Australian Coal Research Ltd.: Brisbane, Australia, 1997.
48. Yip, K.; Wu, H.; Zhang, D.-k., Effect of Inherent Moisture in Collie Coal during Pyrolysis Due to in-Situ Steam Gasification. *Energy & Fuels* **2007,** 21, (5), 2883-2891.
49. Yip, K.; Wu, H.; Zhang, D.-k., Pyrolysis of Collie Coal Briquettes To Produce Char as a Metallurgical Reductant†. *Energy & Fuels* **2006,** 21, (2), 419-425.
50. Yip, K.; Wu, H.; Zhang, D.-k., Mathematical modelling of Collie coal pyrolysis considering the effect of steam produced in situ from coal inherent moisture and pyrolytic water. *Proceedings of the Combustion Institute* **2009,** 32, (2), 2675-2683.
51. Vuthaluru, H. B.; Brooke, R. J.; Zhang, D. K.; Yan, H. M., Effects of moisture and coal blending on Hardgrove Grindability Index of Western Australian coal. *Fuel Processing Technology* **2003,** 81, (1), 67-76.
52. Wee, H. L.; Wu, H.; Zhang, D.-k., Heterogeneity of Ash Deposits Formed in a Utility Boiler during PF Combustion†. *Energy & Fuels* **2006,** 21, (2), 441-450.
53. Ngee, N., Characterisation of Mineral Matter in Selected Australian Coals and Its Relation to the Formation of Fine Ash and Cenospheres. Ph.D. Thesis, Department of Chemical Engineering, Curtin University of Technology, Australia, 2008. .
54. Stamatov, V.; Honnery, D.; Soria, J., Combustion properties of slow pyrolysis bio-oil produced from indigenous Australian species. *Renewable Energy* **2006,** 31, (13), 2108-2121.
55. Bernesson, S.; Nilsson, D.; Hansson, P.-A., A limited LCA comparing large- and small-scale production of rape methyl ester (RME) under Swedish conditions. *Biomass and Bioenergy* **2004,** 26, (6), 545-559.
56. Rustandi, F.; Wu, H., Biodiesel Production from Canola in Western Australia: Energy and Carbon Footprints and Land, Water, and Labour Requirements. *Industrial & Engineering Chemistry Research* **2010,** 49, (22), 11785-11796.
57. Bell, S. J.; Barton, A. F. M.; Stocker, L. J., Agriculture for health and profit in Western Australia: The Western Oil Mallee Project. *Ecosystem Health* **2001,** 7, (2), 116-121.
58. Bartle, J.; Cooper, D.; Olsen, G.; Carslake, J., Acacia species as large scale crop plants in the Western Australian weatbelt. *Conserv. Sci. West. Aust.* **2002,** 4, 96.
59. Olsen, G.; Cooper, D.; Huxtable, D.; Carslake, J.; Bartle, J., DeVeloping multiple purpose species for large scale reVegetation, search project final report (nht project 973849); Department of Conservation and Land Management: Perth, Western Australia, 2004.
60. Maciejewska, A.; Veringa, H.; Sanders, J.; Peteves, S. D. *Co-firing of Biomass with Coal: Constraints and Role of Biomass Pre-treatment.*; DG JRC Institute for Energy: 2006.
61. Esteban, L. S.; Carrasco, J. E., Evaluation of different strategies for pulverization of forest biomasses. *Powder Technology* **2006,** 166, (3), 139-151.
62. Svoboda, K.; Pohorelý, M.; Hartman, M.; Martinec, J., Pretreatment and feeding of biomass for pressurized entrained flow gasification. *Fuel Processing Technology* **2009,** 90, (5), 629-635.

63. Bridgewater, A. V., Biomass Fast Pyrolysis. *Thermal Science* **2004,** 8, (2), 21-49.
64. Czernik, S.; Bridgewater, A. V., Overview of Applications of Biomass Fast Pyrolysis Oil. *Energy & Fuels* **2004,** 18, 590-598.
65. Mohan, D.; Pittman, C. U.; Steele, P. H., Pyrolysis of Wood and Biomass For Bio Oil: A Critical Review. *Energy& Fuels* **2006,** 20, 846-889.
66. Garcia-Perez, M.; Chaala, A.; Pakdel, H.; Kretschmer, D.; Rodrigue, D.; Roy, C., Vacuum Pyrolysis of Softwood and Hardwood Biomass Comparison between Products Yields and Bio oil Properties. *J.Anal.Appl.Pyrolysis* **2007,** 78, 104-116.
67. Mulligan, C. J.; Strezov, L.; Strezov, V., Thermal Decomposition of Wheat Straw and Mallee Residue Under Pyrolysis Conditions. *Energy & Fuels* **2010,** 24, 46.
68. Garcia-Perez, M.; Chaala, A.; Pakdel, H.; Kretschmer, D.; Rodrigue, D.; Roy, C., Multiphase Structure of Bio oils. *Energy & Fuels* **2006,** 20, 364-375.
69. Garcia-Perez, M.; Wang, X. S.; Shen, J.; Rhodes, M. J.; Tian, F.; Lee, W.; Wu, H.; Li, C., Fast pyrolysis of oil mallee wood biomass: effect of temperature on the yield and quality of pyrolysis products. *Ind. Eng. Chem. Res.* **2008,** 47, 1846-1854.
70. Abdullah, H.; Mediaswanti, K. A.; Wu, H., Biochar as a Fuel:2. Significant Differences in Fuel Quality and Ash Properties of Biochars from Various Biomass Components of Mallee Trees. *Energy & Fuels* **2010,** 24, (3), 1972-1979.
71. Huber, G. W.; Iborra, S.; Corma, A., Synthesis of Transportation Fuels from Biomass: Chemistry, Catalysts and Engineering. *Chem. Rev.* **2006,** 106, 4044-4098.
72. Yip, K.; Tian, F.; Hayashi, J.; Wu, H., Effect of Alkali and Alkaline Earth Metallic Species on Biochar Reactivity and Syngas Compositions during Steam Gasification. *Energy Fuels* **2010,** 24, (1), 173-181.
73. Baxter, L., Biomass-coal co-combustion: opportunity for affordable renewable energy. *Fuel* **2005,** 84, (10), 1295-1302.
74. Lu, G.; Yan, Y.; Cornwell, S.; Whitehouse, M.; Riley, G., Impact of co-firing coal and biomass on flame characteristics and stability. *Fuel* **2008,** 87, (7), 1133-1140.
75. Tillman, D. A., Biomass cofiring: the technology, the experience, the combustion consequences. *Biomass and Bioenergy* **2000,** 19, (6), 365-384.
76. Wieck-Hansen, K., Co-ring coal and straw in PF boilers performance impact of straw with emphasis on SCR catalyst for DeNOx catalysis. Proceedings of the 16th Annual Pittsburgh Coal Conference, Pittsburgh, PA, October 11-15,1999.
77. Gupta, R. P.; Beacher, C.; Bhargava, A.; Wall, T. F., The Fate of Inorganic Matter in Biomass During Combustion. *19th Annual Pittsburgh Coal Science Conference, Pittsburgh, 2002.*
78. Baxter, L. L., Ash deposition during biomass and coal combustion: A mechanistic approach. *Biomass and Bioenergy* **1993,** 4, (2), 85-102.
79. Lokare, S. S.; Dunaway, J. D.; Moulton, D.; Rogers, D.; Tree, D. R.; Baxter, L. L., Investigation of Ash Deposition Rates for a Suite of Biomass Fuels and Fuel Blends. *Energy & Fuels* **2006,** 20, (3), 1008-1014.
80. Wall, T. F., Mineral matter transformations and ash deposition in pulverised coal combustion. *Symposium (International) on Combustion* **1992,** 24, (1), 1119-1126.
81. Harb, J. N.; Smith, E. E., Fireside corrosion in pc-fired boilers. *Progress in Energy and Combustion Science* **1990,** 16, (3), 169-190.

82. Davidsson, K. O.; Korsgren, J. G.; Pettersson, J. B. C.; Jäglid, U., The effects of fuel washing techniques on alkali release from biomass. *Fuel* **2002,** 81, (2), 137-142.
83. Robinson, A. L.; Junker, H.; Baxter, L. L., Pilot-Scale Investigation of the Influence of Coal−Biomass Cofiring on Ash Deposition. *Energy & Fuels* **2002,** 16, (2), 343-355.
84. Christensen, K. A. The formation of submicron particles form the combustion of straw. PhD dissertation. Technical University of Denmark, Lyngby, Denmark, 1995.
85. Johansson, L. S.; Tullin, C.; Leckner, B.; Sjövall, P., Particle emissions from biomass combustion in small combustors. *Biomass Bioenerg.* **2003,** 25, (4), 435-446.
86. Strand, M.; Bohgard, M.; Swietlicki, E.; Gharibi, A.; Sanati, M., Laboratory and Field Test of a Sampling Method for Characterization of Combustion Aerosols at High Temperatures. *Aerosol Sci. Tech.* **2004,** 38, (8), 757–765.
87. Lipsky, E. M.; Robinson, A. L., Effects of Dilution on Fine Particle Mass and Partitioning of Semivolatile Organics in Diesel Exhaust and Wood Smoke. *Environmental Science & Technology* **2005,** 40, (1), 155-162.
88. Hinds, W., *Aerosol Technology: Properties, Behavior, and Measurement of Airborne Particles.* 2 ed.; Wiley-Interscience: New York, 1999.
89. Hildemann, L. M.; Cass, G. R.; Markowski, G. R., A Dilution Stack Sampler for Collection of Organic Aerosol Emissions: Design, Characterization and Field Tests. *Aerosol Science and Technology* **1989,** 10, (1), 193-204.
90. McElroy, M. W.; Carr, R. C.; Ensor, D. S.; Markowski, G. R., Size Distribution of Fine Particles from Coal Combustion. *Science* **1982,** 215, (4528), 13-19.
91. Markowski, G. R.; Ensor, D. S.; Hooper, R. G.; Carr, R. C., A submicron aerosol mode in flue gas from a pulverized coal utility boiler. *Environmental Science & Technology* **1980,** 14, (11), 1400-1402.
92. Wehner, B.; Bond, T. C.; Birmili, W.; Heintzenberg, J.; Wiedensohler, A.; Charlson, R. J., Climate-Relevant Particulate Emission Characteristics of a Coal Fired Heating Plant. *Environmental Science & Technology* **1999,** 33, (21), 3881-3886.
93. Markowski, G. R.; Filby, R., Trace element concentration as a function of particle size in fly ash from a pulverized coal utility boiler. *Environmental Science & Technology* **1985,** 19, (9), 796-804.
94. Lipsky, E.; Stanier, C. O.; Pandis, S. N.; Robinson, A. L., Effects of Sampling Conditions on the Size Distribution of Fine Particulate Matter Emitted from a Pilot-Scale Pulverized-Coal Combustor. *Energy Fuels* **2002,** 16, (2), 302-310.
95. Jiménez, S.; Ballester, J., A Comparative Study of Different Methods for the Sampling of High Temperature Combustion Aerosols. *Aerosol Science and Technology* **2005,** 39, (9), 811-821.
96. Kauppinen, E. I.; Pakkanen, T. A., Coal combustion aerosols: a field study. *Environ.Sci.Technol.* **1990,** 24, (12), 1811-1818.
97. Valmari, T.; Lind, T. M.; Kauppinen, E. I.; Sfiris, G.; Nilsson, K.; Maenhaut, W., Field Study on Ash Behavior during Circulating Fluidized-Bed Combustion of Biomass. 1. Ash Formation *Energy Fuels* **1999,** 13, (2), 379-389.
98. Johansson, L. S.; Leckner, B.; Gustavsson, L.; Cooper, D.; Tullin, C.; Potter, A.,

Emission characteristics of modern and old-type residential boilers fired with wood logs and wood pellets. *Atmos. Environ.* **2004,** 38, (25), 4183-4195.
99. Buhre, B. J. P.; Hinkley, J. T.; Gupta, R. P.; Wall, T. F.; Nelson, P. F., Submicron ash formation from coal combustion. *Fuel* **2005,** 84, (10), 1206-1214.
100. Boman, C.; Nordin, A.; Westerholm, R.; Pettersson, E., Evaluation of a constant volume sampling setup for residential biomass fired appliances--influence of dilution conditions on particulate and PAH emissions. *Biomass Bioenerg.* **2005,** 29, (4), 258-268.
101. Jimenez, S.; Ballester, J., Effect of co-firing on the properties of submicron aerosols from biomass combustion. *Proc. Combust. Inst.* **2005,** 30, 2965–2972.
102. Liu, X.; Xu, M.; Yao, H.; Yu, D.; Gao, X.; Cao, Q.; Cai, Y., Effect of Combustion Parameters on the Emission and Chemical Composition of Particulate Matter during Coal Combustion. *Energy & Fuels* **2006,** 21, (1), 157-162.
103. Takuwa, T.; Mkilaha, I. S. N.; Naruse, I., Mechanisms of fine particulates formation with alkali metal compounds during coal combustion. *Fuel* **2006,** 85, (5-6), 671-678.
104. Linak, W. P.; Yoo, J.-I.; Wasson, S. J.; Zhu, W.; Wendt, J. O. L.; Huggins, F. E.; Chen, Y.; Shah, N.; Huffman, G. P.; Gilmour, M. I., Ultrafine ash aerosols from coal combustion: Characterization and health effects. *Proceedings of the Combustion Institute* **2007,** 31, (2), 1929-1937.
105. Zhang, L.; Masui, M.; Mizukoshi, H.; Ninomiya, Y.; Koketsu, J.; Kanaoka, C., Properties of water-soluble and insoluble particulate matter emitted from dewatered sewage sludge incineration in a pilot-scale ash melting furnace. *Fuel* **2008,** 87, (6), 964-973.
106. Bäfver, L. S.; Rönnbäck, M.; Leckner, B.; Claesson, F.; Tullin, C., Emission from combustion of oat grain and its potential reduction by addition of limestone or kaolin. *Fuel Process.Technol.* **2009,** 90, (3), 353-359.
107. Wiinikka, H.; GrÖnberg, C.; Öhrman, O.; BostrÖm, D., Influence of TiO2 Additive on Vaporization of Potassium during Straw Combustion. *Energy Fuels* **2009,** 23, (11), 5367-5374.
108. Ninomiya, Y.; Wang, Q.; Xu, S.; Mizuno, K.; Awaya, I., Effect of Additives on the Reduction of $PM_{2.5}$ Emissions during Pulverized Coal Combustion. *Energy Fuels* **2009,** 23, (7), 3412-3417.
109. Ninomiya, Y.; Wang, Q.; Xu, S.; Teramae, T.; Awaya, I., Evaluation of a Mg-Based Additive for Particulate Matter (PM)2.5 Reduction during Pulverized Coal Combustion. *Energy Fuels* **2010,** 24, 199-204.
110. Vassilev, S. V.; Baxter, D.; Andersen, L. K.; Vassileva, C. G., An overview of the chemical composition of biomass. *Fuel* **2010,** 89, (5), 913-933.
111. Obernberger, I.; Brunner, T.; Bärnthaler, G., Chemical properties of solid biofuels—significance and impact. *Biomass and Bioenergy* **2006,** 30, (11), 973-982.
112. Williams, A.; Pourkashanian, M.; Jones, J. M., Combustion of pulverised coal and biomass. *Progress in Energy and Combustion Science* **2001,** 27, (6), 587-610.
113. Wu, H.; Yip, K.; Kong, Z.; Li, C.-Z.; Liu, D.; Yu, Y.; Gao, X., Removal and Recycling of Inherent Inorganic Nutrient Species in Mallee Biomass and Derived

Biochars by Water Leaching. *Industrial & Engineering Chemistry Research* **2011**.
114.Zevenhoven-Onderwater, M., Ash-forming Matter in Biomass Fuels; Ph.D. Thesis, Department of Chemical Engineering, Åbo Akademi University, Åbo/Turku, Finland, 2002.
115.Marschner, H., Mineral Nutrition of Higher Plants, 2nd ed.: Academic Press: London, 2002; pp229-404.
116.Baxter, L. L., Pollutant emissions and deposit formation during combustion of biomass fuels Third Contractors Meeting 'Alkali Deposits Found in Biomass Power Plants', Sandia National Laboratory, Livermore, California (November 30 1993). .
117.van Lith, S. C.; Jensen, P. A.; Frandsen, F. J.; Glarborg, P., Release to the Gas Phase of Inorganic Elements during Wood Combustion. Part 2: Influence of Fuel Composition. *Energy & Fuels* **2008,** 22, (3), 1598-1609.
118.Dayton, D. C.; French, R. J.; Milne, T. A., Direct Observation of Alkali Vapor Release during Biomass Combustion and Gasification. 1. Application of Molecular Beam/Mass Spectrometry to Switchgrass Combustion. *Energy & Fuels* **1995,** 9, (5), 855-865.
119.Franceschi, V. R.; Horner, H. T., Jr., Calcium Oxalate Crystals in Plants. *Botanical Review* **1980,** 46, (4), 361-427.
120. Jenkins, B. M.; Baxter, L. L.; Miles, T. R.; Miles, T. R.; Oden, L. L.; Bryers, R. W.; Winther, E., Composition of ash deposits in biomass fueled boilers: results of full-scale experiments and laboratory simulations, American Society of Agriculture Engineers, Kansas City (June 19–22 1994). .
121. Korbee, R.; Shah, K. V.; Cieplik, M. K.; Betrand, C. I.; Vuthaluru, H. B.; van de Kamp, W. L., First Line Ash Transformations of Coal and Biomass Fuels during PF Combustion. *Energy & Fuels* 24, (2), 897-909.
122. Shah, K. V.; Cieplik, M. K.; Betrand, C. I.; van de Kamp, W. L.; Vuthaluru, H. B., Correlating the effects of ash elements and their association in the fuel matrix with the ash release during pulverized fuel combustion. *Fuel Processing Technology* **2010,** 91, (5), 531-545.
123. Knudsen, J. N.; Jensen, P. A.; Dam-Johansen, K., Transformation and Release to the Gas Phase of Cl, K, and S during Combustion of Annual Biomass. *Energy & Fuels* **2004,** 18, (5), 1385-1399.
124. Knudsen, J. N.; Jensen, P. A.; Lin, W.; Frandsen, F. J.; Dam-Johansen, K., Sulfur Transformations during Thermal Conversion of Herbaceous Biomass. *Energy & Fuels* **2004,** 18, (3), 810-819.
125. van Lith, S. C.; Alonso-Ramírez, V.; Jensen, P. A.; Frandsen, F. J.; Glarborg, P., Release to the Gas Phase of Inorganic Elements during Wood Combustion. Part 1: Development and Evaluation of Quantification Methods. *Energy & Fuels* **2006,** 20, (3), 964-978.
126. Olsson, J. G.; Jäglid, U.; Pettersson, J. B. C.; Hald, P., Alkali Metal Emission during Pyrolysis of Biomass. *Energy & Fuels* **1997,** 11, (4), 779-784.
127. Dayton, D. C.; Jenkins, B. M.; Turn, S. Q.; Bakker, R. R.; Williams, R. B.; Belle-Oudry, D.; Hill, L. M., Release of Inorganic Constituents from Leached Biomass during Thermal Conversion. *Energy & Fuels* **1999,** 13, (4), 860-870.

128. Keown, D. M.; Favas, G.; Hayashi, J.-i.; Li, C.-Z., Volatilisation of alkali and alkaline earth metallic species during the pyrolysis of biomass: differences between sugar cane bagasse and cane trash. *Bioresource Technology* **2005,** 96, (14), 1570-1577.
129. Keown, D. M.; Hayashi, J.-i.; Li, C.-Z., Effects of volatile–char interactions on the volatilisation of alkali and alkaline earth metallic species during the pyrolysis of biomass. *Fuel* **2008,** 87, (7), 1187-1194.
130. Quyn, D. M.; Wu, H.; Li, C. Z., Volatilisation and catalytic effects of alkali and alkaline earth metallic species during the pyrolysis and gasification of Victorian brown coal. Part I. Volatilisation of Na and Cl from a set of NaCl-loaded samples. . *Fuel* **2002,** 81, (2), 143-149.
131. Björkman, E.; Strömberg, B., Release of Chlorine from Biomass at Pyrolysis and Gasification Conditions. *Energy & Fuels* **1997,** 11, (5), 1026-1032
132. Zintl, F.; Stromberg, B.; Bjorkman, E., Release of Chlorine from Biomass at Gasification Conditions. Proceedings of the 10th European Conference on Biomass for Energy and Industry, Wurzburg, Germany, 1998. .
133. Yu, C.; Bai, J.; Nie, H.; Li, L.; Wang, Q.; Luo, Z., Experimental Study on the Characteristics of Self-Desulfurization during Sugarcane Leaf Combustion in a Circulating Fluidized Bed. *Energy & Fuels* **2011,** 25, (9), 3885-3891.
134. Wang, X.; Si, J.; Tan, H.; Ma, L.; Pourkashanian, M.; Xu, T., Nitrogen, Sulfur, and Chlorine Transformations during the Pyrolysis of Straw. *Energy & Fuels* **2010,** 24, (9), 5215-5221.
135. Khalil, R. A.; Seljeskog, M.; Hustad, J. E., Sulfur Abatement in Pyrolysis of Straw Pellets. *Energy & Fuels* **2008,** 22, (4), 2789-2795.
136. Johansen, J. M.; Jakobsen, J. G.; Frandsen, F. J.; Glarborg, P., Release of K, Cl, and S during Pyrolysis and Combustion of High-Chlorine Biomass. *Energy & Fuels* **2011**.
137. Sonoyama, N.; Okuno, T.; Mašek, O.; Hosokai, S.; Li, C.-Z.; Hayashi, J.-i., Interparticle Desorption and Re-adsorption of Alkali and Alkaline Earth Metallic Species within a Bed of Pyrolyzing Char from Pulverized Woody Biomass. *Energy & Fuels* **2006,** 20, (3), 1294-1297.
138. Okuno, T.; Sonoyama, N.; Hayashi, J.-i.; Li, C.-Z.; Sathe, C.; Chiba, T., Primary Release of Alkali and Alkaline Earth Metallic Species during the Pyrolysis of Pulverized Biomass. *Energy & Fuels* **2005,** 19, (5), 2164-2171.
139. Wu, H.; Quyn, D. M.; Li, C.-Z., Volatilisation and catalytic effects of alkali and alkaline earth metallic species during the pyrolysis and gasification of Victorian brown coal. Part III. The importance of the interactions between volatiles and char at high temperature. *Fuel* **2002,** 81, (8), 1033-1039.
140. Davidsson, K. O.; Stojkova, B. J.; Pettersson, J. B. C., Alkali Emission from Birchwood Particles during Rapid Pyrolysis. *Energy & Fuels* **2002,** 16, (5), 1033-1039.
141. Jensen, P. A.; Frandsen, F. J.; Dam-Johansen, K.; Sander, B., Experimental Investigation of the Transformation and Release to Gas Phase of Potassium and Chlorine during Straw Pyrolysis. *Energy & Fuels* **2000,** 14, (6), 1280-1285.

142. Baxter, L. L.; Miles, T. R.; Dayton, D.; Bryers, R. W.; Oden, L. L., The behavior of inorganic material in biomass-fired power boilers: field and laboratory experiences. *Fuel Process.Technol.* **1998,** 54, (1-3), 47-78.
143. Quyn, D. M.; Wu, H.; Bhattacharya, S. P.; Li, C.-Z., Volatilisation and catalytic effects of alkali and alkaline earth metallic species during the pyrolysis and gasification of Victorian brown coal. Part II. Effects of chemical form and valence. *Fuel* **2002,** 81, (2), 151-158.
144. Skrifvars, B. J.; Lauren, T.; Hupa, M.; Korbee, R.; Ljung, P., Ash behaviour in a pulverized wood fired boiler—a case study. *Fuel* **2004,** 83, (10), 1371-1379.
145. Shah, A. D.; Huffman, G. P.; Huggins, F. E.; Shah, N.; Helble, J. J.; Peterson, T. W.; Sarofim, A. F., Reactions of calcium and sodium during combustion of lignite, International ash utilization symposium. Center for Applied Energy Research, (1999), p. 69.
146. Osborn, G. A., Review of sulphur and chlorine retention in coal-fired boiler deposits. *Fuel* **1992,** 71, (2), 131-142.
147. Obernberger, I.; Biedermann, F.; Widmann, W.; Riedl, R., Concentrations of inorganic elements in biomass fuels and recovery in the different ash fractions. *Biomass and Bioenergy* **1997,** 12, (3), 211-224.
148. Mohanty, B. P.; Shores, D. A., Role of chlorides in hot corrosion of a cast Fe–Cr–Ni alloy. Part I: Experimental studies. *Corrosion Science* **2004,** 46, (12), 2893-2907.
149. Nielsen, H. P.; Baxter, L. L.; Sclippab, G.; Morey, C.; Frandsen, F. J.; Dam-Johansen, K., Deposition of potassium salts on heat transfer surfaces in straw-fired boilers: a pilot-scale study. *Fuel* **2000,** 79, (2), 131-139.
150. Zheng, Y.; Jensen, A. D.; Johnsson, J. E., Laboratory Investigation of Selective Catalytic Reduction Catalysts: Deactivation by Potassium Compounds and Catalyst Regeneration. *Industrial & Engineering Chemistry Research* **2004,** 43, (4), 941-947.
151. Zheng, Y.; Jensen, A. D.; Johnsson, J. E., Deactivation of V2O5-WO3-TiO2 SCR catalyst at a biomass-fired combined heat and power plant. *Applied Catalysis B: Environmental* **2005,** 60, (3-4), 253-264.
152. Christensen, K. A.; Livbjerg, H., A Field Study of Submicron Particles from the Combustion of Straw. *Aerosol Science and Technology* **1996,** 25, (2), 185-199.
153. Christensen, K. A.; Stenholm, M.; Livbjerg, H., The formation of submicron aerosol particles, HCl and SO2 in straw-fired boilers. *Journal of Aerosol Science* **1998,** 29, (4), 421-444.
154. Wu, H.; Glarborg, P.; Frandsen, F. J.; Dam-Johansen, K.; Jensen, P. A., Dust-firing of straw and additives: Ash chemistry and deposition behavior. *Energy and Fuels* **2011,** 25, (7), 2862-2873.
155. Jiménez, S.; Ballester, J., Formation of alkali sulphate aerosols in biomass combustion. *Fuel* **2007,** 86, (4), 486-493.
156. Lind, T.; Kauppinen, E. I.; Hokkinen, J.; Jokiniemi, J. K.; Orjala, M.; Aurela, M.; Hillamo, R., Effect of Chlorine and Sulfur on Fine Particle Formation in Pilot-Scale CFBC of Biomass. *Energy & Fuels* **2005,** 20, (1), 61-68.

157. Sippula, O.; Lind, T.; Jokiniemi, J., Effects of chlorine and sulphur on particle formation in wood combustion performed in a laboratory scale reactor. *Fuel* **2008,** 87, (12), 2425-2436.
158. Jensen, J. R.; Nielsen, L. B.; Schultz-Møller, C.; Wedel, S.; Livbjerg, H., The Nucleation of Aerosols in Flue Gases with a High Content of Alkali - A Laboratory Study. *Aerosol Science and Technology* **2000,** 33, (6), 490-509.
159. Iisa, K.; Lu, Y.; Salmenoja, K., Sulfation of Potassium Chloride at Combustion Conditions. *Energy & Fuels* **1999,** 13, (6), 1184-1190.
160. Jokiniemi, J. K.; Lazaridis, M.; Lehtinen, K. E. J.; Kauppinen, E. I., Numerical simulation of vapour-aerosol dynamics in combustion processes. *Journal of Aerosol Science* **1994,** 25, (3), 429-446.
161. Liu, K.; Xie, W.; Li, D.; Pan, W.-P.; Riley, J. T.; Riga, A., The Effect of Chlorine and Sulfur on the Composition of Ash Deposits in a Fluidized Bed Combustion System. *Energy & Fuels* **2000,** 14, (5), 963-972.
162. Yang, T.; Kai, X.; Sun, Y.; He, Y.; Li, R., The effect of coal sulfur on the behavior of alkali metals during co-firing biomass and coal. *Fuel* **2011,** 90, (7), 2454-2460.
163. Broström, M.; Kassman, H.; Helgesson, A.; Berg, M.; Andersson, C.; Backman, R.; Nordin, A., Sulfation of corrosive alkali chlorides by ammonium sulfate in a biomass fired CFB boiler. *Fuel Processing Technology* **2007,** 88, (11-12), 1171-1177.
164. Zheng, Y.; Jensen, P. A.; Jensen, A. D., A kinetic study of gaseous potassium capture by coal minerals in a high temperature fixed-bed reactor. *Fuel* **2008,** 87, (15-16), 3304-3312.
165. Lowe, A. J.; McCaffrey, D. J. A.; Richards, D. G., An investigation into the effectiveness of fireside fuel additives. *Fuel Processing Technology* **1993,** 36, (1-3), 47-53.
166. Chen, J.-C.; Wey, M.-Y.; Lin, Y.-C., The adsorption of heavy metals by different sorbents under various incineration conditions. *Chemosphere* **1998,** 37, (13), 2617-2625.
167. Öhman, M.; Nordin, A., The Role of Kaolin in Prevention of Bed Agglomeration during Fluidized Bed Combustion of Biomass Fuels. *Energy & Fuels* **2000,** 14, (3), 618-624.
168. Zhou, K.; Xu, M.; Yu, D.; Liu, X.; Wen, C.; Zhan, Z.; Yao, H., Formation and Control of Fine Potassium-Enriched Particulates during Coal Combustion. *Energy & Fuels* **2010,** 24, (12), 6266-6274.
169. Tran, Q. K.; Steenari, B.-M.; Iisa, K.; Lindqvist, O., Capture of Potassium and Cadmium by Kaolin in Oxidizing and Reducing Atmospheres. *Energy & Fuels* **2004,** 18, (6), 1870-1876.
170. Li, Y.; Li, J.; Jin, Y.; Wu, Y.; Gao, J., Study on Alkali-Metal Vapor Removal for High-Temperature Cleaning of Coal Gas. *Energy & Fuels* **2005,** 19, (4), 1606-1610.
171. Latva-Somppi, J.; Kauppinen, E. I.; Valmari, T.; Petri, A.; Gurav, A. S.; T. Kodas, T.; Johanson, B., The ash formation during co-combustion of wood and

sludge in industrial fluidized bed boilers. *Fuel Processing Technology* **1998,** 54, (1-3), 79-94.

172. Valmari, T.; Kauppinen, E. I.; Kurkela, J.; Jokiniemi, J. K.; Sfiris, G.; Revitzer, H., Fly ash formation and deposition during fluidized bed combustion of willow. *Journal of Aerosol Science* **1998,** 29, (4), 445-459.

173. Hupa, M., Ash related issues in fluidized bed combustion of biomasses - recent research highlights. *Energy Fuels* **2011**, (Copyright (C) 2011 American Chemical Society (ACS). All Rights Reserved.), ACS Just Accepted.

174. Shao, Y.; Xu, C.; Zhu, J.; Preto, F.; Wang, J.; Li, H.; Badour, C., Ash Deposition in Co-firing Three-Fuel Blends Consisting of Woody Biomass, Peat, and Lignite in a Pilot-Scale Fluidized-Bed Reactor. *Energy Fuels* **2011,** 25, 2841-2849.

175. Pedersen, A. J.; van, L. S.; Frandsen, F. J.; Steinsen, S. D.; Holgersen, L. B., Release to the gas phase of inorganic metals, S and Cl from waste fractions during combustion. *Int. Tech. Conf. Clean Coal Fuel Syst.* **2009,** 34, 979-987.

176. Vainikka, P.; Enestam, S.; Silvennoinen, J.; Taipale, R.; Yrjas, P.; Frantsi, A.; Hannula, J.; Hupa, M., Bromine as an ash forming element in a fluidised bed boiler combusting solid recovered fuel. *Fuel* **2011,** 90, 1101-1112.

177. Jim; Nez, S.; Ballester, J., Particulate matter formation and emission in the combustion of different pulverized biomass fuels. *Combustion science and technology* **2006,** 178, (4), 655-683.

178. Jim; nez, S.; Ballester, J., Formation and Emission of Submicron Particles in Pulverized Olive Residue (Orujillo) Combustion. *Aerosol Science and Technology* **2004,** 38, (7), 707-723.

179. Gluskotor, H. H.; Shimp, N. F.; Ruch, R. R., Chemistry of Coal Utilization, Second Supplement, M. A. Elliot (ed.), 369-424, John Wiley and Son, New York ,1981.

180. Vassilev, S. V.; Vassileva, C. G., Occurrence, abundance and origin of minerals in coals and coal ashes. *Fuel Processing Technology* **1996,** 48, (2), 85-106.

181. Vassilev, S. V.; Kitano, K.; Vassileva, C. G., Some relationships between coal rank and chemical and mineral composition. *Fuel* **1996,** 75, (13), 1537-1542.

182. Raask, E., Mineral Impurities in Coal Combustion: Behaviour, Problems and Remedial Measures. Hemisphere Publishing Corporation, United States of America, 1985.

183. Littlejohn, R. F., Mineral matter and ash distribution in "as-fired" samples of pulverized fuels. *J. Inst. Fuel* **1966,** 39, 59-67.

184. Russell, N. V.; Méndez, L. B.; Wigley, F.; Williamson, J., Ash deposition of a Spanish anthracite: effects of included and excluded mineral matter. *Fuel* **2002,** 81, (5), 657-663.

185. Speight, J. G., The Chemistry and Technology of Coal, Mardel Dekker Inc., Now York, 1994.

186. Reifenstein, A. P.; Kahraman, H.; Coin, C. D. A.; Calos, N. J.; Miller, G.; Uwins, P., Behaviour of selected minerals in an improved ash fusion test: quartz, potassium feldspar, sodium feldspar, kaolinite, illite, calcite, dolomite, siderite, pyrite and apatite. *Fuel* **1999,** 78, (12), 1449-1461.

187. Gupta, S. K.; Gupta, R. P.; Bryant, G. W.; Wall, T. F., The effect of potassium on the fusibility of coal ashes with high silica and alumina levels. *Fuel* **1998,** 77, (11), 1195-1201.
188. Huggins, F. E.; Kosmack, D. A.; Huffman, G. P., Correlation between ash-fusion temperatures and ternary equilibrium phase diagrams. *Fuel* **1981,** 60, (7), 577-584.
189. Srinivasachar, S.; Helble, J. J.; Boni, A. A.; Shah, N.; Huffman, G. P.; Huggins, F. E., Mineral behavior during coal combustion 2. Illite transformations. *Progress in Energy and Combustion Science* **1990,** 16, (4), 293-302.
190. Gupta, R. P.; Wall, T. F.; Kajigaya, I.; Miyamae, S.; Tsumita, Y., Computer-controlled scanning electron microscopy of minerals in coal--Implications for ash deposition. *Progress in Energy and Combustion Science* **1998,** 24, (6), 523-543.
191. Srinivasachar, S.; Boni, A. A., A kinetic model for pyrite transformations in a combustion environment. *Fuel* **1989,** 68, (7), 829-836.
192. Yan, L., CCSEM Analysis of Mineral in Pulverized Coal and Ash Formation Modeling, Ph.D. Thesis, The University of Newcastle, 2000.
193. Helble, J. J.; Srinivasachar, S.; Boni, A. A., Factors influencing the transformation of minerals during pulverized coal combustion. *Progress in Energy and Combustion Science* **1990,** 16, (4), 267-279.
194. ten Brink, H. M., Silica fines from included quartz in pulverized coal combustion. *Fuel and Energy Abstracts* **1997,** 38, (4), 252-252.
195. Baxter, L. L., The evolution of mineral particle size distributions during early stages of coal combustion. *Progress in Energy and Combustion Science* **1990,** 16, (4), 261-266.
196. ten Brink, H. M.; Eenkhoorn, S.; Weeda, M., The behaviour of coal mineral carbonates in a simulated coal flame. *Fuel Processing Technology* **1996,** 47, (3), 233-243.
197. McLennan, A. R.; Bryant, G. W.; Bailey, C. W.; Stanmore, B. R.; Wall, T. F., An Experimental Comparison of the Ash Formed from Coals Containing Pyrite and Siderite Mineral in Oxidizing and Reducing Conditions. *Energy & Fuels* **2000,** 14, (2), 308-315.
198. Bool Iii, L. E.; Peterson, T. W.; Wendt, J. O. L., The partitioning of iron during the combustion of pulverized coal. *Combustion and Flame* **1995,** 100, (1-2), 262-270.
199. Slater, P. N.; Richards, G. H.; Harb, J. N., Pyrite and illite associations in two eastern US bituminous coals. *Fuel Processing Technology* **1995,** 44, (1-3), 55-69.
200. Liu, X.; Xu, M.; Yao, H.; Yu, D.; Lv, D.; Zhou, K., The Formation and Emission of Particulate Matter during the Combustion of Density Separated Coal Fractions. *Energy & Fuels* **2008,** 22, (6), 3844-3851.
201. Damle, A. S.; Ensor, D. S.; Ranade, M. B., Coal combustion aerosol formation mechanisms: A review. *Aerosol Science and Technology* **1982,** 1, (C), 119-133.

202. Lighty, J. S.; Veranth, J. M.; Sarofim, A. F., Combustion aerosols: Factors governing their size and composition and implications to human health. *Journal of the Air and Waste Management Association* **2000,** 50, (9), 1565-1618.
203. Yao, Q.; Li, S. Q.; Xu, H. W.; Zhuo, J. K.; Song, Q., Studies on formation and control of combustion particulate matter in China: A review. *Energy* **2009,** 34, (9), 1296-1309.
204. Yu, D.; Xu, M. H.; Liu, X.; Huang, J.; Li, G., Mechanisms of submicron and residual ash particle formation during pulverised coal combustion: A comprehensive review. *Developments in Chemical Engineering and Mineral Processing* **2005,** 13, (3-4), 467-482.
205. Kang, S. G., Fundamental Studies of Mineral Matter Transformation during Pulverized Coal Combustion: Residual Ash Formation, Ph.D. Thesis, Department of Chemical Engineering, MIT, 1991.
206. Yan, L.; Gupta, R. P.; Wall, T. F., The implication of mineral coalescence behaviour on ash formation and ash deposition during pulverised coal combustion. *Fuel* **2001,** 80, (9), 1333-1340.
207. Hurley, J. P.; Schobert, H. H., Ash formation during pulverised subbituminous coal combustion. 2. Inorganic transformations during middle and late stages of burnout. *Energy & Fuels* **1993,** 7, (4), 542-553.
208. Smoot, L. D.; Smith, P. J., Coal Combustion and Gasification, Plenum, New York (1985). .
209. Kang, S. G.; Sarofim, A. F.; Beér, J. M., Effect of Char structure on residual ash formation during pulverized coal combustion. *Symposium (International) on Combustion* **1992,** 24, (1), 1153-1159.
210. Wibberley, L. J.; Wall, T. F., An Investigation of Factors Affecting the Physical Characteristics of Flyash Formed in a Laboratory Scale Combustor. *Combustion science and technology* **1986,** 48, (3-4), 177-190.
211.Baxter, L. L., Char fragmentation and fly ash formation during pulverized-coal combustion. *Combustion and Flame* **1992,** 90, (2), 174-184.
212. Helble, J. J.; Sarofim, A. F., Influence of char fragmentation on ash particle size distributions. *Combustion and Flame* **1989,** 76, (2), 183-196.
213. Liu, G.; Wu, H.; Gupta, R. P.; Lucas, J. A.; Tate, A. G.; Wall, T. F., Modeling the fragmentation of non-uniform porous char particles during pulverized coal combustion. *Fuel* **2000,** 79, (6), 627-633.
214. Liu, Y.; Gupta, R.; Sharma, A.; Wall, T.; Butcher, A.; Miller, G.; Gottlieb, P.; French, D., Mineral matter–organic matter association characterisation by QEMSCAN and applications in coal utilisation. *Fuel* **2005,** 84, (10), 1259-1267.
215. Wang, H.; Harb, J. N., Modeling of ash deposition in large-scale combustion facilities burning pulverized coal. *Progress in Energy and Combustion Science* **1997,** 23, (3), 267-282.
216. Kang, S.-G.; Helble, J. J.; Sarofim, A. F.; Beér, J. M., Time-resolved evolution of fly ash during pulverized coal combustion. *Symposium (International) on Combustion* **1989,** 22, (1), 231-238.
217. Mitchell, R. E.; Akanetuk, A. E. J., The impact of fragmentation on char

conversion during pulverized coal combustion. *Symposium (International) on Combustion* **1996,** 26, (2), 3137-3144.
218. Sundback, C. A.; Beér, J. M.; Sarofim, A. F., Fragmentation behavior of single coal particles in a fluidized bed. *Symposium (International) on Combustion* **1985,** 20, (1), 1495-1503.
219. Helble, J.; Neville, M.; Sarofim, A. F., Aggregate formation from vaporized ash during pulverized coal combustion. *Symposium (International) on Combustion* **1988,** 21, (1), 411-417.
220. Wu, H.; Wall, T.; Liu, G.; Bryant, G., Ash Liberation from Included Minerals during Combustion of Pulverized Coal: The Relationship with Char Structure and Burnout. *Energy Fuels* **1999,** 13, (6), 1197-1202.
221. Wang, Q.; Zhang, L.; Sato, A.; Ninomiya, Y.; Yamashita, T., Effects of coal blending on the reduction of PM10 during high-temperature combustion 1. Mineral transformations. *Fuel* **2008,** 87, (13-14), 2997-3005.
222. Helble, J. J.; Sarofim, A. F., Factors determining the primary particle size of flame-generated inorganic aerosols. *Journal of Colloid and Interface Science* **1989,** 128, (2), 348-362.
223. Quann, R. J.; Sarofim, A. F., Vaporization of refractory oxides during pulverized coal combustion. *Symposium (International) on Combustion* **1982,** 19, (1), 1429-1440.
224. Flagan, R. C.; Friedlander, S. K., D.T. Shaw, Editor, Recent Developments in Aerosol Science, Wiley–Interscience, New York (1978), pp. 25–59.
225. Linak, W. P.; Wendt, J. O. L., Toxic metal emissions from incineration: Mechanisms and control. *Progress in Energy and Combustion Science* **1993,** 19, (2), 145-185.
226. Xu, M.; Yan, R.; Zheng, C.; Qiao, Y.; Han, J.; Sheng, C., Status of trace element emission in a coal combustion process: a review. *Fuel Processing Technology* **2004,** 85, (2-3), 215-237.
227. Helble, J. J.; Mojtahedi, W.; Lyyränen, J.; Jokiniemi, J.; Kauppinen, E., Trace element partitioning during coal gasification. *Fuel* **1996,** 75, (8), 931-939.
228. Fisher, G. L.; Chang, D. P. Y.; Brummer, M., Fly ash collected from electrostatic precipitators: microcrystalline structures and the mystery of the spheres. *Science* **1976,** 192, (4239), 553-555.
229. Smith, R. D.; Campbell, J. A.; Nielson, K. K., Characterization and formation of submicron particles in coal-fired plants. *Atmospheric Environment (1967)* **1979,** 13, (5), 607-617.
230. Ramsden, A. R., A microscopic investigation into the formation of fly-ash during the combustion of a pulverized bituminous coal. *Fuel* **1969,** 48, 121–137.
231. Holve, D. J., In Situ Measurements of Flyash Formation from Pulverized Coal. *Combustion science and technology* **1986,** 44, (5-6), 269-288.
232. Sadakata, M.; Mochizuki, M.; Sakai, T.; Okazaki, K.; Ono, M., Formation and behavior of submicron fly ash in pulverized coal combustion furnace. *Combustion and Flame* **1988,** 74, (1), 71-80.
233. Baxter, L. L.; Mitchell, R. E.; Fletcher, T. H., Release of inorganic material

during coal devolatilization. *Combustion and Flame* **1997,** 108, (4), 494-502.
234. Zhang, L.; Ninomiya, Y.; Yamashita, T., Occurrence of Inorganic Elements in Condensed Volatile Matter Emitted from Coal Pyrolysis and Their Contributions to the Formation of Ultrafine Particulates during Coal Combustion. *Energy & Fuels* **2006,** 20, (4), 1482-1489.
235. Zhang, L.; Ninomiya, Y.; Yamashita, T., Formation of submicron particulate matter (PM1) during coal combustion and influence of reaction temperature. *Fuel* **2006,** 85, (10-11), 1446-1457.
236. Fix, G.; Seames, W. S.; Mann, M. D.; Benson, S. A.; Miller, D. J., The effect of oxygen-to-fuel stoichiometry on coal ash fine-fragmentation mode formation mechanisms. *Fuel Process. Technol.* **2011,** 92, 793-800.
237. Carbone, F.; Beretta, F.; D'Anna, A., Factors Influencing Ultrafine Particulate Matter (PM0.1) Formation under Pulverized Coal Combustion and Oxyfiring Conditions. *Energy & Fuels* **2010,** 24, (12), 6248-6256.
238. Zhang, L.; Wang, Q.; Sato, A.; Ninomiya, Y.; Yamashita, T., Interactions among Inherent Minerals during Coal Combustion and Their Impacts on the Emission of PM10. 2. Emission of Submicrometer-Sized Particles. *Energy & Fuels* **2007,** 21, (2), 766-777.
239. Wang, Q.; Zhang, L.; Sato, A.; Ninomiya, Y.; Yamashita, T., Interactions among Inherent Minerals during Coal Combustion and Their Impacts on the Emission of PM10. 1. Emission of Micrometer-Sized Particles. *Energy & Fuels* **2007,** 21, (2), 756-765.
240. Zhou, K.; Xu, M.; Yu, D.; Wen, C.; Zhan, Z.; Yao, H., The effects of coal blending on the formation and properties of particulate matter during combustion. *Chinese Science Bulletin* **2010,** 55, (30), 3448-3455.
241. Ninomiya, Y.; Wang, Q.; Xu, S.; Teramae, T.; Awaya, I., Evaluation of a Mg-Based Additive for Particulate Matter (PM)2.5 Reduction during Pulverized Coal Combustion†. *Energy & Fuels* **2009,** 24, (1), 199-204.
242. Teramae, T.; Takarada, T., Fine Ash Formation during Pulverized Coal Combustion. *Energy & Fuels* **2009,** 23, (4), 2018-2024.
243. Heinzel, T.; Siegle, V.; Spliethoff, H.; Hein, K. R. G., Investigation of slagging in pulverized fuel co-combustion of biomass and coal at a pilot-scale test facility. *Fuel Processing Technology* **1998,** 54, (1-3), 109-125.
244. ASTM Standard E871 - 82, 2006, " Standard Test Method for Moisture Analysis of Particulate Wood Fuels," ASTM International, West Conshohocken, PA, 2006, DOI: 10.1520/E0870-82R06, www.astm.org.
245. ASTM Standard D7582 - 10, 2010, " Test Methods for Proximate Analysis of Coal and Coke by Macro Thermogravimetric Analysis ", ASTM International, West Conshohocken, PA, 2006, DOI: 10.1520/D7582-10, www.astm.org.
246. Standards Australia. AS1038.6.4-2005, Coal and Coke—Analysis and Testing—Higher Rank Coal and Coke—Ultimate Analysis—Carbon, Hydrogen and Nitrogen—Instrumental Method; Standards Australia: Sydney, Australia, 2005.
247. Standards Australia. AS1038.6.3.1-1997, Coal and Coke—Analysis and Testing—Higher Rank Coal and Coke—Ultimate Analysis—Total Sulfur—Eschka

Method; Standards Australia: Sydney, Australia, 1997.
248. Standards Australia. AS1038.8.1-1999, Coal and Coke—Analysis and Testing—Coal and Coke—Chlorine—Eschka Method; Standards Australia: Sydney, Australia, 1999.
249. Carrasco-Marín, F.; Alvarez-Merino, M. A.; Moreno-Castilla, C., Microporous activated carbons from a bituminous coal. *Fuel* **1996,** 75, (8), 966-970.
250. Ghosal, R.; Smith, D. M., Micropore characterization using the Dubinin-Astakhov equation to analyze high pressure CO₂ (273 K) adsorption data. *Journal of Porous Materials* **1996,** 3, (4), 247-255.
251. Yu, D.; Xu, M.; Zhang, L.; Yao, H.; Wang, Q.; Ninomiya, Y., Computer-Controlled Scanning Electron Microscopy (CCSEM) Investigation on the Heterogeneous Nature of Mineral Matter in Six Typical Chinese Coals†. *Energy & Fuels* **2006,** 21, (2), 468-476.
252. Zygarlicke, C. J.; Steadman, E. N., Advanced SEM techniques to characterize coal minerals. *Scanning Microscopy* **1990,** 4, (3), 579-590.
253. Lee, S. W., Fine particulate matter measurement and international standardization for air quality and emissions from stationary sources. *Fuel* **2010,** 89, (4), 874-882.
254. Pagels, J. M.; Strand, J. R., Characteristics of aerosol particles formed during grate combustion of moist forest residue. *J. Aerosol Sci.* **2003,** 34, (8), 1043–1059.
255. Hindiyarti, L.; Frandsen, F.; Livbjerg, H.; Glarborg, P.; Marshall, P., An exploratory study of alkali sulfate aerosol formation during biomass combustion. *Fuel* **2008,** 87, (8-9), 1591-1600.
256. Hanby, V. I., Sodium Sulphate Formation and Deposition in Marine Gas Turbines. *J. Eng. Power* **1974,** 96, 129-133.
257. Kohl, F. J.; Santoro, G. J.; Stearns, C. A.; Rosner, D. E., Theoretical and Experimental Studies of the Deposition of Na_2SO_4 from Seeded Combustion Gases. *J. Electrochem. Soc.* **1979,** 126, (6), 1054–1061.
258. Fielder, W. L.; Stearns, C. A.; Kohl, F. J., Reactions of NaCl with Gaseous SO_3, SO_2, and O_2. *J. Electrochem. Soc.* **1984,** 131, 2414–2417.
259. Steinberg, M.; Schofield, K., The chemistry of sodium with sulfur in flames. *Prog.Energ.Combust.* **1990,** 16, (4), 311–317.
260. Steinberg, M.; Schofield, K., The controlling chemistry in flame generated surface deposition of Na_2SO_4 and the effects of chlorine. *Proc. Combust. Inst.* **1996,** 26, (2), 1835–1843.
261. Srinivasachar, S.; Helble, J. J.; Ham, D. O.; Domazetis, G., A kinetic description of vapor phase alkali transformations in combustion systems. *Prog.Energ.Combust.* **1990,** 16, (4), 303–309.
262. Verhoff, F. H.; Branchero, J., Predicting Dew Points of Flue gasses. *Chem. Eng. Prog.* **1974,** 70, (8), 71.
263. Kiang, Y. H., Predicting dew points of acid gasses. *Chem. Eng. -New York* **1981,** 88, (2), 127.
264. Boman, C.; Nordin, A.; Boström, D.; Öhman, M., Characterization of

Inorganic Particulate Matter from Residential Combustion of Pelletized Biomass Fuels. . *Energy Fuels* **2004,** 18, (2), 338-348.

265. Mackowski, D. W.; Tassopoulos, M.; Rosner, D. E., Effect of radiative heat transfer on the coagulation dynamics of combustion-generated particles. *Aerosol Sci. Tech.* **1994,** 20, (1), 83–99.

266. Alonso, M.; Alguacil, F. J.; Martin, M. I.; Kousaka, Y.; Nomura, T., Aerosol particle size growth by simultaneous coagulation and condensation with diffusion losses in laminar flow tubes. *J. Aerosol Sci.* **1999,** 30, (9), 1191-1199.

267. Johansson, L. S.; Leckner, B.; Gustavsson, L.; Cooper, D.; Tullin, C.; Potter, A.; Berntsen, M., Particle Emissions from Residential Biofuel Boilers and Stoves-Old and Modern Techniques. In *Proceedings of the international workshop "Aerosols in Biomass Combustion" 18th March 2005*, Graz, Austria., 2005; Vol. 6.

268. Encinar, J. M., Gonzalez, J.F., Rodriguez, J.J., and Ramiro, M.J., Catalysed and Uncatalysed Steam Gasification of Eucalyptus Char: Influence of Variables and Kinetic Study. *Fuel* **2001,** 80, 2025-2036.

269. Wu, H., Yip, K., Tian, F., Xie, Z., and Li, C.-Z., Evolution of Char Structure during the Steam Gasification of Biochars Produced from the Pyrolysis of Various Mallee Biomass Components. *Industrial & Engineering Chemistry Research* **2009,** 48, 10431–10438.

270. Li, C. Z.; Sathe, C.; Kershaw, J. R.; Pang, Y., Fates and roles of alkali and alkaline earth metals during the pyrolysis of a Victorian brown coal. . *Fuel* **2000,** 79, (3-4), 427-438.

271. Yu, Y.; Xu, M.; Yao, H.; Yu, D.; Qiao, Y.; Sui, J.; Liu, X.; Cao, Q., Char characteristics and particulate matter formation during Chinese bituminous coal combustion. *Proceedings of the Combustion Institute* **2007,** 31, (2), 1947-1954.

272. Zhuo, J. K.; Li, S. Q.; Yao, Q.; Song, Q., The progressive formation of submicron particulate matter in a quasi one-dimensional pulverized coal combustor. *Proceedings of the Combustion Institute* **2009,** 32, (2), 2059-2066.

273. Wiinikka, H.; Gebart, R.; Boman, C.; Boström, D.; Nordin, A.; Öhman, M., High-temperature aerosol formation in wood pellets flames: Spatially resolved measurements. *Combustion and Flame* **2006,** 147, (4), 278-293.

274. Wiinikka, H.; Gebart, R.; Boman, C.; Boström, D.; Öhman, M., Influence of fuel ash composition on high temperature aerosol formation in fixed bed combustion of woody biomass pellets. *Fuel* **2007,** 86, (1-2), 181-193.

275. Quyn, D. M.; Wu, H.; Li, C.-Z., Volatilisation and catalytic effects of alkali and alkaline earth metallic species during the pyrolysis and gasification of Victorian brown coal. Part I. Volatilisation of Na and Cl from a set of NaCl-loaded samples. *Fuel* **2002,** 81, (2), 143-149.

276. Neville, M.; Quann, R. J.; Haynes, B. S.; Sarofim, A. F., Vaporization and condensation of mineral matter during pulverized coal combustion. *Symposium (International) on Combustion* **1981,** 18, (1), 1267-1274.

277. Obernberger, I., et al. , Characterisation and formation of aerosol and fly-ashes from fixed-bed biomass combustion. *International IEA seminar* **2001**.

278. Srinivasachar, S.; Helble, J. J.; Boni, A. A., Mineral behavior during coal

combustion 1. Pyrite transformations. *Progress in Energy and Combustion Science* **1990,** 16, (4), 281-292.
279. Richard D, S., The trace element chemistry of coal during combustion and the emissions from coal-fired plants. *Progress in Energy and Combustion Science* **1980,** 6, (1), 53-119.
280. Baxter, L. L.; Mitchell, R. E., The release of iron during the combustion of Illinois No. 6 coal. *Combustion and Flame* **1992,** 88, (1), 1-14.
281. Sarofim, A. F., The physical transformation of the mineral matter in pulverized coal under simulated combustion conditions. *Combustion science and technology* **1977,** 16, (3), 187.
282. Yan, L.; Gupta, R.; Wall, T., Fragmentation Behavior of Pyrite and Calcite during High-Temperature Processing and Mathematical Simulation. *Energy & Fuels* **2001,** 15, (2), 389-394.
283. Yan, L.; Gupta, R. P.; Wall, T. F., A mathematical model of ash formation during pulverized coal combustion. *Fuel* **2002,** 81, (3), 337-344.
284. Buhre, B. J. P.; Hinkley, J. T.; Gupta, R. P.; Nelson, P. F.; Wall, T. F., Fine ash formation during combustion of pulverised coal-coal property impacts. *Fuel* **2006,** 85, (2), 185-193.
285. Wee, H. L.; Wu, H.; Zhang, D., Heterogeneity of Ash Deposits Formed in a Utility Boiler during PF Combustion. *Energy Fuels* **2007,** 21, 441-450.
286. Raask, E., The mode of occurrence and concentration of trace elements in coal. *Progress in Energy and Combustion Science* **1985,** 11, (2), 97-118.
287. van Dyk, J. C.; Baxter, L. L.; van Heerden, J. H. P.; Coetzer, R. L. J., Chemical fractionation tests on South African coal sources to obtain species-specific information on ash fusion temperatures (AFT). *Fuel* **2005,** 84, (14-15), 1768-1777.
288. Miller, S. F.; Schobert, H. H., Effect of the occurrence and composition of iron compounds on ash formation, composition, and size in pilot-scale combustion of pulverized coal and coal-water slurry fuels. *Energy & Fuels* **1993,** 7, (6), 1030-1038.
289. Greer, R. T., Coal microstructure and pyrite distribution, Am. chem. Soc. Symp. Ser. (1977) No.1.
290. Wall, T. F.; Lowe, A.; Wibberley, L. J.; McC. Stewart, I., Mineral matter in coal and the thermal performance of large boilers. *Progress in Energy and Combustion Science* **1979,** 5, (1), 1-29.
291. Saastamoinen, J. J.; Aho, M. J.; Hämäläinen, J. P.; Hernberg, R.; Joutsenoja, T., Pressurized Pulverized Fuel Combustion in Different Concentrations of Oxygen and Carbon Dioxide. *Energy & Fuels* **1996,** 10, (1), 121-133.
292. Sarofim, A. F.; Howard, J. B.; Padia, A. S., The Physical Transformation of the Mineral Matter in Pulverized Coal Under Simulated Combustion Conditions. *Combustion science and technology* **1977,** 16, (3-6), 187-204.
293. Kang, S.-W.; Sarofim, A. F.; Beér, J. M., Particle rotation in coal combustion: statistical, experimental and theoretical studies. *Symposium (International) on Combustion* **1989,** 22, (1), 145-153.
294. Sadhukhan, A. K.; Gupta, P.; Saha, R. K., Modeling and experimental studies on single particle coal devolatilization and residual char combustion in

fluidized bed. *Fuel* **2011,** 90, (6), 2132-2141.
295. Levendis, Y. A.; Joshi, K.; Khatami, R.; Sarofim, A. F., Combustion behavior in air of single particles from three different coal ranks and from sugarcane bagasse. *Combustion and Flame* **2011,** 158, (3), 452-465.
296. Atal, A.; Levendis, Y. A., Comparison of the combustion behaviour of pulverized waste tyres and coal. *Fuel* **1995,** 74, (11), 1570-1581.
297. Bejarano, P. A., 2007, 179, (8), 1569., Combustion of coal chars in oxygen-enriched atmospheres. *Combustion science and technology* **2007,** 179, (8), 1569-1578.